



European Spatial Data Research

August 2011

**Registration Quality – Towards Integration of
Laser Scanning and Photogrammetry**

by Petri Rönholm

Atlas of INSPIRE Implementation Methods

by Ingrid Vanden Berghe, Joep Crompvoets,
Walter de Vries and Jantien Stoter

The present publication is the exclusive property of
European Spatial Data Research

All rights of translation and reproduction are reserved on behalf of EuroSDR.
Published by EuroSDR

Printed by Gopher, Amsterdam, The Netherlands

EUROPEAN SPATIAL DATA RESEARCH

PRESIDENT 2010 – 2012:

Jean-Philippe Lagrange, France

VICE-PRESIDENT 2009 – 2011:

Dieter Fritsch, Germany

SECRETARY-GENERAL:

Kevin Mooney, Ireland

DELEGATES BY MEMBER COUNTRY:

Austria: Michael Franzen

Belgium: Ingrid Vanden Berghe; Jean Theatre

Croatia: Željko Hećimović; Ivan Landek

Cyprus: Christos Zenonos; Michael Savvides

Denmark: Thorben Hansen; Lars Bodum

Finland: Risto Kuittinen; Juha Vilhomaa

France: Jean-Philippe Lagrange; Xavier Briottet

Germany: Dietmar Grünreich; Klement Aringer; Dieter Fritsch

Ireland: Colin Bray; Ned Dwyer

Italy: Fabio Crosilla

Netherlands: Jantien Stoter; Aart-jan Klijnjan

Norway: Jon Arne Trollvik; Ivar Maalen-Johansen

Spain: Antonio Arozarena; Emilio Domenech

Sweden: Anders Olsson; Anders Östman

Switzerland: Francois Golay; André Streilein-Hurni

United Kingdom: Malcolm Havercroft; Jeremy Morley

COMMISSION CHAIRPERSONS:

Sensors, Primary Data Acquisition and Georeferencing: Michael Cramer, Germany

Image Analysis and Information Extraction: Norbert Pfeifer, Austria

Production Systems and Processes: André Streilein-Hurni, Switzerland

Data Specifications: Ulf Sandgren, Sweden

Network Services: Lars Bernard, Germany

OFFICE OF PUBLICATIONS:

Bundesamt für Kartographie und Geodäsie (BKG)
Publications Officer: Andreas Busch
Richard-Strauss-Allee 11
60598 Frankfurt
Germany
Tel.: + 49 69 6333 312
Fax: + 49 69 6333 441

CONTACT DETAILS:

Web: www.eurosd.net
President: president@eurosd.net
Secretary-General: secretary@eurosd.net
Secretariat: admin@eurosd.net

EuroSDR Secretariat
Faculty of the Built Environment
Dublin Institute of Technology
Bolton Street
Dublin 1
Ireland
Tel.: +353 1 4023933

The official publications of EuroSDR are peer-reviewed.

ABSTRACT.....	11
1 INTRODUCTION.....	11
2 DESCRIPTION OF THE PROJECT	13
2.1 Aims of the project.....	13
2.2 Participants.....	13
2.3 Description of test data	14
2.4 Reference data.....	17
2.5 Test procedure	19
3 SHORT DESCRIPTIONS OF THE APPLIED METHODS	20
3.1 Method of the Aalto University School of Engineering (Aalto).....	20
3.2 Method of the Dublin Institute of Technology (DIT)	20
3.3 Method of the Finnish Geodetic Institute, Aalto University School of Engineering and TerraSolid Oy (FGI et al.).....	20
3.4 Method of the Independent Research Group on Geospatial (IRGG).....	21
3.5 Method 1 of the National Geographic Institute, Spain (IGN-1)	21
3.6 Method 2 of the National Geographic Institute, Spain (IGN-2)	21
3.7 Planar patches method of the University of Calgary (UofC-1).....	22
3.8 Straight lines method of the University of Calgary (UofC-2).....	22
3.9 Combined method of the University of Calgary (UofC-3)	22
3.10 Method of the University College London (UCL).....	23
3.11 ICP-based method of the University of Stuttgart (IFP-1).....	23
3.12 Point-Based method of the University of Stuttgart (IFP-2)	23
3.13 Method of the Vienna University of Technology (IPF)	23
4 RESULTS AND DISCUSSION.....	24
4.1 Comparison of planimetric accuracies.....	24
4.2 Comparison of vertical accuracies	26
4.3 Comparison of accuracies in rotations.....	29
4.4 Influence of the type of tie features.....	31
4.5 Influence of the analytical characteristics of the applied methods	33
4.6 Influence of the level of automation	36
4.7 Processing time	37
5 SUMMARY AND CONCLUSIONS.....	38
6 ACKNOWLEDGEMENTS	39
7 REFERENCES	39
APPENDIX A. DETAILED STATISTICAL ANALYSIS OF THE RESULTS	42
A.1 Aalto University School of Sciences and Technology (Aalto)	42
A.2 Dublin Institute of Technology (DIT).....	43
A.3 Finnish Geodetic Institute, Aalto University School of Engineering and TerraSolid Oy (FGI et al.).....	45
A.4 National Geographic Institute Spain (IGN-1, IGN-2)	48
A.5 Independent Research Group on Geospatial (IRGG)	49
A.6 University College London (UCL)	50
A.7 University of Calgary (UofC-1, UofC-2, UofC-3).....	51
A.8 University of Stuttgart (IFP-1, IFP-2).....	55
A.9 Vienna University of Technology (IPF).....	56

APPENDIX B. TECHNICAL REPORTS OF THE PARTICIPANTS	58
Report of the Aalto University School of Engineering	59
Report of the Dublin Institute of Technology	66
Report of the Finnish Geodetic Institute, Aalto University School of Engineering and TerraSolid Oy	72
Report of the Independent Research Group on Geospatial	79
Report of the National Geographic Institute Spain	103
Report of the University of Calgary	141
Report of the University College London	163
Report of the Institute for Photogrammetry, University of Stuttgart	229
Report of the Vienna University of Technology	238

ABSTRACT	257
1 INTRODUCTION.....	258
2 QUESTIONNAIRE.....	259
2.1 Introduction.....	259
2.2 Questions.....	259
2.3 Analysis of the questionnaire responses	259
2.4 Conclusions of the questionnaire	260
3 REPORT OF 1ST PROJECT WORKSHOP, 29 & 30 APRIL 2009.....	261
3.1 Introduction.....	261
3.2 Brief description of the Workshop 29 - 30 April 2009.....	262
3.3 Research questions identified by the participants	263
3.4 Main observations during the workshop.....	263
3.5 Remarkable quotes.....	264
4 REPORT OF 2ND PROJECT WORKSHOP 14/15 JANUARY 2010	265
4.1 Introduction.....	265
4.2 Successes and disappointments.....	266
4.3 Propositions.....	268
4.4 Research agenda.....	270
4.5 Concluding remarks	272
5 PRE-CONFERENCE INSPIRE WORKSHOP, 22 JUNE 2010	273
6 CONCLUSION.....	276
ACKNOWLEDGMENTS.....	276
APPENDIX I PRESENTATION AT INSPIRE CONFERENCE, KRAKOW, JUNE 2010	278

EuroSDR Project

Commission 2 “Image analysis and information content”

“Registration Quality – Towards Integration of Laser Scanning and Photogrammetry”

Final Report

Report by Petri Rönnholm

Institute of Photogrammetry and Remote Sensing
Aalto University School of Engineering, Finland
petri.ronnholm@aalto.fi

Abstract

Laser scanning and photogrammetry are powerful 3D data acquisition methods providing both overlapping and complementary information. Currently, integration of laser data and images provides the most complete information for various surveying and 3D modelling tasks. However, this integration requires that both data sets are accurately oriented to the same coordinate system. In 2008, the EuroSDR launched the project “Registration Quality – Towards Integration of Laser Scanning and Photogrammetry” in order to collect knowledge about current registration methods and their performance. The project attracted the involvement of numerous research institutes and companies. Therefore, this test gives a quite extensive set of examples and comparisons of the most important registration strategies today. The empirical results indicated that the relative orientation of airborne laser scanning data and aerial images is a feasible method in order to get data sets within the common coordinate frame. The experiment revealed that, currently, the level of automation was not the most significant factor affecting the quality of registration. More important factors included the type of tie features and the implementation of the methods. The processing time was shortest with most automatic methods, whereas the amount of manual work tended to increase the processing times. It should be noted that many of the methods were still at the developmental stage. It is expected that the performance and processing speed, in most cases, can be enhanced in the future. The test data represented an urban area and many of the methods relied upon certain objects, such as buildings. Therefore, the performance of applied methods in non-built environments should be investigated separately.

1 Introduction

Images provide much complementary information for laser scanning – and vice versa. The integration of airborne laser scanning (ALS) point clouds and aerial images has a great potential for improving, for example, 3D modelling and the recognition and classification of objects in our environment. Some of the most promising end applications include, for example, automatic object recognition, the accurate classification of individual trees, point cloud densification, the automatic classification of land use, system calibration, and the generation of photorealistic 3D models. When integrating data from different sources, however, it is essential to have all data sets within the common coordinate frame. This can be achieved using one of the following principal strategies (Rönnholm et al., 2007):

1. System calibration of the hybrid device for simultaneous data acquisition
2. Separate orientation of images and laser scanning data to a common ground coordinate system
3. Relative orientation of images and laser scanning data.

The focus of this EuroSDR project is on the accuracy of the methods developed for solving a relative orientation between ALS data and aerial images at urban areas. Two other strategies for getting data sets to the same coordinate frame, therefore, are introduced very briefly.

Mounting all sensors to a common platform and calibrating the system provides parameters for relative orientation. Therefore, data sets can be automatically transformed to the common coordinate frame without additional post processing. In order to ensure similar contents for both data sets, simultaneous data collection is required. Otherwise, for example, moving objects at the scene cause differences between data sets. Currently, only 3D range cameras (Ray et al., 2001) are able to fulfil all such conditions. Unfortunately, the range, resolution and accuracy of such devices are not yet sufficient for professional airborne applications.

In some cases, simultaneous data acquisition is not possible or desired. For example, ALS data can also be collected at night-time, which is not feasible for taking aerial images. Another reason for separate data acquisition can be, for example, different requirements for the optimal flying height. Direct orientation sensors, such as GPS/IMU, separately provide approximate orientations for both data sets. A more detailed overview of direct orientation sensors is given, for example, in Skaloud (2006). The accuracies of direct orientation sensors are reported to be as high as 5–10 cm in position and better than 0.006° for ω and ϕ , and 0.01° for κ in rotations (Schwarz, 1995; Cramer, M., 1999; Kremer, 2001; Heipke et al., 2002; Honkavaara et al., 2003; Legat et al., 2006). Unfortunately, the GPS and IMU systems have no inherent quality control (Schenk and Csathó, 2002), which may lead to some systematic or gross errors. Usually, the accuracy of GPS/IMU is not enough to ensure that data sets are precisely within the same coordinate system.

One strategy for transforming separately acquired data sets to fit into the common coordinate frame is to use signalized or natural ground control features and detect corresponding features from both images and ALS data. In the case of aerial images, an aerial triangulation is the standard process for solving accurate exterior orientations of images. For ALS data, no corresponding standard process exists yet. In addition, the most suitable ground control features for ALS point clouds are not necessarily optimal for photogrammetric measurements, and vice versa. Typically, for example, targets designed for ALS data need to be quite large in order to ensure enough laser measurements within them. Suggested ground control features have included, for example, large circular targets (Toth and Grejner-Brzezinska, 2005; Csanyi and Toth, 2007; Yastikli et al., 2008) and pavement markings (Toth et al., 2007). One alternative is to use several small surface areas instead of artificial targets. These reference surface areas are typically modelled using differential GPS (DGPS). However, as pointed out, for example in Vosselman (2008), measuring many ground control targets or areas is not necessarily feasible in laser scanning campaigns.

A relative orientation between ALS data and aerial images has the advantage that only one data set has to be georeferenced. This reduces field work, because less ground control features are needed. Solving a relative orientation requires that enough corresponding features are identified from ALS data and aerial images. Extracting tie features typically follows one of the three basic strategies or a combination of them:

1. Extracting corresponding 3D features from laser scanning data and images
2. Extracting 3D features from laser scanning data and corresponding 2D features from images
3. Creating a synthetic 2D image from a 3D laser scanning point cloud and then extracting 2D features from both the laser-derived synthetic image and the photographic image.

Especially in the case of ALS data, a low point density may be an obstacle when the corresponding features are searched and extracted. Even if modern ALS systems are able to acquire quite dense point clouds, which can be further densified by acquiring overlapping scanning strips, the economical reasons usually lead to moderate point densities. According to Baltsavias (1999), finding accurate corresponding points from ALS data is difficult or even impossible. Usually, if the point density is relatively high, tie-points can be identified with moderate accuracy. Therefore, tie-points are often used only for giving an approximate orientation for a more accurate orientation that uses other types of tie-features.

The foundation for a successful relative orientation is that the internal quality of both data sets is as good as possible. In the case of aerial images, a proper camera calibration is required (Cramer, 2009). Laser scanning data can suffer from various factors that reduce the quality. A detailed description of such error sources is given by Schenk (2001). The quality of ALS data can be improved by collecting overlapping and crossing laser strips and by calculating a strip adjustment. According to Pfeifer

(2005), the main correcting methods are data-driven methods (e.g., Kilian et al., 1996; Crombaghs et al., 2000; Kraus and Pfeifer, 2001; Vosselman and Maas, 2001; Kornus and Ruiz, 2003) and sensor-based methods (e.g., Burman, 2002; Filin, 2003; Kager, 2004). Data-driven methods can be applied to plain 3D laser scanning point clouds when sensor-based methods typically require trajectory and sensor parameter information for each laser point.

The aims of this EuroSDR project are listed in more detail in the next chapter.

2 Description of the project

2.1 Aims of the project

The aims of the EuroSDR project “Registration Quality – Towards Integration of Laser Scanning and Photogrammetry” can be summarized as follows:

- to emphasize the importance of accurate registration
- to gather knowledge about existing methods for registering ALS data with aerial images
- to make comparison between different registration methods
- to find out the current level of automation and processing time.

2.2 Participants

The project received input from nine participants (Table 1). Because some research groups applied more than one registration method, total of 13 variations were included in the final comparisons. Some participants conducted experiments using several variations of their methods. However, from each basic method only one example was included in the comparison.

Research institute or company	Abbreviation	Number of applied registration methods
Aalto University School of Sciences and Technology, Finland	Aalto	1
Dublin Institute of Technology, Ireland	DIT	1
Finnish Geodetic Institute, Aalto University School of Engineering, and TerraSolid Oy, Finland	FGI et al.	1
Independent Research Group on Geospatial, Iran	IRGG	1
National Geographic Institute, Spain	IGN-1, IGN-2	2
University of Calgary, Canada	UofC-1, UofC-2, UofC-3	3
University College London, UK	UCL	1
IFP University of Stuttgart, Germany	IFP-1, IFP-2	2
IPF Vienna University of Technology, Austria	IPF	1
	total	13

Table 1. Participants and the number of registration methods tested.

2.3 Description of test data

The test area was located in Espoonlahti (approximately 60° 8'N, 24° 38'E), close to Helsinki in Finland. The area can be characterized as a residential urban area consisting mainly of terrace houses and detached houses. Photogrammetric data included DMC panchromatic and RGB/IR image blocks of four images having forward overlap of 60% and side overlap of 20% (Figure 1).

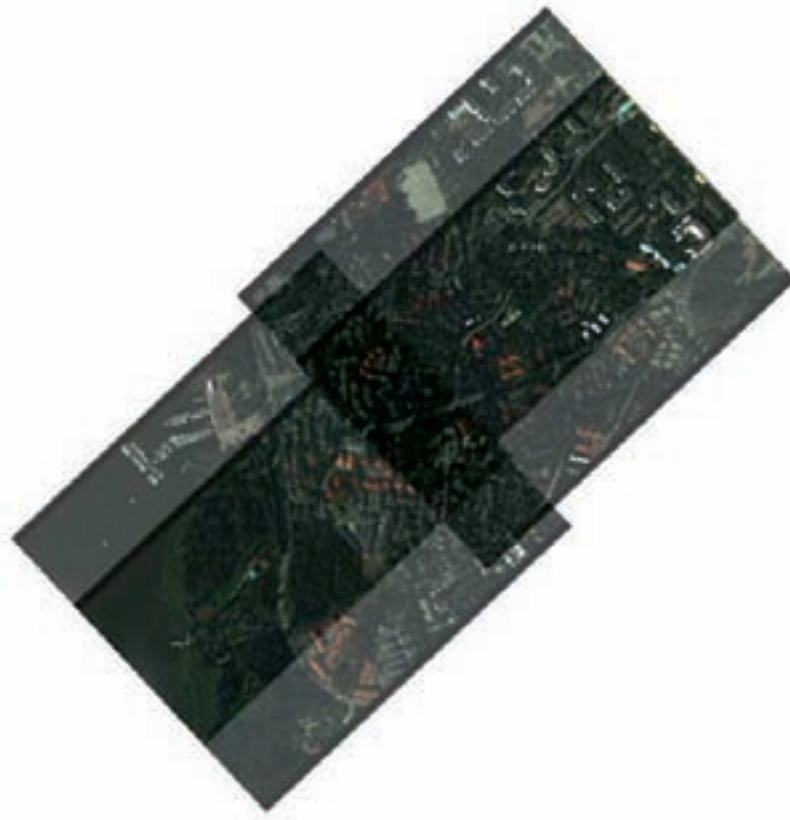


Figure 1. Overview of the DMC (RGB) image block.

The pixel depth of panchromatic images was 16 bits, the image size was 13824x7680 pixels and the ground resolution approximately five cm. In addition, the corresponding image block of DMC multispectral images was available (RGB and infrared channels, Figure 2). However, none of the participants used the infrared channel. The pixel depth of delivered RGB and infrared images was reduced to 8 bits, the image size was 3072x2048 pixels and the ground resolution approximately 22 cm. It should be noted that, usually, the original RGB images are not used, but they are pan-sharpened (Perco, 2005). However, in this test the original geometrical resolution of the RGB images was kept in order to make comparisons between different image resolutions. Otherwise, the imaging geometry of the RGB image block corresponds with the panchromatic image block, but the image scale of the RGB images is different because of the smaller sensor format and shorter focal length. Also, the optics of the camera types is different, leading to larger lens distortions for the RGB images. However, in the case of the RGB images, the effect of lens distortions was reduced with additional self-calibration in aerial triangulation. Panchromatic DMC images were post-processed using DMC Post Processing Software v. 4.4. The interior and exterior orientations of images were provided by the Finnish Geodetic Institute.

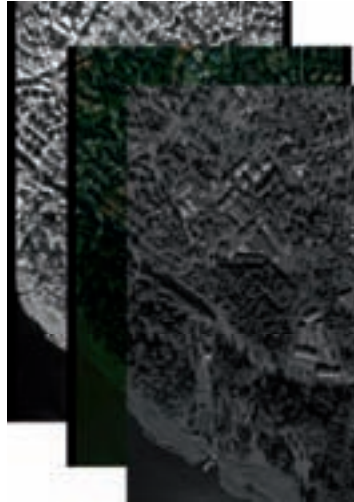


Figure 2. DMS panchromatic (top), RGB (middle) and infrared images (under most).

Aerial triangulations of both panchromatic and multispectral image blocks were calculated using Leica Photogrammetry Suite version 9.2 (Erdas LPS). In order to improve the accuracy of aerial triangulation a block of eight images was used (Figure 3). The four delivered images are located at the centre of this block. In aerial triangulation, for example, pit cover plates and corners of roofs were used as ground control targets. The Finnish Geodetic Institute measured the ground control points using real time kinematic (RTK) GPS. In the cases of panchromatic and RGB/infrared images, the estimated accuracies of exterior orientations are presented in Table 2 and Table 3. The residuals of ground control points and check points for both panchromatic and RGB image blocks are illustrated in Table 4. The panchromatic image block has six check points and the RGB image block seven check points. As expected, the RGB image block has higher mean standard deviations, which indicates the effect of lower image resolution.

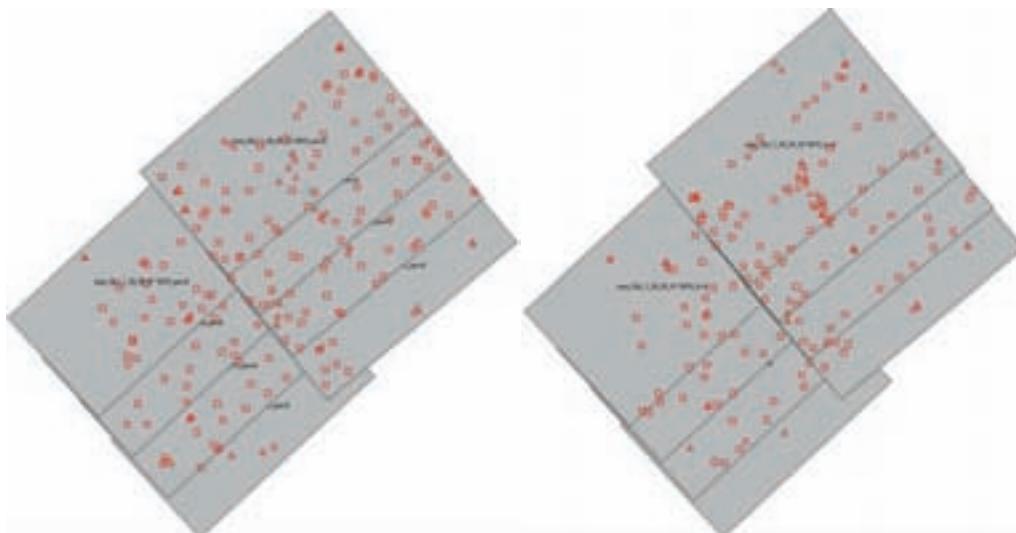


Figure 3. Distribution of tie points and ground control points within image blocks. Left image: panchromatic image block; Right image: RGB image block

Image	mX (m)	mY (m)	mZ (m)	mOmega (deg)	mPhi (deg)	mKappa (deg)
Espo_5b2_1_09_05_01~0013_pan	0.0438	0.0414	0.0180	0.0043	0.0047	0.0014
Espo_5b2_1_09_05_01~0014_pan	0.0436	0.0377	0.0191	0.0038	0.0046	0.0015
Espo_5b2_1_09_05_02~0013_pan	0.0288	0.0283	0.0117	0.0028	0.0028	0.0009
Espo_5b2_1_09_05_02~0014_pan	0.0259	0.0271	0.0107	0.0027	0.0025	0.0009

Table 2. Estimated accuracies (mean standard deviations) for the exterior orientation parameters of panchromatic images included in the EuroSDR test.

Image	mX (m)	mY (m)	mZ (m)	mOmega (deg)	mPhi (deg)	mKappa (deg)
Espo_5b2_1_09_05_01~0013_RGB	0.2189	0.2070	0.0937	0.0214	0.0236	0.0061
Espo_5b2_1_09_05_01~0014_RGB	0.2123	0.1958	0.1048	0.0194	0.0226	0.0071
Espo_5b2_1_09_05_02~0013_RGB	0.1370	0.1460	0.0927	0.0147	0.0138	0.0047
Espo_5b2_1_09_05_02~0014_RGB	0.0981	0.1275	0.0937	0.0131	0.0097	0.0039

Table 3. Estimated accuracies (mean standard deviations) for the exterior orientation parameters of RGB images included in the EuroSDR test.

	aX (m)	aY (m)	aZ (m)	mX (m)	mY (m)	mZ (m)
Ground control points, pan	0.0000	0.0000	0.0000	0.0217	0.0217	0.0108
Check points, pan	-0.0288	-0.0219	-0.0145	0.0451	0.0367	0.0650
Ground control points, RGB	0.0000	0.0000	0.0000	0.0426	0.0427	0.0664
Check points, RGB	0.0185	0.0028	0.0488	0.0982	0.0939	0.2494

Table 4. Residuals of ground control points and check points (averages and mean standard deviations)

As test data, two airborne laser scanning data were acquired using Optech ALTM 3100 (in 2005) and Leica ALS50-II (in 2007) scanners. Only one flying strip was included for the EuroSDR test from both laser scanning campaigns. These strips covered each other quite well and also a stereo model of the aerial images (Figure 4). The flying height for Optech ALTM 3100 ALS data was approximately 1000 m, resulting in a point density of 2-3 points/m². The scanning angle was 24 degrees, out of which 20 degrees were processed and used ($\pm 10^\circ$). The point repetition frequency (PRF) was 100 kHz, the scanning frequency 67 Hz, and the flying speed 75 m/s. Also, the strip adjustment was applied. Corresponding information for Leica ALS50-II scanning included a flying height of 500 m, a point density of 4-5 points/m², a scanning angle of 40 degrees ($\pm 20^\circ$), a PRF of 148 kHz, a scanning frequency of 42.5 Hz, and a flying speed of 72 m/s. No additional strip adjustment was applied. The Finnish Geodetic Institute provided and pre-processed the ALS data. In order to ensure that the ALS data sets were not at the same coordinate system as the images, ALS data were shifted and rotated. The rotations were minor and practically only the kappa rotation was included. The shifts and rotations were different for each ALS data set.

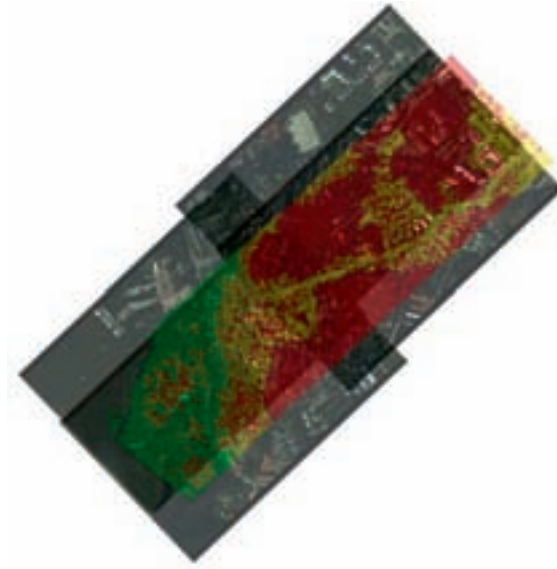


Figure 4. Overview of Leica ALS50-II data cover.

Because of the time gap of two years between data acquisitions, the data sets included some minor differences due temporal changes (Figure 5). In addition, the distribution of point clouds differs in each of the data sets.

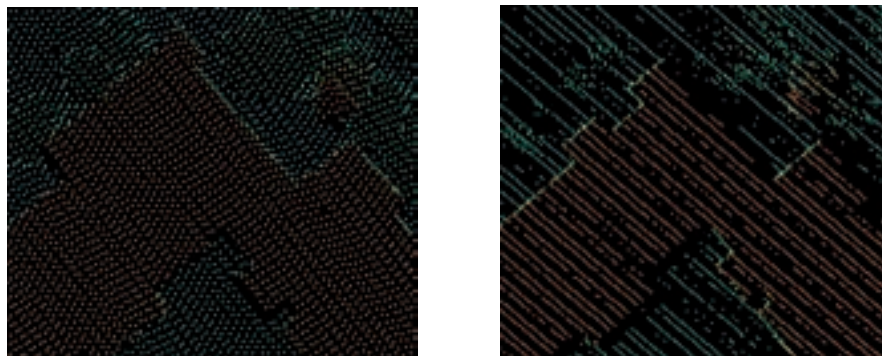


Figure 5. Samples of Optech's (left image) and Leica's (right image) data. Because the data was acquired from different years, some changes are detectable.

2.4 Reference data

In order to create reference data, six local reference areas were measured. The distribution of the reference areas is illustrated in Figure 6. These areas were selected on the basis that several planes or surfaces with different orientations should be visible. The common ground coordinate frame was brought to each test areas by measuring two to three ground control points using static GPS observations. The GPS receiver was a Leica SR530 dual-frequency instrument with Ashtech Choke Ring GPS-antennas. Each GPS observation session lasted more than 45 minutes at 15 seconds intervals.

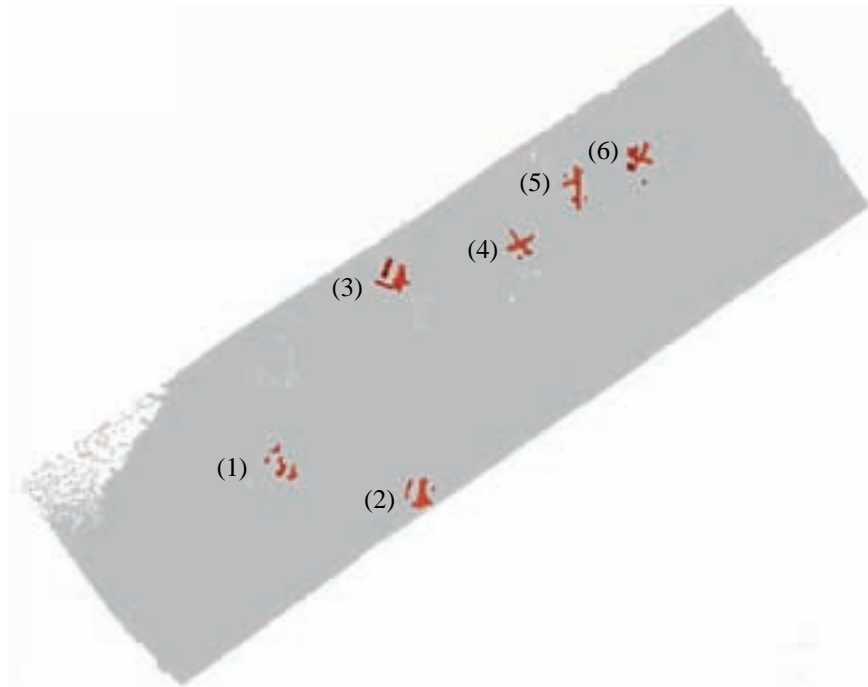


Figure 6. Distribution of six reference areas over Leica's ALS data.

Planes and free surfaces with different orientations were used as control features. In order to model such features, terrestrial laser scanning data was acquired with Leica HDS6000 terrestrial laser scanner. Terrestrial laser scanning point clouds were georeferenced using several spherical targets. The location of each spherical target was measured using a total station that was oriented with GPS-derived ground control points. As the result, very dense georeferenced point clouds were available (Figure 7).

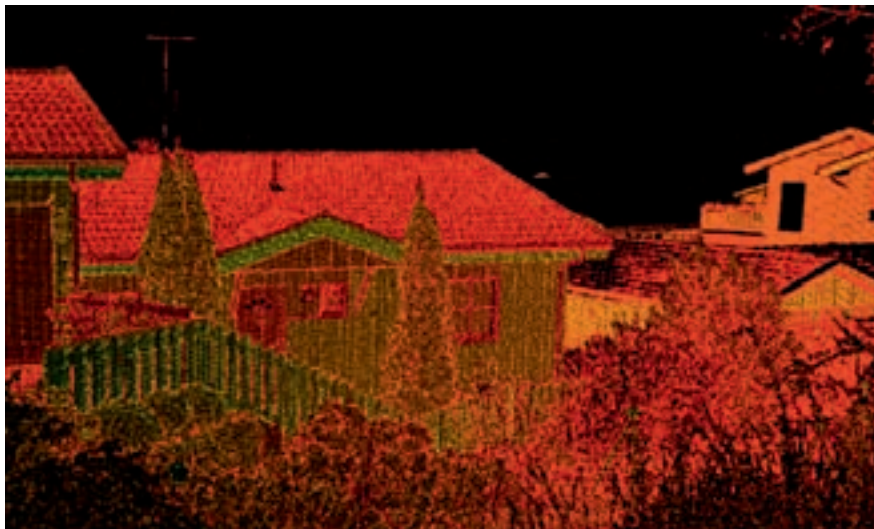


Figure 7. Sample of Leica's HDS6000 terrestrial laser scanning data.

Further processing of terrestrial laser scanning point clouds was continued using Geomagic software, in which the tools for the creation of TIN surfaces were applied. Correspondingly, a set of planes or surfaces with different orientations were achieved from each local reference area. In Figure 8, the set of test planes are illustrated from reference area 1.

The experiment by the Independent Research Group on Geospatial was applied only to two small sub-areas and not to the complete laser data sets. These sub-areas were not completely covered by any of the six reference areas. One of the test areas partially overlapped with reference area 4, but another test area included no terrestrial laser scanning reference data. In order to get some reference also for this approach, a seventh reference area was created using merged Leica's and Optech's data. The original ALS data sets were georeferenced separately using all six reference areas and the Iterative Closest Point (ICP) registration method. After both laser data sets were in the same coordinate frame, they were merged into a single point cloud. From this merged point cloud, planes and surfaces were extracted using Geomagic software. Also, the reference area 4 was expanded using a similar technique. However, this ALS-based reference data is not assumed to be as accurate as in the cases of the six TLS-derived reference areas.

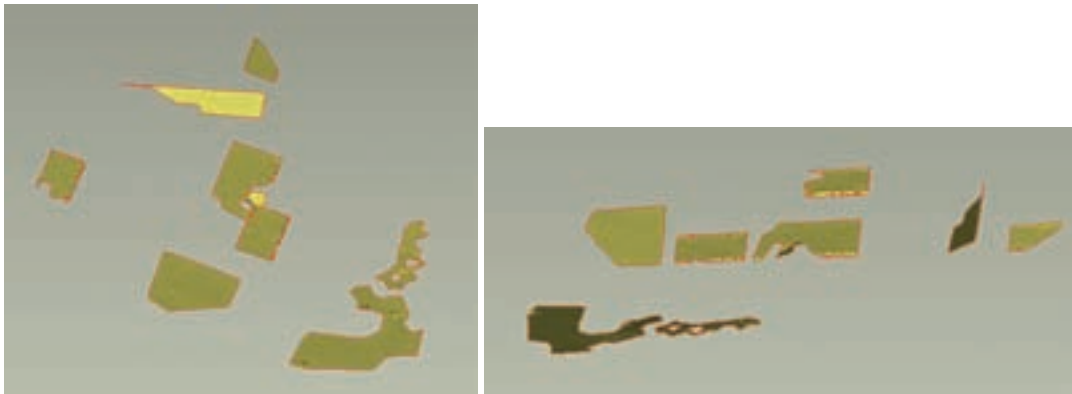


Figure 8. Set of georeferenced reference planes and surfaces from local test area 1. Screen shots were taken from two different perspectives.

2.5 Test procedure

All of the test data was delivered to the participants through an ftp-server. The images were in TIF format, and ALS data, including coordinate and intensity information, were delivered as ASCII text files. A separate document was produced in which all of the test data was described and the common objectives were given. The document also included information about the interior and exterior orientations of the images.

The participants were asked to apply their registration methods with the test data in such a way that the ALS data was transformed to fit into the same coordinate system as the images. As a result, the participants were asked to return the transformed ALS point clouds and technical reports that included descriptions of their methods.

The evaluation of the results was done by comparing the transformed ALS point clouds with the reference data. The reference data included georeferenced 3D models of roof planes and road surfaces acquired using a terrestrial laser scanner. At each reference area, shift differences between the

transformed ALS data and the reference planes and surfaces were solved using the ICP method. The origins of the point clouds were temporarily transformed within the local test area in order to minimize the effect of possible rotation errors. Rotation errors were estimated separately using all of the differences found in the shifts at reference areas 1 to 6. All of the rotations were expressed around a common point which was located in the middle of reference area 4.

3 Short descriptions of the applied methods

In this chapter, short descriptions of the methods included in this EuroSDR project are listed. More details can be found from the reports of the participants (Appendix B).

3.1 Method of the Aalto University School of Engineering (Aalto)

In the Aalto method, the registration is done in 3D space. An operator visually examines an unfiltered laser point cloud superimposed onto a stereo image pair. Therefore, both the image and the laser scanning point cloud are seen in 3D. The registration is solved interactively by changing the image orientation parameters simultaneously for both images. The methods and algorithms are depicted in detail in Rönholm et al. (2003) and Rönholm et al. (2009). The registration is performed separately in several small test areas that are distributed on different sides of an image block. Only local shifts are solved from each of the test areas. The final 3D rigid body transformation parameters, including shifts and rotation (no scale), of a complete laser point cloud are solved using the local result from each test area. The process was repeated twice in order to ensure a successful relative orientation between the ALS data and the aerial image block. The method is performed manually.

3.2 Method of the Dublin Institute of Technology (DIT)

This method creates greyscale images from both laser-derived and image-derived digital surface models (DSM). The image-derived DSM is calculated using automatic image correlation software. The approach searches corresponding features in 2D image spaces. Detecting and identifying corresponding points was performed manually, hence there is the apparent potential for an automated process. Unlike with other methods, only 2D rigid body transformation was applied. Therefore, this method was not included in comparisons in which registration accuracies were examined in the vertical direction.

3.3 Method of the Finnish Geodetic Institute, Aalto University School of Engineering and TerraSolid Oy (FGI et al.)

This method solves the relative orientation of ALS data and a single aerial image at a time using laser-derived 3D lines and corresponding image-derived 2D lines. These lines are selected in such a way that they represent the ridges of roofs. The ridges are found automatically from laser scanning point clouds. The process includes planes fitting into those laser scanning points that represent roofs and intersecting these planes in order to find potential ridge lines. Corresponding ridges are searched for automatically from images using image-processing tools. The relative orientation is solved in an adjustment that uses a coplanarity model. More details are given in Karjalainen et al. (2006). The final transformation of the

laser scanning point cloud uses a 3D rigid body transformation model. The process is almost completely automatic. However, an initial manual orientation is needed in order to find correspondences between laser-derived and image-derived tie features.

3.4 Method of the Independent Research Group on Geospatial (IRGG)

In this approach, the digital image is split into small sub-areas, according to the geometry of the objects and the terrain, using image analysis. Each of these small areas is matched with a corresponding area in a 3D laser point cloud. Correspondences are searched for by extracting boundaries or the patterns of objects from both data sets. The approach is able to solve a local 3D rigid body transformation separately for each pixel of the image expressed in a 3D camera coordinate system – if only correct correspondence is found.

The method requires an initial relative orientation between ALS data and images. In this case, the initial orientation was solved manually by identifying ground control points, which were measured with RTK-GPS. Note that the aerial images and these ground control points were in the same coordinate frame. Registrations were done separately within two relatively small local test areas. The transformation model was a 3D rigid body transformation with translations, rotation and scale. In conclusion, this part of the method describes an approach in which laser data is georeferenced using only ground control information.

Because the main part of the method was applied in such a way that image information was transformed onto the laser point cloud, and not vice versa, only the initial orientation of the ALS data is meaningful in the comparison part presented later in this document. However, visual illustrations in Appendix B shows that colour information from images can be attached with laser point clouds with good accuracy using this method.

3.5 Method 1 of the National Geographic Institute, Spain (IGN-1)

Several homologous 3D tie points are identified from stereo images and ALS data. A DSM is created from a laser scanning point cloud. Shading, colour coding and including the intensity values of the DSM assist in finding manually correct tie points from the laser scanning data. The parameters for translations and rotations of a 3D rigid body transformation are solved in such a way that, during the adjustment, all of the points having residuals of over one metre are rejected. Also, another experiment, which included a scale in the transformation model, was applied. However, because including a scale did not show any significant improvement in residuals, the simplest transformation was chosen. The method was fully manual.

3.6 Method 2 of the National Geographic Institute, Spain (IGN-2)

In order to enable the use of image processing and matching tools, this method creates synthetic 2D images from the 3D ALS data. Therefore, a 3D rigid body transformation between ALS data and aerial images is solved using 2D tie features extracted from image spaces. Solving the parameters of transformations includes separate treatment of the plane and elevation errors.

A synthetic laser-derived image is created from the ALS data. The optimal pixel size of the resulting image depends on the point density of the laser point cloud. In order to maximize similarity, the aerial images are re-sampled in order for them to meet the resolution of the laser-derived images. In addition, it is recommended to have as similar a perspective as possible for both image types. Applying Daubechies D4 wavelets (Jensen and la Cour-Harbo, 2001, pp. 157–160) to both image types leads to very a similar appearance for the final images. Furthermore, the images are binarized before searching for the interest points. Because an automatic search of the interest points leads to many outliers, an optimal set of corresponding tie points are searched using statistical methods.

The method is nearly automatic. Some monitoring and manual assisting are, however, needed during the process of finding the interest points and their correlation with the corresponding points extracted from the other data set.

3.7 Planar patches method of the University of Calgary (UofC-1)

This method uses 3D tie features from laser scanning data and 2D features from multi-image measurements in order to solve the relative orientation of the data sets. The photogrammetric measurements are manual. Planar patches are modelled by identifying a minimum of three points from all overlapping images. Corresponding planar patches are extracted semi-automatically from the ALS data. An operator manually defines a local search area and then a segmentation algorithm (Kim et al., 2007) finds planar patches within this limited area. The centroids of the patches are extracted from both data sets. The resulting centroids from the ALS data and imagery are not necessarily conjugate, but they should lie on the same plane. Therefore, the weight matrix of the adjustment is modified in a way that allows the centroids to move only along the plane direction. As a result, the 3D rigid body transformation is solved and applied to the ALS data.

3.8 Straight lines method of the University of Calgary (UofC-2)

This method uses the same principles than the previous method of planar patches. Again, laser-derived features are in 3D and image-derived corresponding features are in 2D. In this case, ridges of the roofs are desired tie features. 3D lines are extracted from ALS data by intersecting neighbouring planes. From 2D image planes ridges are defined by measuring manually two end points and a sequence of intermediate points. These points do not have to be conjugate in different images. Again, the weight matrix is limiting the allowed movement of selected points (end points) during the adjustment.

3.9 Combined method of the University of Calgary (UofC-3)

In this method, both planar patches and straight lines are extracted with the methods described in the two previous chapters. Therefore, this method also uses 3D laser-derived and 2D image-derived tie features. Both types of tie features are included in one adjustment which uses weight matrixes for restricting the directions of the corrections.

3.10 Method of the University College London (UCL)

End points from the ridges of the roofs are extracted from 3D laser data and 2D image spaces. In order to find the end points of the ridges, roof planes are identified semi-automatically from classified laser point clouds. Ridges and their end points are found by intersecting the adjacent planes of roofs. The corresponding end points of the ridges are extracted manually from the images. These tie points are included in an adjustment that solves a 3D rigid body transformation using translations, rotations and scale.

Also, two other experiments were presented which were not included in the comparison. One used the corners of the roofs and another both corners of the roofs and the end points of the ridges. However, because the corners of the roofs are difficult to accurately locate from the ALS data, the performance was worse than with the method using the end points of the roofs. Therefore, only the case with the end points was included in this project.

3.11 ICP-based method of the University of Stuttgart (IFP-1)

The method finds a relative orientation between ALS and the imagery using DSMs as 3D tie geometry. Image-derived DSMs with a high point density are created automatically using stereo image correlation tools. The resulting image-derived point clouds are filtered in order to remove noisy-type areas, such as vegetation. The distance between the two DSMs is minimized using an automatic ICP method. The 3D rigid body transformation included translations and rotations, but no scale. In this case, however, the initial orientation of the data sets was spread too far apart leading to the need for additional initial orientation, which required the manual identification of three corresponding points. If an initial orientation is close enough, this method has the potential to be fully automatic.

3.12 Point-Based method of the University of Stuttgart (IFP-2)

A synthetic ortho image representation of the ALS data and its intensity information is created by interpolating laser data in a regular grid in the XY plane. The corresponding tie points are identified manually from laser-derived and physical images. Even if the selection of the ALS tie points is done in 2D representation, the connection with 3D information remains. Therefore, the actual transformation between a single image and the ALS data is done using laser-derived 3D points and 2D image points. The 3D rigid transformation includes rotations and translations. Even if the selection of tie points was, in this case, manual, the method has the potential to be automatic.

3.13 Method of the Vienna University of Technology (IPF)

The method is based on image- and laser-derived DSMs as 3D tie features. The principles of the method can also be found in the study by Ressel et al. (2008, 2009). The image-derived DSMs result from automatic stereo image matching. In order to enable the least squares matching between the DSMs, a grid is interpolated from the ALS points using local adjusting planes. Only smooth surfaces, however, are included in the least squares matching in order to ensure correct matching. Therefore, rough areas are filtered using so-called sigma-grids and eccentricity-grids. The sigma-grid stores the standard deviation of the nearest laser points from the adjusted plane at each grid point. The

eccentricity-grid contains the 2D distance between each grid point and the centre of gravity of the ALS points used for the determination of the local plane.

The experiments included three different transformation models; 3D affine transformation, 3D rigid body transformation and a simple 3D shift. From these, the case of 3D affine transformation was selected to be included in the comparisons of the EuroSDR project. This method is practically fully automatic.

4 Results and discussion

In this chapter, the results of the comparisons are presented and discussion is given. At first, the results of the total shift errors are divided into planimetric and vertical parts. Then, the errors in the rotations are illustrated. In addition, the results are reorganized in order to highlight the effect of the type of selected tie features, the analytical characteristics of the applied registration methods and the level of automation. The original numeric results of the comparisons with the reference areas can be found in Appendix A.

4.1 *Comparison of planimetric accuracies*

Figure 9 presents the planimetric accuracies of the registration methods when Optech's ALS data was oriented using panchromatic aerial images. However, the method of the Independent Research Group differs from others in this comparison because it represents a case in which laser scanning data is separately oriented to the ground coordinate system using GPS-derived ground control points. Even if some variations in accuracies between methods can be detected, most of the methods achieved an average accuracy of fewer than 20 cm when compared with the ground reference. At best, the average accuracy of planimetric registration was just a couple of centimetres in both the X and Y directions.

In the case of the relative orientation of Leica's ALS data and panchromatic aerial images, again the averages for the planimetric errors were fewer than 20 cm with most of the methods (Figure 10). However, the standard deviations were significantly larger than in the case of the Optech data. Because no strip adjustment was applied, Leica's data included some internal geometrical problems. Therefore, a 3D rigid body transformation leads to higher variations of local accuracies at the reference areas. The experiment by the IPF Vienna University of Technology differs from the others because it used an affine transformation model. The effect of different transformation models is visible from the results through smaller standard deviations because the affine transformation has been able to reduce some of the strip-wise geometrical problems. The reports by the IPF Vienna University of Technology and IFP Stuttgart University in Appendix B also include graphical illustrations that reveal some internal geometrical problems with Leica's data when the ALS-derived DSM is compared against the image-derived DSM.

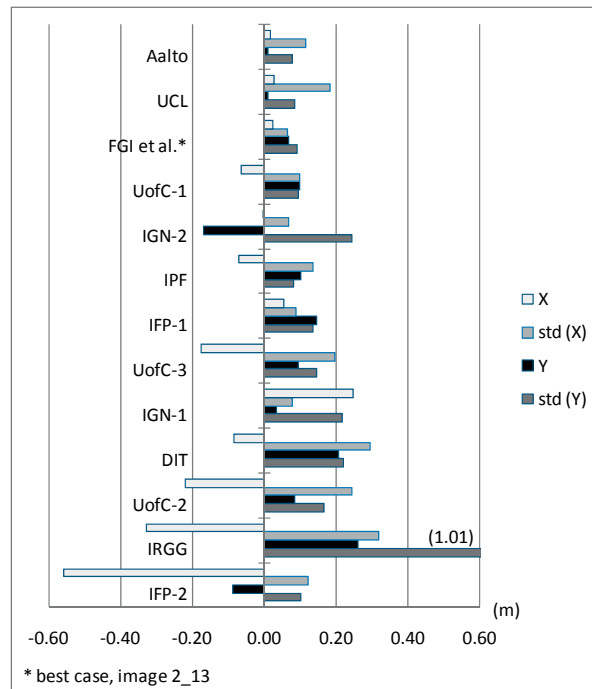


Figure 9. Averages and standard deviations of the planimetric errors (XY) of the registration methods (Optech's ALS data and panchromatic aerial images).

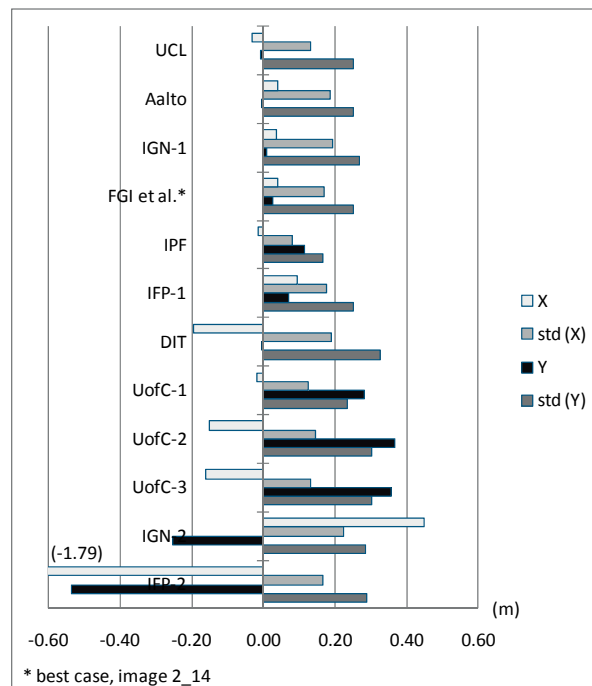


Figure 10. Averages and standard deviations of the planimetric errors (XY) of the registration methods when Leica's ALS data was oriented using panchromatic aerial images.

Comparison of planimetric accuracies in the case of ALS data registered with RGB aerial images (Figure 11 and Figure 12) brought about the expected results. Both the average accuracies and standard deviations were typically larger than in the case of panchromatic images. The lower resolution of images had negatively affected the accuracies. However, it must be noted that these results might also have been affected by the lower accuracy of the aerial triangulation of images, which also occurred due to the lower image resolution. According to Table 3, the estimated accuracy for the camera origins was approximately 0.10-0.20 m, depending on the image. Unfortunately, not all participants applied their methods using RGB images. Therefore, a comprehensive evaluation is not available.

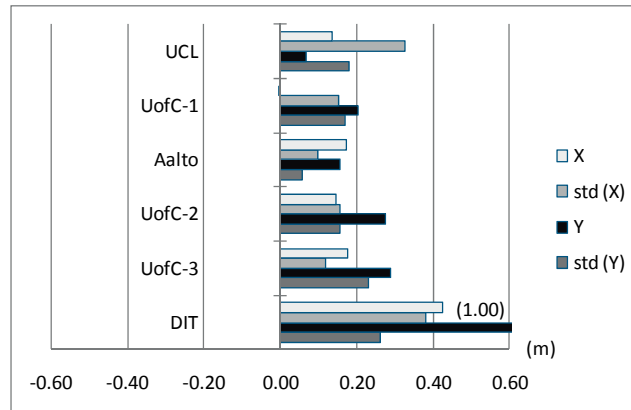


Figure 11. Averages and standard deviations of the planimetric errors (XY) of the registration methods when Optech's ALS data was oriented using RGB aerial images.

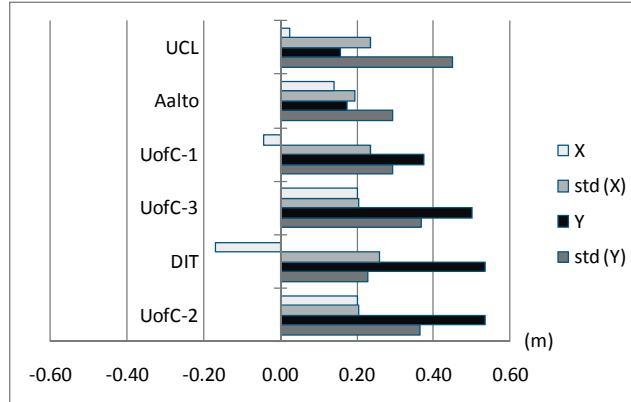


Figure 12. Averages and standard deviations of the planimetric errors (XY) of the registration methods when Leica's ALS data was oriented using RGB aerial images.

4.2 Comparison of vertical accuracies

The majority of the methods have succeeded in achieving better accuracy in the vertical direction than in the planimetric directions when the ALS data is oriented using panchromatic aerial images. The case of Optech's data (Figure 13) reveals that some of the registrations methods have managed to achieve an average accuracy within a couple of centimetres. In those cases, the results indicate both the

successful relative orientation between the ALS data and aerial images and the accurate aerial triangulation of the image blocks. The case of Leica's ALS data oriented using panchromatic images also shows relatively good results (Figure 14), even if in many cases a small increase in the standard deviations is detectable because of unadjusted data. In this case, it seems that the internal errors of an ALS strip have less of an effect in the vertical direction than in the planimetric directions.

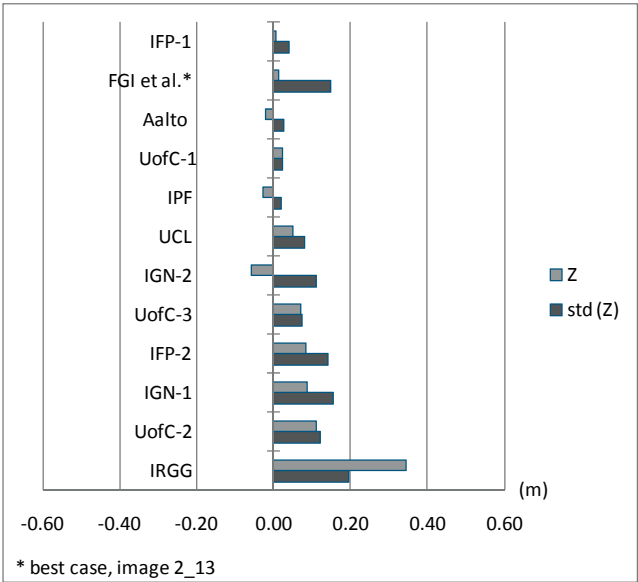


Figure 13. Averages and standard deviations of the errors in heights (Z) when Optech's ALS data was oriented using panchromatic aerial images.

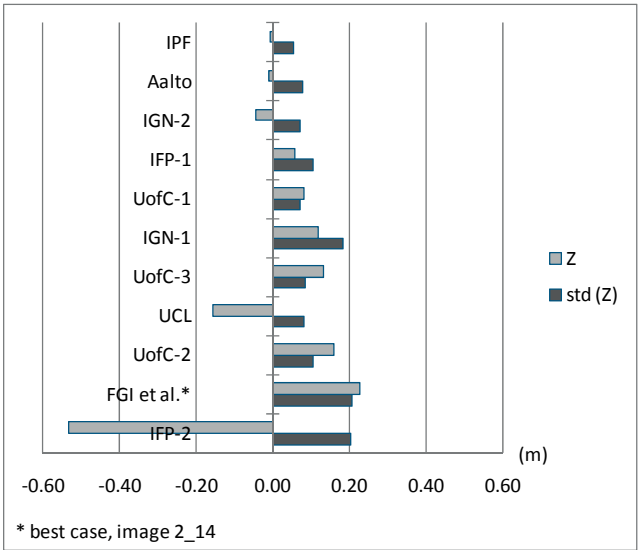


Figure 14. Averages and standard deviations of the errors in heights (Z) when Leica's ALS data was oriented using panchromatic aerial images.

The lower resolution of RGB aerial images is clearly detectable from the results when the ALS data were registered using RGB images (Figure 15 and Figure 16). Again, the number of experiments was too few and the effect of less accurate aerial triangulation prevent us from making strong statements. However, it seems that the image resolution has a significant effect on the vertical accuracy. This was an expected result, because image measurements are less accurate if the image resolution is lower.

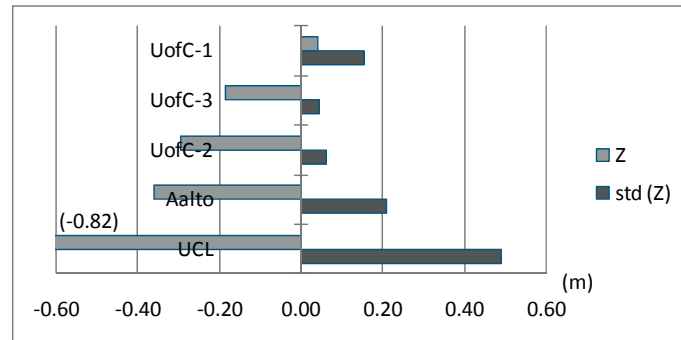


Figure 15. Averages and standard deviation of the errors in heights (Z) when Optech's ALS data was oriented using RGB aerial images.

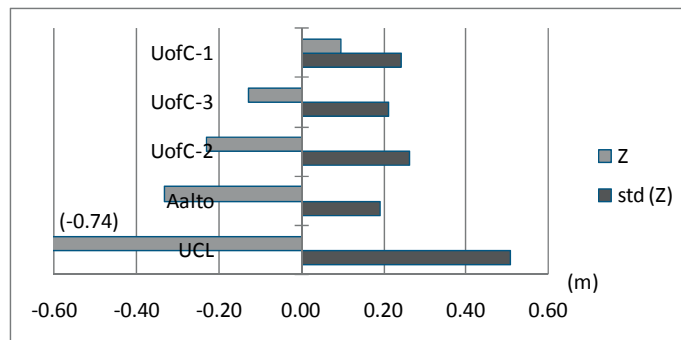


Figure 16. Averages and standard deviation of errors in heights (Z) when Leica's ALS data was oriented with RGB aerial images.

As was shown in this section, the resolution, imaging geometry and quality of the panchromatic aerial images provide such accurate tie features that many registration methods have been able to find registration using ALS data within a vertical accuracy of a couple of centimetres. In the planimetric directions, however, several of the methods encountered more difficulties, most likely because of the relatively low point density. In this project, only laser scanning point densities of 2-3 and 4-5 points/m² were examined. Increasing the point density would most likely have had a positive effect on the planimetric accuracies of many of the registration methods. However, the point density is not as significant for the methods that used surfaces as tie features as it is with other types of methods.

4.3 *Comparison of accuracies in rotations*

Almost all of the participants applied a 3D transformation model when the ALS data was transformed within the same coordinate frame as the aerial images. As an exception, the method of the Dublin Institute of Technology (DIT) used only one rotation (κ), because they applied a 2D rigid body transformation model. It should be noted that a 2D transformation is not able to solve truly 3D problems. However, in this case, both of the ALS data sets were initially quite well levelled and, therefore, the ω and ϕ rotation errors were relatively small. Essentially, the ω and ϕ rotation errors of the DIT method describe the amount of initial rotation errors (Figure 17 and Figure 18). In the cases when Optech's data was registered using panchromatic images, almost all of the methods have succeeded in finding an orientation which has relative small rotation errors (Figure 17).

The case of Leica's data illustrates that the rotations have larger errors than with Optech's data (Figure 18). However, it should be noted that some of the errors in the results are not necessarily caused by the applied registration methods. As mentioned before, the strip adjustment was not applied to Leica's ALS data. Therefore, this data included some local problems in strip-wise internal geometry. In this case, when comparing the results with the ground reference, these errors reduced the accuracy in the planimetric directions in particular. On the other hand, according to an evaluation of the rotation errors, no clear trends are detectable. Only in the case of ϕ rotations, have almost all registration methods suggested small ϕ rotation errors pointing to the common direction, which may suggest a minor trend. If there had been more than six reference areas, geometrically inhomogeneous parts of the ALS data would have been revealed more clearly.

The accuracy of the evaluation could have been improved by adding more reference areas. However, measuring such reference areas is time consuming. In addition, the number of optimal reference areas within the test area was limited. Essentially, adding more reference areas would have required that the terrestrial laser scanner should have been lifted much higher than a tripod allowed. Alternatively, some vegetation should have been removed.

In the cases of relative orientation of the RGB images with Optech's (Figure 19) and Leica's ALS data (Figure 20), the results of the rotation accuracies are more controversial. Even if the differences in accuracies between these two cases generally behave as expected, some results with RGB images are better than in the cases with panchromatic images. Because of too small a number of experiments, the reason for this cannot be reliably concluded. However, one explanation can be that the lower resolution of the images increases the effect of coincidence in such a way that, in some cases, measurement errors have compensated for other errors caused by, for example, the problems in the strip-wise internal geometry.

Optech's ALS data was noisier than Leica's data. However, if the results are compared with Leica's data, it can be concluded that, from the perspective of orientations, the strip-wise internal geometry has a greater influence than noise.

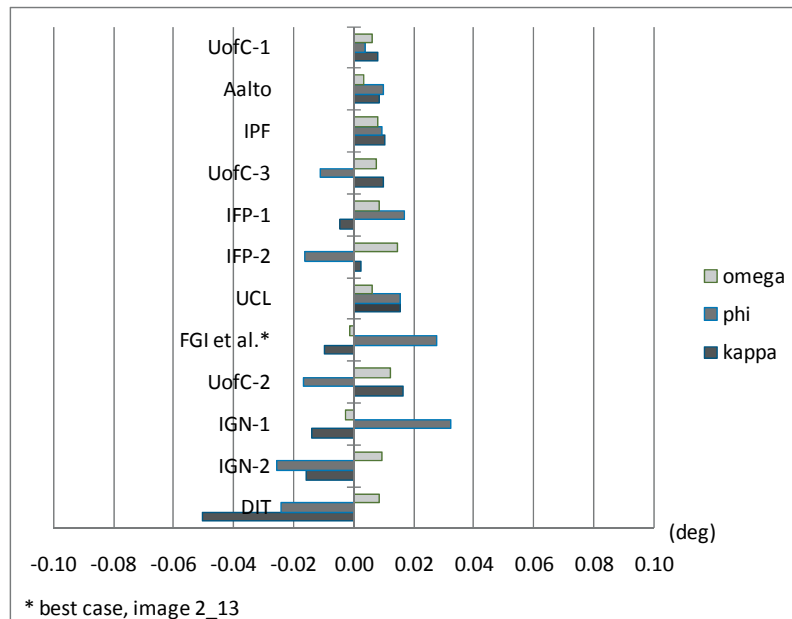


Figure 17. Strip-wise rotation errors (Optech's ALS registered using panchromatic images).

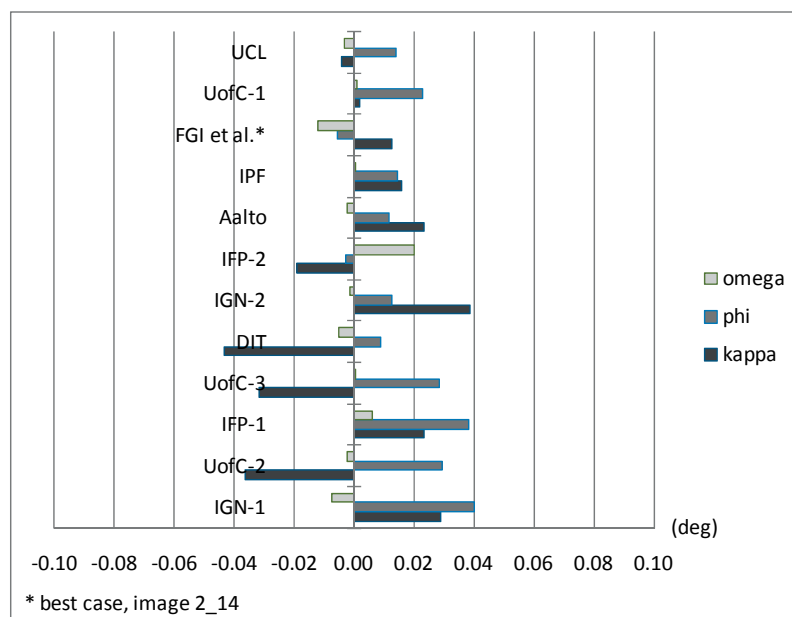


Figure 18. Strip-wise rotation errors (Leica's ALS data registered using panchromatic images).

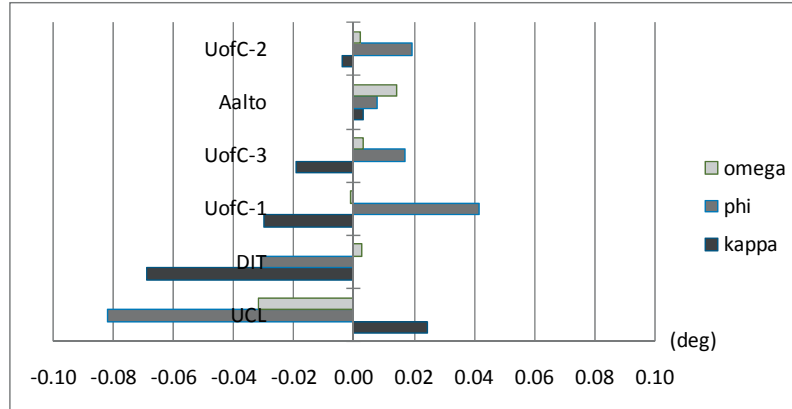


Figure 19. Strip-wise rotation errors (Optech's ALS data registered using RGB images).

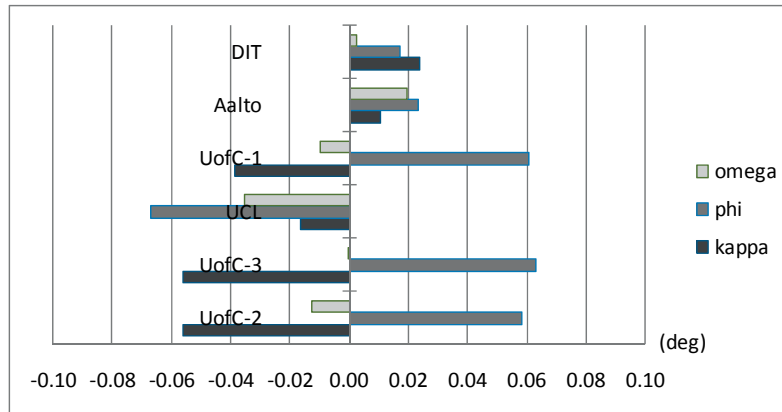


Figure 20. Strip-wise rotation errors (Leica's ALS data registered using RGB images).

4.4 Influence of the type of tie features

All of the results from the relative orientation of the ALS data with the panchromatic images were reorganized by the type of tie features (Figure 21). The cases with the RGB images were rejected because too few experiments were included and the lower image resolution caused more random errors. In this project, several types of tie features, such as points, linear features, surfaces, unfiltered laser point clouds, and the combined use of surfaces and linear features were included. In the IRGG method, Leica's and Optech's data were merged together. Therefore, the registration accuracy was the same for both ALS data sets.

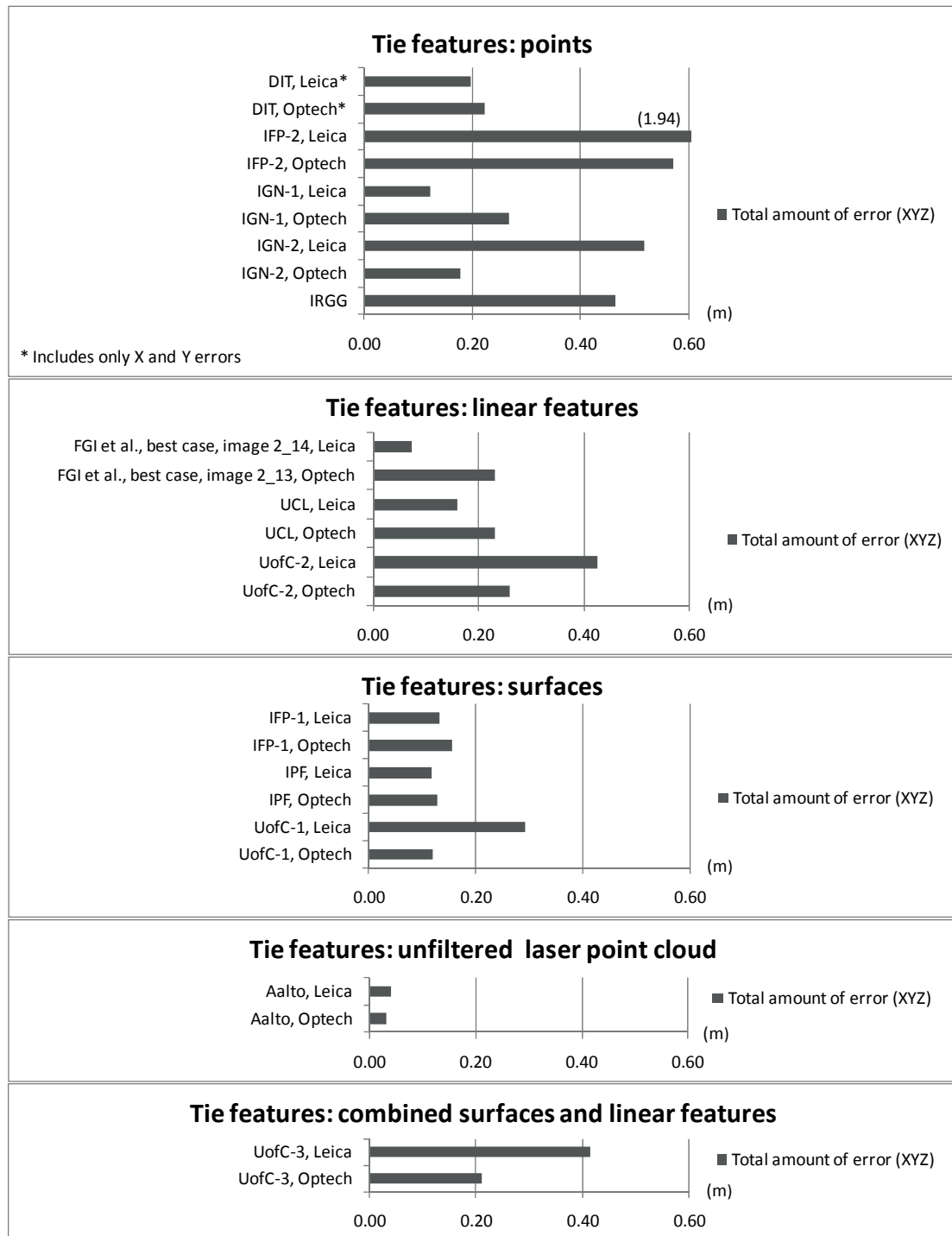


Figure 21. Accuracies of the registration methods organized by the types of tie features. Only the cases with panchromatic images were included.

In this case, a total error was defined as

$$total\ error = \sqrt{dX_A^2 + dY_A^2 + dZ_A^2} \quad (1)$$

In this equation, dX_A , dY_A and dZ_A are the average errors in shifts calculated from the local accuracy evaluations at each of the six reference areas. Note that the examples by the Dublin Institute of Technology (DIT) included only dX_A and dY_A , because the vertical direction was not included in the adjustment. Therefore, the results regarding the DIT experiment in Figure 21 are not exactly comparable with the other results.

The results indicate that, besides the implementation itself, the selection of the type of tie features is one of the main factors affecting the accuracy of registrations. The methods using tie points have greatest variations in accuracies. It was expected that point-like tie features might not be as good as other types of tie features, but surprisingly some methods managed to achieve reasonable accuracy even using tie points.

Linear features also performed quite well. However, in the case of the experiment by FGI et al. (Appendix B), it should be noted that significant variations in accuracies can occur depending on the selected set of tie lines and their geometrical distribution on images. Also, one deficiency might be that the intersections of the roof planes do not always represent exactly the real heights of the ridges. For example, a ridge can be round and not sharp. In such a case, the photogrammetrically-derived ridges would be at a different height level than the ALS-derived ridges.

According to these comparisons, the surface-based methods and interactive orientation using unfiltered ALS point clouds as tie features resulted in relatively good orientations in each case. The strength of the interactive orientation method with unfiltered point clouds and a stereoscopic examination is its capability to use all of the small details of the ALS point clouds during the orientation, which usually allows for a good interpretation of planimetric shifts as well as heights. In the two methods using DSMs as tie features (IFP-1 and IPF), the complete test area was included in the registration process. Therefore, these methods use a lot of information during the registration and thus seem to be very robust. Surfaces with different orientations enable a reliable orientation in all directions. In addition, such methods are also able to detect strip-wise internal geometric problems of the ALS data. However, these methods rely upon the accuracy of automatic image matching that creates image-derived DSMs. In addition, the filtering of vegetation from laser point clouds is highly important, because only corresponding surfaces should be included in these kinds of approaches. In this test, including both surfaces and linear features (UofC-3) in the registration did not prove to be a significant advance over using only surfaces (UofC-1).

4.5 *Influence of the analytical characteristics of the applied methods*

In this chapter, the results were reorganized according to the analytical characteristics of the applied methods (Figure 22). The first category includes methods that extracted truly 3D tie features and also applied 3D transformation to the ALS data. Also, the second category applied a 3D transformation to the ALS data, but the ALS point clouds were registered using either a single image or multiple images. In other words, the transformation was solved between 3D ALS data and 2D image observations or, alternatively, tie features were extracted from both data sources in 2D. The latter method required the creation of synthetic images from the ALS data. In the third category, only 2D transformation was applied. In this case, also tie features from all of the data sources were extracted in 2D image spaces. The last category includes the case in which only the ground control points were used.

In principle, the Aalto, IFP-1 and IPF methods minimize the distance between ALS-derived 3D surfaces and image-derived 3D surfaces, even if surfaces are not physically created when using the Aalto method. The performance of these methods resulted in corresponding accuracies with both Leica's and Optech's data, indicating a high reliability.

All of the methods which registered ALS data with a single image or multiple images using 2D tie features (3D-2D or 2D-2D) resulted in visible differences in accuracies between Leica's and Optech's data. In general, the results of this project suggest that the reliability and accuracy of this category are no better than in the case of using completely 3D tie features. However, the accuracy of the best cases matched well with the completely 3D methods. Therefore, more evidence should be collected before a strong statement could be made about the ranking order of these categories. Within the second category, the UCL method had less variation in registration accuracies between Leica's and Optech's data than the other methods. The FGI et al. method was very similar in principle as the UCL method, but it had less human interaction. The current implementation of the FGI et al. method seems to be less reliable than the UCL method.

Generally, some of the differences in accuracies between the cases of Leica's and Optech's data can be explained with different point distribution as well as with the selected type of tie features, as was discussed in the previous chapters. The UofC-1, UofC-2 and UofC-3 methods reveal that, for example, in their cases using planar patches leads to better results than using linear features or a combination of planar patches and linear features. In the case of Optech's data, the UofC-1 method using planar patches is as accurate as the IFP-1 and IPF methods, which applied DSMs as tie features.

The amount of tie features is also important, especially if not all of the measurements are accurate. For example, the IGN-1 method had 35 to 37 manually measured tie points and, therefore, performed quite well, even if using point-like tie features. The IFP-2 method interpolated the ALS data into regular grids of 1 m and 0.5 meter and extracted only seven tie points, which have caused significantly less accurate results compared with any other method. In this method, the difference in accuracies between Leica's and Optech's data was also large. The IGN-2 method also had large variation in accuracies. One explanation is that the method relies on only five tie points. Therefore, the method currently seems to be sensitive to detecting inaccurate tie points.

Even if the DIT method included only 2D transformation and, thus, has limitations, it was able to achieve similar accuracies for both ALS data sets. If combined with some other method able to remove the remaining rotation errors and vertical misalignments, this method could improve planimetric registration. The IRGG method suffers from the same difficulties as, for example, the IPF-2 method: it is not an easy task to identify the exact points from the ALS data. Again, the extraction of inaccurate corresponding points leads to reduced registration accuracy. However, the IRGG method used ground control points as an initial orientation for a more accurate orientation later. Unfortunately, the more accurate orientation was done by transforming image data into laser point clouds and, therefore, the accuracy of the final transformation could not be evaluated using the reference areas prepared for this EuroSDR test.

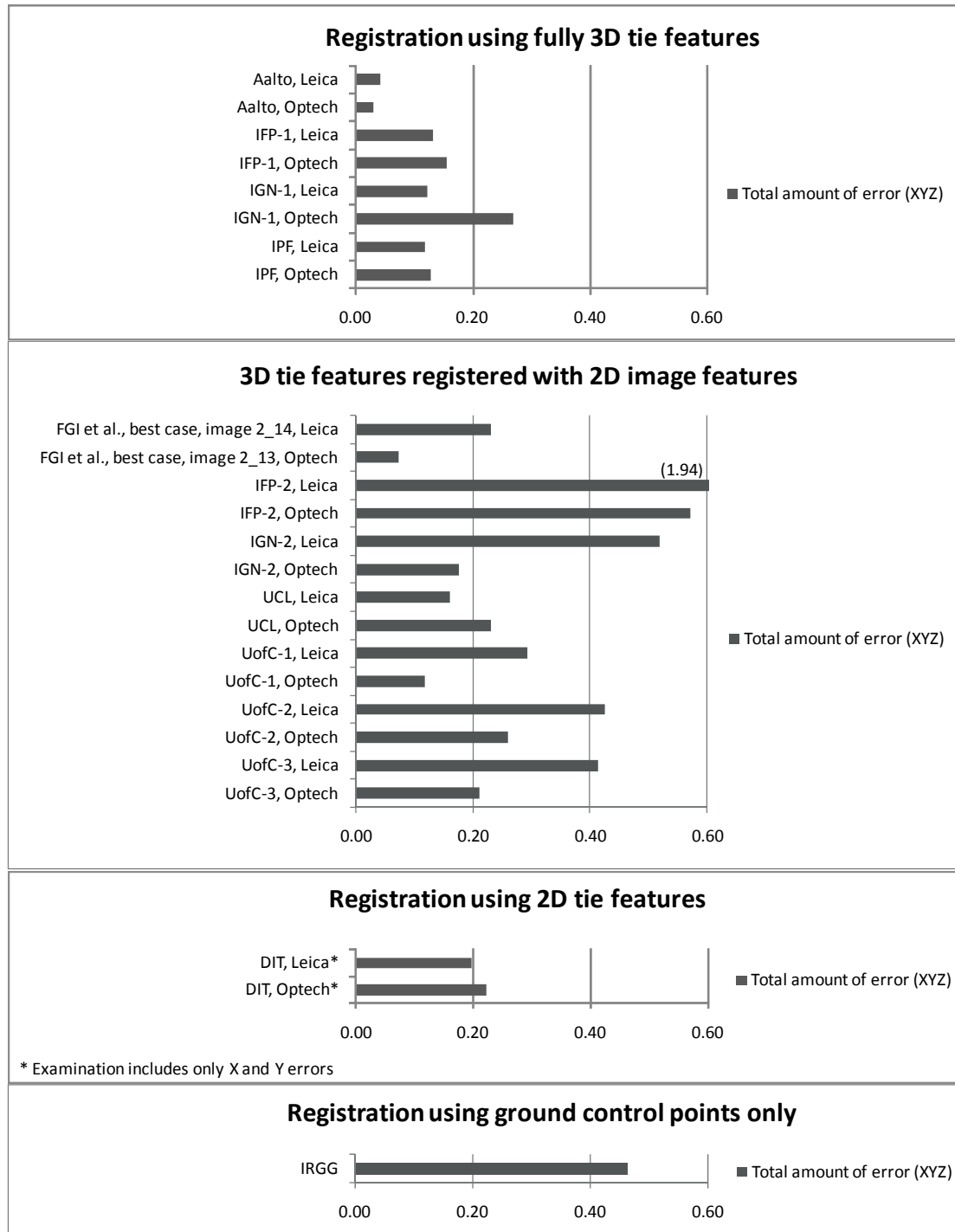


Figure 22. Accuracies of the registration methods organized by the analytical characteristics of the applied methods.

4.6 Influence of the level of automation

Automation is a key issue when huge amounts of data are processed. In addition, automation usually reduces costs and, therefore, it is desired. Thus, the results of this project were reorganized in such a way that the methods were in an ascending order according to the level of automation. The methods were divided into three groups: manual, semi-automatic and (almost) automatic methods. Between the three main categories, there is an empty space in order to enhance readability. Because the most automatic methods were not applied using RGB images, only the cases of panchromatic images were included in this comparison.

Figure 23 and Figure 24 illustrate the total number of shift errors (equation 1) of dX , dY and dZ in the cases of Optech's and Leica's ALS data oriented using panchromatic images. The evaluation suggests that the level of automation is currently not a critical obstacle for finding shifts between the ALS data and aerial images. However, successful registrations were also achieved using manual or semiautomatic methods.

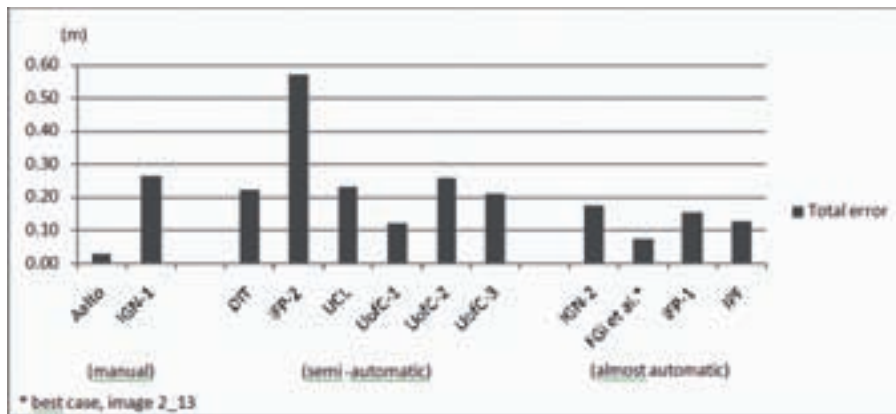


Figure 23. Total shift errors against the level of automation (Optech/pan). The level of automation increases to the right.

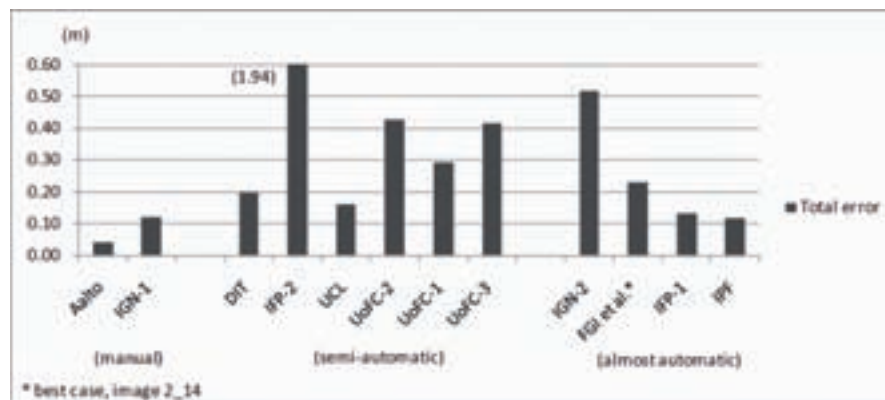


Figure 24. Total shift errors against the level of automation (Leica/pan). The level of automation increases to the right.

As shown in Figure 25 and Figure 26, an evaluation of the rotation errors against the level of automation illustrates that reasonable accuracy can be achieved using any level of automation. Therefore, according to this test, factors other than the levels of automation are the most significant. In the previous chapters, it was discussed how the successful implementation of the method and the type of tie features seem to be the most significant factors explaining the level of accuracy. The results are encouraging, suggesting that automatic methods are also available and feasible for solving registration between ALS data and aerial images.

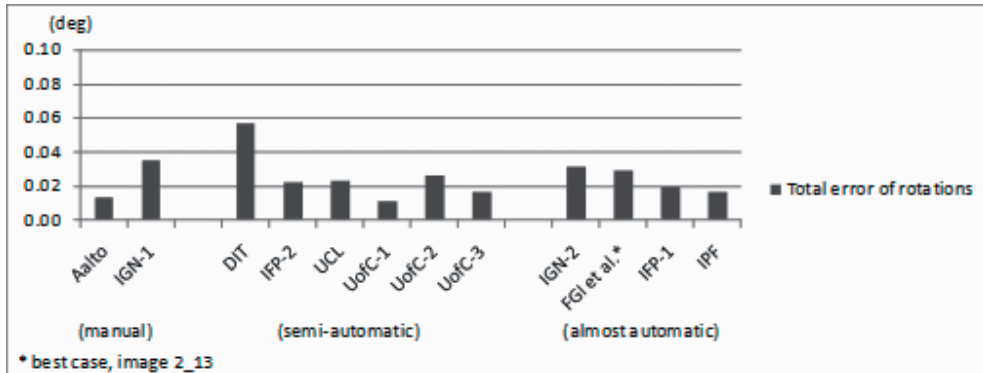


Figure 25. Total rotation errors against the level of automation (Optech/pan). The level of automation increases to the right.

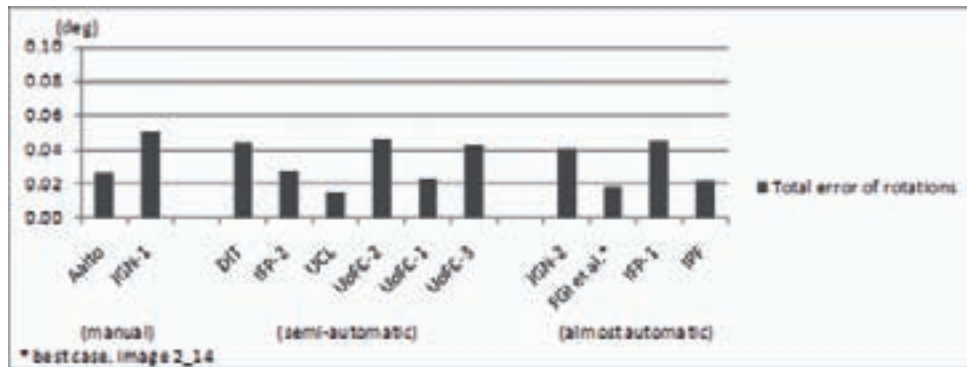


Figure 26. Total rotation errors against the level of automation (Leica/pan). The level of automation increases to the right.

4.7 Processing time

Even if all of the participants did not provide information about the processing times, it seems that the automatic methods took the least amount of time to complete. The amount of manual work slows down the orientation process. The quicker automatic methods took about 20 minutes to calculate. However, setting the project parameters and preparing the data increased the total processing time. The majority of the methods took 1-3 hours to complete, whereas the most time-consuming process took seven hours to complete. Many methods were still in the development stage and thus it is expected that the processing time can be reduced in the future.

5 Summary and conclusions

This EuroSDR test has focused on comparing the methods for solving relative orientations between ALS data and aerial images and their performance. A relative orientation of data sets enables the transformation of data sets within the common coordinate frame. It is expected that in the future the integrated use of laser scanning data and imagery will be a standard procedure for, for example, automatic object recognition, the accurate classification of individual trees, point cloud densification, the automatic classification of land use, system calibration, and the generation of photorealistic 3D models.

The test included thirteen types of orientation methods developed by the participants and applied using a common data set. Fortunately, the applied registration methods covered all major types of tie features and many strategies for how to find them. Major strategy types included the extraction of corresponding 3D features from both data sources, the extraction of 3D features from ALS data and the corresponding 2D features from images, or the creation of a synthetic image from laser data and the extraction of corresponding 2D features from both synthetic laser-derived images and aerial images. The types of tie features included points, lines, surfaces, unfiltered laser point clouds and a combination of lines and surfaces.

The outcomes of this project provide a good overview of potential methods for getting two different aerial data sources within the common coordinate frame. One of the main results of the project was that solving the relative orientation between ALS data and aerial images seems to be a feasible method for getting different data sets within the common coordinate frame in urban areas. Even if this project illustrated many successful registrations, these results, however, are not necessarily valid in non-built environments. Many of the methods, for example, needed certain structures, such as buildings, in order to be applicable.

One of the ALS data sets included some strip-wise internal geometric problems, which were not corrected in a strip adjustment. This increased the amount of errors, which was especially visible in the standard deviations when the results of the registration methods were compared with the ground reference. This experience emphasizes the importance of pre-processing and system-calibration phases, because possible strip-wise geometric inhomogeneities limit the registration accuracies. When using the 3D affine transformation, slight improvements can be achieved if compared to the 3D rigid body transformation, because the affine transformation can compensate for strip-wise geometrical problems to a certain extent. However, the most accurate correction of ALS data typically requires access to the system parameters and trajectory data.

The ground reference included six local reference areas, from which several planes and surfaces with different orientations were measured and modelled. The reference surfaces were measured using a terrestrial laser scanner. Terrestrial laser scanning point clouds were oriented towards the ground coordinate system using spherical targets. The locations of the spherical targets were known via static GPS and total station measurements.

Examples of reasonably good relative orientations were achieved using manual, semi-automatic and nearly automatic methods. Therefore, the level of automation was not the most significant factor for registration accuracies. The accuracy of registrations was more dependent upon the implementation of the methods and the types of tie features.

According to the results, it is difficult to select one method as being superior to all of others. More than one method resulted in good registration accuracies. However, automatic methods that used image- and ALS-derived DSMs as tie features were very promising. Because the DSMs covered the complete

test area, their performance was very robust, thus providing a large amount of information for the registration process. In addition, the complete coverage of surface-like tie features enables checking of the internal geometric quality of ALS data. These methods rely upon automatic image matching, which is needed in order to create image-based DSMs. Therefore, the quality of the image-derived DSMs and the conditions that affect the DSM creation should be further examined.

The lower image resolution of the RGB images usually caused more uncertainty for the relative orientations. Unfortunately, not all registration methods were applied to the RGB images. Therefore, the number of experiments was too few for a detailed analysis.

This EuroSDR project highlights the importance, performance and possibilities of current data registration methods and represents one step towards a future integration of ALS data and aerial images. It must be noted that many methods applied by the participants were still at the developmental stage. Therefore, the performance and execution time of most of the methods can be improved in the future.

6 Acknowledgements

The author would like to acknowledge the people in the institutes and companies who actively participated in this EuroSDR project. Their valuable contributions were essential for the project. Special thanks go to the staff of the Finnish Geodetic institute: most of all to Juha Hyypä, who was the primus motor when this project was established, and to Eero Ahokas, Eija Honkavaara, Harri Kaartinen, Lauri Markelin, and Kimmo Nurminen, who prepared the test materials and measured the ground references.

7 References

- Baltsavias, E., 1999. A comparison between photogrammetry and laser scanning. *ISPRS Journal of Photogrammetry and Remote Sensing*, 54(2/3), pp. 83–94.
- Burman, H., 2002. Laser strip adjustment for data calibration and verification. *International Archives of Photogrammetry and Remote Sensing*, 34(3), pp. 67–72.
- Cramer, M., 1999. Direct geocoding – is aerial triangulation obsolete? In Fritsch/Spiller (eds.): *Photogrammetric Week 1999*, Wichmann Verlag, Heidelberg, Germany, pp. 59-70. <http://www.ifp.uni-stuttgart.de/publications/phowo99/cramer.pdf>
- Cramer, M., 2009. *Digital Camera Calibration*, EuroSDR Official Publication No 55, 257 pages.
- Crombaghs, M., Brügelmann, R., and De Min, E., 2000. On the adjustment of overlapping strips of laseraltimeter height data. *International Archives of Photogrammetry and Remote Sensing*, 33(Part B3), pp. 230–237.
- Csanyi, N. and Toth, C., 2007. Improvement of lidar data accuracy using lidar-specific ground targets. *Photogrammetric Engineering & Remote Sensing*, 73(4), pp. 385–396.
- Filin, S., 2003. Recovery of systematic biases in laser altimetry data using natural surfaces. *Photogrammetric Engineering & Remote Sensing*, 69(11), pp. 1235–1242.

- Heipke, C., Jacobsen K., and Wegmann H., 2002. Analysis of the results of the OEEPE test Integrated Sensor Orientation. Test Report and Workshop Proceedings, OEEPE Official Publication n. 43, pp. 31–45.
- Honkavaara, E., Ilves, R., and Jaakkola, J., 2003. Practical results of GPS/IMU/camera-system calibration. Proceedings of International Workshop: Theory, Technology and Realities of Inertial/GPS Sensor Orientation, Castelldefels, Spain, 10 pages. http://www.isprs.org/commission1/theory_tech_realities/pdf/p06_s3.pdf (accessed September 29, 2009)
- Jensen, A. and la Cour-Harbo, A., 2001. Ripples in Mathematics: The Discrete Wavelet Transform. Springer-Verlag, Berlin, 246 p. ISBN 3-540-41662-5.
- Kager, H., 2004. Discrepancies between overlapping laser scanning strips – simultaneous fitting of aerial laser scanner strips. International Archives of Photogrammetry and Remote Sensing and Spatial Information Sciences, 35(PartB/1), pp. 555–560.
- Karjalainen, M., Hyypä, J., and Kuittinen, R., 2006. Determination of Exterior Orientation Using Linear Features from Vector Maps. The Photogrammetric Record 21(116), pp. 329 - 341.
- Kilian, J., Haala, N., and Englich, M., 1996. Capture and evaluation of airborne laser scanner data. International Archives of Photogrammetry and Remote Sensing, 31(Part B3), pp. 383–388.
- Kim, C., Habib, A., and Mrstik, P., 2007. New Approach for Planar Patch Segmentation using Airborne Laser Data. Proceedings of the ASPRS 2007, Tampa, Florida.
- Kornus, W. and Ruiz, A., 2003. Strip adjustment of LiDAR data. International Archives of Photogrammetry and Remote Sensing. 34(3), pp. 47–50.
- Kraus, K. and Pfeifer, N., 2001. Advanced DTM generation from LIDAR data. International Archives of Photogrammetry and Remote Sensing, 34(3/W4), pp. 23–30.
- Kremer, J., 2001. CCNS and AEROcontrol: Products for efficient photogrammetric data collection. In Fritsch/Spiller (eds.), Photogrammetric Week 2001, Wichmann Verlag, Heidelberg, Germany, pp. 85–92.
- Legat, K., Skaloud, J., and Schmidt, R., 2006. “Reliability of Direct Georeferencing: A Case Study on Practical Problems and Solutions” Final Report on Phase 2. In EuroSDR Official Publication No 51, pp. 169-184. <http://bono.hostireland.com/~eurosdrr/publications/51.pdf>
- Perko, R., 2005. Digital pansharpening versus full color film: A comparative study. Manuscript, 6 pages. <http://www.gtbi.net/export/sites/default/GTBiWeb/soporte/descargas/DigitalPansharpeningVsColorFilm.pdf>
- Pfeifer, N., 2005. Airborne laser scanning strip adjustment and automation of tie surface measurement. Boletim de Ciências Geodésicas, 11(1), Curitiba, Brasil, pp. 3-23.
- Ray, L., Gabello, L., and Repich, K., 2001. Approaches to a color scannerless range imaging system. 3rd International Conference on 3D Digital Imaging and Modeling (3DIM 2001), Quebec City, Canada, pp. 20-27.
- Ressl, C., Kager, H., and Mandlbürger, G., 2008. Quality Checking Of ALS Projects Using Statistics Of Strip Differences. International Archives of Photogrammetry, Remote Sensing and Spatial Information Sciences, 37(Part B3b), pp. 253 – 260.
- Ressl, C., Mandlbürger, G., Pfeifer, N., 2009. Investigating Adjustment of Airborne Laser Scanning Strips Without Usage Of GNSS/IMU Trajectory Data, International Archives of Photogrammetry, Remote Sensing and Spatial Information Sciences, 38(Part 3/W8), pp. 195 – 200.

- Rönnholm, P., Hyypä, H., Pöntinen, P., Haggrén, H. and Hyypä, J., 2003. A Method for Interactive Orientation of Digital Images Using Backprojection of 3D Data, the Photogrammetric Journal of Finland, 18(2), pp. 58-69.
- Rönnholm, P., Honkavaara, E., Litkey, P., Hyypä, H., and Hyypä, J., 2007. Integration of Laser Scanning and Photogrammetry. International Archives of Photogrammetry, Remote Sensing and Spatial Information Sciences, 36(3/W52): 355-362.
- Rönnholm, P., Hyypä, H., Hyypä, J., and Haggrén, H., 2009. Orientation of Airborne Laser Scanning Point Clouds with Multi-View, Multi-Scale Image Blocks. Sensors, 9, pp. 6008-6027.
- Schenk, T., 2001. Modeling and analyzing systematic errors in airborne laser scanners. Technical Notes in Photogrammetry No 19, The Ohio State University, Columbus, USA, 46 pages.
- Schenk, T. and Csathó, B., 2002. Fusion of LIDAR data and aerial imagery for a more complete surface description. International Archives of the Photogrammetry, Remote Sensing and Spatial Information Sciences, 34 (3), pp. 310–317.
- Schwarz, K.P., 1995. Integrated airborne navigation systems for photogrammetry. In Fritsch/Hobbie (eds.): Photogrammetric Week 1995, Wichmann Verlag, pp. 139-154. <http://www.ifp.uni-stuttgart.de/publications/phowo95/Schwarz.pdf>
- Skaloud, J., 2006. "Reliability of Direct Georeferencing: An Overview of the Current Approaches and Possibilities" Final Report on Phase 1. In EuroSDR Official Publication No 51, pp. 143-164. <http://bono.hostireland.com/~eurosdrr/publications/51.pdf>
- Toth, C. and Grejner-Brzezinska, D., 2005. Traffic flow estimation from airborne imaging sensors: a performance analysis. ISPRS Workshop "High-Resolution Earth Imaging for Geospatial Information", 17-20 May, Hannover, Germany, 7 pages. <http://www.ipi.uni-hannover.de/fileadmin/institut/pdf/141-toth.pdf> (accessed September 9, 2009)
- Toth, C., Paska, E., and Brzezinska, D., 2007. Using pavement markings to support the QA/QC of lidar data. International Archives of Photogrammetry, Remote Sensing and Spatial Information Sciences, 36 (Part 3/W49B), pp. 173–178.
- Vosselman, G. and Maas, H.-G., 2001. Adjustment and filtering of raw laser altimetry data. Proceedings of OEEPE Workshop on Airborne Laserscanning and Interferometric SAR for Detailed Digital Terrain Models, Stockholm, Sweden, 11 pages. http://www.tu-dresden.de/ipf/photo/publikationen/aelttere/Vosselmann_Maas_OEEPEStockholm2001.pdf (Accessed October 25, 2010)
- Vosselman, G., 2008. Analysis of planimetric accuracy of airborne laser scanning surveys. International Archives of Photogrammetry, Remote Sensing and Spatial Information Sciences, 37(Part 3A), pp. 99-104.
- Yastikli, N., Toth, C., and Brzezinska, D., 2008. Multi sensor airborne systems: The potential for in situ sensor calibration. International Archives of Photogrammetry, Remote Sensing and Spatial Information Sciences, 37(Part B1/I), pp. 89-94.

Appendix A. Detailed Statistical Analysis of the Results

In this chapter, the numeric results for the shift differences (dX, dY and dZ) at each reference area are presented. The rotation errors describe the strip-wise rotation around a common point that is located in the middle of reference area 4.

The average errors after local ICP registrations at the reference areas were typically 1-3 cm for Leica's laser data and 6-8 cm for Optech's data. The main reason for these average errors is noise within the laser data. Optech's data included more noise than did Leica's data.

All of the results in shifts represent deviations from the references expressed in metres. In the case of rotations, the results represent deviations expressed in degrees.

A.1 Aalto University School of Sciences and Technology (Aalto)

Optech data, pan images

	dX (m)	dY (m)	dZ (m)
Area 1	0.1253	-0.0903	0.0014
Area 2	-0.0942	0.0452	0.0176
Area 3	-0.0024	-0.0400	-0.0550
Area 4	-0.1388	0.1053	-0.0157
Area 5	0.1548	0.0901	-0.0408
Area 6	0.0585	-0.0413	-0.0403
Average	0.0172	0.0115	-0.0221
Std	0.1179	0.0799	0.0281

Optech data, RGB images

	dX (m)	dY (m)	dZ (m)
Area 1	0.3046	0.1340	-0.2992
Area 2	0.0077	0.1311	-0.7393
Area 3	0.2206	0.1021	-0.1022
Area 4	0.2050	0.2598	-0.3058
Area 5	0.1639	0.1345	-0.3272
Area 6	0.1451	0.1783	-0.3886
Average	0.1745	0.1566	-0.3604
Std	0.0988	0.0561	0.2092

Leica data, pan images

	dX (m)	dY (m)	dZ (m)
Area 1	0.1106	-0.0573	-0.0037
Area 2	0.3430	-0.4630	0.1388
Area 3	-0.2192	0.2631	-0.0551
Area 4	0.0020	-0.0132	-0.0347
Area 5	-0.0297	0.1513	-0.0527
Area 6	0.0285	0.0943	-0.0529
Average	0.0392	-0.0041	-0.0101
Std	0.1846	0.2525	0.0755

Leica data, RGB images

	dX (m)	dY (m)	dZ (m)
Area 1	0.1864	0.4591	-0.3020
Area 2	0.4954	-0.3462	-0.6283
Area 3	-0.0721	0.4274	-0.0470
Area 4	0.0555	0.1051	-0.2656
Area 5	0.0455	0.2670	-0.3362
Area 6	0.1329	0.1260	-0.4151
Average	0.1406	0.1731	-0.3324
Std	0.1947	0.2939	0.1904

Estimated rotation errors

	D_omega (deg)	D_phi (deg)	D_kappa (deg)
Optech data, pan images	0.0035	0.0100	0.0086
Optech data, rgb images	0.0144	0.0078	0.0031
Leica data, pan images	-0.0025	0.0116	0.0232
Leica data, rgb images	0.0195	0.0233	0.0104

A.2 Dublin Institute of Technology (DIT)

As can be seen from the results, this registration method was not applied to elevations.

Optech data, pan images

	dX (m)	dY (m)	dZ (m)
Area 1	-0.2771	0.3645	-25.6102
Area 2	-0.4535	0.0896	-25.5829
Area 3	-0.2955	0.2524	-25.5312
Area 4	0.0996	0.3909	-25.4151
Area 5	0.2405	0.3292	-25.3986
Area 6	0.1915	-0.1859	-25.3715
Average	-0.0824	0.2068	-25.4849
Std	0.2944	0.2208	0.1026

Optech data, RGB images

	dX (m)	dY (m)	dZ (m)
Area 1	0.0839	1.4467	-25.6144
Area 2	-0.0981	0.9508	-25.5594
Area 3	0.3720	1.0419	-25.5023
Area 4	0.5566	0.8676	-25.4217
Area 5	0.8872	1.0248	-25.3821
Area 6	0.7388	0.6521	-25.3550
Average	0.4234	0.9973	-25.4725
Std	0.3801	0.2619	0.1031

Leica data, pan images

	dX (m)	dY (m)	dZ (m)
Area 1	-0.3904	0.4027	6.0517
Area 2	-0.1361	-0.4020	6.1897
Area 3	-0.4480	0.2907	6.0265
Area 4	0.0432	0.1080	6.0102
Area 5	-0.1949	-0.0896	6.0100
Area 6	-0.0534	-0.3269	6.0015
Average	-0.1966	-0.0029	6.0483
Std	0.1910	0.3270	0.0715

Leica data, RGB images

	dX (m)	dY (m)	dZ (m)
Area 1	-0.0183	0.5588	6.0517
Area 2	0.2117	0.2482	6.1866
Area 3	-0.3234	0.8885	6.0262
Area 4	-0.4814	0.3206	6.0473
Area 5	-0.3535	0.6188	6.0091
Area 6	-0.0405	0.5680	6.0029
Average	-0.1676	0.5338	6.0540
Std	0.2606	0.2288	0.0679

Estimated rotation errors

Even if this method used only one rotation, because of applied 2D rigid body transformation, errors of all three rotations were calculated.

	D_omega (deg)	D_phi (deg)	D_kappa (deg)
Optech data, pan images	0.0083	-0.0240	-0.0505
Optech data, rgb images	0.0026	-0.0310	-0.0690
Leica data, pan images	-0.0049	0.0088	-0.0434
Leica data, rgb images	0.0024	0.0170	0.0237

A.3 *Finnish Geodetic Institute, Aalto University School of Engineering and Terrasolid Oy (FGI et al.)*

Optech data, pan images

Image Espo_5b2_1_09_05_01~0013_pan

	dX (m)	dY (m)	dZ (m)
Area 1	0.2713	-0.4990	0.3986
Area 2	0.0338	0.0466	0.3474
Area 3	-0.0882	-0.0597	0.4066
Area 4	-0.2915	0.2244	0.4068
Area 5	-0.1613	0.0937	0.3784
Area 6	-0.1273	0.0841	0.3751
Average	-0.0605	-0.0183	0.3855
Std	0.1938	0.2526	0.0232

Image Espo_5b2_1_09_05_01~0014_pan

	dX (m)	dY (m)	dZ (m)
Area 1	0.0605	0.1338	0.3359
Area 2	-0.0874	-0.0438	-0.0332
Area 3	-0.1090	-0.0383	0.2152
Area 4	-0.2871	0.1765	-0.0280
Area 5	-0.1855	0.0447	-0.1484
Area 6	-0.2013	0.0288	-0.2824
Average	-0.1350	0.0503	0.0099
Std	0.1194	0.0896	0.2290

Image Espo_5b2_1_09_05_02~0013_pan

	dX (m)	dY (m)	dZ (m)
Area 1	0.0996	0.2014	0.0897
Area 2	-0.0477	0.0443	0.2771
Area 3	0.0346	0.0253	-0.1339
Area 4	0.0469	0.1651	-0.0098
Area 5	-0.0640	0.0101	-0.0698
Area 6	0.0728	-0.0364	-0.0681
Average	0.0237	0.0683	0.0142
Std	0.0658	0.0937	0.1491

Image Espo_5b2_1_09_05_02~0014_pan

	dX (m)	dY (m)	dZ (m)
Area 1	-0.1089	0.5172	-0.8221
Area 2	-0.3514	0.0761	-0.7517
Area 3	-0.0883	0.2437	0.0091
Area 4	-0.1930	0.2927	0.3354
Area 5	-0.0821	0.1789	0.4722
Area 6	0.0460	0.0783	0.7284
Average	-0.1296	0.2312	-0.0048
Std	0.1330	0.1649	0.6491

Leica data, pan images

Image Espo_5b2_1_09_05_01~0013_pan

	dX (m)	dY (m)	dZ (m)
Area 1	0.0623	0.1518	-0.5686
Area 2	0.2662	-0.2090	-0.1042
Area 3	-0.2403	0.5297	-0.7273
Area 4	-0.0669	0.2521	-0.5222
Area 5	0.0008	0.3750	-0.4936
Area 6	-0.0040	0.2809	-0.4324
Average	0.0030	0.2301	-0.4747
Std	0.1655	0.2501	0.2070

Image Espo_5b2_1_09_05_01~0014_pan

	dX (m)	dY (m)	dZ (m)
Area 1	0.3726	-0.1166	-1.1986
Area 2	0.6140	-0.3559	-1.1478
Area 3	-0.4762	0.3417	1.1846
Area 4	-0.4900	0.4022	1.8547
Area 5	-0.5308	0.6770	2.2567
Area 6	-0.6665	0.7443	2.8516
Average	-0.1962	0.2821	0.9669
Std	0.5437	0.4367	1.7443

Image Espo_5b2_1_09_05_02~0013_pan

	dX (m)	dY (m)	dZ (m)
Area 1	0.0824	-0.0039	0.4573
Area 2	0.3157	-0.1993	0.6979
Area 3	-0.4449	0.4600	-0.3300
Area 4	-0.3097	0.3180	-0.4578
Area 5	-0.3317	0.4984	-0.5891
Area 6	-0.3777	0.4866	-0.7541
Average	-0.1777	0.2600	-0.1626
Std	0.3045	0.2940	0.5953

Image Espo_5b2_1_09_05_02~0014_pan

	dX (m)	dY (m)	dZ (m)
Area 1	0.0881	0.1825	0.1538
Area 2	0.3183	-0.4475	0.6028
Area 3	-0.2076	0.2564	-0.0189
Area 4	-0.0166	0.0001	0.1760
Area 5	0.0190	0.1189	0.1878
Area 6	0.0373	0.0438	0.2561
Average	0.0398	0.0257	0.2263
Std	0.1701	0.2496	0.2059

Estimated rotation errors

	D_omega (deg)	D_phi (deg)	D_kappa (deg)
Optech data, pan, image 1_13	0.0068	0.0085	0.0464
Optech data, pan, image 1_14	0.0105	0.0792	0.0171
Optech data, pan, image 2_13	-0.0011	0.0277	-0.0096
Optech data, pan, image 2_14	0.0310	-0.1746	-0.0211
Leica data, image 1_13	-0.0131	-0.0113	0.0216
Leica data, image 1_14	0.0777	-0.4661	0.1149
Leica data, image 2_13	-0.0283	0.1463	0.0595
Leica data, image 1_14	-0.0120	-0.0057	0.0125

A.4 National Geographic Institute Spain (IGN-1, IGN-2)

Optech data, pan images, method 1 (IGN-1)

	dX (m)	dY (m)	dZ (m)
Area 1	0.3483	0.4655	0.2056
Area 2	0.1329	-0.0612	0.3409
Area 3	0.2950	-0.1008	-0.0507
Area 4	0.2910	0.0584	0.0544
Area 5	0.2420	-0.0906	-0.0037
Area 6	0.1919	-0.0538	-0.0223
Average	0.2502	0.0362	0.0874
Std	0.0781	0.2178	0.1541

Optech data, pan images, method 2 (IGN-2)

	dX (m)	dY (m)	dZ (m)
Area 1	0.0052	0.3032	-0.2005
Area 2	-0.0734	-0.3436	-0.1706
Area 3	0.0609	-0.2997	-0.0756
Area 4	-0.0922	-0.1149	0.0182
Area 5	0.0312	-0.2522	0.0194
Area 6	0.0671	-0.2978	0.0706
Average	-0.0002	-0.1675	-0.0564
Std	0.0680	0.2437	0.1110

Leica data, pan images, method 1 (IGN-1)

	dX (m)	dY (m)	dZ (m)
Area 1	0.1399	-0.0418	0.2428
Area 2	0.3474	-0.4735	0.4342
Area 3	-0.1978	0.3055	0.0302
Area 4	-0.1072	-0.0151	0.0375
Area 5	-0.0016	0.1631	-0.0080
Area 6	0.0366	0.1120	-0.0356
Average	0.0362	0.0084	0.1169
Std	0.1920	0.2677	0.1840

Leica data, pan images, method 2 (IGN-2)

	dX (m)	dY (m)	dZ (m)
Area 1	0.5725	-0.3248	-0.0388
Area 2	0.8419	-0.7898	0.0921
Area 3	0.2073	-0.0138	-0.0747
Area 4	0.3372	-0.2123	-0.0633
Area 5	0.3835	-0.0649	-0.0845
Area 6	0.3559	-0.1126	-0.0933
Average	0.4497	-0.2530	-0.0437
Std	0.2252	0.2854	0.0692

Estimated rotation errors

	D_omega (deg)	D_phi (deg)	D_kappa (deg)
Optech data, pan images, method 1	-0.0026	0.0323	-0.0141
Optech data, pan images, method 2	0.0092	-0.0258	-0.0156
Leica data, pan images, method 1	-0.0072	0.0401	0.0290
Leica data, pan images, method 2	-0.0013	0.0128	0.0385

A.5 Independent Research Group on Geospatial (IRGG)

The approach of Independent Research Group was applied to two local areas and the orientations were not related to each other. One area was partially overlapping test area 4, but another area had no terrestrial laser scanning reference. In order to include this research to the comparison, a new test area (area 7) was created by transforming both Leica's and Optech's laser scanning data using test areas 1-6 as a reference. From these two registered laser scanning data sets a surface was derived. Also, the test area 4 was expanded using similar technique. However, because test areas are not identical with other comparisons, the results should be taken as suggestive. Results from only two reference areas were considered to too few for the reliable evaluating of rotation errors.

Optech/Leica data, pan images

	dX (m)	dY (m)	dZ (m)
Area 4	-0.1009	0.9796	0.3437
Area 7	-0.5517	-0.4529	0.0509
Average	-0.3263	0.2634	0.1973
Std	0.3188	1.0129	0.2070

A.6 University College London (UCL)

Optech data, pan images

	dX (m)	dY (m)	dZ (m)
Area 1	0.3124	0.1210	-0.2131
Area 2	0.0650	-0.0803	-0.0933
Area 3	0.1129	-0.0392	-0.3191
Area 4	-0.1367	0.1101	-0.2279
Area 5	-0.1962	0.0131	-0.3053
Area 6	0.0077	-0.0574	-0.2189
Average	0.0275	0.0112	-0.2296
Std	0.1829	0.0866	0.0809

Optech data, RGB images

	dX (m)	dY (m)	dZ (m)
Area 1	0.7184	0.1593	-1.1609
Area 2	0.1403	0.3334	-0.1311
Area 3	0.2580	-0.0422	-1.5257
Area 4	-0.0616	0.1568	-0.8743
Area 5	-0.0711	-0.0611	-0.7316
Area 6	-0.1661	-0.1464	-0.4961
Average	0.1363	0.0666	-0.8200
Std	0.3247	0.1797	0.4908

Leica data, pan images

	dX (m)	dY (m)	dZ (m)
Area 1	0.0498	0.3102	-0.1330
Area 2	0.1873	-0.2961	-0.0017
Area 3	-0.1871	0.2855	-0.1980
Area 4	-0.0694	-0.0973	-0.1864
Area 5	-0.0865	-0.0602	-0.2057
Area 6	-0.0909	-0.1830	-0.2130
Average	-0.0328	-0.0068	-0.1563
Std	0.1317	0.2497	0.0809

Leica data, RGB images

	dX (m)	dY (m)	dZ (m)
Area 1	0.4083	0.9533	-1.0767
Area 2	0.1889	0.1089	0.0659
Area 3	0.0160	0.3675	-1.4097
Area 4	-0.0837	-0.0738	-0.8312
Area 5	-0.1438	-0.1407	-0.7186
Area 6	-0.2266	-0.2668	-0.4882
Average	0.0265	0.1581	-0.7431
Std	0.2356	0.4477	0.5066

Estimated rotation errors

	D_omega (deg)	D_phi (deg)	D_kappa (deg)
Optech data, pan images	0.0061	0.0156	0.0157
Optech data, RGB images	-0.0319	-0.0816	0.0242
Leica data, pan images	-0.0030	0.0142	-0.0041
Leica data, RGB images	-0.0351	-0.0670	-0.0163

A.7 University of Calgary (UofC-1, UofC-2, UofC-3)

Patch Method (UofC-1)

Optech data, pan images

	dX (m)	dY (m)	dZ (m)
Area 1	0.0975	0.2472	0.0260
Area 2	-0.0846	0.0359	-0.0165
Area 3	0.0195	0.0243	0.0275
Area 4	-0.1622	0.1893	0.0524
Area 5	-0.1171	0.0132	0.0265
Area 6	-0.1268	0.0811	0.0280
Average	-0.0623	0.0985	0.0240
Std	0.0999	0.0973	0.0223

Optech data, RGB images

	dX (m)	dY (m)	dZ (m)
Area 1	-0.1457	0.4708	0.1901
Area 2	-0.2026	-0.0177	0.2734
Area 3	-0.0341	0.2040	-0.0468
Area 4	0.0916	0.3120	0.0003
Area 5	0.0845	0.1546	-0.0656
Area 6	0.1992	0.1086	-0.0989
Average	-0.0012	0.2054	0.0421
Std	0.1540	0.1694	0.1527

Leica data, pan images

	dX (m)	dY (m)	dZ (m)
Area 1	0.0389	0.4579	0.1350
Area 2	0.1917	-0.0674	0.1690
Area 3	-0.1830	0.6071	0.1062
Area 4	-0.0639	0.2405	0.0571
Area 5	-0.0458	0.2903	0.0211
Area 6	-0.0402	0.1573	-0.0098
Average	-0.0171	0.2810	0.0798
Std	0.1247	0.2350	0.0688

Leica data, RGB images

	dX (m)	dY (m)	dZ (m)
Area 1	-0.2992	0.5775	0.3120
Area 2	-0.1969	-0.0479	0.4725
Area 3	-0.2434	0.7982	0.0401
Area 4	0.0659	0.3138	-0.0162
Area 5	0.1700	0.3993	-0.0774
Area 6	0.2558	0.2083	-0.1481
Average	-0.0413	0.3749	0.0972
Std	0.2349	0.2936	0.2424

Estimated rotation errors

	D_omega (deg)	D_phi (deg)	D_kappa (deg)
Optech data, pan images	0.0061	0.0038	0.0081
Optech data, RGB images	-0.0009	0.0414	-0.0297
Leica data, pan images	0.0009	0.0231	0.0020
Leica data, RGB images	-0.0099	0.0606	-0.0387

Linear Feature Method (UofC-2)

Optech data, pan images

	dX (m)	dY (m)	dZ (m)
Area 1	0.1693	0.3664	0.0232
Area 2	-0.1215	0.1392	-0.0920
Area 3	-0.0934	-0.0127	0.1759
Area 4	-0.4241	0.1528	0.1894
Area 5	-0.4434	-0.0772	0.1799
Area 6	-0.3921	-0.0438	0.2006
Average	-0.2175	0.0875	0.1128
Std	0.2443	0.1668	0.1200

Optech data, RGB images

	dX (m)	dY (m)	dZ (m)
Area 1	0.3814	0.4103	-0.2258
Area 2	0.0552	0.4228	-0.2099
Area 3	0.2798	0.2788	-0.3370
Area 4	-0.0042	0.3628	-0.3097
Area 5	0.0086	0.1052	-0.3461
Area 6	0.1538	0.0677	-0.3462
Average	0.1458	0.2746	-0.2958
Std	0.1569	0.1547	0.0620

Leica data, pan images

	dX (m)	dY (m)	dZ (m)
Area 1	-0.3149	0.6714	0.2458
Area 2	-0.1639	0.0277	0.3136
Area 3	-0.3247	0.7706	0.1570
Area 4	-0.0504	0.3457	0.1135
Area 5	-0.0613	0.2874	0.0782
Area 6	0.0170	0.0897	0.0432
Average	-0.1497	0.3654	0.1586
Std	0.1439	0.3014	0.1034

Leica data, RGB images

	dX (m)	dY (m)	dZ (m)
Area 1	-0.0619	0.9762	-0.0126
Area 2	0.0938	0.2599	0.2014
Area 3	0.0588	0.9935	-0.3441
Area 4	0.2898	0.4252	-0.3571
Area 5	0.3727	0.3972	-0.4074
Area 6	0.4635	0.1428	-0.4625
Average	0.2028	0.5325	-0.2304
Std	0.2035	0.3648	0.2638

Estimated rotation errors

	D_omega (deg)	D_phi (deg)	D_kappa (deg)
Optech data, pan images	0.0122	-0.0168	0.0162
Optech data, RGB images	0.0020	0.0191	-0.0039
Leica data, pan images	-0.0021	0.0294	-0.0363
Leica data, RGB images	-0.0127	0.0581	-0.0562

Combined Linear Feature and Patch Method (UofC-3)

Optech data, pan images

	dX (m)	dY (m)	dZ (m)
Area 1	0.1693	0.3116	0.0214
Area 2	-0.1451	0.1802	-0.0623
Area 3	-0.1051	-0.0179	0.1016
Area 4	-0.2416	0.1648	0.1204
Area 5	-0.3362	-0.0011	0.1137
Area 6	-0.3834	-0.0613	0.1271
Average	-0.1737	0.0961	0.0703
Std	0.1991	0.1452	0.0756

Optech data, RGB images

	dX (m)	dY (m)	dZ (m)
Area 1	0.3350	0.6777	-0.1243
Area 2	0.0466	0.3633	-0.1352
Area 3	0.2924	0.2564	-0.2102
Area 4	0.0757	0.3248	-0.1889
Area 5	0.1044	0.0774	-0.2241
Area 6	0.2010	0.0377	-0.2309
Average	0.1759	0.2896	-0.1856
Std	0.1195	0.2310	0.0457

Leica data, pan images

	dX (m)	dY (m)	dZ (m)
Area 1	-0.3073	0.6783	0.2059
Area 2	-0.1385	0.0227	0.2447
Area 3	-0.3309	0.7640	0.1551
Area 4	-0.1400	0.2898	0.1018
Area 5	-0.0644	0.2902	0.0603
Area 6	0.0030	0.0949	0.0247
Average	-0.1630	0.3567	0.1321
Std	0.1322	0.3028	0.0852

Leica data, RGB images

	dX (m)	dY (m)	dZ (m)
Area 1	-0.0597	0.9454	0.0745
Area 2	0.1007	0.2515	0.1852
Area 3	0.0509	0.9647	-0.1599
Area 4	0.2699	0.3890	-0.2101
Area 5	0.3891	0.3366	-0.3257
Area 6	0.4618	0.1056	-0.3245
Average	0.2021	0.4988	-0.1268
Std	0.2043	0.3662	0.2119

Estimated rotation errors

	D_omega (deg)	D_phi (deg)	D_kappa (deg)
Optech data, pan images	0.0077	-0.0110	0.0097
Optech data, RGB images	0.0032	0.0169	-0.0190
Leica data, pan images	0.0008	0.0284	-0.0314
Leica data, RGB images	-0.0003	0.0630	-0.0563

A.8 University of Stuttgart (IFP-1, IFP-2)

Optech data, pan images, method A (IFP-1)

	dX (m)	dY (m)	dZ (m)
Area 1	0.1356	0.3424	0.0531
Area 2	-0.0504	0.0138	-0.0342
Area 3	0.0813	0.0847	0.0440
Area 4	-0.0669	0.2701	0.0271
Area 5	0.0974	0.1492	-0.0166
Area 6	0.1253	0.0108	-0.0320
Average	0.0537	0.1452	0.0069
Std	0.0893	0.1367	0.0392

Optech data, pan images, method B (IFP-2)

	dX (m)	dY (m)	dZ (m)
Area 1	-0.4990	-0.1747	-0.0219
Area 2	-0.7256	-0.1514	-0.1611
Area 3	-0.5337	-0.0386	0.1834
Area 4	-0.6898	0.0426	0.1714
Area 5	-0.4199	0.0077	0.1623
Area 6	-0.4792	-0.2021	0.1683
Average	-0.5579	-0.0861	0.0837
Std	0.1223	0.1031	0.1429

Leica data, pan images, method A (IFP-1)

	dX (m)	dY (m)	dZ (m)
Area 1	0.1489	0.0393	0.1725
Area 2	0.4048	-0.3906	0.0646
Area 3	-0.1297	0.3537	0.1745
Area 4	0.0191	0.0832	0.0426
Area 5	0.0495	0.2131	-0.0209
Area 6	0.0739	0.1328	-0.0873
Average	0.0944	0.0719	0.0577
Std	0.1776	0.2523	0.1042

Leica data, pan images, method B (IFP-2)

	dX (m)	dY (m)	dZ (m)
Area 1	-1.9438	-0.2174	-0.6104
Area 2	-1.5916	-0.9709	-0.8849
Area 3	-2.0105	-0.2129	-0.2781
Area 4	-1.7621	-0.5996	-0.4355
Area 5	-1.7723	-0.5444	-0.4760
Area 6	-1.6402	-0.6646	-0.5091
Average	-1.7868	-0.5350	-0.5323
Std	0.1644	0.2883	0.2040

Estimated rotation errors

	D_omega (deg)	D_phi (deg)	D_kappa (deg)
Optech data, pan images, method A	0.0083	0.0167	-0.0043
Optech data, pan images, method B	0.0146	-0.0165	0.0023
Leica data, pan images, method A	0.0059	0.0383	0.0232
Leica data, pan images, method B	0.0203	-0.0025	-0.0190

A.9 Vienna University of Technology (IPF)

Optech data, pan images

	dX (m)	dY (m)	dZ (m)
Area 1	0.1043	0.0717	-0.0090
Area 2	-0.0198	0.0663	-0.0597
Area 3	-0.0494	0.1324	-0.0305
Area 4	-0.2113	0.2452	-0.0008
Area 5	-0.2574	0.0033	-0.0380
Area 6	0.0041	0.0986	-0.0294
Average	-0.0716	0.1029	-0.0279
Std	0.1370	0.0817	0.0211

Optech data using RGB images were not processed

Leica data, pan images

	dX (m)	dY (m)	dZ (m)
Area 1	-0.0157	0.3178	0.0032
Area 2	0.0950	-0.1316	0.0878
Area 3	0.0469	-0.0057	-0.0011
Area 4	-0.1354	0.0889	-0.0173
Area 5	-0.0085	0.1762	-0.0555
Area 6	-0.0675	0.2518	-0.0662
Average	-0.0142	0.1162	-0.0082
Std	0.0815	0.1671	0.0549

Leica data using RGB images were not processed

Estimated rotation errors

	D_omega (deg)	D_phi (deg)	D_kappa (deg)
Optech data, pan images	0.0082	0.0095	0.0105
Leica data, pan images	0.0002	0.0146	0.0159

Appendix B. Technical Reports of the Participants

Report of the Aalto University School of Engineering

Report of the Dublin Institute of Technology

Report of the Finnish Geodetic Institute, Aalto University School of Engineering and TerraSolid Oy

Report of the Independent Research Group on Geospatial

Report of the National Geographic Institute, Spain

Report of the University of Calgary)

Report of the University College London

Report of the Institute for Photogrammetry, University of Stuttgart

Report of the Vienna University of Technology

Report of the Aalto University School of Engineering EuroSDR ”Registration Quality – Towards Integration of Laser Scanning and Photogrammetry”

Petri Rönnholm
Institute of Photogrammetry and Remote Sensing
Aalto University School of Engineering
Finland
petri.ronnholm@aalto.fi



Description of the method

The Institute of Photogrammetry and Remote Sensing, Aalto University School of Engineering, participated in the “Registration Quality” project using the interactive orientation method. Originally, the method was applied to solve the relative orientation between a laser scanning point cloud and a single image (Rönnholm et al., 2003) or an image block (Rönnholm et al., 2008). In this case, the use of stereo image pairs enabled stereoscopic vision during the orientation process. However, it was noticed that, during the interactive orientation, it was difficult to use the complete image block or even a single stereo pair because of the large image sizes. Instead, the interactive orientation was performed in several, relatively small, sample areas. A total of six sample areas were distributed around the image block (Figure 1).

If distinguishable features are located quite close to one another, as in the case of a small test area, it may be difficult to find accurate rotation parameters for the orientations. Therefore, only shifts were included in local interactive orientations. Finally, unknown parameters of a 3D rigid transformation between the ALS data and images were solved by means of the least squares method using the local shifts from each sample area. The scale of the transformations was assumed to be a constant and, therefore, was not included. In order to use point-like data in the least squares method, each sample area was represented with an original laser point chosen arbitrarily within the current test area, and its virtual tie point, which was calculated using the corresponding local shifts.

In order to ensure a successful relative orientation, the orientation process was done twice. The second orientation round used the results from the first orientation as the initial rotations.

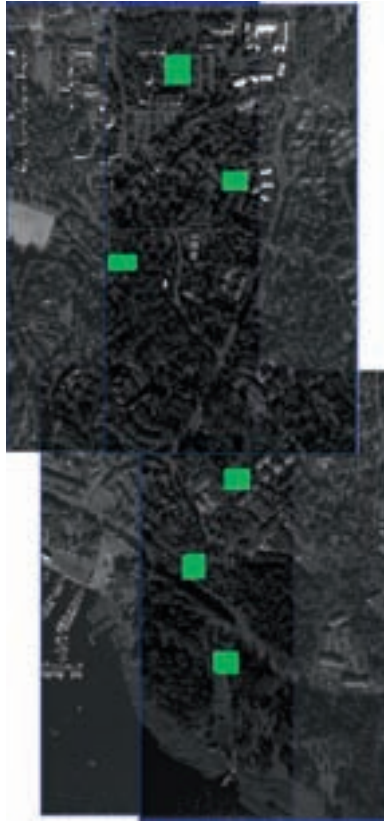


Figure 1. Local sample areas (Leica's laser scanning data) in which interactive orientations were applied.

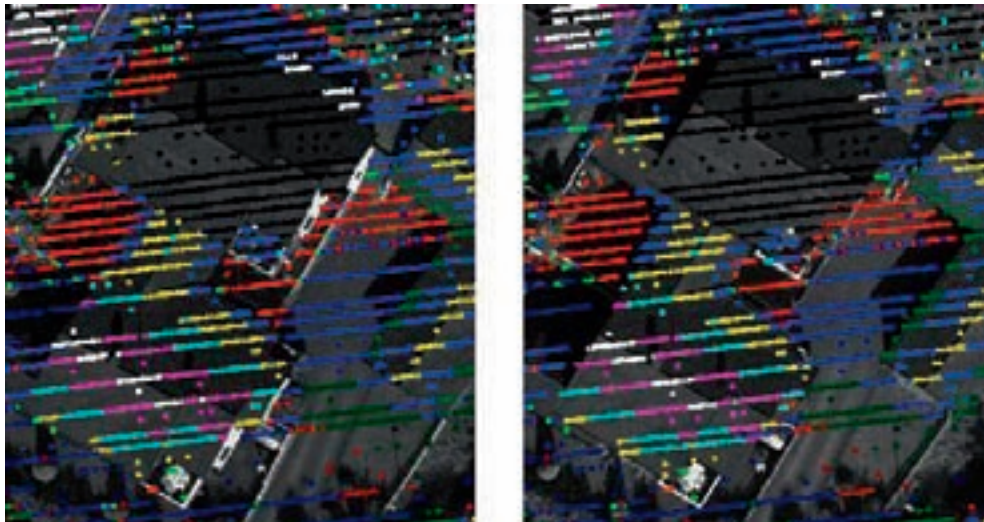


Figure 2. Example of a local sample area (Leica's data) after the first orientation round (cross-eye stereo).

Results

In this chapter, the transformation parameters are presented from the 1st and 2nd orientation rounds. In addition, the residuals of the 3D shifts at each local test area after the orientation rounds are presented. In all cases, system origin was temporarily moved to the first laser scanning point of the current local test area. The same origin was used during the adjustment and transformation. Because the location of the origin and the rotations have a tight connection, the numeric values of the transformation parameters are not directly comparable.

Leica's laser scanning data oriented with panchromatic images

The first orientation round

dX (m)	dY	dZ	dOmega (rad)	dPhi	dKappa
-18.189	-21.596	-6.393	-0.00112	-0.00055	0.000368

Table 1. Parameters for a rigid transformation applied to the complete laser scanning point cloud. (Leica/pan)

	X (m)	Y	Z
Area1	-0.009	-0.046	0.257
Area2	0.060	0.169	-0.179
Area3	0.056	-0.121	-0.207
Area4	-0.224	0.178	0.072
Area5	0.190	-0.148	0.099
Area6	-0.073	-0.032	-0.042
Total RMSE	0.128	0.129	0.162

Table 2. The residuals of shifts at each test area after solving common transformation parameters for complete data. (Leica/pan)

The second orientation round

dX (m)	dY	dZ	dOmega (rad)	dPhi	dKappa
0.083	-0.009	0.451	0.001203	0.000673	-0.00012

Table 3. Parameters of a rigid transformation applied to the complete laser scanning point cloud. (Leica/pan)

	X (m)	Y	Z
Area1	0.073	0.021	0.051
Area2	0.007	0.068	-0.049
Area3	0.072	-0.006	-0.004
Area4	-0.240	0.180	0.007
Area5	0.177	-0.178	-0.028
Area6	-0.090	-0.085	0.024
Total RMSE	0.134	0.113	0.033

Table 4. The residuals of shifts at each test area after solving common transformation parameters for complete data. (Leica/pan)

Optech's laser scanning data oriented with pan images.

The 1st orientation round

dX (m)	dY	dZ	dOmega (rad)	dPhi	dKappa
23.622	-17.809	25.693	0.00061	0.00000	0.00007

Table 5. Parameters of a rigid transformation applied to the complete laser scanning point cloud. (Optech/pan)

	X (m)	Y	Z
Area1	-0.138	-0.119	-0.137
Area2	0.135	0.195	0.174
Area3	0.228	0.048	0.012
Area4	-0.052	0.140	-0.085
Area5	-0.097	-0.137	0.119
Area6	-0.077	-0.127	-0.083
Total RMSE	0.134	0.135	0.114

Table 6. The residuals at each test area after solving common transformation parameters for complete data. (Optech/pan)

The 2nd orientation round

dX (m)	dY	dZ	dOmega (rad)	dPhi	dKappa
-0.015	0.030	-0.022	-0.00007	-0.00005	0.00004

Table 7. Parameters of a rigid transformation applied to the complete laser scanning point cloud. (Optech/pan)

	X (m)	Y	Z
Area1	-0.035	-0.060	-0.012
Area2	-0.008	0.015	0.025
Area3	0.022	0.009	-0.002
Area4	0.000	0.013	-0.009
Area5	0.011	0.021	-0.005
Area6	0.010	0.001	0.003
Total RMSE	0.018	0.027	0.012

Table 8. The residuals at each test area after solving common transformation parameters for complete data. (Optech/pan)

Leica's laser scanning data oriented with RGB images

The 1st orientation round

dX (m)	dY	dZ	dOmega (rad)	dPhi	dKappa
-18.095	-21.499	-6.233	-0.00207	-0.0025	0.000287

Table 9. Parameters of a rigid transformation applied to the complete laser scanning point cloud. (Leica/RGB)

	X (m)	Y	Z
Area1	0.355	0.231	-0.243
Area2	0.044	0.181	0.319
Area3	0.005	-0.082	0.080
Area4	-0.300	0.216	-0.155
Area5	0.198	-0.259	-0.109
Area6	-0.301	-0.285	0.109
Total RMSE	0.241	0.219	0.189

Table 10. The residuals at each test area after solving common transformation parameters for complete data. (Leica/RGB)

The 2nd orientation round

dX (m)	dY	dZ	dOmega (rad)	dPhi	dKappa
0.111	0.047	-0.022	0.00009	0.00017	-0.00007

Table 11. Parameters of a rigid transformation applied to the complete laser scanning point cloud. (Leica/RGB)

	X (m)	Y	Z
Area1	0.231	0.207	0.038
Area2	0.081	0.072	-0.022
Area3	0.075	0.004	-0.002
Area4	-0.080	0.264	0.000
Area5	0.033	-0.301	-0.040
Area6	-0.340	-0.245	0.026
Total RMSE	0.177	0.212	0.027

Table 12. The residuals at each test area after solving common transformation parameters for complete data. (Leica/RGB)

Optech's laser scanning data oriented with RGB images

The 1st orientation round

dX (m)	dY	dZ	dOmega (rad)	dPhi	dKappa
23.850	-17.741	25.266	-0.00307	-0.00315	-0.00018

Table 13. Parameters of a rigid transformation applied to the complete laser scanning point cloud. (Optech/RGB)

	X (m)	Y	Z
Area1	0.490	0.269	-0.014
Area2	0.001	-0.185	0.079
Area3	-0.217	0.082	-0.020
Area4	0.125	0.212	0.011
Area5	-0.186	-0.191	-0.115
Area6	-0.212	-0.187	0.059
Total RMSE	0.253	0.196	0.063

Table 14. The residuals at each test area after solving common transformation parameters for complete data. (Optech/RGB)

The 2nd orientation round

dX (m)	dY	dZ	dOmega (rad)	dPhi	dKappa
0.054	0.023	0.195	0.00179	0.00097	0.00001

Table 15. Parameters of a rigid transformation applied to the complete laser scanning point cloud. (Optech/RGB)

	X (m)	Y	Z
Area1	0.294	0.243	-0.085
Area2	-0.113	-0.151	0.077
Area3	-0.091	-0.099	0.068
Area4	0.034	0.124	0.013
Area5	0.050	0.017	-0.074
Area6	-0.175	-0.134	0.002
Total RMSE	0.154	0.145	0.063

Table 16. The residuals at each test area after solving common transformation parameters for complete data. (Optech/RGB)

Discussion

In this experiment, the feasibility of the interactive orientation method for solving a relative orientation between airborne laser scanning data and images was investigated. In some cases, clear shifts were detectable after the first orientation round. Therefore, the second orientation round was useful for ensuring a more accurate orientation. In this case, the rotation errors for the complete ALS data were relatively small, causing no interpretation difficulties. However, it is assumed that if larger orientation errors exist, the first orientation round can eliminate most of such rotation errors, thus enabling easier interpretation for the second orientation round.

The orientation part of the method was fully manual, based on the Operator's ability to interpret and adjust the relative orientation of images and laser scanning data. Each interactive orientation within a local test area required a number of minutes. However, the complete process for each case required approximately 2-3 hours, including data transferring, searching for suitable local test areas, selecting a corresponding sets of laser scanning points, making interactive orientations, calculating the final transformation parameters for laser scanning data, and transforming the laser point cloud – all of this was repeated twice. Typically, the second orientation round was completed much more quickly because the initial orientation was already quite close to the correct one. In the future, processing time may be reduced by implementing all of the functions in the common software.

References

Rönnholm, P., H. Hyypä, P. Pöntinen, H. Haggrén and J. Hyypä, 2003. A Method for Interactive Orientation of Digital Images Using Backprojection of 3D Data, the Photogrammetric Journal of Finland, Vol 18, No. 2, pp. 58-69.

Rönnholm, P., H. Hyypä, J. Hyypä, H. Haggrén, 2009. Orientation of Airborne Laser Scanning Point Clouds with Multi-View, Multi-Scale Image Blocks. Sensors, 9, pp. 6008-6027.

Report of the Dublin Institute of Technology Registration Quality - Towards Integration of Laser Scanning and Photogrammetry

*Contribution from DIT – Dublin Institute of Technology
10th December 2009*

Mr. Kevin Mooney
Department of Spatial Information Sciences
The Dublin Institute of Technology
Bolton Street
Dublin 1.
Ireland.
Tel. +353-1-4023730
Fax. +353-1-4023999
e-mail: kevin.mooney@dit.ie



The Department of Spatial Information Sciences (SIS), at the Dublin Institute of Technology (DIT), participated in the EuroSDR research project, Registration Quality - Towards Integration of Laser Scanning and Photogrammetry, during 2009.

The quality of registration of airborne LiDAR and image data is of interest at DIT because a PhD study at the department of SIS is developing automated methods for the extraction of roadside objects from these data sources. The study is undertaken within the context of the National Roads Authority (NRA) of Ireland's need to produce a noise model for its network of national roads in order to meet the requirements of the EC noise directive (Directive 2002/49/EC).

The PhD study envisages that the NRA will have airborne LiDAR and imagery available to it for future road surveys, which will be acquired with direct sensor orientation at different times. In order to check the correspondence of the orientation of each sensor, our method compares the digital surface models (DSM) independently generated from each data set.

For the purpose of the EuroSDR project, the following data sets were utilised:

- Optech ALTM 3100 airborne laser data: This airborne laser scanning data was acquired in July 2005. The flying height was approximately 1000 m resulting in a point density of 2 - 3 points/m². One laser strip was provided, with its orientation intentionally deflected;
- Leica ALS50II airborne laser data: This airborne laser scanning data was acquired in April 2007. The flying height was approximately 500 m resulting in a point density of 4 - 5 points/m². One laser strip was provided, with its orientation intentionally deflected;
- DMC panchromatic images: This test data set included four DMC panchromatic images at a ground resolution of approximately 5 cm, forward overlap 60% and side overlap 20%. The images were collected in September 2005 and the interior and exterior orientation of the images was provided;
- DMC multispectral images (RGB): This test data set included four DMC RGB images at a ground resolution of approximately 22 cm, forward overlap 60%, and side overlap 20%

and the registration between

- Optech ALTM 3100 airborne laser data and DMC panchromatic images;
- Leica ALS50II airborne laser data and DMC panchromatic images;
- Optech ALTM 3100 airborne laser data and DMC multispectral images (RGB);
- Leica ALS50II airborne laser data and DMC multispectral images (RGB)

was checked.

In each case, the unfiltered and unclassified LiDAR point cloud was used to generate a DSM using 'first' and 'only' echo data. Terrasolid software, Terrascan, was used for this purpose. The DSM resolution was 0.5 m. A sample window (Upper left: 369099.763E, 6670314.621N and Lower right: 369922.762E, 6669538.621N) was extracted from the DSM for registration testing purposes.

A DSM was also generated from each image data set using the provided sensor orientation and a sample window using the same coordinate values extracted.

A greyscale image of each generated DSM was used for the purpose of the registration evaluation. Matching pixels were identified in the two DSMs being compared.

The steps taken in the DIT approach can be identified as follows:

1. Generate a DSM from each dataset. The Ground sample resolution was 0.5 m.
2. Extract a sample DSM greyscale image file within specified rectangular bounds
3. Identify matching image pixels. Ten matching pairs were selected.
4. Compute the parameters of a 2D linear transformation relating both datasets and the RMSE for the X and Y fit in pixels
5. Apply the parameters of the transformation to the x,y values of the original LiDAR point cloud.

The method has the potential for considerable automation. However, as the Department's PhD study is still ongoing, automation has not yet been prioritised. Hence, the above steps were executed manually in the EuroSDR test.

Approximate times taken for each step:

- Creating DSMs from LiDAR and Aerial Images using Match-T - approximately five minutes for each DSM
- Find and match common points in pairs of DSM - fifteen minutes for ten points for each pair of DSMs
- Populating the Microsoft excel transformation and computing the transformation parameters - five minutes for each pair of DSMs
- Using Terrasolid TerraScan to apply the transformation to LiDAR data - ten minutes for each LiDAR data set.

Results:

Registration between Optech's laser data and DMC panchromatic images.

The parameters of the transformation:

$$X = ax - by + C_X$$

$$Y = bx + ay + C_Y$$

are computed to be:

$$a: 1.000508$$

$$b: -0.001018$$

$$C_X: -6953.95 \text{ m}$$

$$C_Y: -3029.81 \text{ m}$$

$$\text{RMSE X: } 0.8 \text{ pixel} = 0.39 \text{ m}$$

$$\text{RMSE Y: } 0.7 \text{ pixel} = 0.35 \text{ m}$$

$$\text{Rotation } (\theta = \tan^{-1}\left(\frac{b}{a}\right)): -0.0010 \text{ Rads about origin of coordinate system}$$

$$\text{Scale } (\lambda = \sqrt{a^2 + b^2}): 1.0005$$

Because, the above transformation is applied about the origin of the coordinate reference system, the shift parameters, C_X and C_Y are not indicative of the actual shifts between the LiDAR and image data sets. These have been analysed separately, following the application of the transformation to the LiDAR data set. Following the transformation of the LiDAR point cloud, and based on a sample of 1000 points, the following shifts exist between the original LiDAR points and the transformed LiDAR points:

X shift Mean: 24.06 m

Y shift Mean: -17.89 m

Registration between Leica's laser data and DMC panchromatic images.

The parameters of the transformation:

$$X = ax - by + C_x$$

$$Y = bx + ay + C_y$$

are computed to be:

a: 0.999846

b: -0.001109

C_x : -7358.28 m

C_y : 1415.07 m

RMSE X: 0.7 pixel = 0.33 m

RMSE Y: 0.6 pixel = 0.29 m

Rotation ($\theta = \tan^{-1}\left(\frac{b}{a}\right)$): -0.0011 Rads about origin of coordinate system

Scale ($\lambda = \sqrt{a^2 + b^2}$): 0.9998

Because, the above transformation is applied about the origin of the coordinate reference system, the shift parameters, C_x and C_y are not indicative of the actual shifts between the LiDAR and image data sets. These have been analysed separately, following the application of the transformation to the LiDAR data set. Following the transformation of the LiDAR point cloud, and based on a sample of 1000 points, the following shifts exist between the original LiDAR points and the transformed LiDAR points:

X shift Mean: -18.84 m

Y shift Mean: -21.22 m

Registration between Optech's laser data and DMC RGB images.

The parameters of the transformation:

$$X = ax - by + C_X$$

$$Y = bx + ay + C_Y$$

are computed to be:

$$a: \quad 0.999819$$

$$b: \quad -0.001138$$

$$C_X: \quad -7499.45 \text{ m}$$

$$C_Y: \quad 1610.74 \text{ m}$$

$$\text{Rotation } (\theta = \tan^{-1}\left(\frac{b}{a}\right)): \quad -0.0011 \text{ Rads about origin of coordinate system}$$

$$\text{Scale } (\lambda = \sqrt{a^2 + b^2}): \quad 0.9998$$

Because, the above transformation is applied about the origin of the coordinate reference system, the shift parameters, C_X and C_Y are not indicative of the actual shifts between the LiDAR and image data sets. These have been analysed separately, following the application of the transformation to the LiDAR data set. Following the transformation of the LiDAR point cloud, and based on a sample of 1000 points, the following shifts exist between the original LiDAR points and the transformed LiDAR points:

$$\text{X shift Mean:} \quad 24.17 \text{ m}$$

$$\text{Y shift Mean:} \quad -17.39 \text{ m}$$

Registration between Leica's laser data and DMC RGB images.

The parameters of the transformation:

$$X = ax - by + C_X$$

$$Y = bx + ay + C_Y$$

are computed to be:

$$a: \quad 0.999493$$

$$b: \quad -0.000082$$

$$C_X: \quad -377.89 \text{ m}$$

$$C_Y: \quad 3390.75 \text{ m}$$

$$\text{Rotation } (\theta = \tan^{-1}\left(\frac{b}{a}\right)): \quad -0.0001 \text{ Rads about origin of coordinate system}$$

$$\text{Scale } (\lambda = \sqrt{a^2 + b^2}): \quad 0.9995$$

Because, the above transformation is applied about the origin of the coordinate reference system, the shift parameters, C_X and C_Y are not indicative of the actual shifts between the LiDAR and image data sets. These have been analysed separately, following the application of the transformation to the LiDAR data set. Following the transformation of the LiDAR point cloud, and based on a sample of 1000 points, the following shifts exist between the original LiDAR points and the transformed LiDAR points:

$$\text{X shift Mean:} \quad -18.09 \text{ m}$$

$$\text{Y shift Mean:} \quad -20.87 \text{ m}$$

Report of the Finnish Geodetic Institute, Aalto University School of Engineering and TerraSolid Oy EuroSDR "Registration Quality – Towards Integration of Laser Scanning and Photogrammetry"

Use of Roof Ridges as 3D Line Features in Registration of Aerial Images and Laser Scanning Point Clouds

Mika Karjalainen, Finnish Geodetic Institute, mika.karjalainen@fgi.fi
Petri Rönnholm, Aalto University School of Engineering, petri.ronnholm@aalto.fi
Arttu Soininen, TerraSolid Oy, arttu.soininen@terrasolid.fi
Finland

Description of the method

Precise co-registration of different remotely sensed data sets require tie features, which have to be located and matched on data sources to be co-registered. For example, in the registration of similar aerial images, tie points are typically exploited, and are widely used in commercial photogrammetric software packages. However, in the case of images and laser scanning point clouds, general tie point algorithms cannot be used directly, because of difficulties in finding point-like features accurately from laser scanning data. One alternative approach is to use laser-derived and image-derived surfaces to locate tie points. For example, the DSM based surface matching is a sound and versatile approach (e.g., Akca, 2007); however, it presumably is a relatively computing intensive approach as well. Another approach would be the use of linear features in co-registration, and several reports dealing with the subject have been published in, for example, Tommaselli and Tozzi (1996) and Habib and Alruzouq (2004). In our approach, we have decided to use line type of tie features in the registration of aerial images and laser scanning point clouds, which could lead to a fast and reliable co-registration process.

First, we needed to extract line features from the laser scanning point clouds. However, a direct extraction of line features, such as building outlines, from laser scanning data is usually impractical. In this case, the point density was not high enough to describe true breaklines accurately. Therefore, in our approach, an indirect extraction method was applied. The indirect method included two phases: 1) planes were fitted to the filtered laser scanning points that represent roofs and 2) the ridge of the roof was considered to be an intersection of two roof planes. Extraction of the ridges of roofs was completed using a beta version of TerraMatch software by TerraSolid Oy.

In the second stage, our goal was to locate the roof ridges from aerial images, that is, to find such image points (edge pixels), which most likely represent the roof ridges on the aerial images. In general, the problem of locating edge pixels is known as edge detection. Edge detection typically includes typically the following stages: noise filtering, edge enhancement, finding edges, sub-pixel detection

(Sonka et al., 1993). In order to locate edge pixels from images, the 3D line features (3D roof ridges) were projected on the images using the initial exterior orientation parameters and the collinearity equations. Then, image intensity value profiles were digitized perpendicularly to the projected line features. Thus, each scan line is a 1D signal containing image intensity signal, for which edge detection can be carried out in order to locate edge pixels. The projection of 3D line features, digitizing of the intensity profiles and the edge detection algorithm were carried out automatically. The result of the whole process is a set of 3D line features (representing roof ridges) and some image pixels that plausibly correspond to the roof ridges on the images. It should be noted that automatic edge detection tends to produce erroneous edge pixels, because some of the roof ridges may be invisible due to occlusion or shadows etc. Therefore, outlier detection was applied in order to discard erroneous image points from further calculations. In the edge detection phase, it was required that the located edge pixels should be nearly collinear (roof ridge should be a straight line). Moreover, in the phase of calculation of orientation parameters (see below), edge pixels, which do not fit to the functional model, can be discarded.

Finally, relative orientations of laser point cloud and images were solved using roof ridges (3D lines) and their corresponding image pixels (2D image points). In contrast to point based space resection, there are no exact point-to-point correspondences in data sets. It is only known, that an image point corresponds to a certain 3D line feature. In such cases, orientation parameters can be solved using a coplanarity model, where the idea is that three vectors: β (3D roof ridge vector), c (vector from 3D roof ridge to the perspective centre) and p (vector from image point to the perspective centre) should lie on the same plane i.e. $|\beta \ c \ p| = 0$ (Figure 1). The unknowns in this equation are the orientation parameters of the image. The method is described in more detail, for example, in Mulawa et al. (1988). The detection of edge pixels and the approach used for calculating the orientation parameters are described in Karjalainen et al. (2006). As a result, new exterior orientation parameters for the images were obtained. These parameters described image orientations in the coordinate system of the delivered laser scanning data.

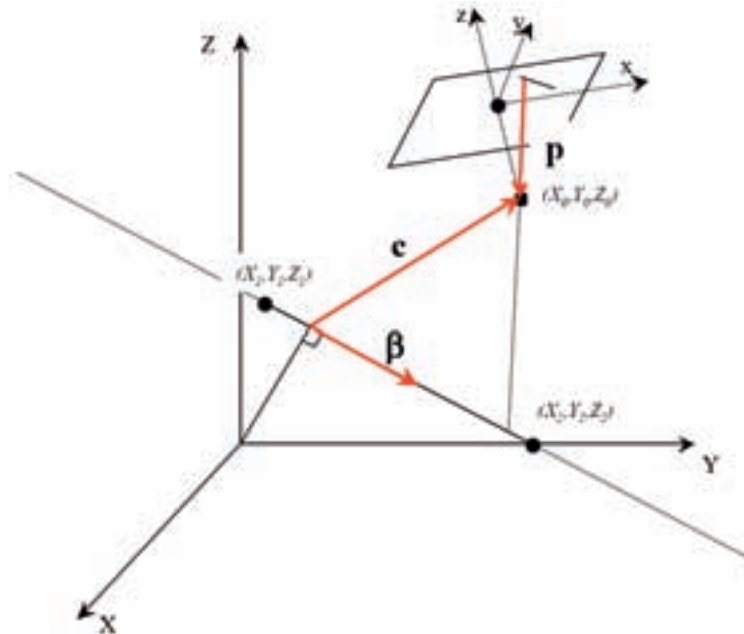


Figure 1. Linear features and coplanarity model.

Because it was required to transform laser scanning data into the original coordinate system of the aerial images, the reverse transformation was applied to the laser scanning data. The equations for the reverse transformation are described in Rönnholm et al. (2009). The complete workflow of the registration method is illustrated in Figure 2. Practically, all sub-parts of the registration method were automatic. However, our approach requires orientation parameters relatively close to the true ones in order to locate edge pixels representing roof ridges on the images. Therefore, in the beginning, a manual orientation was required, because the roof ridges projected using the initial orientation parameters were too far away from their true locations.

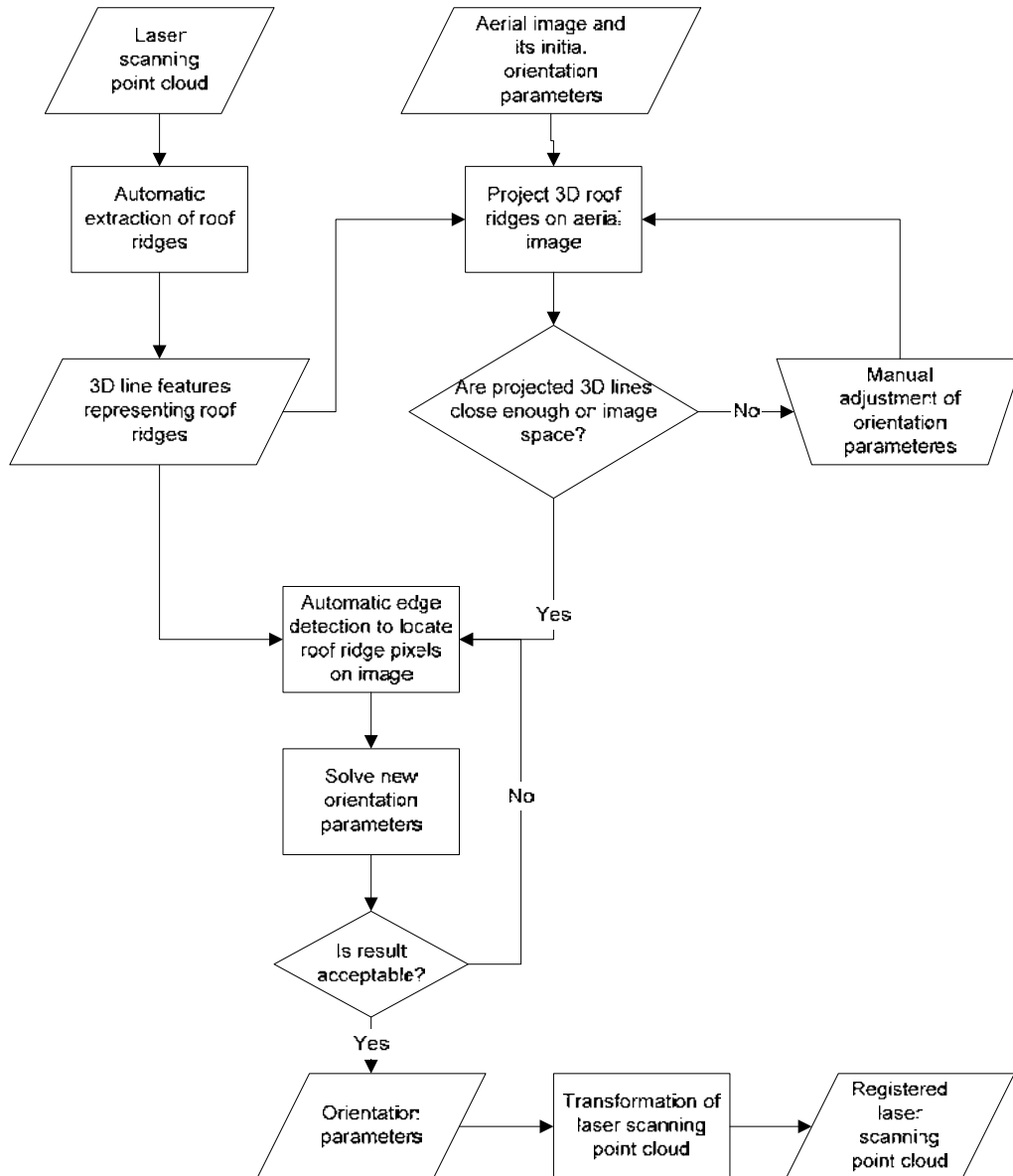


Figure 2. The workflow illustrating how to solve the relative orientation between laser scanning point clouds and aerial images and how to transform laser point clouds into the ground coordinate system, of the images.

Results

In Tables 1 and 3, the new exterior orientation parameters of the provided images are listed and Tables 2 and 4 illustrate how much the adjusted orientation parameters differ from the original image orientations. Orientation parameters in Tables 1 and 3 describe images in the same coordinate system as the laser scanning point clouds.

Adjusted EO parameters (using Leica ALS roof ridges as ground control features)						
PAN	Meters			Degrees		
Image-ID	X0	Y0	Z0	omega	phi	kappa
Espo...01~0013_pan	369156.476	6669525.320	539.653	-0.5297	-0.3890	-47.1337
Espo...01~0014_pan	369055.054	6669655.116	541.623	-1.0402	-0.3870	-47.1243
Espo...02~0013_pan	369543.722	6669930.703	568.467	0.6269	-0.4264	129.8300
Espo...02~0014_pan	369446.320	6670050.712	569.159	0.7526	-0.4487	129.8249

Table 1. Exterior orientation parameters of aerial images after adjustment. Case: Leica laser scanning data and panchromatic images.

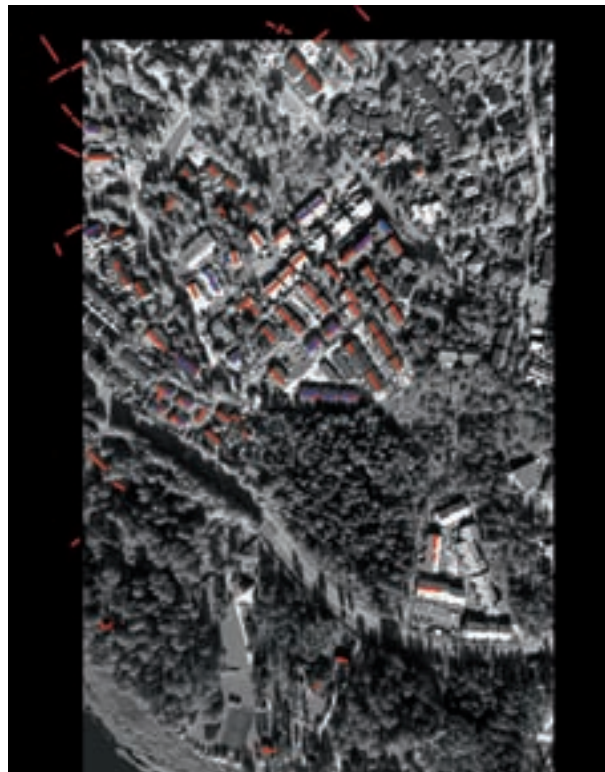


Figure 3. Laser-derived ridges are illustrated with red lines. Blue lines represent those ridges that have been used for registration.

Image-ID	Difference (Adjusted-Original)					
	X0	Y0	Z0	omega	phi	kappa
Espo...01~0013_pan	19.014	20.790	6.568	0.067	0.097	0.024
Espo...01~0014_pan	17.600	26.130	6.840	-0.489	-0.033	-0.088
Espo...02~0013_pan	18.587	19.926	6.288	0.163	0.037	-0.023
Espo...02~0014_pan	18.791	21.125	5.993	0.068	0.095	0.019
average	18.498	21.993	6.422	-0.048	0.049	-0.017

Table 2. Differences of adjusted exterior orientation parameters and the original ones. Case: Leica laser scanning data and panchromatic images.

Adjusted EO parameters (using Optech ALS roof ridges as ground control features)						
PAN	Meters			Degrees		
Image-ID	X0	Y0	Z0	Omega	phi	kappa
Espo...01~0013_pan	369113.487	6669522.386	507.066	-0.5882	-0.5101	-47.1941
Espo...01~0014_pan	369012.805	6669646.921	508.655	-0.5556	-0.4684	-47.0576
Espo...02~0013_pan	369501.881	6669927.720	536.654	0.5506	-0.4196	129.8550
Espo...02~0014_pan	369403.982	6670048.523	537.269	0.5474	-0.5368	129.8291

Table 3. Exterior orientation parameters of aerial images following adjustment. Case: Optech laser scanning data and panchromatic images.

Image-ID	Difference (Adjusted-Original)					
	X0	Y0	Z0	omega	phi	kappa
Espo...01~0013_pan	-23.975	17.855	-26.019	0.008	-0.024	-0.036
Espo...01~0014_pan	-24.648	17.935	-26.128	-0.004	-0.114	-0.021
Espo...02~0013_pan	-23.253	16.943	-25.525	0.087	0.044	0.002
Espo...02~0014_pan	-23.548	18.935	-25.897	-0.138	0.007	0.024
average	-23.856	17.917	-25.892	-0.012	-0.022	-0.008

Table 4. Differences of adjusted exterior orientation parameters and the original ones. Case: Optech laser scanning data and panchromatic images.

Discussion

This experiment revealed that an almost automatic process using linear features is feasible. However, there are also challenges to overcome. For example, it turned out that the orientation algorithm seemed to discard the majority of all possible 3D roof edges from the adjustment of the orientation parameters. The reason is probably that too high rejection threshold values were used in the outlier detection. Also, the quality of 3D lines extracted from laser scanning data varied. Particularly, more complex roof shapes may cause some error to extracted ridges. Therefore, lower threshold values for outlier rejection could have been used in order to get more edge points in to the adjustment. On the other hand, also the

lighting conditions affect the results of image-based edge detection. Moreover, laser scanning and image-derived roof ridges may not always correspond exactly. For example, a roof ridge might not be sharp but round, which may cause some vertical differences, because laser-derived ridges were always expected to be sharp. Figure 4 illustrates some examples of superimposed laser-derived ridges following registration.

In this experiment, co-registration was carried out for a single image at a time. It can be expected that block adjustment with image-to-image tie points would most likely increase the achievable accuracy. At the moment, the quality of final registration depends highly on the number of successfully located roof ridges and the distribution of line features. Ideally, the line features should be distributed evenly around the frame area and there should be line features in all orientations (using all near parallel lines only would not be an ideal situation). The advantage of the method is in its automatic nature. Moreover, the method seemed to be fast, and near real-time processing is achievable given that 3D line features are calculated in advance. It is recommended that the quality of the registration results is separately verified, for example, by inspecting the result visually. If the initial orientation parameters are too far away from the true ones with respect to the width of the digitized intensity profiles, the algorithm is not able to find correct orientation and manual adjustment is required.



Figure 4. Examples of how laser-derived ridges correspond with aerial images after registration. Left image: good alignment. Right image: Some differences are detectable.

References

- Acka, D., 2007. Matching of 3D surfaces and their intensities, *ISPRS Journal of Photogrammetry and Remote Sensing*, 62(2):112-121.
- Habib, A. F. and Alruzouq, R. I., 2004. Line-based Modified Iterated Hough Transform for Automatic Registration of Multi-source Imagery, *The Photogrammetric record*, 19(105):5-21.
- Karjalainen, M., Hyypä, J., Kuittinen, R., 2006. Determination of Exterior Orientation Using Linear Features from Vector Maps. *The Photogrammetric Record* 21(116), pp. 329 - 341.

Mulawa, D. C. and Mikhail, E.M., 1988. Photogrammetric treatment of linear features, *International Archives of Photogrammetry and Remote Sensing*, Volume XXVII, Part B3, p. 383-393.

Rönnholm, P., H. Hyypä, J. Hyypä, and H. Haggrén, 2009. Orientation of Airborne Laser Scanning Point Clouds with Multi-View, Multi-Scale Image Blocks. *Sensors*, 9, pp. 6008-6027.

Sonka, M., Hlavac, V., and Boyle, R., 1993. *Image Processing, Analysis and Machine Vision*, Chapman & Hall, University Press, Cambridge, ISBN 0-412-45570-6, 555 pages.

Tommaselli, A. M. G. and Tozzi, C. L., 1996. A recursive approach to space resection using straight lines. *Photogrammetric Engineering & Remote Sensing*, 62(1): 57–66.

Report of the Independent Research Group on Geospatial EuroSDR "Registration Quality – Towards Integration of Laser Scanning and Photogrammetry"

Dr. Amir Saeed HOMAINIJAD
Independent Research Group on Geospatial, Tehran, IR IRAN
s_homain@yahoo.com

Image Registration based on Image Splitting and Pixel Registration

Abstract

A novel approach to image registration will be explained. The approach has been developed and created in response to illuminate typical errors which traditionally are part of images such as lens distortions and relief displacement, and provides a robust and reliable output. The output has versatile applications in mapping, visualisation, thematic map, classification, etc. Using this approach, images were initially split into sub areas based on geometry of an object and topography of terrain. Then sub areas were registered pixel by pixel on a 3D model of laser scanning data. Two sets of laser scanning data (individually and combined) were utilised in this approach and their results were analysed. The result is that point clouds data and pixels of image were transferred to points which have X, Y, Z coordinates and colour values. Indeed, with this approach raster images were converted to vector and transferred to 3D spaces of laser scanning data or DTM. The output is free of image distortions and has map characteristics.

Keywords: Digital Image, Laser Scanning, Transformation, Ortho-image, DTM

1. Introduction

1.1. Definition

Data fusion or data merging is a part of digital image processing aimed at providing an accurate and precise output from a number of images of terrain which were acquired with a sensor at different times, or images acquired with different sensors simultaneously or at different times. According to Zitova and Flusser (2003) data fusion consists of the following processing; object detecting, matching, transform model estimation, and image resample and transformation.

1.1.1. Object Detecting

Image analysis for object detection is achieved within two broad categories of feature-based and pixel-based methods. The feature-based method concentrates on the geometric appearance of features; in contrast, the pixel-based method focuses on pixel values. Each of these methods its advantages and is utilised for a specific propose. For fast object detection especially in real time, a feature-based method

is preferred rather than pixel-based method. For example, Viola and Jones (2001) employed a feature-based method along with encoding ad hoc domain knowledge for fast object detection. They develop a method of object detection based on Haar-Like feature and AdaBoost approaches. AdaBoost was utilised for image classification and employment of Haar-Like feature was carried out for object detection. Their study concerned the detection of a human eye from a grey level video footage in real time.

The task of automated feature extraction, particularly in real time video imagery, goes back many years. For example Ruetz and Brodersen (1988) applied vertical and horizontal edge detection masks for extracting features in real time from video footages, or Tomita (1988) developed Interactive Modelling and Automatic Recognition System (IMARS) to automatically recognise an object with minimum knowledge of image processing algorithms.

Since the early 80s when CCD cameras have been employed in photogrammetry, particularly in close range photogrammetry, automatic object detection methods have been developed and employed in order to automate the whole or part of photogrammetric processing. For example, Förstner and Gülch (1987) applied the Förstner operator for detecting points from images for digital image matching. The Förstner operator is a commonly applied operator for object detection for many years. For example, Rongxing Li and Kaichang Di (2007) employed the Förstner operator for detecting interest objects in their study for matching of Mars Stereo images using the Cross Correlation method. However, Jazayeri and Fraser (2008) claim that the FAST operator is more optimal interest operator for close range photogrammetry rather than the Förstner operator.

The objective of pixel-based image segmentation is to automatically categorise all pixels in an image into themes, or to cluster pixels into salient image regions. In this method, a group of pixels where their intensities are within a range of threshold will be clustered and a particular intensity value will be assigned to them for discrimination from other pixels. For example, Vogelmann and Rock (1989) utilised pixel-based image segmentation method on five bands of Landsat TM for detection of forest damage caused by the pear thrips. Bosch et al (2008) classified a range of images according to probabilistic Latent Semantic Analysis (pLSA) in order to classify each image to defined images which were labelled such as forest, river, coastal, etc.

1.1.2. Matching

Automatic digital image matching is a distinctive task in digital image processing and pattern recognition, particularly in digital photogrammetry since the early 1980s, and is categorised in two broad groups of area-based and feature-based matching. Area-based matching aims at extracting a pixel in left image and its corresponding pixel in the right image according to the pixel intensity as Eq 1 describes.

$$I_L(X_L, Y_L) + n(X_L, Y_L) = I_R(X_R, Y_R) \quad (1)$$

Where $I_L(X_L, Y_L)$ and $I_R(X_R, Y_R)$ are the intensity values of corresponding pixels in the left and right images, and $n(X_L, Y_L)$ is noise causing a difference between two corresponding pixels. To detect a corresponding pixel on the right image, a window sweeps the right image and values of pixels inside the window are evaluated according to Eq.1 in order to find the corresponding pixel. Mustaffar and Mitchell (2001) by transforming the detected pixel to the origin image improve the area-based matching; however, their method is very dependent to initial pixel detection, window size, and the transformation's mathematical modelling. Shimizu and Okutomi (2005) developed a method of sub-pixel estimation from an image pair for improving the accuracy of area-based matching.

The objective of feature-based matching is to extract a feature from an image which is stable in the course of viewpoint and match its corresponding attributes to the feature on the source image. Features consist of edges, intersections points, corners, and line segments. There are a number of feature detection operators which can be carried out for object detection. For example, edges can be extracted by an edge detection operator such as Canny edge detector (Canny 1986), or corners and intersection points can be detected by one of the point detectors such as the Förstner operator. The detected objects in an image pair have to be evaluated in order to make the best match, in this regard; Maas (1996) implemented an epipolar lines method for matching the extracted points within left and right images and Homajnejad (1997) applied a mathematical transformation model to match two corresponding points.

1.1.3. Transform Model Estimation

Transform-model-estimation aims at finding the parameters of orientation of an image with the original image, a map, a 3D model from object and terrain, or object and terrain themselves. The parameters and mathematical model will be defined according to a proposed strategy on image transformation, and consequently the number of Control Points (CP) has to be calculated. CPs are required to obtain the parameters of orientation but the location and coverage of CPs has to be selected very carefully in order to achieve an optimal precision. Equations 2, 3, and 4 describe three different mathematical models of image orientations.

$$\begin{aligned} U &= s (x \cos (\phi) - y \sin (\phi)) + t_x \\ v &= s (x \sin (\phi) + y \cos (\phi)) + t_y \end{aligned} \quad (2)$$

$$\begin{aligned} U &= a_0 + a_1 x + a_2 y \\ V &= b_0 + b_1 x + b_2 y \end{aligned} \quad (3)$$

$$\begin{aligned} U &= \frac{a_0 + a_1 x + a_2 y}{1 + c_1 x + c_2 y} \\ V &= \frac{b_0 + b_1 x + b_2 y}{1 + c_1 x + c_2 y} \end{aligned} \quad (4)$$

In order to obtain the parameters of the above equations, at least two, three, and 4 control points are needed respectively.

1.1.4. Image Resampling and Transforming

Re-sampling is the digital process of changing the sample rate or dimensions of digital imagery by analysing and sampling the original data. Basically, re-sampling is an important process in digital image processing and computer graphics to resize, convert, render, and transfer digital images. Figure 1 demonstrates a typical process of re-sampling.

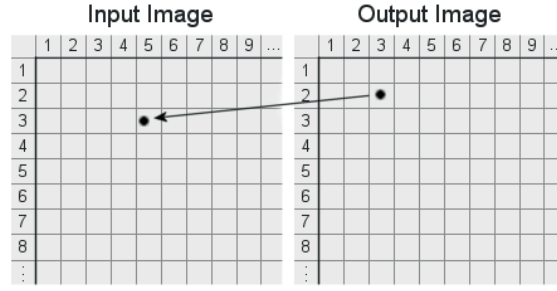


Figure 1: Demonstration of typical process of image re-sampling.

Re-sampling based on precision maybe divided into seven methods of Nearest-Neighbour, Bilinear Interpolation, Cubic Convolution, Cubic Spline (Direct Computation), Cubic Spline (Using FFT), Radial Function with local support, and Gaussian (using FFT). The re-sampling equation generally follows a two-dimensional polynomial as Eq 5 describes.

$$f(x, y) = \sum_{i=-a}^b \sum_{p=-a}^b \sum_{j=0}^{n-1} \sum_{q=0}^{n-1} K_{i,j,p,q} t^j s^q f_{\alpha+i, \beta+p} \quad (5)$$

Where:

$$K_{i,j,p,q} = k_{i,j} \times k_{p,q}$$

Dodgson (1992) gives a comprehensive address on re-sampling as well as details on the above equation.

Besides conventional applications of re-sampling such as image transformation, image rendering, and image registration; a number of studies have implemented re-sampling for motion and depth estimation, or object tracking, or recognition of a 3D shape, or object detection. For example, Xiong et al (2005) implement re-sampling techniques in rendering images for scene depth recognition in real time. Zöller and Buhmann (2007) utilised an unsupervised method of Parametric Distributional Clustering (PDC) for image segmentation along re-sampling technique for object recognition. Charif and McKenna (2006) employed Sampling Importance Re-sampling (SIR) filter for object tracking. They implemented SIR versus Iterated Likelihood Weighting (ILK) to find a robust method for object tracking in real time. In their study, they reached the result that SIR has high variance and poor approximation in accuracy, but ILK has good accuracy on object tracking and low variance. Crowley and Stern (1984) utilised re-sampling techniques in order to speed up the process of Difference of Low-Pass transform for bandpass image matching.

1.2. Approaches

The operation of multi-temporal merging aims at merging two or more images which are acquired by a sensor at different times for improving classification. For example, Allen (1990) carried out a study for NASS on the monitoring of crops of cotton and rice of part of the USA and utilised a Landsat TM image and eight SPOT images from the study area. This study, in general, was implemented on the combination of multi-temporal merging and change detection and multi-sensor image merging

operations, but the study area was reduced in order to a sub area that was acquired by SPOT in different times for implementation of multi-temporal merging operation. Mattia et al (2009) utilised 11 L-Band SAR images which were acquired from a European agricultural area within the period of April to July 2006. Their study's outcome was to develop an algorithm to retrieve the moisture of land from multi-temporal L Band SAR images. Almeida-Filho et al (2007) utilised multi-temporal L Band SAR images for detecting deforestation. McCauley and Goetz (2004) utilised Landsat TM images from an area of Montgomery, County, Maryland UAS for discrimination of residential areas from commercial and industrial and agricultural areas and providing data for residential mapping. They registered the classified image on a digitised map from the same area to produce a residential map from the study area.

Change detection procedures have the objective of monitoring a process of natural phenomena or manmade objects over a period of time by implementing a multi-temporal data set. El Hajj et al (2009) utilised images of SPOT 5 time series for monitoring the growing of sugarcane harvest. They implemented Fuzzy Interface System (FIS) for classifying input data. Montesano et al (2009) studied vegetation cover changes in Eurasia and North America. They Utilised Quickbird imagery in Google Earth to validate and assess MODIS Vegetation Continuous Fields (VCF). Anderssohn et al (2009) applied least-squares adjustment on 65 Envisat IM and WSM images which were acquired within the period of 2003 to 2008 from the Altiplano-Puna plateau of the Central Volcanic Zone of the Andes between Chile and Argentina for defining surface deformation in this area. They combined the IM and WSM images for achieving maximum result. Le Hégarat-Masclé et al (2005) monitored South East France's forest as well as agricultural watershed in Saône (France) by implementing a method of change detection on the Course Resolution SPOT/VGT-S10, SPOT/VGT-P, and NOAA/AVHRR data. For forest monitoring, they classified a HRV/SPOT5 (2003) and simulated on the CR images and using iterative estimation method they detected the changes. And for agricultural purposes, they utilised the database which was obtained from NOAA/AVHRR images during the period from 1988 to 2003, and implemented SPOT/VGT-S10 and SPOT/VGT-P for change detection. They implemented the unsupervised method for classifying S10 and P images and detected the changes using iterative t estimation. To avoid errors they used the t_{i-1} output as initial information for t_i iterative.

Multi-sensor image merging aspires to fuse different terrain images which were acquired by different type of imaging systems to improve the output. In the medical field, image registration has a very wide application in diagnosing and identifying different type of cancers, organ failure, tumour growth, etc. and it provides a powerful tool for detecting early signs of illness (Yanovsky 2009). Earlier, Maintz and Viergever (1998) gave a comprehensive survey of various types of the image registration in medical field. Walimbe and Shekhar (2006) presented an algorithm for automatic elastic registration of 3D medical images. Elastic registration refers to techniques of recovering of non-rigid mismatches between different images. They implemented their algorithm on 15 Computed Tomography and Positron Emission Tomography (CT-PET) pair images which were acquired from whole body. Wu et al (2004) developed a method for automatic registration of images which were acquired by Magnetic Resonance Spectroscopy Imaging (MRSI) and Magnetic Resonance Imaging (MRI) for detecting prostate cancer. Their aim was to refine acquired images which were deformed during the imaging process or, better to say, that prostate was moved during the imaging process.

Producing a synthetic stereoscopic image generated by simulation of DEM or topographic map and airborne or spaceborne images such as Landsat, SAR, etc, is one of the applications of merging image data with ancillary information. This is a technique to allow interactive exploration of a 3D environment with stereoscopic depth cues. Utilising this technique in remote sensing gives an outlook to images for accurate interpretation and scene analysis. For example, Dean et al (1982) superimpose the thermal and SAR images which were acquired from Pilgrim Springs, Alaska to study thermal anomalies and structural elements of the area, and Lu et al (2004) combined a DEM with SAR and

Landsat images for mapping lava flows at Westdahl volcano, Alaska. As providing a stereo image from Landsat or SPOT images is not practically applicable, and as stereo imagery can provide the benefit of analysing a landscape or topography of a region, Salvi (1995) produced a synthetic Stereoscopic image by combining Landsat-5 TM and a 1:25,000 DEM from Velino-Sirente, Italy for geological purposes to study fault scrap in this area. Berthier and Toutin (2008) compared a DEM derived from SPOT 5 HRS and a DEM derived from Shuttle Radar Topographic Mission (SRTM) which were obtained from North-West Canada and South-East Alaska.

Integration of spaceborne and airborne data in GIS is another application of data fusion and a number of studies have focused on this area of data fusion. For example, Abdallah et al (2005) integrated a number of data retrieved from various resources such as topographic map, rainfall map, geological map, soil map, and remote sensing data (SPOT 4 data) from north of Lebanon in a GIS overlay to study the mass movement of ground in this area. Generation of a model from global change phenomena with GIS was one of the objectives of Hastings and Di's (1994) research. They integrated NOAA's data base data related to global change in a GIS to provide the model. Ballester et al (2003) implemented a GIS data base and Landsat 7-ETM images to investigate the effect of land-use in Amazônia on the ecosystem of this area.

Despite the methods explained above, there is diversity in implementation of image registration base on the diverse studies. The main objective of remote sensing and photogrammetry from image registration is to orient images with the terrain and object; consequently most studies in these areas have concentrated on obtaining the parameters of orientation for image transformation. Buiten and Putten (1997) studied a mathematical solution for reducing residuals from the following equation (Eq. 6). The residuals (u , and v) at any point on the image represent the amount and direction of the image which didn't match with the next image at that corresponding point.

$$\begin{aligned}x &= a_1 + a_2X + a_3Y + a_4X^2 + a_5XY + a_6Y^2 + u \\ y &= b_1 + b_2X + b_3Y + b_4X^2 + b_5XY + b_6Y^2 + v\end{aligned}\tag{6}$$

They this report a novel approach of registration of an aerial digital image on Laser Scanning data is presented. The approach focused on registration of each pixel of the digital image on its corresponding point in the Laser Scanning Data. In order to achieve the aspects of the proposed method, the digital image was split into small areas according to the geometry of object and terrain, and then pixels of each small part were individually registered on corresponding points on a 3D space. This approach has advantages in comparison with methods which were discussed above, and latter will be mentioned in this report. The organisation of this report includes the following chapters. The next chapter will explain the proposal and the methodology for implementing the proposal. Chapter 3 will give details on the study area and technical information. The evaluation of output along with data analysis will be given in Chapter 4. Finally, Chapter 5 will provide a summary and conclude the report.

Photography, at the heart of photogrammetry, is the art of creating still or moving pictures from objects and follow the central projection law, and captured pictures from objects are laid from the centre to the sides according to this law. In addition if an object has depth or height, its image will have had the third dimension which is called relief displacement (Figure 2). The relief displacement is one of the issues in photogrammetry which reduce the reliability of the final product of an ortho-rectify-image process; however, there are a number of methods for improving this issue but none of those methods are able to eliminate this issue. Figure 3 is a very good example of the result of this issue on an orthorectified image. With implementing digital images in photogrammetry, the application of ortho-image and ortho-rectify-image has been significantly raised. On the other hand, a digital image represents a restricted area array and has a limitation for its physical shape. However, one of the

advantages of digital imagery over film-based photos is its physical stability. In contrast to film-based photos, dimensions of a digital image are always constant and will not be deformed. Therefore, the output of image processing is also a digital image which has a restricted area array. Assuming an image acquired over flat terrain, image processing and image transformation of the image is successful because there is no relief displacement issue in the image. In contrast, an image acquired over a rough area which includes objects with significant height and depth, the image processing and transformation is not simple and the output will be affected by relief displacement.

2. Proposal and Methodology

2.1. Proposal

Photography, as the heart of photogrammetry, is the art of creating still or moving pictures from objects and follow central projection law, and captured pictures from objects are laid from the centre to the sides according to this law. In addition if an object has depth or high, its image will have had the third dimension which is called relief displacement (Figure 2). The relief displacement is one of issues in photogrammetry which reduce the reliability of final product of an ortho-rectify-image processing; however, there are a number of methods for improving this issue but none of those methods are able to eliminate this issue. Figure 3 is a very good example of remaining of this issue on an ortho-rectify-image. With implementing digital images in photogrammetry, the application of ortho-image and ortho-rectify-image has been significantly raised. In other hand, a digital image is a restrict area array and has a limitation for its physical shape, but, one of the advantages of digital image over film-based photo is its physical stability. In contrast of film-based photo, dimensions of a digital image are always constant and will not be deformed. Therefore, output of an image processing also is a digital image which has a restrict area array. Assuming there is an image which acquired from a flat terrain; so image processing and image transformation of the image is much unadorned because there is no any relief displacement issue on the image. In contrast, if there is an image which acquired from rough area which includes objects with significant heights and depths the image processing and transformation is not simple and the output will be affected by relief displacement issue.

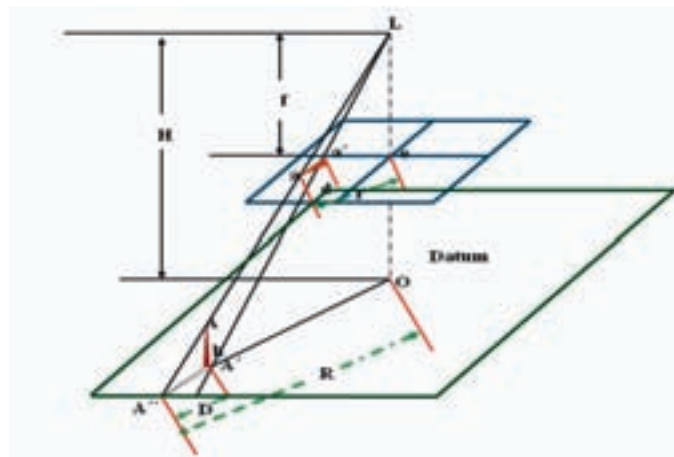


Figure 2: As can be seen the increase in elevation of AA' causes its image on the perspective plane (aa') to be replaced outwards from principal point.



Figure 3: An ortho-image from the centre of a city with high raises rise buildings. The relief displacement clearly can be clearly seen. The highlighted building leans to towards the next building and its side can be seen.

An image orientation to the terrain is initially required before image transformation. A number of GCPs must be defined on the image and the terrain, in order to obtain the parameters of orientation; also GCPs are required for image transformation. Regardless of the mathematical model employed for image transformation, the transformation algorithm will transfer the whole of the image at once; so GCPs must cover the whole of the image and make a good balance according to the topography of terrain. It has to be mentioned that the transformation of an image at once causes a deformation of the final output to some extent because the terrain has 3D shape and the image is a 2D plane and the transformation will transform a 2D plane to a 2D plane according to a 3D model.

A proposal for this project has been given according to the knowledge about the strengths and weaknesses of image processing, digital imagery, laser scanner, data fusion, and also according to the aspects and objectives of this project. The theme of this project was initially proposed by EuroSDR in order to find a method of fusing an aerial photograph and laser scanning data which can reduce land surveying practice for pre-processing and post-processing of data fusion, and the requirement of Ground Control Points in the terrain, thereby increasing the reliability and precision of the final output. The final output of this project is an ortho-rectify-image which will be obtained by fusing an aerial photograph on laser scanning data. Despite other methods which fulfil image processing and transformation on the whole of the image at once, in this project, it is proposed that the image will be split into small areas according to geometry and topography of the terrain and each sub area will be separately and individually transferred to the corresponding part in the laser scanning data. It should be mentioned that each sub area will not be transferred at once; hence, some distortion will remain. Therefore, each sub area will be transferred pixel by pixel and each pixel transferred individually. This means the parameters of transformation for each pixel will be different. Each pixel will be transferred on a 3D model and will be converted to vector mode. The transformed pixel is not a pixel; indeed it will be a dot which has three coordinates (X, Y, Z) and three values of (RGB). The transferred image is a collection of point clouds in a 3D space. There are a number of advantages to utilising this method over other methods of transformation. For example, by utilising this method the issue of relief displacement and other image distortions will be eliminated. The output is a vector model of higher resolution than an image. The output data can be easily utilised in visualisation, and a visualised model is more accurate than other methods of visualisation. This method can be used to fuse any image on a 3D model such as DTM, DEM, and DSM as well as laser scanning data.

The origin of a digital image is located in the top left corner of the first pixel on the left of the first row (Figure 4) and X accumulates from top to down and Y accumulates from left to right. In this project the origin of the image is selected to be the centre of the first pixel on the left of the first row and the top of first column, because it was an attempt to make a mathematical relationship between the centre of a pixel and a dot.

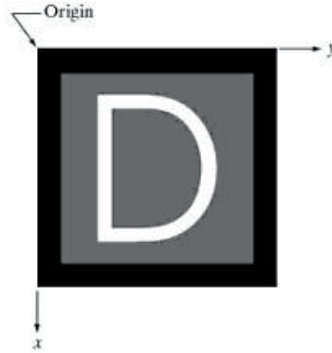


Figure 4: The origin of the image is located in the top left corner of the image, the Y accumulates increases from left to right, and x accumulates from top to down.

The following steps have been designed for fusing an aerial photograph with laser scanning data.

1. Retrieve laser scanning data on a 3D model.
2. Split the aerial photo into small areas according to geometry of the object and the terrain topography .
3. Detect the corresponding small area in the 3D model.
4. Transfer each pixel of small area individually to the corresponding point in the 3D model.

2.2. Methodology

The methodology for implementation of the proposal will be discussed in this section. An image represents a central projection of an object on a plane. The presence of the object in the image is very much dependent on the direction of viewpoint. Usually, a single image from an object cannot clearly identify the object because the object could be occluded by other objects and some areas and boundaries are hidden. There are several studies in computer vision and pattern recognition for matching an image with its 3D model. The main idea is to extract the boundary of an object or a pattern from the image and use a transformation approach and a defined database or generic algorithms to match with the corresponding boundary or pattern in the 3D model. Lamdan and Wolfson (1988) applied an approach for matching occluded images of objects to their corresponded 3D models. Their approach consisted of two steps. The first step was to provide an initial database from objects. Then in step 2, they transferred extracted boundaries for matching with the corresponding boundary on the 3D model according to provided database. Niblock et al (2007) developed a method based on model-based matching to match an airport's band's lights for assisting landing aircraft. Nashida (1995) developed a method of model-based shape-matching for recognising handwriting. Stevens and Beveridge (1997) developed an approach of 3D matching of extracted targets from multi sensor images with a 3D model according to defined models. Similarity, Liu et al (2001), Cesar Jr. et al (2005), Grosky el al (1992), Henikoff and Shapiro (1993), Chang and Leou (1992), Gérard, and Gagalowicz (2000) have developed approaches for model-based matching to match extracted patterns from images to defined models.

Tsang and Yu (2003) developed a generic algorithm for model-based matching. In their approach they transferred the extracted patterns from an image to a model space according to the developed generic algorithm.

In this project for implementing the registration of the extracted features or patterns from aerial photographs on laser scanning data the following practices have been fulfilled. Initially, the aerial image was oriented with the laser scanning model. In this part of image registration, parameters of translation, scale factor and rotation angle around the Z axis (κ) were considered (Eq 7). Then, the extracted feature or pattern was refined. The refining process consisted of omitting some parts which caused to distort the output such as relief displacement. The developed algorithm would apply a special filter along a logical assessment to define these areas. Then, the refined patterns and features were transferred to the space of laser scanning space according to Eq. 7. In this step, the extracted pattern or feature would be matched with the corresponding pattern on the laser scanning data according to a developed algorithm. The algorithm would assess each extracted patterns or features with the corresponding patterns on the laser scanning data and would find the optimum parameters in order to fit the corresponding extracted patterns.

$$\begin{bmatrix} x_t \\ y_t \\ z_t \end{bmatrix} = \begin{bmatrix} x_s \\ y_s \\ z_s \end{bmatrix} + sR_\kappa \begin{bmatrix} x_i \\ y_i \\ z_i \end{bmatrix} \quad (7)$$

Point uncertainty was the main issue which affected the accuracy of output. As the accuracy of output is very much in the range of the accuracy of the laser scanning data, the point uncertainty is always on the part of point clouds. There are different approaches for refining the point clouds, but refined point clouds include these errors. If a set of data with higher accuracy and precision was available the accuracy of output was much higher. The author is implementing a similar project for transferring a very poor image to very high accuracy surveying data. The accuracy of first transferred data indicated that the output is very much dependent on the accuracy of the host data and not on the accuracy of the slave data (image). The report relating to the latest study will be published very soon. In chapter 4 the accuracy of the output will be analysed.

3. Study Area and Technical Information

The test area is located in Espoonlahti (approximately 60° 8'N, 24° 38'E) in the southern part of Finland. The area can be characterized as a low residential urban area having mainly terraced and detached houses with multistorey buildings and apartments in some areas.

Additionally required and applicable data were provided such as photographs orientation parameters and GCPs.

GCPs were measured using real time kinematic (RTK) GPS and some of the GCPs represent cornices of roofs.

Laser Scanning images were acquired with Optech ALTM 3100 and Leica ALS50-II scanners during 2005 and 2007. Technical details of imagery systems and camera are presented below.

Optech ALTM 3100

Scanning angle 24 degrees, 20 degrees is processed ($\pm 10^\circ$)
PRF 100 kHz
Scanning frequency 67 Hz
Flying speed 75 m/s

Leica ALS50-II

Scanning angle 40 degrees ($\pm 20^\circ$)
PRF 148 kHz
Scanning frequency 42.5 Hz
Flying speed 72 m/s

DMC Photogrammetric Images

Pixel depth	16 bit
Size	13824x7680
ground resolution	5 cm
Forward overlap	60%
Side Overlap	20%

Interior Orientation

Focal length: 120.0000 mm (10000 pixels)
Principle point (differences from the image centre):
Px=0.000 mm
Py=0.000 mm
Pixel size: 0.012 mm
Image size: 13824x7680 pixels (165.888x92.16 mm)

4. Implementation of Proposal and Assessment of Output

4.1. Implementation

Before discussing the implementation of the proposal and the assessment of output, it should be mentioned that all programs and algorithms for this project were developed by the author in VC++ and VBA. It was assumed that radiometric and geometric corrections were applied to the provided Laser Scanning data and there was no requirement for further correction. In the first step more than 6 million point clouds, acquired by Leica ALS50-II and Optech ALTM 3100 were retrieved and captured, and put on a 3D model (Figure 5). Then the aerial photographs were captured and processed for splitting into small area according to the geometry of the object and topography of the terrain (Figure 6). The DMC camera is able to acquire panchromatic and multispectral images. The panchromatic consists of four CCD areas which mosaic and a large area image and multispectral consists of red, green, blue, and infrared sensors (Figure 7). In this project, the panchromatic and colour images were used.



Figure 5: Demonstration of captured Leica and Optech point clouds on a 3D model. The Optech's point clouds show in blue colour and Leica point clouds show in yellow colour.



Figure 6: demonstration of typical splitting image to sub area according to geometry of object.

The coordinate system and datum of both point clouds acquired by Optech and Leica were initially transferred and matched with the coordinate systems provided by EuroSDR. Aerial photographs were transferred to Optech, Leica, and a combined model of Optech and Leica data. There were small differences between Optech and Leica data as well as the presence of some gaps between each of the scanning data, so the combined data would represent an integrated data which can improve the output.

The following figure shows a typical installation of the DMC system in an aircraft.

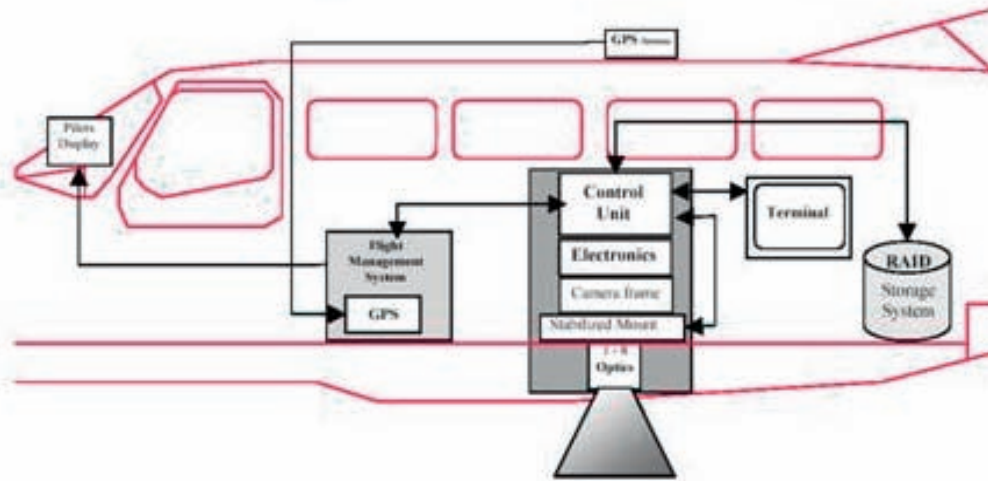


Figure 7: DMC configuration (Figure is derived from Intergraph website).

In this study, laser scanning data are considered as topographic data which has some photography attributes such as intensity values. Therefore, it is an understanding in this project that each point cloud has an individual identity and differs from other points even those points are in the neighborhood. On board GPS and IMU help to find the parameters of orientation as well as coordinate system and datum for each laser scanner. It is an assumption that geometric and radiometric corrections were initially given to all provided laser scanning data by EuroSDR and there is no requirement for further correction; however, after investigation it was found that some intensity values exceed the limit value; consequently those data were removed.

As was mentioned earlier there was a differences between coordinate system and datum of two Optech and Leica laser scanning data, and in order to have a unique coordinate system, it was required to transfer those coordinate system and datum to provided coordinate system and datum. In addition, Leica data has small gaps over the whole of the terrain and this is a drawback of using this data and it was necessary to create some points for that area which reduce the reliability of the outcome of the project. In contrast, Optech data has good coverage of the terrain and there are no gaps between data; however, there is not full coverage of Optech data over the Leica data. A combined 3D model from two data sets is a precise 3D model because the whole of terrain is covered by point clouds. Also as was mentioned earlier, in this study each point cloud has an individual identity that means each point cloud presents an individual point on a 3D space and there is very low likelihood that two Laser scanners acquire a specific point on an object. If there is a requirement of having a specific point on an object on two 3D models, it needs to construct the surface on that area and then extract the point. Figures 5 show an area on two 3D models, for example building “A” can be recognised in two 3D models. According to the earlier explanation, “c” one of the corners of building is in different location with its corresponding point “c” on the figure 5, because a number parameters such as time of flying, position of laser scanning at time of acquiring, swing angle of laser scanners, rate of pulse signal, etc of two laser scanners cause this difference in location.

The implementation of the project consists of the following steps:

1. Transferring the Optech and Leica coordinate systems to provided coordinate system,
2. Retrieve Optech data in a 3D space,
3. Retrieve Leica data in a 3D space,
4. Retrieve combined Optech and Leica data in a 3D space,
5. Split the colour DMC image according to the geometry of the object and topography of terrain,
6. Split the DMC panchromatic image according to the geometry of the object and terrain,
7. Initially transfer aerial photographs according to Equation 7,
8. Define corresponding areas on the 3D models,
9. Transfer sub area of the colour image to the Optech 3D space pixel by pixel,
10. Transfer sub area of the colour image to the Leica 3D space pixel by pixel
11. Transfer sub area of the colour image to combined 3D space pixel by pixel
12. Transfer sub area of the panchromatic image to the Optech 3D space pixel by pixel
13. Transfer sub area of the panchromatic image to the Leica 3D space pixel by pixel
14. Transfer sub area of the panchromatic image to the combined 3D space pixel by pixel

A combined 3D model from two data sets is a precise 3D model because the whole of the terrain is covered by point clouds. Figure 8 shows the 3D model from Leica data which are captured by yellow colour and the small gaps can be recognised clearly, Figure 9 shows the same area in Optech 3D model, and there are no gaps between data and it has very good and balanced coverage by Optech data from the area. Combined data (Figure 5) has a good coverage over the area and there are no gaps between data. An area which is on both DMC panchromatic and colour image as well as Optech and Leica 3D models was chosen which has a maximum distortion due to relief displacement and lens distortion (Figure 10). This area was located near the edge of the aerial photograph and precisely chosen for the implementation of the proposal. The main reason for choosing this area was to test the proposal aspects. The area includes multistorey buildings with car parking and park areas. The chosen area from DMC colour and panchromatic photographs were individually transferred to Optech, Leica, and combined 3D models. Outputs of transformed images are 3D models of point clouds (Figures 11 and 12). As was explained, each pixel after transferring is converted to a point that has three coordinates of X, Y, Z and three values of Red, Green, and Blue. Indeed, the outputs look like an image. The output of colour and panchromatic photographs on Leica 3D model has lower accuracy than outputs from transferring colour and panchromatic photographs on Optech and combined 3D models because there are no gaps between Optech data and Optech data acquired more details from the terrain and object. The coordinates of some distinct points on Optech and Leica 3D models are very close to each other and their differences are less than tolerance errors of Optech and Leica. Especially, planar coordinates are in the range of the tolerance, but the Z value for some special points is relatively different. For example the Z values on top of pipes on the building “A” derived from transferred colour and panchromatic images on Leica 3D models are one meter less than Z values of the same point on transferred colour and panchromatic images on Optech and combined 3D models. These differences mostly related to Leica data, because there are too many gaps on Leica data and Leica data couldn’t acquire all area, and some very small objects were missed by Leica data acquisition. In contrast, Optech was able to acquire small objects and so the final output from transferring the photographs on Optech and combined 3D models have more precise. If the trees and bushes are investigated, it can be realised that very good coverage is available from trees and bushes, and this enabled us to develop a 3D visualised model from trees without having terrestrial data. 3D visualised model from buildings is possible but for more detail and precision, terrestrial data is required.

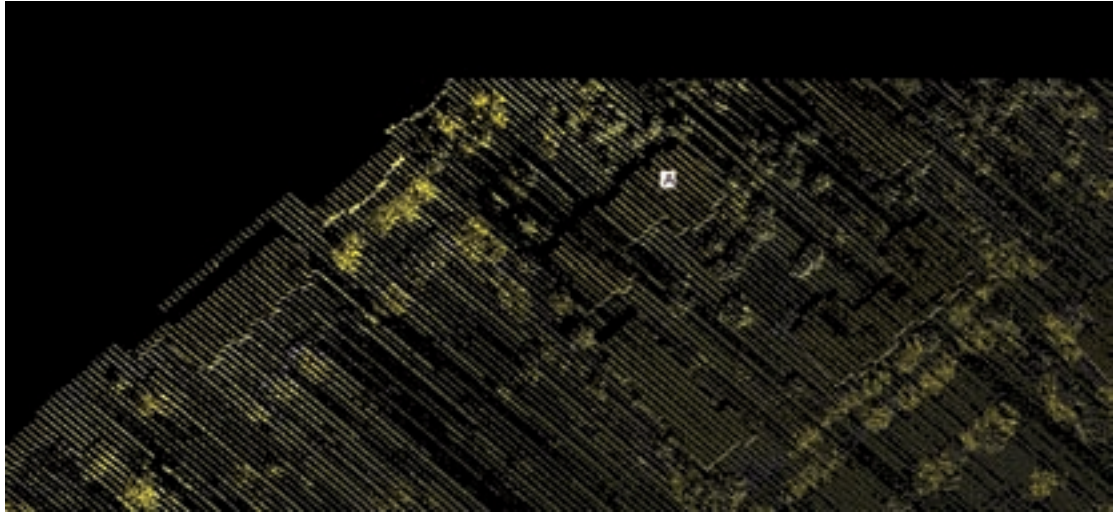


Figure 8: 3D model of Leica point clouds. Some gaps between data in this area can be seen.

Figure 13 demonstrates the 3D view of transferred colour image on combined data. The figure shows all captured points from south to north view. The figure shows the building roofs with some rooftop equipment, trees and small bushes, and ground. This is a very interesting presentation from the terrain and it enables us to visualise the 3D model. Certainly, if a terrestrial point clouds and images from building and area are available, the visualisation is more accurate and more details can be captured and present on the 3D visualised model. This approach has some advantages and issues. Illuminating lens distortion and relief displacement is the most important advantage. Figures 11(a), 11(b), and 11(c) show the buildings have not distorted by effect of relief displacement and this effect is completely illuminated.

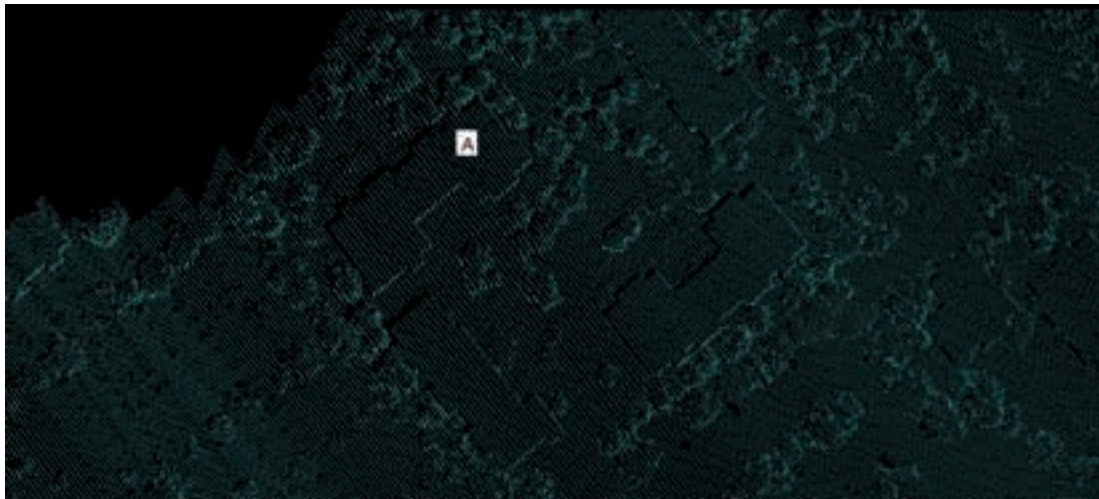


Figure 9: A 3D model from Optech's point clouds.



Figure 10: The sub area has been chosen for data fusing implementation. The effects of releaf displacement can be clearly seen.

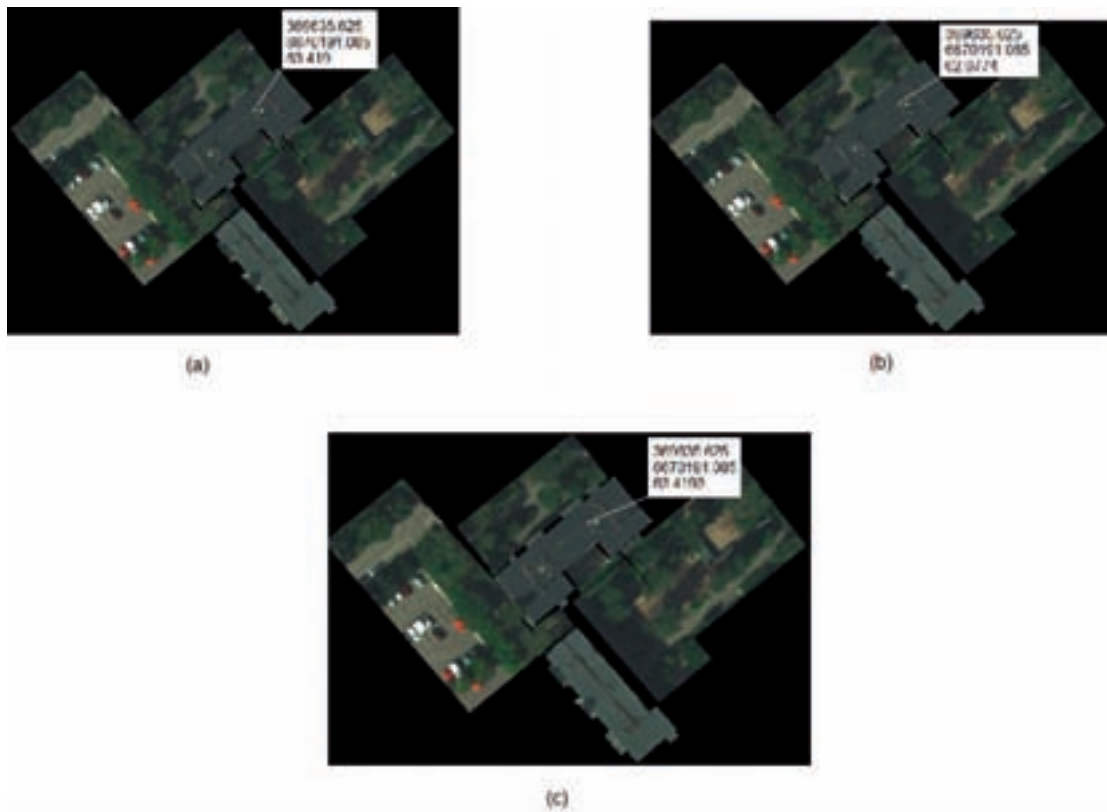


Figure 11: Figures (a), (b), and (c) present the transformed image on the Leica 3D data, Optech 3D data, and combined 3D data respectively. They look like image but their elements are points which are include colour values.

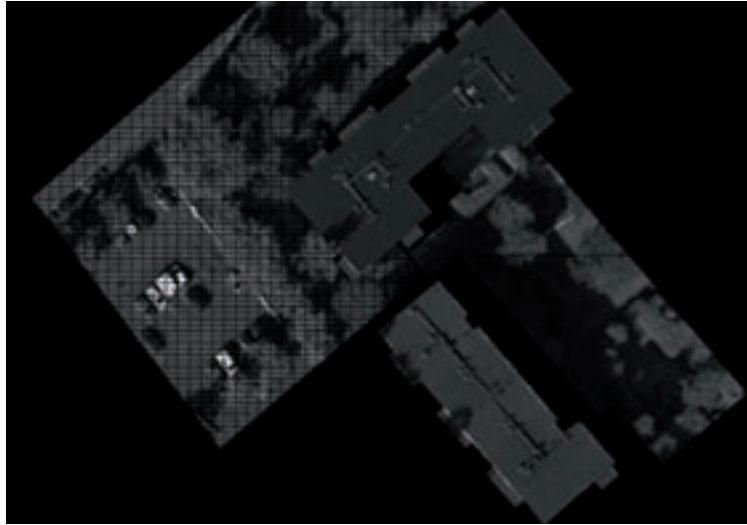


Figure 12: The transferred panchromatic image, the blank area between the green area and building represent the effect of relief displacement after transformation.

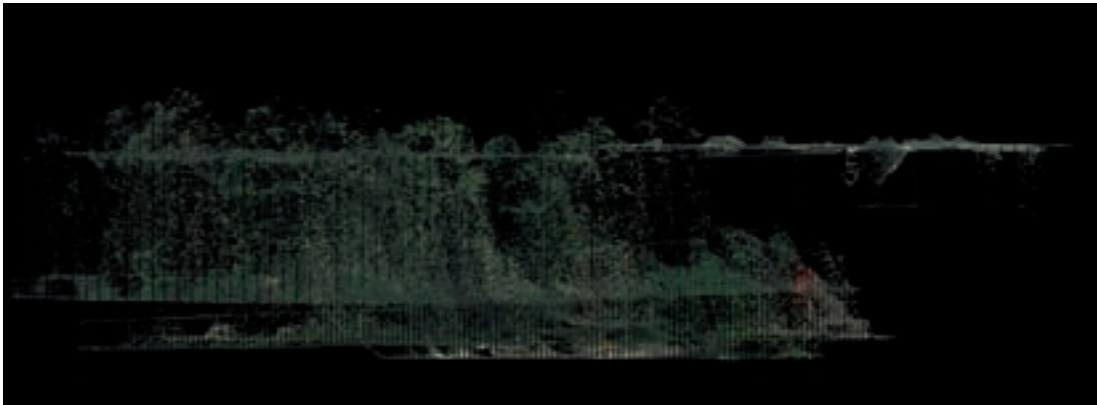


Figure 13: A 3D model of transformed image on the combined 3D model. Roofs, trees, ground, and small bushes can be clearly recognised.

4.2. Analysis of output

This section will compare the data obtained after transformation with the provided data. Figure 14 represents the location of provided GCPs on the area. All GCPs were captured on laser scanning data. It was realised that the majority of those data outside of laser scanning data, and only a small fraction of those data were in the laser scanning data. Therefore, that small part was transferred from images to the laser scanning data (Figure 15), and then the corresponding points on the transferred data were measured. It should be noted that it was assumed that all provided GCPs had no errors and the differences between extracted data and provided GCPs related to transforming processing; however, as was mentioned earlier it was assumed that all corrections were introduced to the laser scanning data, but it has to be considered that all cloud points consists of point uncertainties and the final output would be affected by those point uncertainties.

Table 1 presents the extracted data versus provided GCPs. The range of differences on X, Y but the ΔZ for most of points are higher than range of errors because those areas are covered by trees and trees affected the height value of points. To avoid those errors the image would be transferred on the laser scanner data for a second time, but this time a filter would be applied on the data for reducing the effect of trees on points. Table 2 presents the filtered data versus provided GCPs. The range of errors is significantly reduced except for a few points. Those points are covered by trees and it needs to apply a special filter on those points for rectifying.

This assessment proves that the proposed approach is able to transfer an image to a 3D model and improve the output with the highest reliability. The author is conducting a terrestrial project and digital images were transferred according to this proposal to a high precise 3D data, and the precision of output is in the range of 3D data and is around 1ppm.

5. Summary

A new approach for data fusion has been created and developed based on illumination of image distortions such as lens distortion and relief displacements. In this approach the image is split into sub areas and each area transferred to a 3D model pixel by pixel and the output is a point clouds or a vector image. This approach opens a new window to the Geospatial, especially to photogrammetry and remote sensing and presents a new way for illuminating distortions and provides an accurate and reliable output which can be used for mapping, GIS, Visualization, planning, traffic control, etc. even in medical photogrammetry. Obviously, the output of this approach is undermined by some situations of image acquisition and accuracy of the 3D model, but these issues can be illuminated by acquiring image and data from different views in order to have more details from the object and terrain. Also some dynamic object will affect the accuracy of the output, for example, parked cars and travelling cars on the terrain at the time of acquiring the laser scanning or aerial photography will affect on the output. Generally, cars are considered as a dynamic object whether they are parked or moving. Obviously, this issue can be fixed by removing the cars from the 3D model. This method has broad application in most sciences which rely on measurement.



Figure 14: Location of provided GCPs on the terrain.

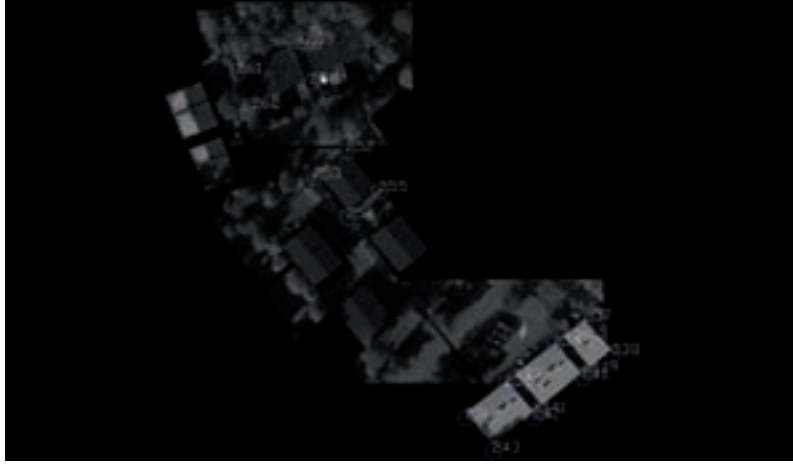


Figure 15: Transferred image on the 3D data plus provided GCPs on the area.

		Provided GCPs by EuroSDR			Extracted coordinates					
		X	Y	Z	X	Y	Z	Δx	Δy	Δz
231	roof	369450.817	6669932.425	46.612	369451.094	6669934.064	46.916	-0.277	-1.639	-0.304
232	roof	369461.458	6669941.186	46.627	369461.781	6669942.167	42.585	-0.323	-0.981	4.042
233	roof	369463.587	6669942.948	46.355	369463.906	6669944.099	46.666	-0.320	-1.151	-0.311
234	roof	369474.240	6669951.763	46.221	369474.313	6669952.147	46.850	-0.073	-0.384	-0.629
236	roof	369476.371	6669953.505	46.021	369476.594	6669954.026	46.581	-0.223	-0.521	-0.560
237	roof	369482.108	6669958.239	45.974	369481.938	6669958.211	46.504	0.171	0.028	-0.530
238	roof	369489.357	6669949.420	46.032	369488.781	6669950.373	46.613	0.576	-0.953	-0.581
239	roof	369483.633	6669944.693	46.044	369483.375	6669946.031	46.290	0.258	-1.338	-0.246
240	roof	369481.512	6669942.919	46.240	369481.063	6669944.206	46.829	0.450	-1.288	-0.589
241	roof	369470.833	6669934.162	46.286	369470.813	6669936.050	46.790	0.020	-1.888	-0.504
242	roof	369468.716	6669932.422	46.619	369468.531	6669934.065	42.900	0.185	-1.642	3.719
243	roof	369458.071	6669923.642	46.648	369457.938	6669925.532	47.119	0.134	-1.890	-0.471
252	roof	369419.814	6670002.791	49.997	369419.937	6670002.383	50.619	-0.123	0.408	-0.623
253	roof	369411.332	6669995.758	49.986	369412.562	6669996.306	50.541	-1.230	-0.548	-0.555
254	roof	369420.059	6669985.199	50.004	369420.125	6669987.165	45.920	-0.066	-1.966	4.084
255	roof	369428.533	6669992.232	50.027	369427.438	6669993.242	44.163	1.096	-1.010	5.864
258	roof	369410.359	6670020.668	46.229	369408.750	6670021.269	46.468	1.608	-0.601	-0.239
259	roof	369409.560	6670031.107	46.231	369408.468	6670031.604	45.401	1.092	-0.497	0.830
260	roof	369406.495	6670029.815	46.239	369405.406	6670030.118	46.576	1.089	-0.303	-0.337
261	roof	369391.299	6670023.475	46.217	369391.709	6670023.952	46.405	-0.410	-0.477	-0.188
262	roof	369395.166	6670014.322	46.239	369395.250	6670015.046	45.053	-0.084	-0.723	1.186

Table 1: Comparison of extracted data after transformation versus provided GCPs. As it can be seen the most critical differences related to Z values.

		Provided GCPs by EuroSDR			Extracted coordinates					
		X	Y	Z	X	Y	Z	Δx	Δy	Δz
231	roof	369450.817	6669932.425	46.612	369451.000	6669933.080	46.930	-0.183	-0.655	-0.318
232	roof	369461.458	6669941.186	46.627	369461.781	6669941.910	46.915	-0.323	-0.724	-0.288
233	roof	369463.587	6669942.948	46.355	369463.812	6669943.427	46.896	-0.226	-0.479	-0.541
234	roof	369474.240	6669951.763	46.221	369474.219	6669951.617	46.960	0.021	0.146	-0.739
236	roof	369476.371	6669953.505	46.021	369476.469	6669953.664	46.711	-0.098	-0.159	-0.690
237	roof	369482.108	6669958.239	45.974	369481.813	6669957.981	46.504	0.295	0.258	-0.530
238	roof	369489.357	6669949.420	46.032	369488.750	6669949.902	46.403	0.607	-0.482	-0.371
239	roof	369483.633	6669944.693	46.044	369483.250	6669945.364	46.472	0.383	-0.672	-0.428
240	roof	369481.512	6669942.919	46.240	369481.031	6669943.538	46.538	0.481	-0.620	-0.298
241	roof	369470.833	6669934.162	46.286	369470.812	6669935.072	46.658	0.021	-0.910	-0.372
242	roof	369468.716	6669932.422	46.619	369468.531	6669933.080	46.984	0.185	-0.657	-0.365
243	roof	369458.071	6669923.642	46.648	369458.000	6669924.170	48.850	0.071	-0.528	-2.202
252	roof	369419.814	6670002.791	49.997	369419.375	6670003.175	50.325	0.439	-0.384	-0.329
253	roof	369411.332	6669995.758	49.986	369411.531	6669996.655	50.601	-0.199	-0.897	-0.615
254	roof	369420.059	6669985.199	50.004	369420.062	6669986.463	50.270	-0.003	-1.264	-0.267
255	roof	369428.533	6669992.232	50.027	369428.344	6669993.148	50.110	0.189	-0.916	-0.083
257	roof	369413.376	6670021.940	46.257	369411.844	6670022.035	46.669	1.532	-0.095	-0.412
258	roof	369410.359	6670020.668	46.229	369408.906	6670020.586	46.128	1.452	0.082	0.101
259	roof	369409.560	6670031.107	46.231	369408.406	6670030.349	46.531	1.154	0.758	-0.300
260	roof	369406.495	6670029.815	46.239	369405.500	6670029.115	46.387	0.995	0.700	-0.148
261	roof	369391.299	6670023.475	46.217	369391.937	6670023.322	46.635	-0.638	0.153	-0.418
262	roof	369395.166	6670014.322	46.239	369395.500	6670014.902	45.053	-0.334	-0.580	1.186

Table 2: This table shows a comparison of extracted data after transforming and filtering versus provided GCPs. As it can be seen all differences are in the range of the point uncertainty of point clouds except at point 262 and 243 which it needs the application of a special filtering.

6. Acknowledgment

The author appreciates the EuroSDR, especially Mr. Petri Rönholm for providing opportunity to participate in project of EuroSDR Registration quality project, and correcting the report so that it would fit a proper English language structure and grammar.

References

- Abdallah C., Chorowicz J., Bou Kheir R., Khawlie M., (2005), "Detecting major terrain parameters relating to mass movements' occurrence using GIS, remote sensing and statistical correlations, case study Lebanon" *Remote Sensing of Environment* 99: Pages 448-461
- Akca D., (2007) "Matching of 3D surfaces and their intensities" *ISPRS Journal of Photogrammetry & Remote Sensing* 62
- Almeida-Filho R., Rosenqvist A., Shimabukuro Y.E., Silva R.P., (2007) "Detecting deforestation with multitemporal L-band SAR imagery: a case study in Western Brazilian Amazônia" *International Journal of Remote Sensing*, 28: Pages 1383-1390
- Allen J.D., (March 1990) "Remote Sensor Comparison For Crop Area Estimation Using Multitemporal Data" NASS Research Report No. SRB-90-03
- Anderssohn J., Motagh M., Walter T.R., Rosenau M., Kaufmann H., Oncken O., (2009) "Surface deformation time series and source modeling for a volcanic complex system based on satellite wide swath and image mode interferometry: The Lazufre system, central Andes" *Remote Sensing of Environment* 113: Pages 2062-2075
- Ayoub F., Leprince S., Avouac J-P, (2009) "Co-registration and Correlation of Aerial Photographs for Ground Deformation Measurements" *ISPRS Journal of Photogrammetry and Remote Sensing*
- Ballester M.V.R., Victoriaa D., Kruschea A.V., Coburnb R., Victoriaa R.L., Richeyb J.E., Logsdonb M.G., Mayorgab E., Matricardic E., (2003), "A Remote Sensing/GIS-Based Physical Template to Understand the Biogeochemistry of the Ji-Paraná river basin Western Amazo`nia)" *Remote Sensing of Environment* 87: Pages 429-445
- Berthier E., Toutin T., (2008) "SPOT5-HRS Digital Elevation Models and the Monitoring of Glacier Elevation Changes in North-West Canada and South-East Alaska" *Remote Sensing of Environment* 112: Pages 2443-2454
- Bosch A., Zisserman A., Muñoz X., (APRIL 2008) "Scene Classification Using a Hybrid Generative/Discriminative Approach" *IEEE Transactions on Pattern Analysis and Machine Intelligence*, Vol. 30, No. 4
- Bouillon A., Bernard M., Gigord P., Orsoni A., Rudowski V., Baudoin A., (2006) "SPOT 5 HRS Geometric Performances: Using Block Adjustment as a Key Issue to Improve Quality of DEM Generation" *ISPRS Journal of Photogrammetry & Remote Sensing* 60: Pages 134-146
- Buitena H.J., van Putten B., (1997) "Quality Assessment of Remote Sensing Image Registration-and Testing of Control Point Residuals Analysis" *ISPRS Journal of Photogrammetry & Remote Sensing* 52: Pages 57-73
- Cesar Jr., R.M., Bengoetxea, E., Bloch, I., Larrañaga, p., (2005), "Inexact graph matching for model based recognition: Evaluation and comparison of optimisation algorithms", *Pattern Recognition*, Vol 38, 2009-2013
- Chang, Y.L., Leou, J.J., (1992), "A model-based approach to representation and matching of object shape patterns", *Pattern Recognition, Letter* 13, 707-714
- Charif H.N., McKenna S.J., (2006) "Tracking the activity of participants in a meeting" *Machine Vision and Applications*

- Crowley J.L., Stern R.M., (MARCH 1984) "Fast Computation of the Difference of Low-Pass Transform", IEEE Transactions on Pattern Analysis and Machine Intelligence, Vol. PAMI-6, No. 2: Pages 212-222
- Dean K.G., Forbes R.B., Turner D.L., Eaton F.D., Sullivan K.D., (1982) "Radar and Infrared Remote Sensing of Geothermal Features at Pilgrim Springs, Alaska" REMOTE SENSING OF ENVIRONMENT 12: Pages 391-405
- Dodgson N.A., (1992) "Image Resampling" Technical Report, University of Cambridge No. 261
- El Hajj M., Bégué A., Guillaume S., Martiné J.F., (2009) "Integrating SPOT-5 time series, crop growth modelling and expert knowledge for monitoring agricultural practices - The case of sugarcane harvest on Reunion Island" Remote Sensing of Environment 113: Pages 2052-2061
- Förstner, W., E., Gülch, (1986), "A fast Operator for Detection and Precise Location of Distinct Point" ISPEs Intercommission Workshop on Fast Processing of Photogrammetric Data: Pages 281-305
- Gérard, P., Gagalowicz, A., (2000), "Three dimensional model-based tracking using texture learning and matching", Pattern Recognition, Letters 21, 1095-1103
- Grosky, W.I., Neo, P., Mehrota, R., (1992), "A pictorial index mechanism for model-based matching", Data & Knowledge Engineering, Vol. 8, 309-327
- Gruen A., Akca D., (2005) "Least squares 3D surface and curve matching" ISPRS Journal of Photogrammetry & Remote Sensing 59: Pages 151-174
- Hastings D.A., Liping Di L., (1994) "Modeling of Global Change Phenomena with GIS Using the Global Change Data Base. II: Prototype Synthesis of the AVHRR-Based Vegetation Index from Terrestrial Data" Remote Sensing Environment 49: Pages 13-24
- Hégarat-Masclé S., Le, Otlé C., Guérin C., (2005) "Land cover change detection at coarse spatial scales based on iterative estimation and previous state information" Remote Sensing of Environment 95: Pages 464-479
- Henikoff, J., Shapiro, L.G., (1993), "Representative patterns for model-based matching", Pattern Recognition, Vol. 26, No. 7, 1087-1098
- Homajnejad A. S., (1997) "REAL TIME PHOTOGRAMMETRIC PROCESSING", PhD Dissertation, University of Melbourne
- Horaud R., Niskanen M., Dewaele G., Boyer E., (JANUARY 2009) "Human Motion Tracking by Registering an Articulated Surface to 3D Points and Normals" IEEE Transactions on Pattern Analysis and Machine Intelligence, Vol. 31, No. 1: Pages 281-305
- Jazayeri I., Fraser C.S., (2008) "INTEREST OPERATORS IN CLOSE-RANGE OBJECT RECONSTRUCTION" The International Archives of the Photogrammetry, Remote Sensing and Spatial Information Sciences. Vol. XXXVII. Part B5. Beijing: Pages 69-74
- Kornus W., Lehner M., Schroeder M., (2000) "Geometric in-flight calibration of the stereoscopic line-CCD scanner MOMS-2P" ISPRS Journal of Photogrammetry & Remote Sensing 55: Pages 59-71
- Lamdan, Y., Wolfson, H.J., (1988) "Geometric Hashing: A General and Efficient Model-Based Recognition Scheme", The Second International Conference on Computer Vision, 238-249
- Li R., Di K., (2007) "Integration of Orbital, Descent and Ground Imagery for Topographic Capability Analysis in Mars Landed Missions" Report for NASA Applied Information Systems Research Program, The Ohio State University

- Liu, C.L., Kim, I.J., Kim, K.H., (2001), Model-based stroke extraction and matching for handwritten Chinese character recognition", *Pattern Recognition*, Vol. 34, 2339-2352
- Lu Z., Rykhus R., Masterlark T., Dean K.G., (2004) "Mapping recent lava flows at Westdahl Volcano, Alaska, using radar and optical satellite imagery" *Remote Sensing of Environment* 91: Pages 345-353
- Maas H.G., (July 9-19 1996), "Automatic DEM generation by multi-image feature based matching" 18th ISPRS Congress, Vienna, IAPRS Vol. 31, Part B3: Pages 484-489
- Mattia F., Satalino G., Pauwels V.R.N., Loew A., (2009) "Soil moisture retrieval through a merging of multi-temporal L-band SAR data and hydrologic modelling" *Hydrol. Earth Syst. Sci.*, 13: Pages 343-356
- McCAULEY S., GOETZ S.J., (20 MARCH, 2004) "Mapping residential density patterns using multi-temporal Landsat data and a decision-tree classifier" *INT. J. REMOTE SENSING*, VOL. 25, NO. 6: Pages 1077-1094
- Montesano P.M., Nelson R., Sun G., Margolis H., Kerber A., Ranson K.J., (2009) "MODIS tree cover validation for the circumpolar taiga-tundra transition zone" *Remote Sensing of Environment* 113: Pages 2130-2141
- Monserrat O., Crosetto M., (2008) "Deformation measurement using terrestrial laser scanning data and least squares 3D surface matching" *ISPRS Journal of Photogrammetry & Remote Sensing* 63: Pages 142-154
- Mustaffar M., Mitchell H.L., (2001) "Improving area-based matching by using surface gradients in the pixel co-ordinate transformation" *ISPRS Journal of Photogrammetry & Remote Sensing* 56: Pages 42-52
- Niblock, J., Peng, J.-X., McMenemy, K., Irwin, G.W., (2007), "Fast model-based-feature matching technique applied to airport lighting", *IET Science, Measurement, and Technology*, Vol. 2, No. 3, 160-176
- Nishida, H., (1995), "Model-based shape matching with structural feature grouping", *IEEE transactions on pattern analysis matching intelligence*, Vol. 17, No. 3, 315-320
- Radhadevi P.V., Solanki S.S., Jyothi M.V., Nagasubramanian V., Varadan G., (2009) "Automated co-registration of images from multiple bands of Liss-4 camera" *ISPRS Journal of Photogrammetry and Remote Sensing* 64: Pages 17-26
- Reitberger J., Schnörr C.I., Krzystek P., Stilla U., (2009) "3D segmentation of single trees exploiting full waveform LIDAR data" *ISPRS Journal of Photogrammetry and Remote Sensing*
- Ruetz, P. A., Brodersen, R. W., (1988) "An Image-Recognition System Using Algorithmically Dedicated Integrated Circuits", *Machine Vision and Applications* 1: Pages 3-22
- Salvi S., (1995) "Analysis and Interpretation of Landsat Synthetic Stereo Pair for the Detection of Active Fault Zones in the Abruzzi Region (Central Italy)" *REMOTE SENS. ENVIRON.* 53: Pages 153-163
- Shimizu M., and Okutomi M., (2005) "Two-Dimensional Simultaneous Subpixel Estimation for Area-Based Matching" *Systems and Computers in Japan*, Vol. 36, No. 2
- Stevens, M.R., Beveridge, J.R., (1997), "Precise matching of 3-D target models to multisensory data", *IEEE Transactions on Image Processing*, Vol. 6, No. 1, 126-142

- Sundaresan A., Chellappa R., (OCTOBER 2008) "Model-Driven Segmentation of Articulating Humans in Laplacian Eigenspace" IEEE Transactions on Pattern Analysis and Machine Intelligence, VOL. 30, NO. 10
- Tomita F., (1988) "Interactive and Automatic Image Recognition System" Machine Vision and Applications 1: Pages 59-69
- Viola, P., Jones, M., (JULY 13, 2001) "Robust Real-time Object Detection", SECOND INTERNATIONAL WORKSHOP ON STATISTICAL AND COMPUTATIONAL THEORIES OF VISION – MODELING, EARLY, COMPUTING, AND SAMPLING VANCOUVER, CANADA
- Vogelmann J.E., Rock B.N., (1989) "Use of Thematic Mapper Data for the Detection of Forest Damage Caused by the Pear Thrips" REMOTE SENS. ENVIRON. 30: Pages 217-225
- Walimbe V., Shekhar R., (2006) "Automatic elastic image registration by interpolation of 3D rotations and translations from discrete rigid-body transformations" Medical Image Analysis 10: Pages 899-914
- Wang C., Menenti M., Stoll M-P., Feola A., Belluco E., Marani M., (JULY 2009) "Separation of Ground and Low Vegetation Signatures in LiDAR Measurements of Salt-Marsh Environments" IEEE TRANSACTIONS ON GEOSCIENCE AND REMOTE SENSING, VOL. 47, NO. 7
- Wu X., Dibiase S.J., Gullapalli R., Yu C.X., (2004) "Deformation Image Registration for the Use of Magnetic Resonance Spectroscopy in Prostate Treatment Planning" Int. J. Radiation Oncology Biol. Phys., Vol. 58, No. 5: Pages 1577-1583
- Xiong Y., Olson C.F., Matthies L.H., (2005) "Computing depth maps from descent images" Machine Vision and Applications 16: Pages 139–147
- Yanovsky I., Leow A.D., Lee S., Osher S.J., Thompson P.M., (2009) "Comparing registration methods for mapping brain change using tensor-based morphometry" Medical Image Analysis 13: Pages 679-700
- Zitova, B., Flusser, J., (2003) "Image Registration Methods: a survey", Image and Vision Computing 21, Pages 977–1000
- Zöllner T., Buhmann J.M., (JULY 2007) "Robust Image Segmentation Using Resampling and Shape Constraints" IEEE TRANSACTIONS ON PATTERN ANALYSIS AND MACHINE INTELLIGENCE, VOL. 29, NO. 7: Pages 1147-1164

Report of the National Geographic Institute Spain EuroSDR Registration Quality – Towards Integration of Laser Scanning and Photogrammetry

Jorge Martínez Luceño, Instituto Geográfico Nacional, jmluceno@fomento.es
Juan Carlos Ojeda Manrique, Instituto Geográfico Nacional, jcojeda@fomento.es
Eduardo González Cristóbal, Instituto Geográfico Nacional, egonzalezc@fomento.es
Francisco Papí Montanel, Instituto Geográfico Nacional, fpapi@fomento.es
Andrés Díez Galilea, ETSI Topografía, Geodesia y Cartografía UPM, andres.diez@upm.es;
Ricardo Rodríguez Cielos, ETSI Topografía Geodesia y Cartografía UPM, ricardo.rodriguez@upm.es;
Julián Aguirre de Mata, ETSI Topografía, Geodesia y Cartografía UPM, julian.aguirre@upm.es;
Alejandro Sáenz Echeverría, ETSI Topografía, Geodesia y Cartografía UPM, asaenz69@telefonica.net
Alfonso Gómez, Stereocarto, agomez@stereocarto.com
Tomás Fernández de Sevilla, InfoterraSGSA, tomas.sevilla@infoterra.es



Introduction:

IGN-Spain under an agreement with Universidad Politécnica de Madrid (UPM) and the Stereocarto company, presents two different methods to solve the registration of lidar and photogrammetric data. First, Method 1, based on manual measurements and 3D processing was performed with the purpose of obtaining information on processing time and accuracy in the coordinates of the point cloud, which could serve to assess the results of the designed automatic method, which is the that is identified as Method2, which is called *“Automatic measurements base on synthetic LiDAR images with 3D transformations”*.

This second method combines the methodologies and developments achieved in two research projects conducted jointly with IGN, UPM and Stereocarto. These projects are called *"Special Agreement for research and development of the integration of image information and optical radar in surveying and mapping applications"* and *"Special Agreement for the development of algorithms that facilitate the detection of temporal changes using satellite imagery"*.

Based on these two internal projects of IGN-Spain, a methodology was developed and adapted work developments (algorithms) to serve the purpose of this research project EuroSDR.

Methods:

Method 1: Manual measurements with 3D transformation

Method 1 is based on manual measurements of homologous points in DMC Panchromatic images and LiDAR Digital Surface Model. Then a 3D transformation for translation and rotations is calculated and applied, estimating the internal and external accuracy. The tools and steps were the following:

1. Create an Inpho Match-AT 5.0 project importing DMC PAN Images and external orientation.
2. Select over 50 existing homologous points between images and LiDAR point cloud.
3. Measure photocordinates and extract terrain coordinates for images points using Match-AT.
4. Import XYZ Intensity cloud points with Globalmapper v10 and generate a Digital Surface Model.
5. Measure 3D XYZ terrain point coordinates from Digital Surface Model.
6. Calculate transformation parameters for translations and rotation using the 3D measured coordinates data set. Points with residual greater than 1 m were rejected. The Terrascan (Terrasolid) transformation tool was used for this step.
7. Import LiDAR point cloud with Terrascan (Terrasolid) and apply the transformation parameters for getting the registered photogrammetric data.
8. Estimate internal precision using the residuals point data from the 3D transformation.
9. Estimate external accuracy using ground control points. Elevation accuracy was estimated using the Terrascan tool comparing elevation from known field points and laser points for a planimetric position. Planimetric accuracy was estimated measuring points over the Digital Surface Model from the corrected LiDAR point cloud.

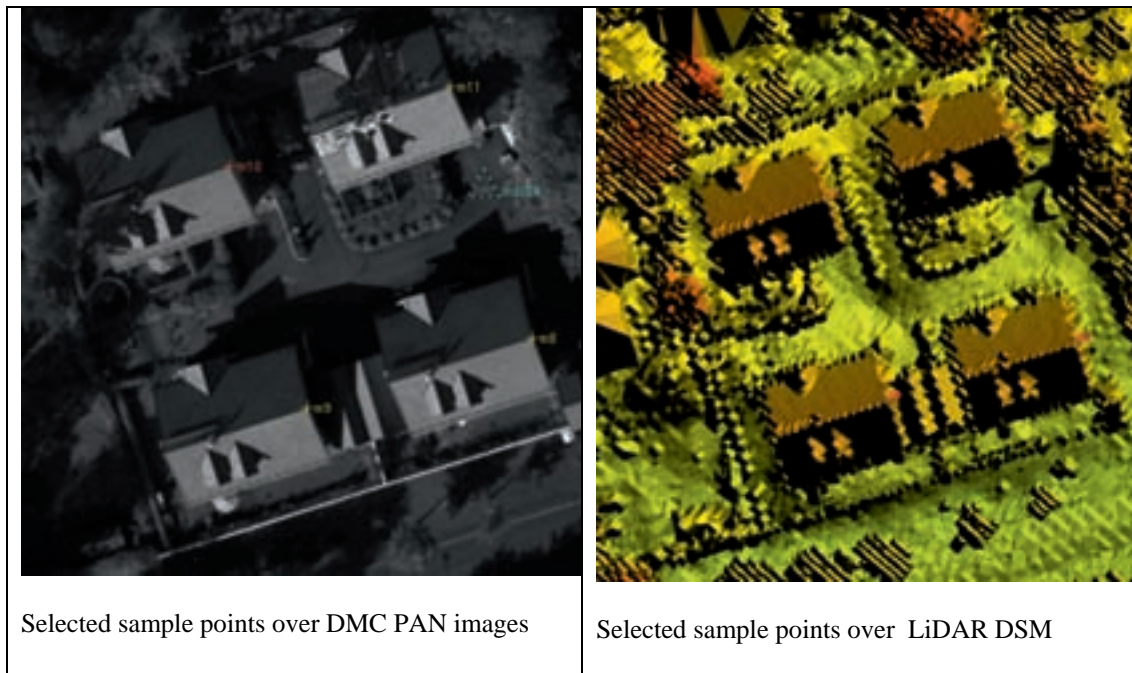


Fig.1. Extracted point in both data sets.

Results. Method 1:

Panchromatic images, Method 1, case Leica ALS50_II:

a) Transformation parameters for 3D translation and rotation using 37 homologous points, from LiDAR to Images:

Dx 17.98325633 Dy 21.67819285 Dz 5.93302306 Ox 369442.98291837 Oy 6669871.63042857 Oz 53.57577551 Rx 7.471021489501609e-004 Ry 3.395677686097900e-004 Rz 2.898328662446877e-004	Dx, Dy, Dz meters. Translations Ox, Oy, Oz meters. Rotation centre Rx, Ry, Rz arc degree. Rotations
---	---

b) Measured coordinates and residuals for each point – Method 1. Case Leica ALS50_II:

See “Method 1: Appendix 1” for the detailed coordinates and residual list.

c) Descriptive statistics for point transformation residuals – Method 1. Case Leica ALS50_II

STATISTIC	X	Y	Z
Mean	0,000	0,000	0,000
Standard error	0,053	0,051	0,041
Median	-0,030	0,005	0,003
Standard Deviation	0,369	0,357	0,284
Sample Variance	0,136	0,128	0,081
Kurtosis	0,067	0,132	3,879
Skewness	0,461	-0,132	0,215
Range	1,638	1,552	1,919
Minimum	-0,758	-0,819	-0,941
Maximum	0,879	0,733	0,978
Sum	0,000	0,000	0,000
Count	49	49	49

d) Quality control for elevations – Method 1. Case Leica ALS50_II:

Number	Easting	Northing	Known Z	Laser Z	Dz m
289	369442.979	6669958.546	45.160	slope	*
999965	369028.017	6669225.908	25.852	outside	*
999975	369079.774	6669357.282	23.416	23.870	+0.454
999976	369085.686	6669359.584	23.379	23.880	+0.501
999977	369086.108	6669355.649	23.447	23.970	+0.523
999978	369083.568	6669354.668	23.492	24.010	+0.518
999988	369077.904	6669645.350	26.261	slope	*
999989	369078.392	6669641.341	26.264	slope	*
999990	369072.887	6669644.746	26.257	slope	*
99997	369080.660	6669652.213	24.258	24.380	+0.122
999987	369083.201	6669653.901	24.485	24.570	+0.085
999948	369456.822	6669556.146	40.857	outside	*
999947	369463.146	6669564.884	40.672	outside	*
999982	369540.596	6669833.380	39.649	39.890	+0.241
999981	369542.279	6669853.709	39.414	39.600	+0.186
999979	369545.668	6669847.081	39.427	39.650	+0.223
999980	369545.212	6669848.501	39.442	39.630	+0.188
99991	369341.209	6669691.230	40.240	40.490	+0.250
999970	369340.291	6669692.091	40.260	40.540	+0.280
999971	369336.474	6669651.668	40.569	40.910	+0.341
999972	369337.280	6669650.516	40.587	40.870	+0.283
999973	369333.919	6669628.119	41.305	41.670	+0.365
999974	369334.813	6669626.834	41.356	41.710	+0.354

- Descriptive statistics:

Average dz +0.307
 Minimum dz +0.085
 Maximum dz +0.523
 Average magnitude 0.307
 Root mean square 0.335
 Std deviation 0.138

e) Quality control for planimetric – Method 1. Case Leica ALS50 _II:

Comparison between field ground control points and measured points over the digital surface model generated from the transformed LiDAR point cloud:

Field GPS point			DSM Measure		Differences m	
Number	X m	Y m	X m	Y m	Delta X	Delta Y
231	369450.82	6669932.43	369450,91	6669932,73	-0,09	-0,31
232	369461.46	6669941.19	369461,40	6669941,18	0,05	0,00
233	369463.59	6669942.95	369463,49	6669943,08	0,09	-0,13
234	369474.24	6669951.76	369474,36	6669952,02	-0,11	-0,25
235	369476.37	6669953.50	369476,12	6669952,93	0,26	0,58
237	369482.11	6669958.24	369482,21	6669958,77	-0,10	-0,53
238	369489.36	6669949.42	369489,89	6669950,33	-0,53	-0,91
239	369483.63	6669944.69	369484,10	6669944,97	-0,47	-0,27
240	369481.51	6669942.92	369481,75	6669943,00	-0,24	-0,08
243	369458.07	6669923.64	369458,33	6669924,16	-0,26	-0,52
244	369449.80	6669986.75	369450,23	6669987,70	-0,43	-0,95
247	369458.31	6669993.76	369457,97	6669994,30	0,34	-0,54
248	369438.36	6670018.00	369438,59	6670017,94	-0,23	0,07
249	369447.07	6670007.44	369446,40	6670007,34	0,67	0,10
250	369438.52	6670000.43	369439,39	6670000,73	-0,87	-0,30
254	369420.06	6669985.20	369420,52	6669985,39	-0,46	-0,19
255	369428.53	6669992.23	369428,49	6669992,40	0,04	-0,17
256	369428.58	6670028.30	369428,92	6670028,53	-0,34	-0,22
257	369413.38	6670021.94	369413,50	6670021,90	-0,12	0,04
258	369410.36	6670020.67	369410,39	6670020,58	-0,03	0,09

259	369409.56	6670031.11		369410,04	6670031,38		-0,48	-0,28
260	369406.50	6670029.82		369405,97	6670029,62		0,53	0,20
261	369391.30	6670023.48		369391,24	6670023,28		0,06	0,19
263	369395.17	6670014.32		369394,84	6670014,37		0,32	-0,05
287	369445.24	6669964.53		369444,96	6669964,14		0,28	0,38

f) Descriptive statistics for point residuals from planimetric differences DeltaX and DeltaY – Method 1. Case Leica ALS50 _II:

STATISTIC	Delta X	Delta Y
Mean	-0,085	-0,162
Standard error	0,072	0,071
Median	-0,101	-0,165
Standard Deviation	0,362	0,356
Sample Variance	0,131	0,127
Kurtosis	-0,113	0,561
Skewness	0,089	-0,357
Range	1,537	1,528
Minimum	-0,870	-0,950
Maximum	0,667	0,578
Sum	-2,129	-4,047
Count	25	25

Panchromatic images, Method 1, case Optech ALTM 3100

a) Transformation parameters for 3D translation and rotation using 35 homologous points, from LiDAR to Images:

Dx 23.92804423 Dy -17.88329654 Dz 25.56415692 Ox 369429.88321731 Oy 6669856.78729961 Oz 48.18979154 Rx -1.563190181914549e-003 Ry -7.076838877939056e-004 Rz -7.778234344437390e-005	Dx, Dy, Dz meters. Translations Ox, Oy, Oz meters. Rotation centre Rx, Ry, Rz arc degree. Rotations
--	---

b) Measured coordinates and residuals for each point – Method 1. Case Optech ALTM 3100:

See “Method 1: Appendix 1” for the detailed coordinates and residual list.

c) Descriptive statistics for point transformation residuals – Method 1. Case Optech ALTM 3100

STATISTIC	X	Y	Z
Mean	0,000	0,000	0,000
Standard error	0,053	0,057	0,034
Median	0,023	-0,058	-0,007
Standard Deviation	0,380	0,409	0,248
Sample Variance	0,144	0,168	0,062
Kurtosis	-0,505	-0,233	3,752
Skewness	-0,024	0,206	-1,226
Range	1,567	1,781	1,492
Minimum	-0,738	-0,879	-0,927
Maximum	0,829	0,902	0,565
Sum	0,000	0,000	0,000
Count	52	52	52

d) Quality control for elevations – Method 1. Case Optech ALTM 3100:

Number	Easting	Northing	Known Z	Laser Z	Dz m
999975	369079.774	6669357.282	23.416	23.990	+0.574
999977	369086.108	6669355.649	23.447	23.970	+0.523
999976	369085.686	6669359.584	23.379	23.900	+0.521
999978	369083.568	6669354.668	23.492	24.000	+0.508
999971	369336.474	6669651.668	40.569	40.850	+0.281
999974	369334.813	6669626.834	41.356	41.620	+0.264
999973	369333.919	6669628.119	41.305	41.560	+0.255
999972	369337.280	6669650.516	40.587	40.840	+0.253
999987	369083.201	6669653.901	24.485	24.680	+0.195
99997	369080.660	6669652.213	24.258	24.450	+0.192
999970	369340.291	6669692.091	40.260	40.450	+0.190
99991	369341.209	6669691.230	40.240	40.360	+0.120
999980	369545.212	6669848.501	39.442	39.480	+0.038
999979	369545.668	6669847.081	39.427	39.460	+0.033
999982	369540.596	6669833.380	39.649	39.650	+0.001
999981	369542.279	6669853.709	39.414	39.380	-0.034

289	369442.979	6669958.546	45.160	removed	*
999989	369078.392	6669641.341	26.264	removed	*
999988	369077.904	6669645.350	26.261	removed	*
999990	369072.887	6669644.746	26.257	removed	*
999947	369463.146	6669564.884	40.672	outside	*
999948	369456.822	6669556.146	40.857	outside	*
999965	369028.017	6669225.908	25.852	outside	*

- Descriptive statistics:

Average dz	+0.245
Minimum dz	-0.034
Maximum dz	+0.574
Average magnitude	0.249
Root mean square	0.310
Std deviation	0.197

e) Quality control for planimetric – Method 1. Case Optech ALTM3100:

Comparison between field ground control points and measured points over the digital surface model generated from the transformed LiDAR point cloud:

Field GPS Points			DSM Measure			Differences m	
Number	X m	Y m	X m	Y m		Delta X	Delta Y
231	369450,82	6669932,43	369450,71	6669932,73		0,11	-0,30
232	369461,46	6669941,19	369461,40	6669941,21		0,06	-0,03
233	369463,59	6669942,95	369463,58	6669943,33		0,01	-0,38
234	369474,24	6669951,76	369474,39	6669951,89		-0,15	-0,13
235	369476,37	6669953,50	369476,31	6669953,57		0,06	-0,07
237	369482,11	6669958,24	369482,02	6669958,18		0,09	0,06
238	369489,36	6669949,42	369489,27	6669949,20		0,09	0,22
239	369483,63	6669944,69	369483,73	6669944,44		-0,09	0,25
240	369481,51	6669942,92	369481,23	6669942,73		0,28	0,19
242	369468,72	6669932,42	369468,83	6669932,17		-0,11	0,25
243	369458,07	6669923,64	369458,16	6669923,48		-0,09	0,17
244	369449,80	6669986,75	369449,69	6669986,85		0,11	-0,10
247	369458,31	6669993,76	369457,87	6669993,60		0,44	0,16
248	369438,36	6670018,00	369438,46	6670017,72		-0,10	0,28
249	369447,07	6670007,44	369446,47	6670007,29		0,60	0,14
250	369438,52	6670000,43	369438,60	6670000,88		-0,07	-0,45
254	369420,06	6669985,20	369419,89	6669985,52		0,17	-0,32
255	369428,53	6669992,23	369428,43	6669991,85		0,11	0,39

256	369428,58	6670028,30	369428,49	6670028,16		0,10	0,15
257	369413,38	6670021,94	369413,45	6670021,64		-0,08	0,30
258	369410,36	6670020,67	369410,32	6670021,00		0,04	-0,34
259	369409,56	6670031,11	369409,36	6670030,82		0,20	0,28
260	369406,50	6670029,82	369406,04	6670030,28		0,46	-0,46
261	369391,30	6670023,48	369391,33	6670023,91		-0,03	-0,43
263	369395,17	6670014,32	369395,17	6670014,41		0,00	-0,09
287	369445,24	6669964,53	369445,07	6669964,53		0,17	-0,01

*f) Descriptive statistics for point residuals from planimetric differences DeltaX and DeltaY
– Method 1. Case Optech ALTM3100:*

STATISTIC	Delta X	Delta Y
Mean	0,092	-0,010
Standard error	0,036	0,053
Median	0,075	0,026
Standard Deviation	0,186	0,268
Sample Variance	0,035	0,072
Kurtosis	1,309	-1,216
Skewness	1,207	-0,399
Range	0,744	0,850
Minimum	-0,146	-0,464
Maximum	0,598	0,386
Sum	2,392	-0,257
Count	26	26

Level of Automation Method 1:

There is no level of automation for method 1. This is completely based on manual measurements.

Discussion Method 1:

A manually measured method is followed for registering the LiDAR cloud points (both Leica ALS50II and Optech ALTM3100) and DMC panchromatic images. 57 homologous points were selected between photogrammetric images and the digital surface model derived from the point cloud. Then a 3D geometric transformation with translations and rotations was calculated using 52 well distributed points along the LiDAR strip with residuals less than 1m.

It was estimated that using RGB multispectral resolution image, a better result will not be achieved than using the panchromatic images. This type of method needs the best resolution images as fixed data.

Initially a 3D geometric transformation considering 9 parameters for 3 translations, 3 rotations and 3 scale factors was applied, getting similar results to the 3D transformation with just translation and rotations. Scale factors were not significant, so the simplest transformation was chosen.

This method was solved making monoscopic photogrammetric measurements for 2 hours (57 points) and 1 additional hour for measuring points over the LiDAR DSM, for each case, Leica and Optech datasets.

Inner precision (standard deviation) for this transformation method was estimated as ± 40 cm for planimetric and ± 30 cm for elevation data. The results are similar for Leica and Optech data sets.

Inner precision for Method 1 Transformation	Leica	Optech ALTM3100
X standard deviation point residual	0.37 m	0.38 m
Y standard deviation point residual	0.36 m	0.41 m
Z standard deviation point residual	0.28 m	0.25 m

These values are higher than expected due to the relative quality measurements over the LiDAR DSM objects. This manual measurement technique over the LiDAR DSM is only possible for high density LiDAR cloud points, greater than 2 pts/m².

Absolute precision or accuracy for this transformation method was estimated using the field ground control points compared with laser points. The summary result is:

Accuracy for Method 1 Transformation	Leica	Optech ALTM3100
X constant – systematic error	-0.09 m	0.09 m
Y constant – systematic error	-0.16 m	-0.01 m
Z constant – systematic error	0.31 m	0.24 m
X standard deviation	0.36 m	0.19 m
Y standard deviation	0.36 m	0.27 m
Z standard deviation	0.14 m	0.20 m

There is a high systematic error for elevation that could be derived from the inner precision of method 1.

Planimetric accuracy is in the range of the expected magnitude given by the manufacturer. Elevation accuracy is out of tolerance, the expected precision for 500m high LiDAR flight is 0.10 m. This is because planimetric errors in point coordinates extracted on high sloped surfaces, such as the buildings upper corners, produce high elevation errors.

A better elevation result could be achieved using method 1, if the transformation were solved in 2 steps: First planimetric parameters, then elevation parameters, but using different homologous points. Well defined planimetric points from one side, and on the other hand, different points in flat areas for elevation.

Conclusions Method 1:

In spite of being a manual method, it could be useful for getting registration in small flight areas such as field calibration, and then export and apply the transformation for a whole block.

Method 1 is a relatively fast method; in 2 hours you can solve the transformation and choosing by yourself the best homologous well-distributed points around the project area. Also you can solve the transformation using standard photogrammetric and LiDAR tools.

Method 1 does not fulfil the standard quality elevation tolerance. It could be improved solving the 3D transformation in 2 steps: Getting first planimetric parameters, then elevation parameters using different points.

References Method 1:

Constantin-Octavian Andrei, March 2006 .3D affine coordinate transformation. Master's of Science Thesis in Geodesy no. 3091 TRITA-GIT EX 06-004. School of Architecture and the Built Environment. Royal Institute of Technology (KTH) 100 44 Stockholm, Sweden.

Methods:

Method 2: Automatic measurements based on synthetic LiDAR images with 3D transformations

This method integrates a complex process whose operation is based on the automatic image matching originating from a different source for the selection of homologous points. On the one hand, the LiDAR information allows the generation of a number of synthetic images employing as the radiometric information, the pulse intensity returned by the sensor. On the other hand, DMC Pancromatic Images.

Owing to the different characteristics DMC Pancromatic Images present with respect to the images generated from LiDAR data, matching algorithms based on radiometry do not work correctly. For this reason, Digital Image Matchig of these images after having undergone a number of previous transformations is needed.

The main characteristic of this method is the use of the wavelet transform allowing the generation of a number of images from two distinct sources – photogrammetry and LiDAR – presenting equal characteristics.

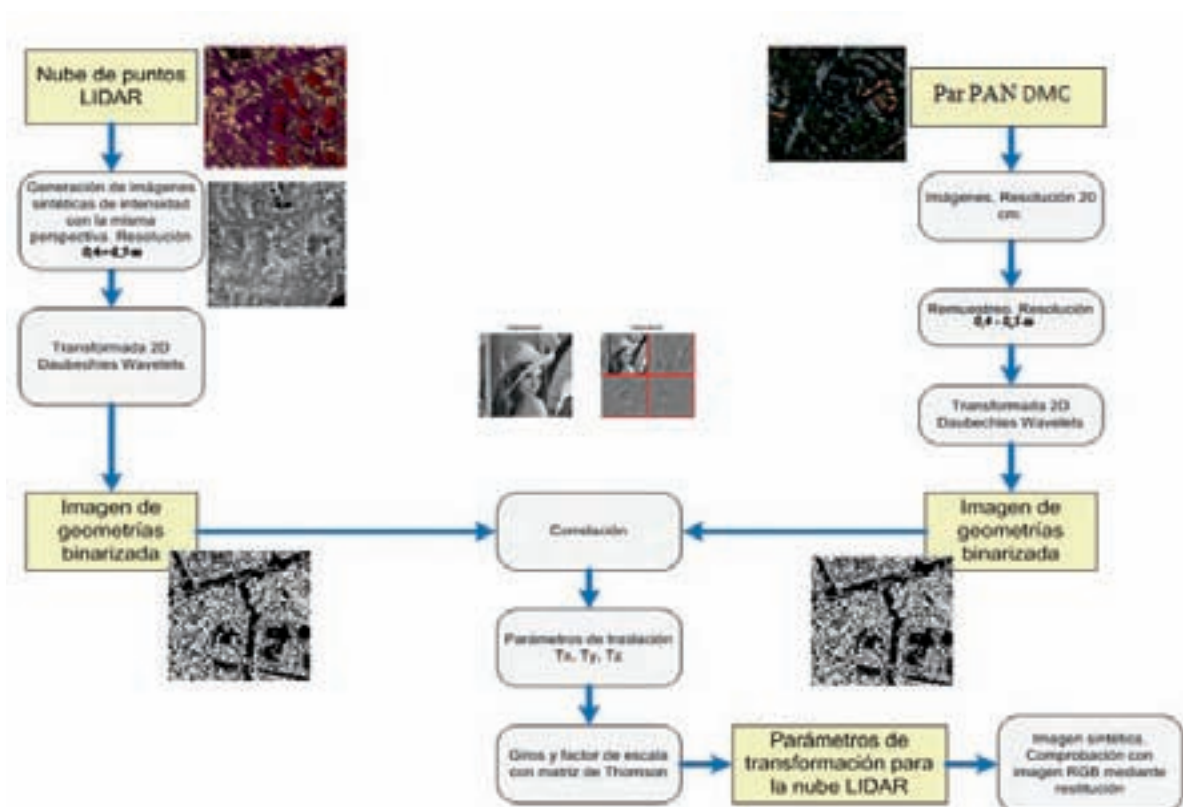


Fig2. Workflow

Basically this automatic procedure needs to obtain two images of similar characteristics for the image matching later, in such a way that it is possible to find homologous points in both. For it, the starting information will be:

- A LiDAR point cloud of sufficient density.
 - Intensity information for the points.
 - Oriented photogrammetric flight or oriented ortho-photography.
- i. From the LiDAR point cloud a number of synthetic images of the zone shared with the external source (PAN DMC) used as the control will be generated. It is relevant to highlight the need for these images to have a pixel size in accordance with the density of the ground points.

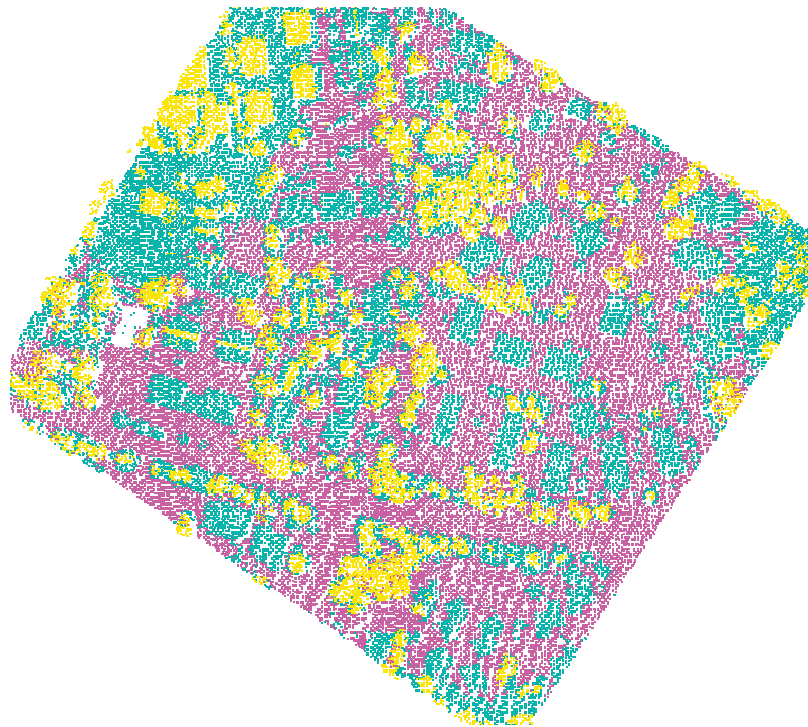


Fig3. LiDAR point cloud

In order to achieve the maximum similarity between these synthetic images with respect to the photogrammetric images (Digital Mapping Camera – DMC), it is advisable for them to have an approximate perspective so that the possible image obscurations should be as close as possible.

- ii. Since the pixel size of the synthetic images is, on the whole, higher than the pixel size of an ordinary photogrammetric image, it will be necessary to resample the images coming from the DMC in order to obtain new images with the same pixel size as the synthetic images, since the correlation algorithms do not work correctly with different pixel size in raster documents.

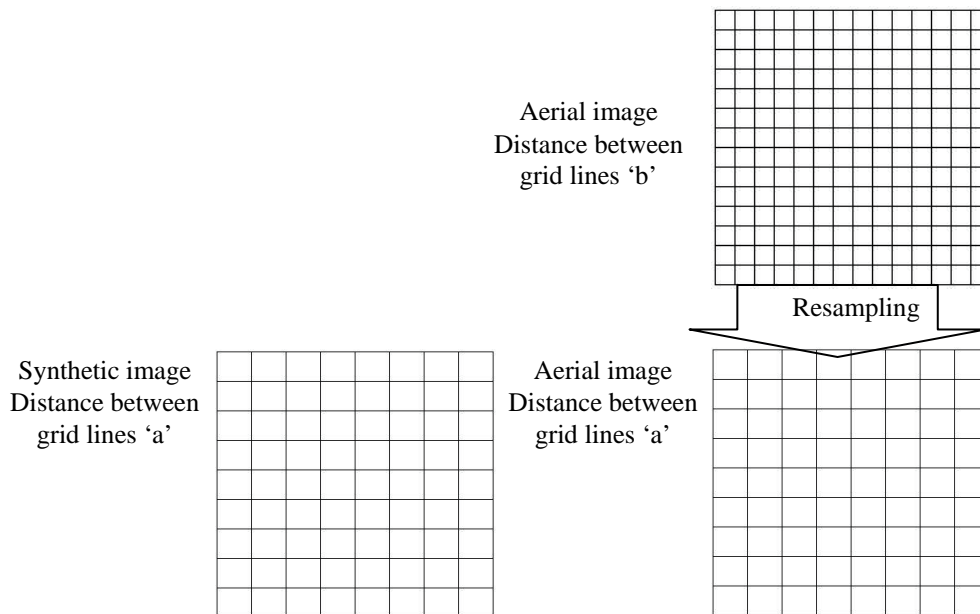


Fig4. Image resampling

Pixel size of syntethic and pancromatic resampling images used in Method 2 are described below:

- Pixel size for Pancromatic DMC images-Synthetic image from Leica ALS-50_II: 0,4m
- Pixel size for Pancromatic DMC images-Synthetic image from Optech ALTM3100: 0,5m

- iii. Next it is necessary to apply a transformed wavelet, to obtain two images as similar as possible in order to achieve the subsequent image matching. The type selected for this process is the so-called Daubechies D4 wavelet.

The algorithms based on wavelet transforms represent a compression system without losses since the image size gets smaller through smoothing in an iterative process, concurrently storing the zones of sharp changes in image colour through a number of coefficients. This series of coefficients allows generating raster files holding only information in the zones of changes (high frequencies).

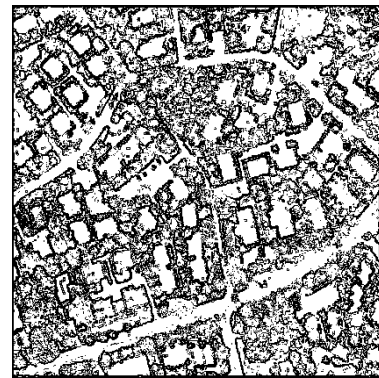
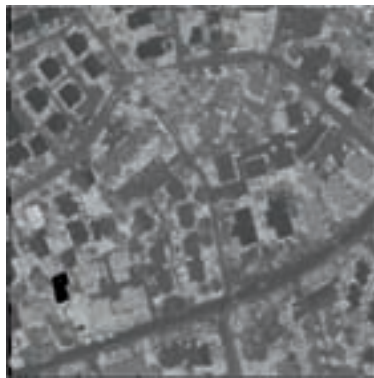
In practice these zones will coincide with changes of elements on the terrain such as corners of buildings in contrast with the ground, vegetation limits, etc.

By applying this type of algorithm to two images that are very different between each other, very similar final images will be obtained radiometrically in high frequency zones. In other words, a sharp colour change in an ordinary photogrammetric image due to a red roof over a black background will also appear in the synthetic image of intensity, although the latter will have another colour range and entirely different characteristics.

- iv. The binarization of a digital image consists of making it into a black-and-white image, so as to preserve its essential properties. The majority of geometry recognition algorithms are

created from binary images, so it is appropriate to apply a binarization filter to images generated through the wavelet transform; besides this allows reducing the bulk of data to be handled.

One of the methods to binarize a digital image is by means of its histogram. This way we obtain a graph showing the number of pixels for each gray level appearing in the image. To accomplish binarization, an appropriate value within the gray levels (threshold) should be selected in such form that the histogram takes the shape of a valley at that level. All gray levels below the calculated threshold will turn into black and all gray levels above the threshold will turn into white.



a) synthetic image



b) pancromatic image

Figure 5. Images after Daubechies D4 wavelet and binarization

- v. The next step is the extraction of characteristics of both images. These characteristic points correspond to zones where the curvature of the image is at a maximum. In this case the algorithm of extraction of characteristics developed by Harris and Stephens that uses differential operators, based on previous work of Moravec, has been applied.

Through this process a quite important number of points eligible to be homologous in both images will be extracted; several hundreds may be obtained. A good number of these points will be erroneous or they will not present the required accuracy in their planimetric position. For this reason it will be necessary to carry out a new selection based on statistical calculations to obtain a minimum of 5 optimal points.

For that purpose highest plausibility algorithms are applied not only to the radiometric characteristics of the image but also to the geometric aspects. By means of statistical variables, the points having a maximum value in the coefficient of a multi-information correlation are selected as homologous points. The parameters used are the radiometry, the point height (extracted of a DSM generated by automatic image matching and used as auxiliary information) and the wavelet coefficients – as studied above – that store the zones presenting sharp changes (high frequencies).

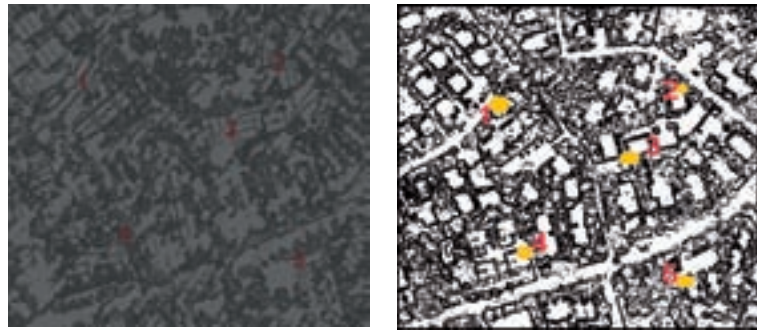


Figure 6. Homologous points in both binary images

- vi. The last step is the calculation of a 3D transformation defining the possible displacement between images now under study, using the Thompson equations for linearization of angles.

This type of equation implies a separate treatment of planimetry and altimetry. In a first step, the centroids of the two sets of points are calculated reducing their coordinates to those points. Then both the translations and the possible scale factor are calculated.

After the transformation parameters corresponding to the planimetry are known, the angles are obtained through the linearized equations mentioned above.

Results. Method 2:

In the present study, only the panchromatic images of the DMC and the LiDAR point cloud obtained with the Leica and Optech companies sensors were used.

In order to test the method, one zone of interest was defined to subsequently verify the similarity between the transformation parameters obtained in each LiDAR point cloud referring to the Method 1. In both cases the end values are very similar, hence acceptable.

Next, the results of data transformation are shown for each LiDAR point cloud.

Panchromatic images, Method 2, case Leica ALS50_II (Modified):

a) Transformation parameters obtained using ALS 50_II:

Dx -17.581 Dy -21.959 Dz -6.096 Rx 0.0001 Ry 0.0000 Rz 0.0002	Dx, Dy, Dz meters. Translations Rx, Ry, Rz arc degree. Rotations
--	---

	Lidar			Restitución		
	X	Y	Z	X	Y	Z
Punto 1	369694,593	6670194,637	60,302	369677,136	6670172,619	54,302
Punto 2	369748,073	6670158,612	58,005	369729,806	6670136,837	52,101
Punto 3	369762,429	6670156,899	56,473	369745,230	6670135,418	49,976
Punto 4	369790,814	6670135,692	57,023	369772,102	6670113,554	51,341
Punto 5	369695,028	6670211,412	60,876	369678,759	6670189,030	54,478
Tx	-17,581					
Ty	-21,959					
Tz	-6,096					
Lambda	1,000000					
Omega	0,0001	g		Rx	Ry	Rz
Fi	0,0000	g		0,124	-0,060	0,096
Kappa	0,0002	g		-0,687	0,184	0,192
				0,382	0,478	-0,401
				-1,132	-0,179	0,414
				1,312	0,345	0,343

Next, graphics with the results of the quality control applied to the transformed point cloud are shown. Some points are not used because of the incorrect identification either due to the huge vegetation or due to the control points not having coincidence with the LiDAR data.

b) Quality control for elevations – Method 2. Case Leica ALS50. Modified:

CONTROL					
ID	X	Y	Z	Z	Ez
231	369450,82	6669932,43	46,61	46,45	0,16
232	369461,46	6669941,19	46,63	46,55	0,08
233	369463,59	6669942,95	46,36	46,21	0,15
234	369474,24	6669951,76	46,22	46,02	0,2
235	369476,37	6669953,5	46,02	45,92	0,1
237	369482,11	6669958,24	45,97	45,82	0,15
238	369489,36	6669949,42	46,03	45,89	0,14
239	369483,63	6669944,69	46,04	45,95	0,09
240	369481,51	6669942,92	46,24	46,1	0,14
241	369470,83	6669934,16	46,29	46,13	0,16
242	369468,72	6669932,42	46,62	46,47	0,15
243	369458,07	6669923,64	46,65	46,52	0,13
245	369441,11	6669997,36	48,3	48,18	0,12
246	369449,63	6670004,35	48,29	48,26	0,03
247	369458,31	6669993,76	48,26	48,21	0,05
248	369438,36	6670018	48,28	48,16	0,12
249	369447,07	6670007,44	48,31	48,15	0,16
250	369438,52	6670000,43	48,28	48,18	0,1
251	369429,85	6670011,04	48,3	48,2	0,1
252	369419,81	6670002,79	50	49,87	0,13
253	369411,33	6669995,76	49,99	49,85	0,14
254	369420,06	6669985,2	50	49,87	0,13
255	369428,53	6669992,23	50,03	49,76	0,27
256	369428,58	6670028,3	46,21	46,09	0,12
257	369413,38	6670021,94	46,26	46,03	0,23
258	369410,36	6670020,67	46,23	46,03	0,2
259	369409,56	6670031,11	46,23	46,05	0,18
260	369406,5	6670029,82	46,24	46,08	0,16
261	369391,3	6670023,48	46,22	46,12	0,1
262	369395,17	6670014,32	46,24	46,33	-0,09
283	369398,32	6670006,17	45,97	45,72	0,25
284	369393,52	6670004,25	46,23	46,11	0,12
285	369397,36	6669994,5	46,27	46,02	0,25
286	369447,25	6669962,01	45,13	45,19	-0,06

287	369445,24	6669964,53	45,67	45,53	0,14
288	369440,93	6669960,98	45,71	45,48	0,23
289	369442,98	6669958,55	45,16	45,12	0,04
999975	369079,77	6669357,28	23,42	23,43	-0,01
999976	369085,69	6669359,58	23,38	23,41	-0,03
999977	369086,11	6669355,65	23,45	23,59	-0,14
999978	369083,57	6669354,67	23,49	23,59	-0,1
999988	369077,9	6669645,35	26,26	26,12	0,14
999989	369078,39	6669641,34	26,26	25,97	0,29
999990	369072,89	6669644,75	26,26	25,99	0,27
99997	369080,66	6669652,21	24,26	24,16	0,1
999987	369083,2	6669653,9	24,49	24,32	0,17
999982	369540,6	6669833,38	39,65	39,67	-0,02
999981	369542,28	6669853,71	39,41	39,41	0
999979	369545,67	6669847,08	39,43	39,43	0
999980	369545,21	6669848,5	39,44	39,45	-0,01
99991	369341,21	6669691,23	40,24	40,26	-0,02
999970	369340,29	6669692,09	40,26	40,29	-0,03
999971	369336,47	6669651,67	40,57	40,61	-0,04
999972	369337,28	6669650,52	40,59	40,58	0,01
999973	369333,92	6669628,12	41,31	41,36	-0,05
999974	369334,81	6669626,83	41,36	41,39	-0,03

c) Descriptive statistics for point residuals from altimetric differences Delta Z – Method 2 (M). Case Leica ALS50:

STATISTIC	Z
Mean	0,095892857
Median	0,12
Standard Deviation	0,010581006
Sample Variance	0,102864019
Kurtosis	-0,5924918
Skewness	0,008708033
Range	2.1
Minimum	-1.11
Maximum	0.99
Count	56

d) Quality control for planimetric – Method 2. Case Leica ALS50- Modified:

Comparison between field ground control points and measured points over the digital surface model generated from the transformed LiDAR point cloud:

CONTROL			LIDAR				
ID	X	Y	ID	X	Y	Dx	Dy
231	369450,82	6669932,43	231	369451,78	6669932,4	-0,96	0,03
232	369461,46	6669941,19	232	369461,72	6669940,21	-0,26	0,98
233	369463,59	6669942,95	233	369464,46	6669943,19	-0,87	-0,24
234	369474,24	6669951,76	234	369474,31	6669950,97	-0,07	0,79
235	369476,37	6669953,5	235	369477,08	6669952,85	-0,71	0,65
237	369482,11	6669958,24	237	369482,33	6669957,25	-0,22	0,99
238	369489,36	6669949,42	238	369488,8	6669949,35	0,56	0,07
239	369483,63	6669944,69	239	369483,66	6669945,03	-0,03	-0,34
240	369481,51	6669942,92	240	369481,33	6669942,55	0,18	0,37
241	369470,83	6669934,16	241	369471,23	6669935,27	-0,4	-1,11
242	369468,72	6669932,42	242	369467,82	6669931,89	0,9	0,53
243	369458,07	6669923,64	243	369458,7	6669924,34	-0,63	-0,7
245	369441,11	6669997,36	245	369441,77	6669997,18	-0,66	0,18
246	369449,63	6670004,35	246	369449,83	6670003,83	-0,2	0,52
247	369458,31	6669993,76	247	369457,31	6669994,68	1	-0,92
248	369438,36	6670018	248	369438,39	6670017,46	-0,03	0,54
249	369447,07	6670007,44	249	369446,53	6670007,11	0,54	0,33
250	369438,52	6670000,43	250	369438,74	6670001,52	-0,22	-1,09
251	369429,85	6670011,04	251	369430,66	6670010,81	-0,81	0,23
252	369419,81	6670002,79	252	369420,09	6670002,42	-0,28	0,37
253	369411,33	6669995,76	253	369412,36	6669995,82	-1,03	-0,06
254	369420,06	6669985,2	254	369420,19	6669986,01	-0,13	-0,81
255	369428,53	6669992,23	255	369428,26	6669991,79	0,27	0,44
256	369428,58	6670028,3	256	369428,33	6670028,09	0,25	0,21
257	369413,38	6670021,94	257	369414,34	6670022,74	-0,96	-0,8
258	369410,36	6670020,67	258	369409,41	6670020,73	0,95	-0,06
259	369409,56	6670031,11	259	369410,52	6670031,03	-0,96	0,08
260	369406,5	6670029,82	260	369406,47	6670029,23	0,03	0,59
261	369391,3	6670023,48	261	369391,65	6670022,91	-0,35	0,57
262	369395,17	6670014,32	262	369396,07	6670014,62	-0,9	-0,3
283	369398,32	6670006,17	283	369397,54	6670005,36	0,78	0,81
284	369393,52	6670004,25	284	369394,38	6670003,67	-0,86	0,58

285	369397,36	6669994,5		285	369398,58	6669995,17		-1,22	-0,67
286	369447,25	6669962,01		286	369446,79	6669962,31		0,46	-0,3
287	369445,24	6669964,53		287	369445,31	6669964,05		-0,07	0,48
288	369440,93	6669960,98		288	369441,78	6669961,22		-0,85	-0,24
289	369442,98	6669958,55		289	369442,53	6669959,09		0,45	-0,54

e) Descriptive statistics for point residuals from planimetric differences DeltaX and DeltaY – Method 2 (M). Case Leica ALS50:

	X	Y
Mean	-0,197567568	0,05837838
Median	-0,22	0,18
Standard Deviation	0,38873003	0,34802508
Sample Variance	0,623482181	0,5899365
Kurtosis	-0,887327034	-0,80194303
Skewness	0,290470778	-0,4297395
Range	2,22	2,1
Minimum	-1,22	-1,11
Maximum	1	0,99
Count	37	37

Panchromatic images, Method 2, case Optech ALTM3100:

a) Transformation parameters obtained using ALTM3100:

Dx 23.702 Dy -18.073 Dz 25.425 Rx 0.0003 Ry 0.0002 Rz 0.0002	Dx, Dy, Dz meters. Translations Rx, Ry, Rz arc degree. Rotations
---	---

Lidar				Restitución			
	X	Y	Z		X	Y	Z
Punto 1	369419.12	6669875.80	20.110		369442.88	6669857.70	45.740
Punto 2	369448.74	6670008.30	13.899		369472.23	6669990.10	39.071
Punto 3	369550.00	6670019.70	13.730		369573.85	6670001.70	39.071
Punto 4	369505.98	6669937.10	13.654		369529.52	6669919.20	39.071
Punto 5	369468.09	6669855.10	14.171		369491.98	6669836.90	39.736
<u>Tx</u>	23,702						
<u>Ty</u>	-18.073			<u>Rx</u>	<u>Ry</u>	<u>Rz</u>	
<u>Tz</u>	25.425			0.058	0.045	0.205	
Lambda	1,000000			-0.216	-0.112	-0.253	
Omega	0,0003g			0.146	-0.013	-0.084	
Fi	0,0002g			-0.168	0.186	-0.008	
Kappa	0,0002g			0.180	-0.106	0.140	

Next, graphics with the results of the quality control applied to the transformed point cloud are shown. Some points are not used because of the incorrect identification either due to the huge vegetation or due to the control points have no coincidence with the LiDAR data.

b) Quality control for elevations – Method 2. Case Optech ALTM3100:

	CONTROL		
ID	Zcontrol	Zlidar	Dz
231	46,6117	46,49	0,1217
232	46,6266	46,71	-0,0834
233	46,3552	46,35	0,0052
234	46,2207	46,53	-0,3093
236	46,0212	46,02	0,0012
237	45,9742	46,02	-0,0458
238	46,0323	46,15	-0,1177
239	46,0436	45,97	0,0736
240	46,24	46,51	-0,27
241	46,2863	46,27	0,0163
242	46,6187	46,67	-0,0513
243	46,6484	46,8	-0,1516
244	48,3252	48,42	-0,0948
245	48,3032	48,56	-0,2568
246	48,2882	48,44	-0,1518
247	48,2552	48,42	-0,1648

248	48,282	48,42	-0,138
249	48,3059	48,42	-0,1141
250	48,2748	48,43	-0,1552
251	48,2962	48,24	0,0562
252	49,9965	50,01	-0,0135
253	49,9859	50,28	-0,2941
254	50,0035	50,13	-0,1265
255	50,0269	50,11	-0,0831
256	46,2124	46,14	0,0724
257	46,2566	46,35	-0,0934
258	46,2291	46,25	-0,0209
259	46,2313	46,17	0,0613
260	46,2387	46,1	0,1387
261	46,2165	46,27	-0,0535
262	46,2392		
272	39,3757	39,23	0,1457
273	39,3909	39,37	0,0209
274	39,375		
281	40,4108	40,45	-0,0392
282	40,397	40,39	0,007
283	45,9663		
284	46,2263		
285	46,2731		
286	45,1309	44,89	0,2409
287	45,6739	45,71	-0,0361
288	45,7141	45,79	-0,0759
289	45,1596		
999975	23,416	23,21	0,206
999976	23,379	23,18	0,199
999977	23,447	23,33	0,117
999978	23,492	23,32	0,172
999988	26,261	26,24	0,021
999989	26,264	26,26	0,004
999990	26,257	26,25	0,007
99997	24,258	24,11	0,148
999987	24,485	24,32	0,165
999982	39,649	39,5	0,149
999981	39,414	39,38	0,034

999979	39,427	39,42	0,007
999980	39,442	39,42	0,022
999991	40,24	40,21	0,03
999970	40,26	40,11	0,15
999971	40,569	40,45	0,119
999972	40,587	40,45	0,137
999973	41,305	41,26	0,045
999974	41,356	41,29	0,066

c) Descriptive statistics for point residuals from altimetric differences Delta Z – Method 2. Case Optech ALTM3100:

STATISTIC	Z
Mean	-0,0032446
Median	0,007
Standard Deviation	0,1294184
Sample Variance	0,0167491
Kurtosis	-0,2034877
Skewness	-0,3845359
Range	0,550
Minimum	-0,309
Maximum	0,241
Count	56

d) Quality control for planimetric – Method 2. Case Optech ALTM3100:

Comparison between field ground control points and measured points over the digital surface model generated from the transformed LiDAR point cloud:

	CONTROL				LIDAR				
ID	X	Y		ID	X	Y		Dx	Dy
231	369450,817	6669932,425		231	369450,980	6669932,420		-0,163	0,005
232	369461,458	6669941,186		232	369461,740	6669940,680		-0,282	0,506
233	369463,587	6669942,948		233	369463,890	6669942,950		-0,304	-0,002
234	369474,240	6669951,763		234	369474,410	6669951,130		-0,170	0,633
236	369476,371	6669953,505		236	369476,530	6669953,240		-0,159	0,265
237	369482,108	6669958,239		237	369482,050	6669957,210		0,058	1,029

238	369489,357	6669949,420		238	369489,110	6669949,500		0,247	-0,080
239	369483,633	6669944,693		239	369483,770	6669944,720		-0,137	-0,027
240	369481,512	6669942,919		240	369481,380	6669942,920		0,132	-0,002
241	369470,833	6669934,162		241	369471,260	6669934,250		-0,427	-0,088
242	369468,716	6669932,422		242	369468,200	6669932,250		0,516	0,172
243	369458,071	6669923,642		243	369458,000	6669924,160		0,071	-0,518
244	369449,801	6669986,749		244	369449,590	6669986,960		0,211	-0,211
245	369441,114	6669997,355		245	369441,590	6669996,960		-0,476	0,395
246	369449,626	6670004,353		246	369449,290	6670003,330		0,336	1,023
247	369458,308	6669993,755		247	369457,770	6669994,090		0,538	-0,335
248	369438,360	6670018,004		248	369438,340	6670017,570		0,020	0,433
249	369447,068	6670007,438		249	369446,230	6670007,610		0,838	-0,172
250	369438,523	6670000,431		250	369438,740	6670000,690		-0,217	-0,259
251	369429,848	6670011,039		251	369430,590	6670011,390		-0,742	-0,351
252	369419,814	6670002,791		252	369420,060	6670002,060		-0,246	0,731
253	369411,332	6669995,758		253	369411,580	6669995,430		-0,248	0,328
254	369420,059	6669985,199		254	369420,160	6669986,040		-0,101	-0,841
255	369428,533	6669992,232		255	369427,610	6669992,470		0,923	-0,238
256	369428,584	6670028,304		256	369427,650	6670028,630		0,934	-0,326
257	369413,376	6670021,940		257	369413,550	6670021,620		-0,174	0,320
258	369410,359	6670020,668		258	369409,600	6670020,430		0,758	0,238
259	369409,560	6670031,107		259	369410,360	6670031,040		-0,800	0,067
260	369406,495	6670029,815		260	369406,320	6670029,420		0,175	0,395
261	369391,299	6670023,475		261	369391,360	6670023,370		-0,061	0,105
262	369395,166	6670014,322		262					
272	369389,737	6670057,617		272	369389,880	6670057,560		-0,143	0,057
273	369379,027	6670058,321		273	369379,040	6670058,390		-0,013	-0,069
274	369380,580	6670082,369		274					
281	369365,450	6670046,555		281	369365,130	6670046,390		0,320	0,164
282	369354,727	6670045,984		282	369354,940	6670045,930		-0,213	0,054
283	369398,321	6670006,166		283					
284	369393,519	6670004,252		284					
285	369397,363	6669994,501		285					
286	369447,247	6669962,011		286	369446,730	6669961,890		0,517	0,121
287	369445,237	6669964,525		287	369444,910	6669963,660		0,327	0,865
288	369440,928	6669960,984		288	369441,530	6669960,970		-0,602	0,014

*e) Descriptive statistics for point residuals from planimetric differences DeltaX and DeltaY
– Method 2. Case Optech ALTM3100:*

	X	Y
Mean	0,03365946	0,118964865
Median	-0,0606	0,0566
Standard Deviation	0,4340708	0,40771166
Sample Variance	0,1884175	0,1662288
Kurtosis	-0,1675906	0,44667626
Skewness	0,3808518	0,34761542
Range	1,735	1,870
Minimum	0,8	-0,841
Maximum	0,934	1,029
Count	37	37

Level of Automation. Method 2:

The entire process as described above may be performed automatically through the correct development of the different algorithms in a computer support system. Monitoring by an operator is only needed at the step of extracting characteristic points and their subsequent correlation to find the optimal points in order to avoid possible higher errors invalidating the results obtained.

In any case, it is believed that this method provides a very high degree of automation. Moreover, the process time spent by the use of the different tools is relatively short, as long as the selected zones to obtain the transformation parameters are not excessively large. This condition is due to the long time and the many resources expended in the generation of synthetic images, as well as the processes of extraction of characteristics and image matching, taking into account that it is necessary to move through all the pixels of the images in both cases.

Time spent in every process is shown below:

Reference DSM generation.

Automatic image matching + manual edition	0 h 45 min
Photogrammetric images resampling	2min (1 min per image)
Stereoscopic pairs generation based on synthetic images	5 min
Wavelet application	5 min
Binarization	2 min
Automatic interesting points extraction (XYZ)	5 min
Solve and analysis of the 3D transformation	5 min
	TOTAL 1 h 09 min

Discussion. Method 2:

A number of problems and limitations were detected in the process that could be obviated through a more detailed study of the method.

Once the optimal points have been automatically selected, the transformation parameters corresponding to the planimetry were calculated and subsequently an automatic extrapolation was employed on a digital surface model (DSM) to obtain the point height. This digital model was created by automatic image matching. At the present time, the automatic image matching algorithms for digital model generation, present serious problems concerning the results achieved; this depends on the image quality and the terrain characteristics. For this reason a subsequent edition by a skilled operator is necessary to achieve a digital model correctly defining the terrain and the elements lying on it.

It is also important to emphasize that the images used correspond to a zone presenting a high number of different features – buildings, vegetation, etc. It would be interesting to test the present method using images with homogeneous features to study its performance in this case.

Finally, the point density that may be achieved by a LiDAR sensor is at present still very restricted. This issue is essential when generating quality synthetic images of intensity since the higher the density of swept points the higher will be the spatial resolution of the generated images. An increase in the spatial resolution of those images would allow removing the step of photogrammetric image resampling, resulting in the enhancement of quality and accuracy of the end product.

The systematic errors of XYZ coordinates of the point clouds both for Leica and Optech LiDAR point cloud present certain differences shown below:

Accuracy for Method 2 Transformation	Leica ALS50_II (M)	Optech ALTM3100
X constant – systematic error	-0,19m	0.03 m
Y constant – systematic error	0.05 m	0.11 m
Z constant – systematic error	0.09 m	-0.003 m
X standard deviation	0.38 m	0.43 m
Y standard deviation	0.34 m	0.41 m
Z standard deviation	0.01 m	0.13 m

Fig 7. Quality results for the LiDAR point cloud transformation-Method2

It is about reasonable values that give a high standard deviation for X and Y coordinates due to the LiDAR data with low density. On the other hand, the Z standard deviation is low in both cases because the altimetric accuracy is higher than the planimetric accuracy.

It is possible to improve the final results using a bigger quantity of points and a better distribution of them over the point cloud.

However, in a flight project like this, the altimetric standard deviation it is about 0.5 meters and the LiDAR accuracy is about 0.15 meters, so the quadratic component could produce an error next to 0.5 meters.

As an additional check, the two methods were compared. The time process is lower in the second method, 1.09 hours in Method2 against 2 hours in Method1, for each Lidar point cloud. The systematic errors are quite similar in some cases but the higher differences are in the Z coordinate. On the other hand, the Z standard deviation is lower in Method 2, but the planimetric standard deviation in Method 2 is higher than Method 1.

Pixel size of syntethic and pancromatic resampling images used in Method 2 are noticed:

- Pixel size for Pancromatic DMC images-Synthetic image from Leica ALS-50_II: 0,4m
- Pixel size for Pancromatic DMC images-Synthetic image from Optech ALTM3100: 0,5m

Accuracy for Method Transformation	Leica Method 2	Leica Method 1	Optech Method 2	Optech Method 1
X constant – systematic error	-0.19 m	-0.20 m	0.03 m	-0.03 m
Y constant – systematic error	0.05 m	-0.27 m	0.11 m	-0.13 m
Z constant – systematic error	0.09 m	0.36 m	-0.003 m	0.25 m
X standard deviation	0.38 m	0.35 m	0.43 m	0.18 m
Y standard deviation	0.34 m	0.35 m	0.41 m	0.26 m
Z standard deviation	0.01 m	0.24 m	0.13 m	0.20 m

Fig 8. Quality results for the LiDAR point cloud transformation- Both Methods

An integrated management of the above-mentioned processes in a stand-alone computer environment would enable the definition of an entirely automatic methodology for the correct integration of LiDAR data and photogrammetric data. At the present time every process is carried out separately and the mediation of an operator introducing all the needed information at every step is required.

Algorithms can be implemented to enhance this automatic method with the aim of improving the determination of the XYZ coordinates of the homologous points over the photogrammetric and synthetic images, necessary for calculation of the transformation parameters between both data sets, through the knowledge of the external orientation of the photographs either through aerotriangulation techniques, or by direct parameters originating from the GPS-IMU systems.

Using the geometry of intersections in space (colinearity equations), advantages such as improved accuracy of the transformed point cloud, a reduction in process time by eliminating the image matching process and the subsequent edition of the reference DSM and the possibility of full automation of the process, could be achieved.

Conclusions. Method 2:

The possibility to use wavelet transform and binarization algorithms to obtain suitable images in order to extract the homologous points in synthetic and DMC images by matching geometric aspects and finally to calculate the transformation between both data sets was evaluated.

The advantages in the time process of Method 2 (automatic measurements) against Method 1 (manual measurement) were proved.

In conclusion, the proper functioning of the developed algorithms was proved as well as the validity of automatic methodology proposed since the accuracies obtained with this method are within the expected range, due to the pixel size of the images used and the number of homologous points selected.

Finally, new developments can easily be performed to improve the automation and accuracy of this method.

References. Method 2:

Articles

“Lidargrammetry” combines the best of two worlds

Martin Flood

General manager

GeoCue Canada

E-mail: mflood@goeocue.com

The Daubechies D4 Wavelet Transform

Ian Kaplan

Lawrence Livermore National Laboratory

http://www.bearcave.com/misl/misl_tech/wavelets/daubechies/index.html

Análisis de imagen basado en texturas mediante la transformada Wavelet

R. Marfil, F. Jiménez, A. Bandera y F. Sandoval

Departamento de Tecnología Electrónica, E.T.S.I. Telecomunicación

Universidad de Málaga, Málaga (Spain)

E-mail: rebeca@dte.uma.es

Books

Photogrammetry and Surveying. A selection of papers 1910-1976

E. H. Thompson

Photogrammetric Society of London

Lieutenant Colonel

Method 1: Appendix 1.

Measured coordinates and residuals for each point – Method 1. Case Leica ALS50_II:

Known point pairs - Images - Lidar - Units meters

03		369614.748	6670149.915	56.190
	=>	369631.800	6670171.906	62.611
04		369668.788	6670139.427	57.632
	=>	369687.216	6670161.811	63.153
05		369675.320	6670153.138	57.639
	=>	369693.875	6670175.128	63.505
08		369483.089	6669851.783	49.258
	=>	369500.778	6669873.348	54.965
09		369461.668	6669845.175	49.404
	=>	369479.085	6669866.690	55.232
10		369454.432	6669868.341	50.797
	=>	369471.997	6669889.672	56.708
11		369475.323	6669875.834	50.391
	=>	369493.046	6669897.190	56.236
12		369465.032	6669936.767	48.097
	=>	369482.951	6669958.190	54.082
15		369429.454	6669982.400	50.877
	=>	369447.296	6670003.940	57.048
16		369347.667	6669899.113	52.653
	=>	369364.758	6669920.770	58.585
17		369395.100	6669881.725	52.075
	=>	369412.508	6669902.995	58.075
18		369410.418	6669888.166	48.864
	=>	369428.367	6669909.589	54.779
19		369346.193	6669823.749	48.203
	=>	369363.957	6669845.318	54.363
25		369446.784	6669793.275	49.403
	=>	369465.016	6669814.925	55.009
30		369258.587	6669705.708	45.774
	=>	369276.538	6669727.022	51.760
26		369407.810	6669765.578	50.524
	=>	369426.139	6669787.432	56.258
31		369237.456	6669695.555	47.110

	=>	369255.488	6669717.142	52.874
27		369401.197	6669772.708	50.588
	=>	369419.266	6669794.520	56.379
32		369254.579	6669681.208	46.684
	=>	369272.671	6669703.181	52.526
33		369261.493	6669642.341	47.983
	=>	369278.900	6669664.089	53.914
29		369298.020	6669639.218	48.122
	=>	369315.415	6669660.867	54.160
35		369241.770	6669619.516	48.414
	=>	369259.354	6669641.321	54.131
36		369261.316	6669602.575	52.060
	=>	369279.330	6669623.493	57.795
41		369017.859	6669613.605	27.357
	=>	369035.758	6669634.448	33.228
42		369025.436	6669473.713	33.394
	=>	369043.813	6669495.264	38.918
38		369164.204	6669604.878	41.466
	=>	369182.460	6669626.286	47.357
45		368914.441	6669399.899	20.027
	=>	368933.303	6669421.537	26.162
50		369618.527	6670059.225	51.030
	=>	369636.510	6670080.901	57.137
46		369038.099	6669380.922	31.175
	=>	369056.700	6669402.260	35.911
51		369629.454	6669977.465	49.895
	=>	369647.514	6669999.023	56.080
48		369555.278	6670059.025	49.614
	=>	369573.348	6670080.813	56.600
53		369534.528	6669964.271	47.089
	=>	369552.323	6669985.391	53.125
49		369572.795	6670067.914	50.567
	=>	369590.908	6670090.055	56.657
54		369543.486	6669924.042	45.017
	=>	369561.103	6669946.576	51.306
55		369591.909	6669958.719	45.454
	=>	369609.854	6669981.232	51.628
v2_100		369726.267	6670049.736	51.816
	=>	369744.321	6670071.092	57.598

v2_103		369707.669	6670058.793	51.648
=>		369726.024	6670080.281	57.619
v2_104		369804.918	6670093.962	53.130
=>		369823.086	6670115.766	58.848
v2_105		369798.968	6670090.743	53.103
=>		369817.233	6670111.828	59.323
v2_106		369748.333	6670140.873	54.080
=>		369766.528	6670162.724	59.626
v2_111		369631.674	6670099.865	57.372
=>		369649.618	6670122.006	63.418
v2_107		369771.811	6670113.324	54.149
=>		369790.176	6670135.047	59.936
v2_112		369195.339	6669795.792	48.572
=>		369213.199	6669817.567	54.589
v2_108		369732.951	6670122.478	53.437
=>		369750.878	6670144.367	59.780
v2_113		369240.231	6669737.138	45.160
=>		369258.470	6669759.090	51.150
v2_109		369676.936	6670172.562	56.497
=>		369694.867	6670194.764	62.339
v2_114		369171.065	6669566.640	42.954
=>		369189.325	6669588.864	48.942
v2_116		368922.329	6669383.656	20.298
=>		368940.796	6669405.354	26.190
v2_117		369194.231	6669525.205	41.452
=>		369212.297	6669546.816	47.598

Residuals – Method 1. Case Leica ALS50

Number	dEasting	dNorthing	dZ
03	+0.8477	-0.2647	-0.3284
04	-0.5252	-0.6426	+0.5452
05	-0.6566	-0.2471	+0.2083
08	+0.2942	+0.1290	+0.2079
09	+0.5678	+0.1724	+0.0891
10	+0.4137	+0.3531	+0.0262
11	+0.2538	+0.3352	+0.0904
12	+0.0388	+0.2669	-0.0002
15	+0.1040	+0.1368	-0.1409

16	+0.8793	-0.0050	+0.0636
17	+0.5674	+0.3965	-0.0332
18	+0.0240	+0.2497	+0.0514
19	+0.2272	+0.0862	-0.2194
25	-0.2319	+0.0333	+0.2776
30	+0.0733	+0.3173	-0.1041
26	-0.3205	-0.1832	+0.1421
31	-0.0039	+0.0374	+0.1173
27	-0.0628	-0.1427	+0.0920
32	-0.0598	-0.3432	+0.0224
33	+0.6361	-0.1178	-0.0972
29	+0.6499	-0.0079	-0.2197
35	+0.4661	-0.1806	+0.1061
36	+0.0425	+0.7091	+0.0690
41	+0.1459	+0.7325	+0.0234
42	-0.2892	+0.0225	+0.2640
38	-0.2041	+0.1992	-0.0530
45	-0.7582	-0.0866	-0.3649
50	-0.0588	+0.0558	-0.0835
46	-0.4873	+0.2409	+0.9781
51	-0.1129	+0.1773	-0.2259
48	-0.1464	-0.0739	-0.9408
53	+0.1550	+0.5907	-0.0548
49	-0.1918	-0.4225	-0.0443
54	+0.3437	-0.8192	-0.3412
55	+0.0062	-0.7845	-0.2166
v2_100	-0.1272	+0.4059	+0.1981
v2_103	-0.4309	+0.2689	+0.0218
v2_104	-0.2532	-0.0204	+0.2684
v2_105	-0.3492	+0.6975	-0.2337
v2_106	-0.2934	-0.0844	+0.4943
v2_111	-0.0296	-0.4098	+0.0034
v2_107	-0.4555	+0.0510	+0.2254
v2_112	+0.1397	-0.1645	-0.0463
v2_108	-0.0210	-0.1263	-0.3107
v2_113	-0.2241	-0.3255	-0.0785
v2_109	-0.0382	-0.4578	+0.2463
v2_114	-0.1959	-0.6157	-0.1800
v2_116	-0.3580	-0.1446	-0.1366
v2_117	+0.0095	+0.0052	-0.3777

Maximums	+0.8793	+0.8192	+0.9781

Measured coordinates and residuals for each point – Method 1. Case Optech ALTM 3100:

Known point pairs - Images - Lidar - Units meters

03	369590.283	6670167.930	31.220
=>	369614.748	6670149.915	56.190
04	369644.733	6670157.261	32.177
=>	369668.788	6670139.427	57.632

01		369702.128	6670067.429	26.158
	=>	369726.339	6670049.701	51.670
50		369594.698	6670077.547	25.528
	=>	369618.527	6670059.225	51.030
48		369531.547	6670077.450	24.843
	=>	369555.278	6670059.025	49.614
49		369549.207	6670086.089	25.127
	=>	369572.795	6670067.914	50.567
55		369568.181	6669977.250	20.099
	=>	369591.909	6669958.719	45.454
51		369605.566	6669995.222	24.631
	=>	369629.454	6669977.465	49.895
53		369510.548	6669981.383	21.739
	=>	369534.528	6669964.271	47.089
54		369519.040	6669942.521	19.803
	=>	369543.486	6669924.042	45.017
12		369440.786	6669954.421	22.604
	=>	369465.032	6669936.767	48.097
15		369406.347	6669999.919	25.743
	=>	369429.454	6669982.400	50.877
13		369391.562	6669987.357	27.630
	=>	369416.220	6669968.580	53.065
10		369430.208	6669885.904	25.138
	=>	369454.432	6669868.341	50.797
11		369450.883	6669893.297	24.730
	=>	369475.323	6669875.834	50.391
09		369437.661	6669862.945	23.741
	=>	369461.668	6669845.175	49.404
08		369459.057	6669869.436	23.495
	=>	369483.089	6669851.783	49.258
17		369370.766	6669899.427	26.415
	=>	369395.100	6669881.725	52.075
18		369386.994	6669905.558	23.287
	=>	369410.418	6669888.166	48.864
16		369323.299	6669917.067	26.508
	=>	369347.667	6669899.113	52.653
25		369423.263	6669811.030	23.846
	=>	369446.784	6669793.275	49.403
27		369377.747	6669790.594	24.907

	=>	369401.197	6669772.708	50.588
26		369384.535	6669783.806	24.519
	=>	369407.810	6669765.578	50.524
19		369322.156	6669841.576	22.728
	=>	369346.193	6669823.749	48.203
31		369213.797	6669713.675	21.300
	=>	369237.456	6669695.555	47.110
30		369234.804	6669722.964	20.203
	=>	369258.587	6669705.708	45.774
32		369230.946	6669698.741	21.093
	=>	369254.579	6669681.208	46.684
33		369237.162	6669660.388	22.306
	=>	369261.493	6669642.341	47.983
29		369273.371	6669657.048	22.388
	=>	369298.020	6669639.218	48.122
36		369236.894	6669619.785	25.820
	=>	369261.316	6669602.575	52.060
34		369203.061	6669638.398	21.330
	=>	369227.642	6669620.591	46.966
35		369217.387	6669637.577	22.472
	=>	369241.770	6669619.516	48.414
39		369106.992	6669639.756	15.285
	=>	369130.930	6669621.044	40.974
38		369140.289	6669622.822	15.888
	=>	369164.204	6669604.878	41.466
41		368994.310	6669630.610	1.923
	=>	369017.859	6669613.605	27.357
42		369001.741	6669491.419	7.509
	=>	369025.436	6669473.713	33.394
46		369014.139	6669398.662	4.217
	=>	369038.099	6669380.922	31.175
45		368890.721	6669418.210	-5.898
	=>	368914.441	6669399.899	20.027
v2_100		369702.128	6670067.429	26.169
	=>	369726.267	6670049.736	51.816
v2_103		369684.507	6670076.535	26.247
	=>	369707.669	6670058.793	51.648
v2_104		369780.860	6670111.507	27.918
	=>	369804.918	6670093.962	53.130

v2_105		369775.191	6670108.421	27.893
=>		369798.968	6670090.743	53.103
v2_106		369724.838	6670158.694	28.565
=>		369748.333	6670140.873	54.080
v2_107		369747.968	6670131.411	28.425
=>		369771.811	6670113.324	54.149
v2_108		369708.758	6670140.578	28.300
=>		369732.951	6670122.478	53.437
v2_109		369652.869	6670190.870	31.216
=>		369676.936	6670172.562	56.497
v2_110		369601.594	6670200.010	31.415
=>		369625.460	6670182.158	56.636
v2_111		369607.823	6670118.215	32.069
=>		369631.674	6670099.865	57.372
v2_112		369171.705	6669813.402	22.989
=>		369195.339	6669795.792	48.572
v2_113		369216.644	6669754.417	19.643
=>		369240.231	6669737.138	45.160
v2_114		369147.550	6669585.028	17.432
=>		369171.065	6669566.640	42.954
v2_117		369170.425	6669543.880	15.800
=>		369194.231	6669525.205	41.452

Residuals	Method 1. Case Optech ALTM 3100		
Number	dEasting	dNorthing	dZ

03	-0.5204	+0.1309	+0.2663
04	-0.1115	-0.0534	-0.1633
01	-0.2705	-0.1732	-0.0393
50	+0.1125	+0.4282	-0.1212
48	+0.2112	+0.5355	+0.5649
49	+0.3548	+0.2845	-0.1050
55	+0.2097	+0.6306	+0.1638
51	+0.0481	-0.1385	+0.2527
53	-0.0430	-0.7813	+0.1214
54	-0.5104	+0.5821	+0.3245
12	-0.3112	-0.2326	-0.0294
15	+0.8287	-0.3594	+0.2350
13	-0.7250	+0.9021	-0.0572
10	-0.2965	-0.3180	-0.0957
11	-0.5121	-0.4210	-0.0943
09	-0.0803	-0.1139	-0.0581
08	-0.1049	-0.2333	-0.1533
17	-0.4065	-0.1730	-0.1593
18	+0.5056	-0.4885	-0.0744
16	-0.4389	+0.0831	-0.7052
25	+0.4013	-0.1277	+0.1186
27	+0.4702	+0.0083	-0.0050
26	+0.6447	+0.3498	-0.3143
19	-0.1118	-0.0498	+0.0812
31	+0.2570	+0.2497	-0.1301
30	+0.1350	-0.6175	+0.1090
32	+0.2820	-0.3391	+0.1247
33	-0.4192	+0.1770	+0.1023
29	-0.7384	-0.0431	+0.0769
36	-0.5163	-0.6544	-0.3972
34	-0.6707	-0.0620	+0.1535
35	-0.4734	+0.1926	-0.1407
39	-0.0236	+0.8408	+0.0312
38	-0.0017	+0.0713	+0.1923
41	+0.3745	-0.8785	+0.2207
42	+0.2132	-0.1694	-0.0082
46	-0.0566	-0.1414	-0.9271
45	+0.1928	+0.4233	-0.0119
v2_100	-0.1983	-0.2076	-0.1747
v2_103	+0.7793	-0.1574	+0.0450
v2_104	-0.1155	-0.3590	+0.2472
v2_105	+0.1652	-0.2261	+0.2497
v2_106	+0.4508	-0.0777	-0.1689
v2_107	+0.1008	+0.1856	-0.3195
v2_108	-0.2478	+0.2020	+0.2256
v2_109	-0.1202	+0.4189	-0.0362
v2_110	+0.0810	-0.0331	-0.0272
v2_111	+0.0893	+0.4650	+0.0234
v2_112	+0.2886	-0.2540	-0.0890
v2_113	+0.3339	-0.5941	+0.1011
v2_114	+0.3936	+0.5169	+0.3117
v2_117	+0.1005	+0.7996	+0.2631

Maximums	+0.8287	+0.9021	+0.9271

Report of the University of Calgary EuroSDR "Registration Quality – Towards Integration of Laser Scanning and Photogrammetry"

Ayman F. Habib, University of Calgary, ahabib@ucalgary.ca
Eunju Kwak, University of Calgary, ekwak@ucalgary.ca
Sendo Wang, University of Calgary, sendo@ucalgary.ca
Ana Paula Kersting, University of Calgary, ana.kersting@ucalgary.ca



1. Introduction

The complementary characteristics of LiDAR and photogrammetric data continuously lead towards the integration of both systems. To fully utilize the synergic characteristics in these data, they should be georeferenced to the same reference frame; hence, the importance of a proper co-registration methodology is obvious and cannot be ignored. However, the lack of standard process for orientation of laser scanning data relative to photogrammetric data leads to the various kinds of registration methods. Therefore, EuroSDR initiated this joint project to compare the existing methods comprehensively.

The objective of this report is to introduce the registration method between LiDAR and images developed by Digital Photogrammetry Research Group (DPRG) while utilizing appropriate primitives that can be extracted from the LiDAR data with a satisfactory level of automation. This report starts with discussing the proposed procedure for the registration, including the automatic extraction of the primitives. Then, the results of registration between images and LiDAR are presented. After the results are evaluated through qualitative analysis, discussion about the amount of time and automation follows. Finally, this report presents some conclusions.

2. Methods

To register any two datasets, common features have to be identified and extracted from both datasets. The decision of primitives influences the subsequent registration steps; therefore, it is crucial to decide upon the primitives to be used for establishing the transformation between the datasets in question. In traditional photogrammetric applications, point primitives are commonly used. However, since the LiDAR footprints are irregularly distributed, it is almost impossible to identify distinct conjugate points in overlapping photogrammetric and LiDAR data. Consequently, straight-lines and planar patches are used as the registration features for photogrammetric and LiDAR dataset integration.

Urban areas are rich with planar patches such as building roofs and manmade monuments. When it comes to the linear features, it is not easy to measure 3D linear features in irregular point clouds. This research indirectly determines 3D lines by intersecting extracted neighboring 3D planar patches.

The co-registration of photogrammetric and LiDAR datasets using planar patches and straight lines can be implemented in the same fashion. Both methodologies are based on preliminary and independent processing of the LiDAR and photogrammetric data, where a photogrammetric model is built relative to a coordinate system defined by the EOP information provided by EuroSDR. Then, conjugate LiDAR and photogrammetric features are utilized in an absolute orientation between the photogrammetric model and the LiDAR reference frame. Figure 1 shows this 2-step procedure of registration. The registration parameters will be determined relative to the image reference frame, then, transformed LiDAR points will be determined through Equation 1 where $(X'_{LiDAR}, Y'_{LiDAR}, Z'_{LiDAR})$ refers to the transformed LiDAR point cloud to the image reference frame.

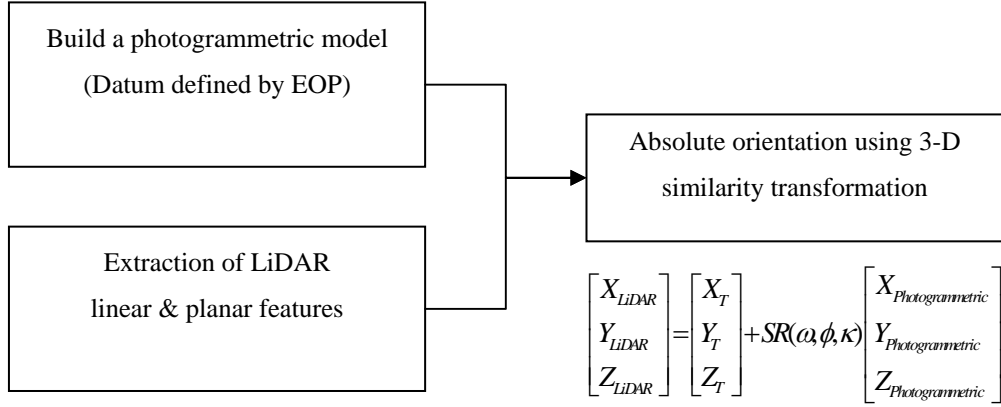


Figure 1: 2-step procedure for the registration of LiDAR and photogrammetric datasets

$$\begin{bmatrix} X'_{LiDAR} \\ Y'_{LiDAR} \\ Z'_{LiDAR} \end{bmatrix} = \frac{R^T}{S} \left(\begin{bmatrix} X_{LiDAR} \\ Y_{LiDAR} \\ Z_{LiDAR} \end{bmatrix} - \begin{bmatrix} X_T \\ Y_T \\ Z_T \end{bmatrix} \right) \quad (1)$$

In the following section, first, we will discuss how to represent and extract the planar and linear features from the photogrammetric data; then, building a 3D photogrammetric model incorporating points and linear features will follow. The mathematical models and similarity measures in the suggested registration methodologies will be addressed after discussing the semi-automatic procedure for extracting LiDAR features.

2.1. Representation and extraction of Photogrammetric features

The photogrammetric planar surface is identified and represented by 3 or more 2D points in the image space; e.g., the points A, B, and C in Figure 2 are observed in the image space and determine a triangular area. Three points are the minimum number of points required to explicitly define a plane.

The vertices should be measured on all overlapping images the points appear in to define a photogrammetric 3D surface.

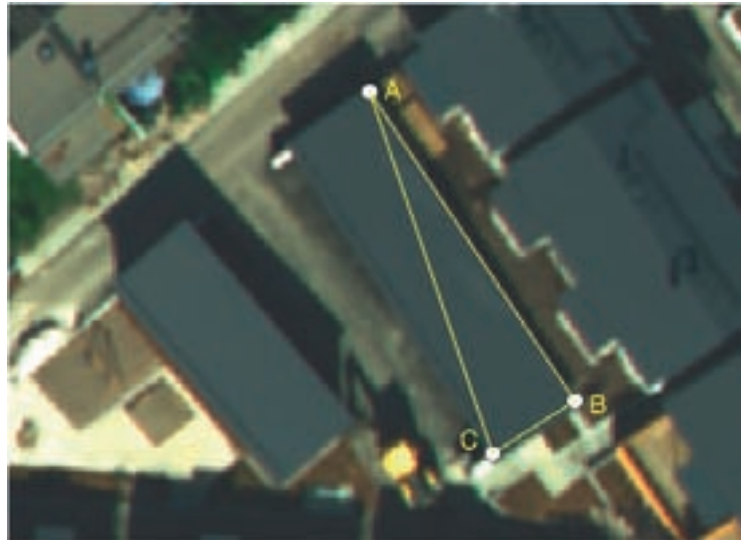


Figure2: Image space planar features represented by three points

Straight lines appearing in a group of overlapping images are represented by two end points which are used to define the corresponding 3D model space line through the collinearity model, and a series of intermediate points. The extraction of image lines starts by identifying two points in one or two images along the line under consideration (e.g., 1A, 1B). One should note that these points need not be identifiable in other images. Intermediate points along the line are measured in all the overlapping images (e.g., 1C). Similar to the end points, the intermediate points need not be conjugate as seen in Figure 3.



Figure 3: Image space straight lines represented by a sequence of intermediate points and two end points

For this project, three vertices of 32 patches and series of points along the 15 lines are measured on the four provided image datasets of RGB, while 30 patches and 15 lines are measured on panchromatic images due to the invisible vertices of two patches on panchromatic images.

2.2. Build a Photogrammetric model

In addition to the aforementioned measurements of all the planar patches and lines in the image space, image coordinates of tie points and ground control points are measured to reconstruct 3D photogrammetric model. The given GCPs are not well distributed enough to perform indirect georeferencing, therefore GPS/INS-assisted bundle adjustment (Integrated Sensor Orientation) is performed considering the given EOP information as the correct location of camera acquired from GPS/INS onboard. Habib et al. (2002) introduced the bundle adjustment using straight-line features based on coplanarity condition. When incorporating linear features, every intermediate point measured along a straight line in image space provides a condition equation in that the point should lie on the plane defined by the perspective centre and the line end points. This constraint can be expressed as Equation 2 which indicates that these three vectors are coplanar.

$$(\vec{V}_1 \times \vec{V}_2) \cdot \vec{V}_3 = 0 \quad (2)$$

In Equation 2, \vec{V}_1 and \vec{V}_2 are the vectors from the perspective centre and to the two end points and \vec{V}_3 is the vector from the perspective centre to any intermediate image point on the line (Figure 4).

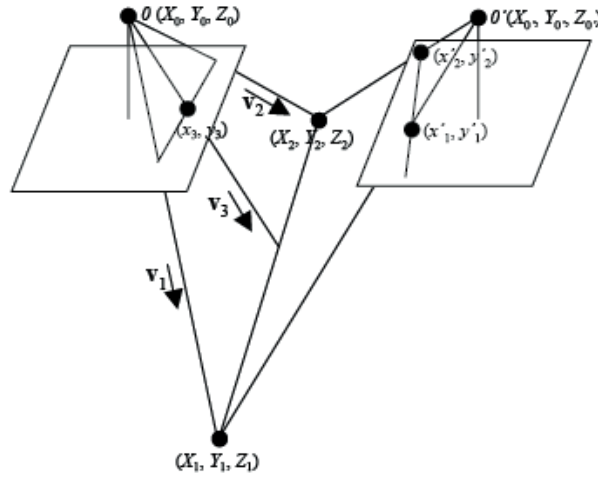


Figure 4: Coplanarity-based Incorporation of Linear Features

As a result of bundle adjustment process, the 15 3D model lines, each represented by two 3D points, and the 32 3D model patches, each represented by three 3D points, are estimated and used in the next co-registration procedure.

2.3. Representation and extraction of LiDAR features

LiDAR patches are represented by the set of 3D points that comprise the patch under consideration. LiDAR_QC program developed by DPRG enables planar patches to be extracted from LiDAR point clouds semi-automatically. The process begins by displaying the LiDAR intensity images in the program window, in which the user selects an area of interest where planar patches exist. The user clicks on the centre of the area after defining the radius of a circle within which the original LiDAR footprints will be extracted. It should be noted that the LiDAR intensity images are only used for visualization purposes. Figure 5a shows a sample area as well as the original LiDAR footprints located in a selected area. Then, a segmentation algorithm (Kim et al., 2007) is used to identify planar patches in the point cloud within the selected area. The outcome from the segmentation is an aggregated set of points representing planar patches in the selected area (Figure 5b).

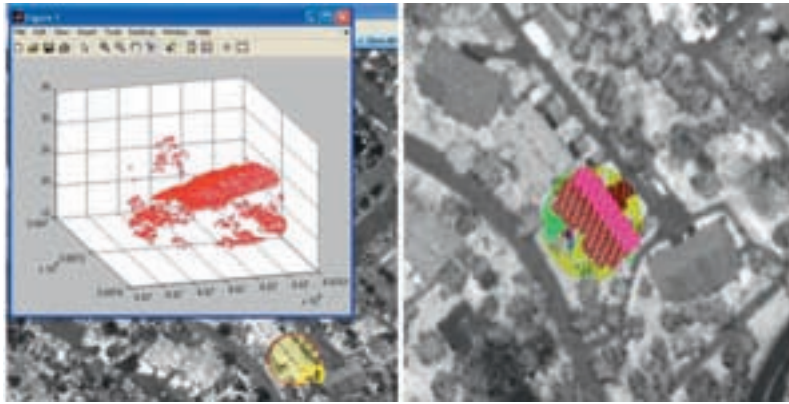


Figure 5: a) Area of interest selection and LiDAR point cloud extraction, b) Segmented planar patches

In addition to the straight-lines extracted from the photogrammetric dataset, a corresponding set of LiDAR straight lines have to be extracted to be used in the registration procedure. LiDAR lines will be represented by two 3D points and they are extracted automatically by intersecting neighbouring segmented planar patches as seen in Figure 6 (Habib et al., 2008).

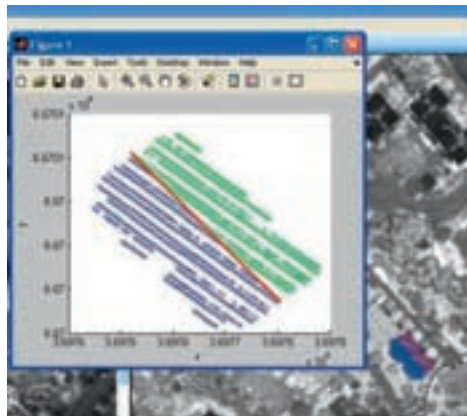


Figure 6: Extracted linear features, through planar patch intersection

Once patch segmentation is finished according to above procedures, neighbouring planar patches are identified and their plane parameters are determined. Intersection of neighbouring planes produces an infinite straight-line and the end points for the intersected line can be defined by projecting all the points that fall within a certain buffer onto the line segment and selecting the extreme points along the line segment to be the endpoints (Figure 7).

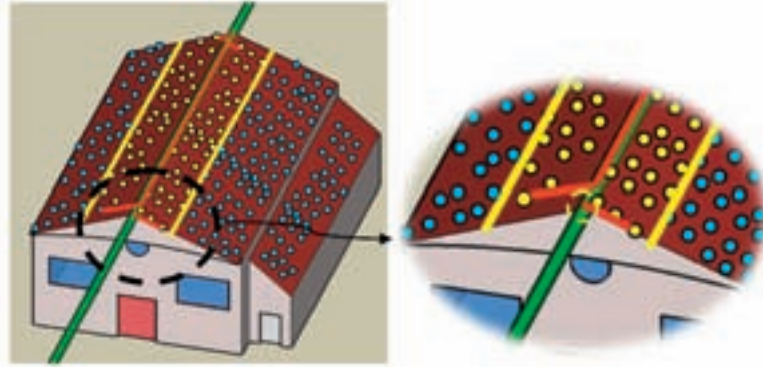


Figure 7: Projecting points within a buffer to define the line endpoints

2.4. Mathematical Model: Point based method

Once we have obtained linear and planar features from the 3D photogrammetric model and LiDAR datasets as a result of the previously described procedure, the relationship between conjugate features must be established. To define the relationship between 3D features from different datasets, 3D conformal transformation parameters, which use three rotations, three translations, and a scale factor, are estimated. In the traditional registration based on correspondent points, least square solution ensures the minimization of the Euclidian distance between two corresponding points after applying the estimated transformation parameters. However, we should consider that the points selected in the imagery and in LiDAR features need not be conjugate. During the absolute orientation procedure, the centroids of the patches were used to define these patches. The advantage of using the centroid is that the centroid pass through the fitted plane through the segmented points. In order to compensate for the non-correspondence between the centroid of vertices defined in the imagery and the centroid of vertices in the LiDAR patch and also the endpoints of lines in the respective datasets, we will restrict the weight of the selected points from both datasets along the plane direction and along the line direction.

First, the modification of the weight matrix of the planar patches to be accommodated in the point based method will be discussed and that of lines will follow. Lastly, incorporating the weight matrix into similarity measurements will be addressed.

The basic idea in this method is to expand the original variance-covariance matrices of the involved points along the direction parallel to the plane, while maintaining the original variance along the direction normal to the plane as conceptually shown in Figure 8 (Habib, et al., 2007).

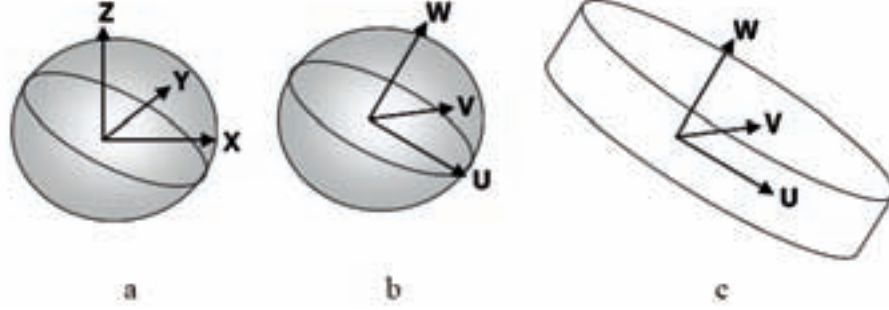


Figure 8: Conceptual basis for using planar patches in a point-based approach for the determination of the conformal transformation parameters between two 3D datasets

The weight restriction procedure for planar patches can be applied as follows. First, the relationship between the original coordinate system (XYZ) and a local coordinate system (UVW) is defined by the rotation matrix R (Equation 3). The local coordinate system (UVW) is defined with the U and V axes aligned along the plane direction. The rotation matrix is derived using the orientation of the normal to the planar patch, which is derived through a plane fitting procedure using all points of the control LiDAR patch.

$$\begin{bmatrix} U \\ V \\ W \end{bmatrix} = R \begin{bmatrix} X \\ Y \\ Z \end{bmatrix} \quad (3)$$

The original weight matrix, P_{XYZ} , is defined as the inverse of the variance-covariance matrix Σ_{XYZ} , which depends on the accuracy of the LiDAR data and the accuracy of photogrammetric reconstruction result as seen in Equation 4.

$$P_{XYZ} = \Sigma_{XYZ}^{-1} \quad (4)$$

The weight of the points in the local coordinate system (P_{UVW}) can be derived using the law of error propagation according to Equation 5.

$$P_{UVW} = R P_{XYZ} R^T = \begin{bmatrix} P_U & P_{UV} & P_{UW} \\ P_{VU} & P_V & P_{VW} \\ P_{WU} & P_{WV} & P_W \end{bmatrix} \quad (5)$$

Then, the weight matrix can be modified according to Equation 6 by assigning a zero value for the weights along the planar patch, to obtain a new weight matrix P'_{UVW} in the plane coordinate system. This weight matrix implies that the points can freely move along the plane direction.

$$P'_{UVW} = \begin{bmatrix} 0 & 0 & 0 \\ 0 & 0 & 0 \\ 0 & 0 & P_w \end{bmatrix} \quad (6)$$

Finally, the modified weight matrix P'_{XYZ} in the original coordinate system can be derived according to Equation 7.

$$P'_{XYZ} = R^T P'_{UVW} R \quad (7)$$

The idea behind the method using linear features is similar to the one with patches. None of the endpoints from photogrammetric and LiDAR data is required to be conjugate points. The only requirement is that the selected points should be along the same line. This approach restricts the weight matrix of the points in the line direction. Consequently, the behaviour of these points will be fixed in all directions except along the line direction which means that the points are free to move only along the line. The modified weight matrix of lines can be derived in the same manner of patches using Equation 8 instead of Equation 6 where U axis is parallel to the line, and the V and W axes are perpendicular to the U axis.

$$P'_{UVW} = \begin{bmatrix} 0 & 0 & 0 \\ 0 & P_v & P_{vw} \\ 0 & P_{wv} & P_w \end{bmatrix} \quad (8)$$

The proposed weight restriction ensures the minimization of the normal distance between conjugate linear and areal features, after applying the estimated transformation parameters. In the Least Square Adjustment (LSA) procedure, the unknown parameters are estimated to minimize the weighted sum of squared residuals as represented by Equation 9. The components (dX, dY, dZ) refer to the differences between the photogrammetric coordinates and the transformed coordinates of LiDAR datasets after applying the estimated rotations, shifts and a scale. Equations 10 – 11 consider the case of an areal feature to show that the LSA target function minimizes the weighted sum of the squared normal distances between conjugate planar patches after the manipulation of the weight matrix according to Equation 6 (Habib et al., 2008).

$$e^T P e = \min \quad \text{Where} \quad e = \begin{bmatrix} X_{\text{photogrammetric}} - X'_{\text{LiDAR}} \\ Y_{\text{photogrammetric}} - Y'_{\text{LiDAR}} \\ Z_{\text{photogrammetric}} - Z'_{\text{LiDAR}} \end{bmatrix} = \begin{bmatrix} dX \\ dY \\ dZ \end{bmatrix} \quad (9)$$

$$\Sigma[dX \ dY \ dZ] P'_{XYZ} \begin{bmatrix} dX \\ dY \\ dZ \end{bmatrix} \rightarrow \Sigma[dX \ dY \ dZ] R^T P'_{UVW} R \begin{bmatrix} dX \\ dY \\ dZ \end{bmatrix} = \min \quad (10)$$

$$\Sigma[dU \ dV \ dW] P'_{UVW} \begin{bmatrix} dU \\ dV \\ dW \end{bmatrix} \rightarrow \Sigma[dU \ dV \ dW] \begin{bmatrix} 0 & 0 & 0 \\ 0 & 0 & 0 \\ 0 & 0 & P_w \end{bmatrix} \begin{bmatrix} dU \\ dV \\ dW \end{bmatrix} = \sum P_w d_w^2 = \quad (11)$$

Where $[dU \ dV \ dW]$ represent the components of the residual vector $[dX \ dY \ dZ]$ in the UVW coordinate system (that is, the planar patch local coordinate system with dW being along the plane normal).

To define the 3D conformal parameters, a minimum of four patches (three non-parallel and one parallel) are required and a minimum of two non-coplanar line segments are necessary. Therefore, planar patches with various slopes and orientations should be used. The distribution of extracted patches and linear features is shown in Figure 9.

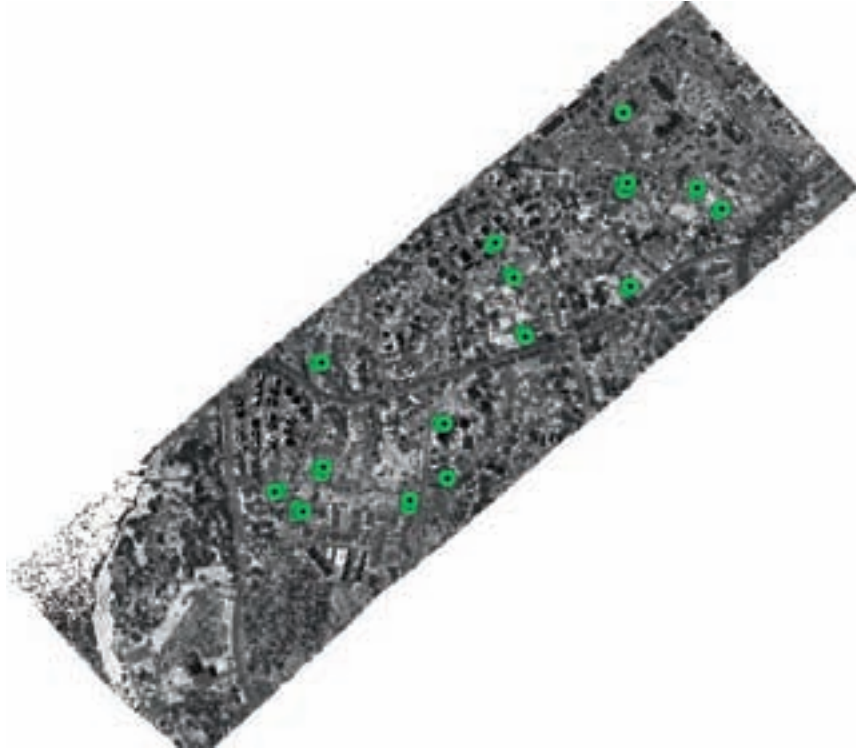


Figure 9: Visualization of the location of planar patches and linear features

3. Results

The final registration parameters are shown from Table 1 to Table 4. The sigma value represents the normal distance between conjugate elements after applying the transformation parameters. Note that the origin of the coordinate system for all the results are as follows, X: 369417.812, Y: 6669870.603, Z: 49.864, which are the coordinates of the centroid of extracted patches.

Two kinds of primitives, linear features and planar patches, are utilized to establish the correspondence between two datasets as discussed in the previous section. After estimating the transformation parameters, laser data will be transformed into the image reference frame using Equation 1.

Table 1 shows the seven 3D conformal registration parameters between Optech's laser data and DMC panchromatic images.

	Linear feature method	Patch method	Line + patch
XT [m]	-23.4124	-23.6283	-23.4266
YT [m]	17.7546	17.7599	17.7562
ZT [m]	-25.5813	-25.4892	-25.5392
S	1.0007	1.0002	1.0006
Omega [deg]	-0.0253	0.0149	-0.0049
Phi [deg]	-0.0375	-0.0146	-0.0243
Kappa [deg]	-0.0287	-0.0031	-0.0252
Sigma	0.105	0.012	0.077

Table 1: Transformation parameters between Optech's laser data and DMC panchromatic images (15 lines + 30 patches)

Table 2 shows the seven 3D conformal registration parameters between Leica's laser data and DMC panchromatic images.

	Linear feature method	Patch method	Line + patch
XT [m]	18.1675	18.0505	18.1699
YT [m]	21.3819	21.45	21.39
ZT [m]	5.9044	5.9818	5.9303
S	1.0004	1.0005	1.0004
Omega [deg]	0.0031	-0.0133	-0.0089
Phi [deg]	-0.014	-0.0256	-0.0253
Kappa [deg]	0.0859	0.0415	0.0827
Sigma	0.168	0.03	0.119

Table 2: Transformation parameters between Leica's laser data and DMC panchromatic images (15 lines + 30 patches)

Table 3 shows the seven 3D conformal registration parameters between Optech's laser data and DMC RGB images.

	Linear feature method	Patch method	Line + patch
XT [m]	-23.7931	-23.6849	-23.8266
YT [m]	17.5412	17.6533	17.5761
ZT [m]	-25.1531	-25.4819	-25.2659
S	1.0007	0.9996	1.0006
Omega [deg]	0.0439	0.0758	0.0378
Phi [deg]	0.0026	0.0137	-0.0033
Kappa [deg]	0.0095	0.0231	0.0152
Sigma	0.356	0.098	0.242

Table 3: Transformation parameters between Optech's laser data and DMC RGB images (15 lines & 32 patches)

Table 4 shows the seven 3D conformal registration parameters between Leica's laser data and DMC RGB images.

	Linear feature method	Patch method	Line + patch
XT [m]	17.7984	18.0053	17.8007
YT [m]	21.21	21.3607	21.2561
ZT [m]	6.3156	5.9854	6.1953
S	1.0005	0.9999	1.0005
Omega [deg]	0.0682	0.0465	0.0369
Phi [deg]	0.0278	0.0021	-0.0011
Kappa [deg]	0.1103	0.087	0.111
Sigma	0.373	0.102	0.263

Table 4: Transformation parameters between Leica's laser data and DMC RGB images (15 lines & 32 patches)

4. Result analysis

Before discussing the final registration quality, to ensure the quality of reconstructed photogrammetric model (Section 2.1), the outcome of the bundle adjustment should be evaluated. Two parameters, the square root of the a posteriori reference variance (σ_0) and the root mean square error (RMSE), are analyzed.

The square root of the a posteriori reference variance is a measure of the quality of fit between the observed quantities and the estimated quantities in the bundle adjustment. It can also be thought of as a measure of the appropriateness of the mathematical model used to represent the data. The value of σ_0 should be within the range of the image coordinate measurement accuracy, which is 1 pixel (0.012 mm) in this project. Therefore, a σ_0 value that is larger than one pixel is not acceptable.

The RMSE analysis, also known as check point analysis, determines the accuracy of the final estimated ground coordinates of some GCPs that are used as check points, for which “true” ground coordinates are available from a more accurate surveying method. This can be achieved by utilizing the available GCPs as check points. Thus, the RMSE analysis gives an indication about the accuracy of the reconstructed object space. They are compared with the expected accuracies (σ_X , σ_Y , and σ_Z) of the reconstructed points computed based on assumed image measurement accuracy, the elevation height, the camera’s focal length, and height-base ratio.

The σ_0 of the panchromatic images is 4.26e-003mm (0.4 pixel), which indicates an acceptable range of residuals from the bundle adjustment procedure. As seen in Table 5, RMSE values can be compared to the expected accuracy computed based on 1 pixel image measurement accuracy.

29 check point analysis			
	X	Y	Z
Mean	0.04	0.03	-0.01
Std	0.06	0.04	0.11
RMSE	0.07	0.05	0.11
Total RMSE	0.14		

Table 5: RMSE of reconstructed point using panchromatic images (unit: m)

Expected accuracy of panchromatic image reconstruction using 1 pixel (0.012 μ m) image measurement accuracy is as below.

$$\sigma_X = \frac{H}{c} \sigma_x = \frac{548.30}{120} \times 0.012 = 0.05 \text{ m}$$

$$\sigma_Y = \frac{H}{c} \sigma_y = \frac{548.30}{120} \times 0.012 = 0.05 \text{ m}$$

$$\sigma_Z = \frac{H}{c} \frac{H}{B} \sigma_{P_x} = \frac{548.30}{120} \times \frac{548.30}{358.90} \times \sqrt{2} \times 0.012 = 0.11 \text{ m}$$

The σ_0 of the RGB images is 6.16e-003mm (0.5 pixel), which indicates the values from this photogrammetric model are acceptable. RMSE analysis in Table 6 shows that the reconstructed points are within expected accuracy computed based on 1 pixel image measurement accuracy.

46 check point analysis			
	X	Y	Z
Mean	0.03	0.17	-0.27
Std	0.14	0.13	0.50
RMSE	0.14	0.21	0.57
Total RMSE	0.63		

Table 6: RMSE of reconstructed point using RGB images (unit: m)

Expected accuracy of RGB image reconstruction using 1 pixel (0.012 μm) image measurement is as below.

$$\sigma_X = \frac{H}{c} \sigma_x = \frac{545.80}{25.263} \times 0.012 = 0.26 \text{ m}$$

$$\sigma_Y = \frac{H}{c} \sigma_y = \frac{545.80}{25.263} \times 0.012 = 0.26 \text{ m}$$

$$\sigma_Z = \frac{H}{c} \frac{H}{B} \sigma_{P_x} = \frac{545.80}{25.263} \times \frac{545.80}{358.96} \times \sqrt{2} \times 0.012 = 0.56 \text{ m}$$

To prove the compatibility between the LiDAR and images qualitatively, four true orthophotos are generated using the angle-based true orthophoto generation methodology, developed by Habib et al. (2007). Figure 10 shows RGB and PAN true orthophoto with respective to Leica and Optech DSM respectively with the grey box showing the underlied DSM. A boundary line between the orthophoto and DSM is continuous which means transformed LiDAR and images are compatible.

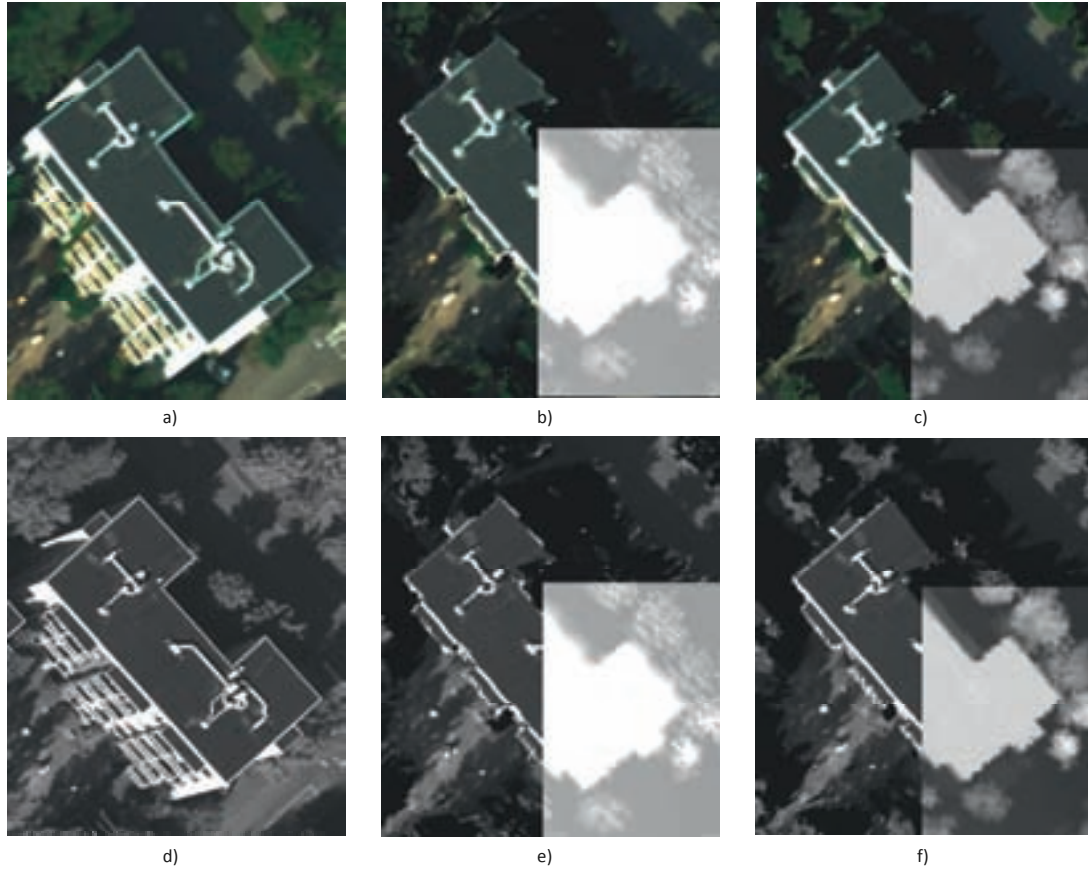
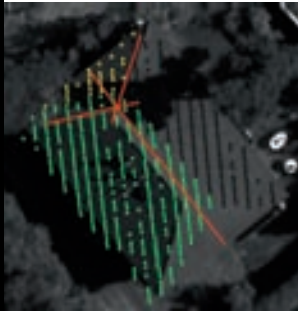
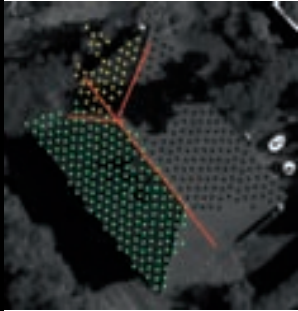
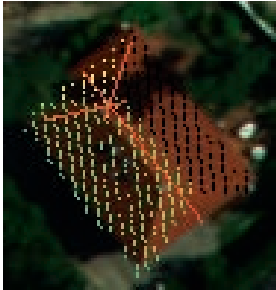
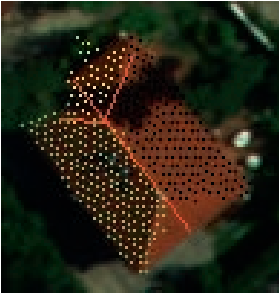
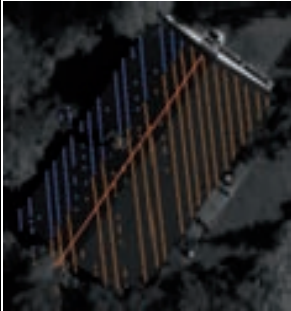
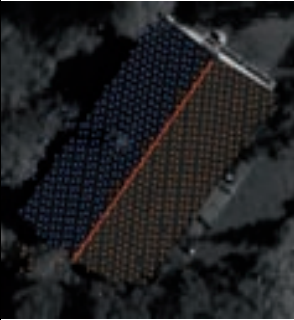


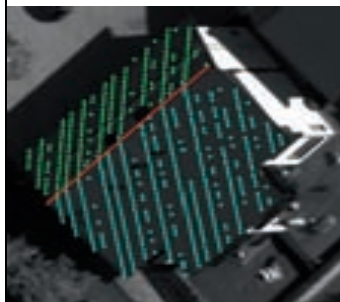
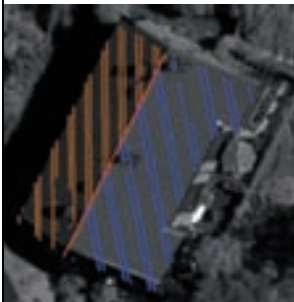
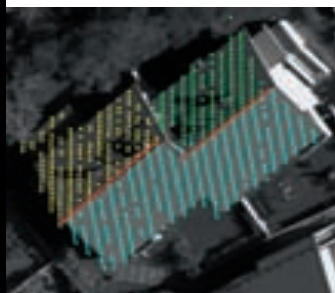
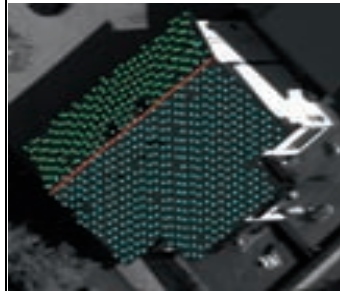
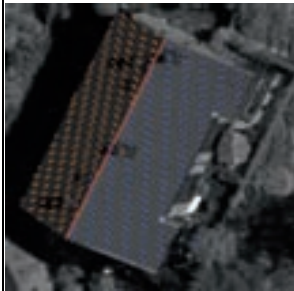
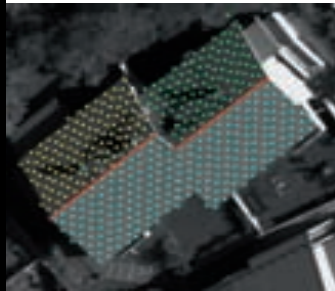
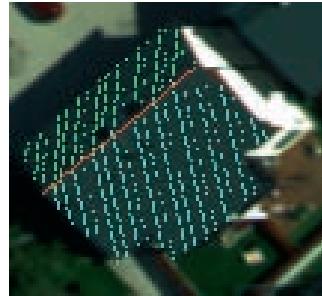
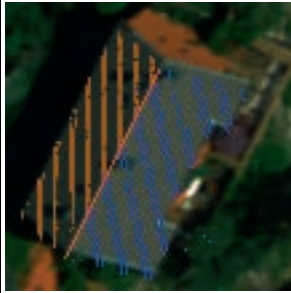
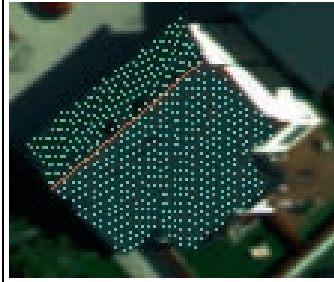


Figure 10: a) original RGB image, b) RGB orthophoto with DSM from Leica, c) RGB orthophoto with DSM from Optech, d) original PAN image, e) PAN orthophoto with DSM from Leica, f) PAN orthophoto with DSM from Optech

Another way to show the quality of the registration parameters can be seen from the Figures in Table 7. Extracted patches and lines from LiDAR are transformed with respect to the image reference frame by applying the estimated seven registration parameters (Equation 1). Then, transformed patches and lines are projected onto imagery using the given EOP and IOP information. The projected features fit to features in the image quite well. The discrepancy between the projected line and the original lines in the images are less than 2 pixels for RGB images and less than 3 pixels for PAN images which corresponds to ground distance of 44 cm and 15 cm respectively. Even though Optech data have lower point density, it shows more uniform point distribution and higher registration accuracy than Leica. Leica data has slightly higher discrepancy between the projected feature and the original feature (a, c vs. b, d in Table 7) and higher sigma values than Optech data (Tables 2, 4 vs. Tables 1, 3).

Table 7: a) Projected transformed Leica lines and patches onto PAN image using parameter from patch method, b) Projected transformed Optech lines and patches onto PAN image using parameter from patch method, c) Projected transformed Leica lines and patches onto RGB image using parameter from patch method, and d) Projected transformed Optech lines and patches onto RGB image using parameter from patch method

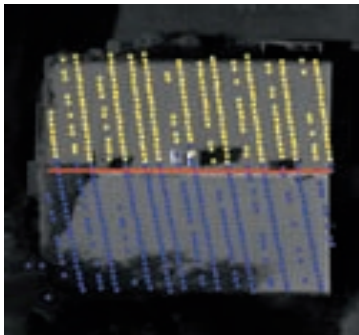
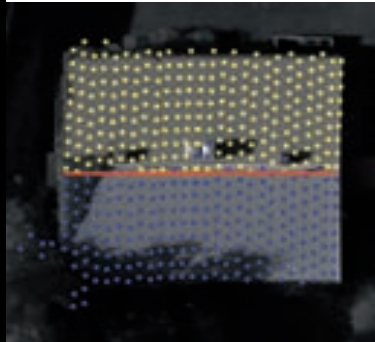
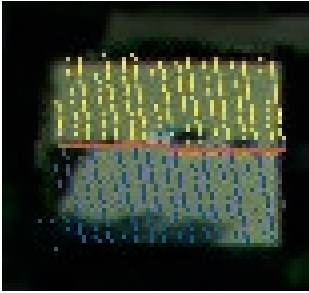
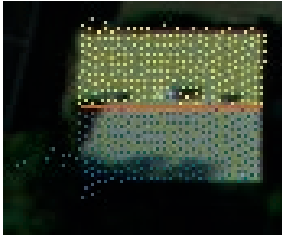
Building No.	a) Leica Data Projection on Panchromatic Images	b) Optech Data Projection on Panchromatic Images	c) Leica Data Projection on RGB Images	d) Optech Data Projection on RGB Images
C1				
C2				



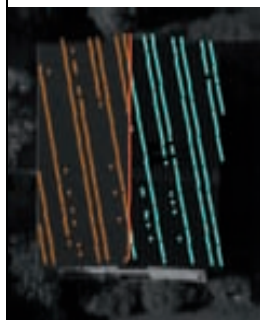
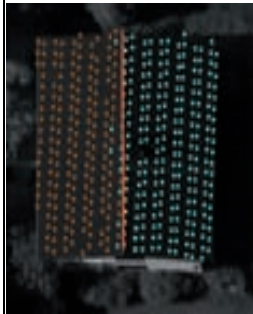
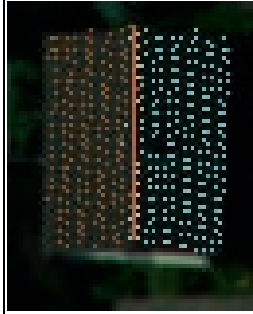
C3

C4

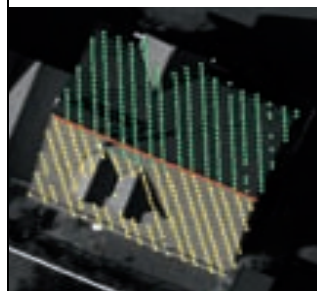
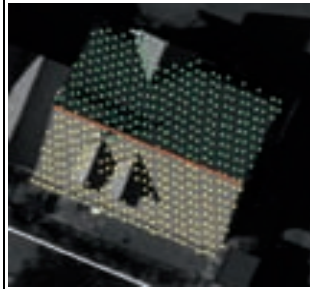
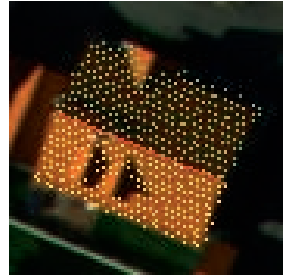
C5



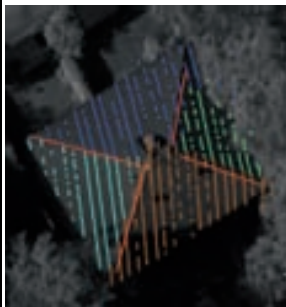
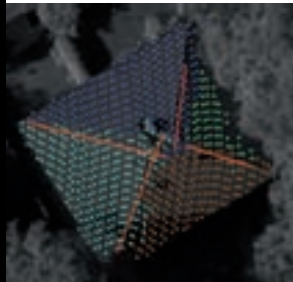
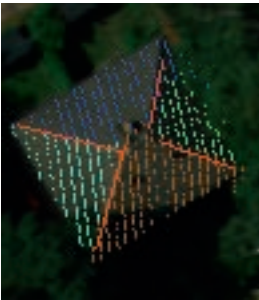
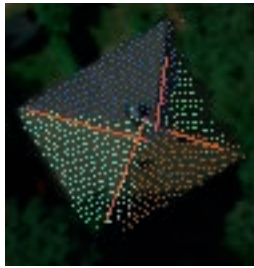
C6



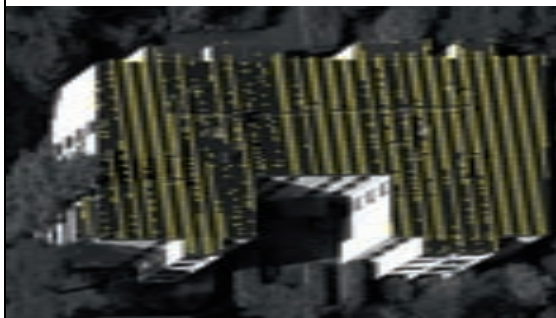
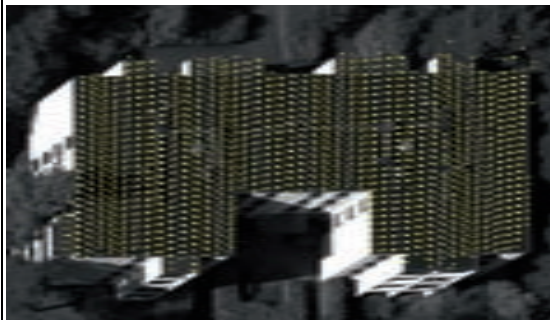
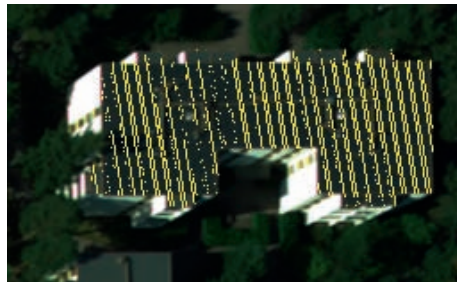
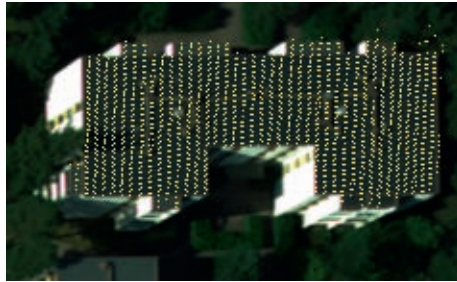
C7



C8

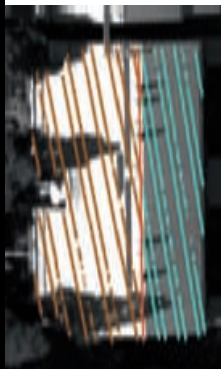
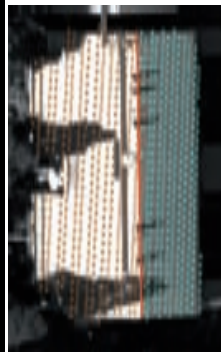


C9

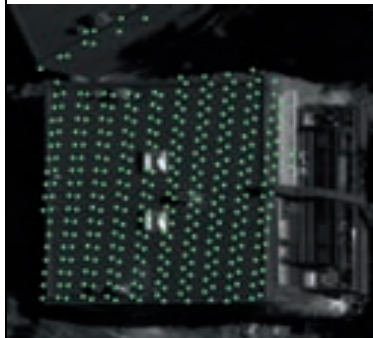


C10

<div data-bbox="256 311 497 607"></div> <div data-bbox="256 656 497 958"></div> <div data-bbox="245 1030 505 1352"></div> <div data-bbox="240 1424 507 1767"></div> <div data-bbox="363 1832 392 1883" data-label="Caption"> <p>C11</p> </div>	<div data-bbox="537 306 738 611"></div> <div data-bbox="526 651 750 963"></div> <div data-bbox="526 1003 748 1375"></div> <div data-bbox="521 1424 753 1769"></div> <div data-bbox="625 1832 654 1883" data-label="Caption"> <p>C13</p> </div>	<div data-bbox="782 306 1086 611"></div> <div data-bbox="775 651 1091 963"></div> <div data-bbox="767 1019 1099 1361"></div> <div data-bbox="769 1429 1098 1762"></div> <div data-bbox="922 1832 951 1883" data-label="Caption"> <p>C14</p> </div>
--	--	--



CI15



CI16

5. Level of Automation

According to the registration method discussed beforehand, first, LiDAR linear and areal features that can be identified in the aerial images are extracted semi-automatically from both of LiDAR strips. The two LiDAR strips can be processed at the same time, because features can be extracted simultaneously from the overlapping LiDAR strips. It took roughly 3 hours to extract 32 patches and 15 lines from both of LiDAR datasets. In addition to the extracted LiDAR features, the used program generates the modified weight matrices of LiDAR features as an output, which can be used directly for the absolute orientation procedure.

To build a photogrammetric model, tie points, GCP, and points defining lines and patches are manually measured on the overlapping images. Around 7 hours took for each set of images. 3D photogrammetric model of patches, lines and tie points are acquired through BA process.

Lastly, registration parameters are computed automatically using absolute orientation program and the program running time is 1 second while organizing the input files took 20 minutes. The amount of automation and time according to the tasks are summarized in Table 8.

Procedure	Tasks	Datasets	Amount of automation	Amount of time
1. Extraction of LiDAR features	LiDAR patch extraction	Optech & Leica	Semi-automatic	3 hours
	LiDAR linear feature extraction			
2. Build a photogrammetric model (bundle adjustment)	Tie points	PAN (4 images)	Manual image measurements	7 hours
	Points along the line			
	Vertices along the patch			
	Tie points	RGB (4 images)		7 hours
	Points along the line			
	Vertices along the patch			
	Perform the BA	PAN	Automatic	30 minutes
	Perform the BA	RGB		30 minutes
3. Absolute orientation	Modified weight matrix	Result from steps 1 and 2	Automatic	20 minutes
	LSA using modified weight matrix			1 second

Table 8: Summary of amount of automation and time for registration method

6. Conclusions

This report presented a 2-step procedure to register LiDAR data into the image reference frame by incorporating linear and areal features that can be extracted from the LiDAR data in a semi-automatic way. The extracted LiDAR linear features are represented by two end points and the planar patches are represented by set of points along its perimeter. Independent photogrammetric model is built relative to a coordinate system defined by the EOP information provided by EuroSDR using linear features and tie points defining the patch vertices. Transformation function between the photogrammetric model and the LiDAR data is established using the two end points of lines and centroid of planar patches. Non-correspondence of the selected points between the two datasets is compensated for by artificially expanding their variance-covariance matrices along the line direction and along the plane direction respectively.

The software developed by DPRG also supports 1-step procedure which incorporates LiDAR-derived linear and areal features as control information for the georeferencing of the photogrammetric data.

The performance of the proposed procedure was evaluated using orthophotos generated from LiDAR DSM and provided images. Another qualitative analysis was performed by projecting the transformed LiDAR features onto the images. The result shows good level of compatibility between transformed LiDAR data with respect to the image reference frame and the image data.

Future research will focus on analyzing the effect of LiDAR performance on the quality of final registration such as how the pattern of LiDAR and point distribution affect the segmentation and registration quality.

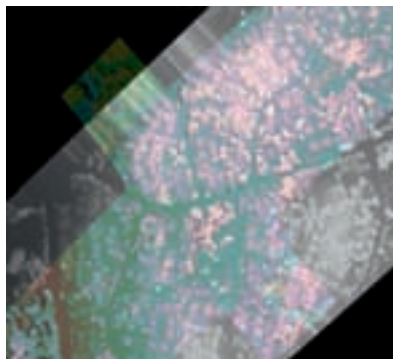
7. References

- Al-Durgham, M. M. (2007). Alternative Methodologies for the Quality Control of LiDAR Systems. Thesis UCGE Reports Number 20259, University of Calgary, AB, Canada.
- Habib, A., M. Morgan, and Y. Lee, (2002). Bundle adjustment with self-calibration using straight lines, *Photogrammetric Record*, 17(100): 635-650.
- Habib, Ayman, Eui-Myoung Kim, C.J. Kim, (2007). New Methodologies for True Orthophoto Generation. *PE&RS Photogrammetric Engineering & Remote Sensing*, 73(1), pp. 25–36.
- Habib, A., Bang, K., Aldelgawy, M., and S. Shin, (2007). Integration of Photogrammetric and LiDAR Data in a Multiprimitive Triangulation Procedure, *Proceedings of the ASPRS 2007, Tampa, Florida*.
- Habib, A., A. Jarvisa, A. P. Kerstinga, and Y. Alghamdia, (2008). Comparative analysis of georeferencing procedure using various sources of control data, *The International Archives of the Photogrammetry, Remote Sensing and Spatial Information Sciences. Vol. XXXVII. Part B4. Beijing 2008*
- Habib, A., A. P. Kersting, Z. Ruifang, M. Al-Durgham, C. Kim, and D. C. Lee, (2008). LiDAR strip adjustment using conjugate linear features in overlapping strips, *The International Archives of the Photogrammetry, Remote Sensing and Spatial Information Sciences. Vol. XXXVII. Part B1. Beijing 2008*
- Kim C., Habib A., and Mrstik P. (2007). New Approach for Planar Patch Segmentation using Airborne Laser Data. *Proceedings of the ASPRS 2007, Tampa, Florida*

Report of the University College London
EuroSDR "Registration Quality – Towards Integration of
Laser Scanning and Photogrammetry"

**REGISTRATION QUALITY
TOWARDS INTEGRATION OF LASER
SCANNING
AND PHOTOGRAMMETRY**

Astrid Caballero Pardo
Department of Civil, Environmental & Geomatic Engineering
University College London



MSc Geographic Information Science

First Supervisor: Mr. Jeremy Morley
Second Supervisor: Prof. Ian Dowman
University College London
2009



Abstract

Registration of digital images and laser scanning point clouds have been receiving particular attention in mapping activities and applications such as change detection, image fusion, orthophoto generation, 3-D city modelling, surface reconstruction, and object recognition due to their complementary characteristics while maintaining low cost and fast mapping.

Experiments were carried out on the extraction of LiDAR data through the acquisition of apex's end points and corners of roofs. The quality of the registration of LiDAR based on the extracted features shows that better accuracy is achieved when using apex's end points of roof.

Two datasets of laser scanning point clouds were provided each one with different point density, from this it was found that density is an important characteristic when selecting and defining the planes that conform an apex, but no sufficient evidence in the quality of the registration was found since Optech (2-3 points/m²) has better horizontal accuracy than Leica (4-5 points/m²). On the other hand, density makes a difference when registration is based on the extracted corners of roof.

The registration of the laser scanning point clouds using panchromatic aerial images as reference exhibits better accuracy than the registration using the multispectral images, the spatial resolution has an important influence in the quality of the process.

Future work will entail more automation when extracting features as well as more experiments on laser scanning point clouds with different point density in order to understand its influence on the registration.

Acknowledgements

I would like to thank my supervisors Mr. Jeremy Morley and Prof. Ian Dowman, for their guidance, patience and time provided throughout this challenging project.

I also want to thank EuroSDR for allowing me to be part of this project and provide the data to experiment, and Mr. Petri Rönnholm for his advice which allowed me to complete my experiments.

Sincere thanks to Dr. Jonathan Iliffe for his timely and invaluable help and for his willingness to share his knowledge.

I extend my thanks to Mr. Dietmar Backes for sharing his knowledge and views as well as spending time to help solving those technical issues that gave me so many headaches.

My gratitude is also due to my classmates from MSc GIS Camilo Vargas, MSc Remote Sensing Steve Sok, Dan Fisher and Steve Williams and Jenny Roan a PhD student for their comments and support given to this project, as well as by the enjoyable environment they gave me.

From my heart my deepest gratitude is due to my father, mother, sister and brother for their love, constant and unconditional support, trust and lessons given to me in every step of my life.

Table of Contents

Abstract.....	164
Acknowledgements.....	164
Table of Contents	165
List of Figures.....	167
List of Tables	169
1 Introduction.....	170
1.1 Aim of this project	170
2 Background	171
2.1 LiDAR	171
2.2 Photogrammetry.....	174
2.3 Registration	178
2.3.1 <i>LiDAR and Photogrammetric data</i>	178
2.3.2 <i>Registration methods available or under development</i>	180
2.3.3 <i>Errors that affect registration</i>	182
3 Research Question.....	182
3.1 Objectives	182
4 Data	183
4.1 LiDAR	183
4.2 Photogrammetric data	183
4.3 Field surveys	188
4.4 Software	188
5 Methodology	189
6 Results.....	190
6.1 Initial assessment of LiDAR data quality	190
6.1.1 <i>Leica</i>	190
6.1.2 <i>Optech</i>	192
6.2 Definition and extraction of features from the two datasets.....	193
6.2.1 <i>Photogrammetry dataset</i>	193
6.2.2 <i>LiDAR dataset</i>	195
6.3 Three-dimensional transformation Function.....	197
6.3.1 <i>10-parameters transformation</i>	198
6.4 LiDAR registered.....	201
7 Analysis & Discussion.....	202
7.1 Extraction of features	202
7.1.1 <i>Block of images</i>	202

7.1.2	<i>LiDAR extraction</i>	204
7.2	Transformation function	205
7.2.1	<i>Apex of Roofs</i>	206
7.2.2	<i>Corners of roofs</i>	207
7.2.3	<i>Apex and corners of roofs together</i>	208
7.3	LiDAR registered	208
8	Conclusions & Future Work	210
8.1	Features extraction	211
8.1.1	<i>Images</i>	211
8.1.2	<i>LiDAR dataset</i>	211
8.2	Transformation Function	212
8.3	Automation	212
	References	212
	Appendix A Initial quality assessment	214
	Appendix B Socet set extracted points	218
	Appendix C Apex of roofs using TerraScan	219
	Appendix D Matlab script	220
	Appendix E Values of Extracted Points	223
	Appendix F Registered LiDAR	228

List of Figures

Figure 1 Basic operation of laser rangefinder by using the time-of-flight (TOF) method.

Figure 2 (a) Coverage of an area by using a laser profile. (b) Coverage of an area by using a laser scanner.

Figure 3 LiDAR system (based on Shan & Toth, 2009).

Figure 4 Principle of pinhole camera from Wolf & Dewitt, 2000.

Figure 5 Array of Charge-Coupled devices –CCDs (based on Wolf and Dewitt, 2000).

Figure 6 Absolute orientation process according to the number of images from Schenk (1999).

Figure 7 Absolute orientation of a stereomodel in the model coordinate system x_m, y_m, z_m , with respect to the object coordinate system X, Y, Z . From Schenk, 1999.

Figure 8 (a) Sensor orientations of the aerial images and LIDAR data independently. (b) Relative orientation of the datasets.

Figure 9 Y parallax.

Figure 10 Distribution on the image block of Ground control points (GCPs) provided by EuroSDR

Figure 11 Image of the ground control points provided by EuroSDR.

Figure 12 Methodology workflow.

Figure 13 GCP Vs Leica Laser scanning data.

Figure 14 TIN leica data Vs GCP.

Figure 15 GCPs Vs Optech Laser scanning data.

Figure 16 (a) Extracted points from panchromatic images. (b) Extracted points from multispectral images.

Figure 17 (a) Lines from roof plane's intersections in the Leica dataset using terraScan. (b) Points from lines.

Figure 18 Orange points are the extracted points from Optech, while green points are the extracted points from Leica using TerraScan (Appendix C).

Figure 19 Extracted Leica points (roof's corners) using LiDAR tool for ArcGIS. (top left) Raster hill-shade of the elevation (top right) Raster using bare-Earth algorithm (bottom left) Raster hill-shade of the previous one (bottom right) Points from extracted building edges based on the Raster using bare-Earth algorithm.

Figure 20 Overview of LiDAR data registered superimposed onto the DEM from the aerial images block. (a) Leica and Panchromatic DEM (new orientation). (b) Optech and Panchromatic DEM (new orientation). (c) Leica and Panchromatic DEM (EuroSDR orientation). (d) Optech and Panchromatic DEM (EuroSDR orientation). (e) Leica and multispectral DEM (EuroSDR orientation). (f) Optech and multispectral DEM (EuroSDR orientation).

Figure 21 Leica dataset before (left) and after registration (right) based on panchromatic images (new orientation).

Figure 22 Optech dataset before (left) and after registration (right) based on panchromatic images (new orientation).

Figure 23 (a) Initial Extracted points. (b) Set of points for registration after rejecting flat roofs.

Figure 24 (Left) TerraScan automatically generates 4 roof's planes (Centre) Only two planes were used to determine the apex (Right) Manually Edited planes.

Figure 25 Z values of Leica Vs GCPs provided by EuroSDR.

Figure 26 Z values of Optech Vs GCPs provided by EuroSDR.

Figure 27 Distribution of the extracted points from the panchromatic images.

Figure 28 Points that were rejected because of their flat roof.

Figure 29 Example of roof plane's intersection using TerraScan.

Figure 30 Overview Optech registered based on panchromatic images.

Figure 31 Overview Leica registered based on panchromatic images.

List of tables

Table 1 General classification of laser scanners (Shaded boxes indicate the laser scanner types that are focus for this work).

Table 2 Exterior orientation parameters for the panchromatic block images provided by EuroSDR.

Table 3 Statistics of the new exterior orientation parameters.

Table 4 New parameters of exterior orientation.

Table 5 Exterior orientation parameters for the multispectral block images provided by EuroSDR.

Table 6 Planimetric analysis Leica dataset.

Table 7 Planimetric analysis Optech dataset.

Table 8 Initial 7- parameters values, calculated from four points of Optech.

Table 9 10-parameters values, calculated from four points of Optech.

Table 10 10-parameter transformation function parameters by using least squares. Points extracted from roof's apex.

Table 11 10-parameter transformation function parameters by using least squares. Points extracted from roof's corners.

Table 12 10-parameter transformation function parameters by using least squares. Points extracted from roof's apex and corners.

Table 13 10 – parameter transformation result values are the same that those obtained with the 3 and 7 parameter transformation. X_o , Y_o and Z_o are the local coordinates for LiDAR dataset.

Table 14 RMSE and standard deviation values using points from the apex of buildings.

Table 15 RMSE and standard deviation values using points from the corners of roofs.

Table 16 RMSE and standard deviation values using points from the apex and corners of roofs together.

Table 17 Profiles of a test area. (a) and (b) represent the longitudinal profile of the Leica (blue) and Optech (green) comparing to the Panchromatic images. (c) Transversal profile of a house in the test area. (d) and (e) represent the longitudinal profile of the Leica (blue) and Optech (green) comparing to the Multispectral images. (f) Transversal profile of a house in the test area

Table 18 Mean standard deviation of a sample area calculated from DEMs.

Table 19 X_s , Y_s and Z_s are the coordinates of the source dataset which in this case is LiDAR whereas X_t , Y_t and Z_t are the coordinates of the corresponding points in the target coordinate system which in this case is the images block's ground coordinate system with the new orientation (ETRS89 / ETRS-TM35FIN) .Blue shaded cells are the points that were removed after cheking the residuals.

Table 20 Leica residuals of 28 points extracted using TerraScan. Blue shaded cells are the points that were removed after checking the residuals.

Table 21 Residuals Optech with 28 points extracted using TerraScan. Blue shaded cells are the points that were removed after checking the residuals.

Table 22 Values of points extracted from the images using the EuroSDR exterior orientation related with the extracted points with TerraScan.

Table 23 Residuals from points extracted with ArcGIS LiDAR tool using the new orientation.

1 Introduction

The evolution of hardware, software and data collection techniques that allows high accuracy and acquire great amount of topographic data at a reasonable cost and time has led in an increase incorporation of them in mapping activities and applications such as change detection, image fusion, orthophoto generation, 3-D city modelling, surface reconstruction, and object recognition. However, the current digital technology has not yet been able to provide data as good as those acquired from analog sensors (SHAN & TOTH, 2009). Therefore, the integration of data collected in different formats (each one with strengths and limitations), has gained interest in order to compensate the weaknesses of each dataset while maintaining low cost and fast mapping. In this regard, *integration* of digital images and laser scanning point clouds have been receiving particular attention due to their complementary characteristics, but an integration can only be possible after accurate *registration* of the datasets to a common reference frame.

From the above the use of data derived from the registration of digital aerial images and airborne laser scanning data has increased, thus it is nowadays a concern For EuroSDR organisation to understand the current methods to performance this process in order to develop more quality integration.

The registration of LiDAR dataset based on aerial images is a process under development where automation plays an important role since the extraction of features that relate the data to align them in a common reference system (registration), is a high time consuming task which requires dealing with more than one software as it is shown throughout this document.

Several approaches for the registration of airborne laser scanning data and aerial images have been carried out using mainly the LiDAR dataset as reference which results have shown acceptable accuracy. However, as the registration of LiDAR and photogrammetric data is an emerging field there is a lot to play, analyze, and understand such performing a registration where the aerial images are the reference and LiDAR is the moving dataset.

1.1 Aim of this project

The aim of this project is to perform a registration of the LiDAR datasets using the images as reference in order to analyse how much a registration method differs in performance and accuracy when laser scanning data have different density and the images have different spatial resolution.

The registration of LiDAR is carried out by extracting the apex's end point of roofs as Laser data is more reliable inside surfaces. Socet Set 5.4.1. is use to extract the features from the images while TerraSolid 9.0 specifically the TerraScan extension is use to extract the features from the LiDAR data.

For comparison, a second method is done by extracting the corners of roofs but the LiDAR data was not registered based on this approach.

The spatial transformation or mapping function used to properly overlay LiDAR and the aerial images is a 10-parameter transformation where it can be obtained the scale, translations on X, Y and Z as well as the rotations.

2 Background

2.1 LiDAR

Laser scanners also called LiDAR –Light Detection and Ranging, belong to the group of active sensors which means that the sensor illuminates the target itself without relying on other sources of radiation such the sun energy (which is the case of the passive sensors). LiDAR operation is based on the use of a laser ranger or laser rangefinder, this device measures the distance or range between the sensor and a target by emitting a beam or pulse of monochromatic radiation in which all the waves are coherent and in phase. The emitted radiation is also highly collimated and directional in the sense that it is emitted as a narrow beam in a specific direction (SHAN & TOTH, 2009).

There are two methods to measure the distance, the first method measures the time-of-flight (TOF) of a pulse of laser radiation from the laser ranger to the object and to return to the instrument after having been reflected from the object (Figure 1). The second method consists in compare the phase difference between a transmitted and received wave pattern of a continuous emitted beam (instead of a pulse). For laser ranging it is commonly used the first method by emitting a short pulse with a very high pulse energy in order to detect the sign and obtain an accurate range (SHAN & TOTH, 2009).

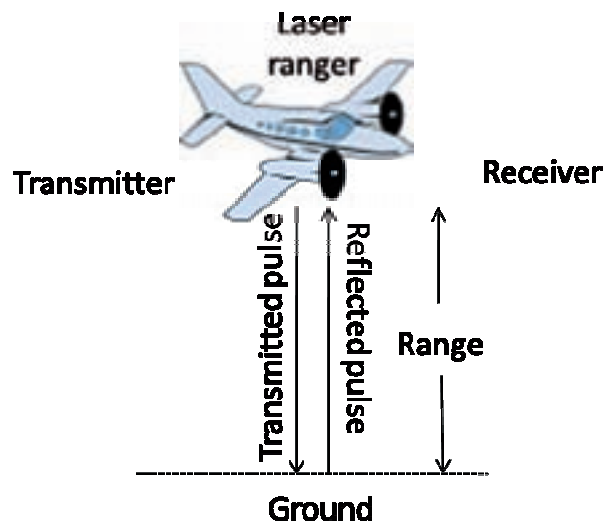


Figure 1 Basic operation of laser rangefinder by using the time-of-flight (TOF) method.

Another key component of a laser scanner is the scanning mechanism such a prism or rotating mirror which allow to acquire data of an area rather than a line which is the case of a laser profiler (Parent device of the laser scanner)(Figure).

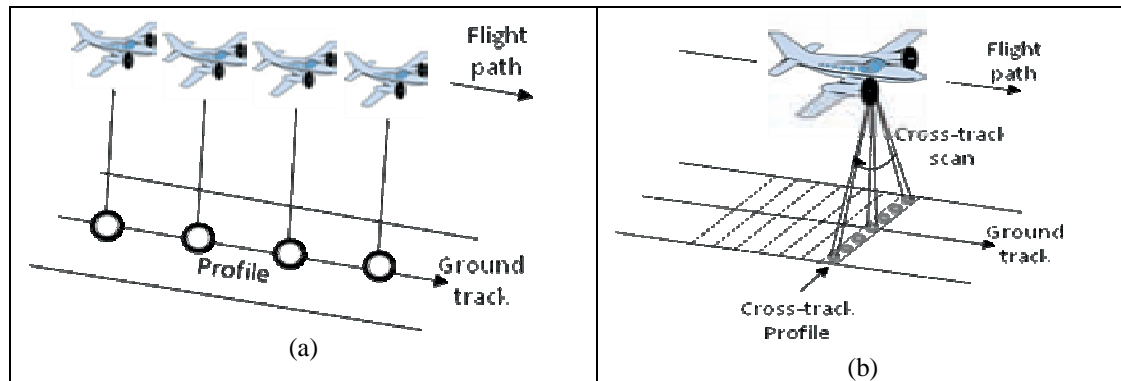


Figure 2 (a) Coverage of an area by using a laser profile. (b) Coverage of an area by using a laser scanner.

Now that it has been presented the main elements of LiDAR, it is time to determine in a general way the types of laser scanners (SHAN & TOTH, 2009: 29-126), as follows:

Laser scanner	Terrestrial	Static (Instrument in a fixed/static position)	Short-Range (Maximum ranges from 50 to 100m)	Using Phase measurement (continuous beam/wave)	
				Using pulse ranging	
			Medium-Range	Maximum ranges from 150 to 350m.	
			Long-Range	Maximum ranges more than 500m.	
		Dynamic (Dynamic vehicular platforms)	Commercial system		
			Custom-Built and In-House Operated systems		
	Research systems				
	Airborne	Topographic	Scanning mechanisms and ground measuring patterns	Single mirror or a pair of oscillating mirrors. Producing a Z-shaped pattern.	
				Optical polygon. Produces parallel lines pattern.	
				Nutating mirror. Produces a en elliptical scan pattern.	
				A pair of linear fibre-optic arrays. Produces a series of scan lines parallel to the flight line.	
		System suppliers	Commercial system. Optech,Leica Geosystems, Riegl, IGI, Toposys, iMAR		
			Custom-Built and In-House Operated systems. Top-Eye, Fugro,TopoSys, Terrapoint		
			Research systems. NASA, RASCAL, SLICER		
Bathymetric	Involves the use of two laser rangefinders.				

Table 1 General classification of laser scanners (Shaded boxes indicate the laser scanner types that are focus for this work).

As it is mention above, there are two main types of laser scanners which are airborne laser scanners and terrestrial laser scanner, but for the purpose of registration LiDAR and aerial photographs only data acquire from airborne topographic laser scanners are relevant. Therefore, it is precise to understand the airborne topographic laser scanners system which in turn will lead to understand the LiDAR data and its characteristics.

Topographic LiDAR systems have two main segments, the airborne segment and the ground segment. The airborne segment is integrated by the airborne platform, LiDAR (compounded by laser ranging unit, scanning device and controlling and data sampling unit) and the Position and orientation system (POS), which gives the geo-reference to the data. POS stores information taken from a GPS and inertial measurement unit -IMU (for attitude determination, pitch, heading and roll) at the same time that LiDAR is sampling the terrain by using its laser ranging unit. The controlling and data sampling unit synchronizes the ranging unit with the scanner and stores the range, intensity, scanning angles and time of the collected dataset.

To guarantee high accuracy on the LiDAR dataset there are GPS reference stations on the ground that makes part, along with processing hardware and software, of the ground segment mentioned before in order to perform a process off-line and finally obtain geocoded 3D LiDAR cloud of points (Figure).

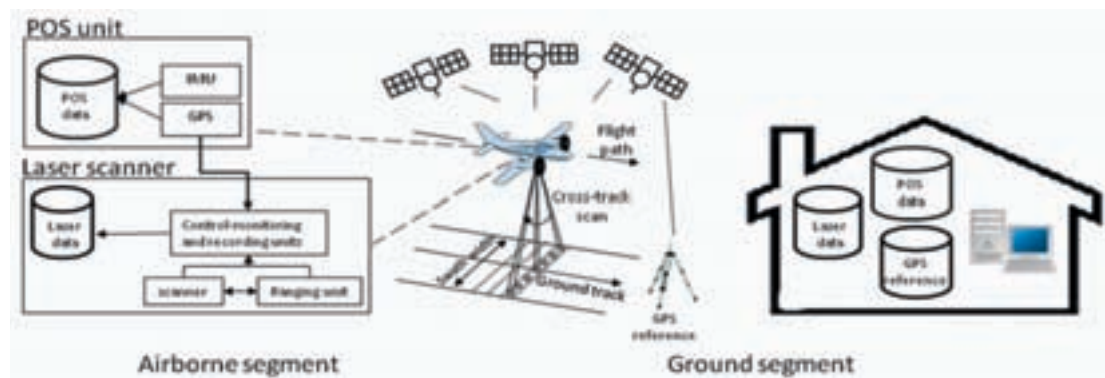


Figure 3 LiDAR system (based on SHAN & TOTH, 2009).

The LiDAR point cloud is collected in strips and to cover parallel areas a overlapping between strips is necessary to ensure a contiguous coverage of the terrain. A point of the LiDAR strip has X,Y (planimetric ground location), Z (elevation), Intensity, GPS time (of the return pulse), number of returns (from an emitted pulse),return number (e.g., return three of four returns), Mirror angle (at the time of this pulse), Point ID and other after processing such a classification (e.g., building)(SHAN & TOTH, 2009: 300).

It has been seen that airborne LiDAR has three interconnected main sensors, which are GPS, IMU and the laser scanner device (in some cases with oscillating mirror) that may introduce systematic and/or random error. An individual sensor calibration, lack of synchronization and misalignment between the sensors are usually the sources of errors in LiDAR data (SHAN & TOTH, 2009: 242). The quality of the LiDAR data relies on the accuracy of the LiDAR system's sensors and their calibration parameters. The accuracy of a LiDAR dataset is provided by the system manufacturer.

2.2 Photogrammetry

Photogrammetry is (REMONDINO, 2005): “The science of obtaining reliable measurements by means of **photographs/images**. The art, science and technology of obtaining reliable information about physical objects and the environment through the process of recording, measuring, and interpreting **photographic images** and pattern of electromagnetic radiant energy and other phenomena. The art of turning **images** into 3D models”. “Any measuring technique allowing the modelling of a 3D space using 2D images” (KASSER & EGELS, 2009).

As it is mentioned above, Photogrammetry relies on the metric aspects of the **photographs/images** in order to extract information of the world such determine the X, Y and Z coordinates of the terrain for topographic mapping purposes. Photograph is an image of objects based on the “pinhole principle” (Figure 4), discovered by “ancient Arabs when inside a dark tent, they could observe inverted images of illuminated outside objects... formed by light rays which passed through tiny holes in the tent. In the 1700s French artist used the pinhole principle as an aid in drawing perspective views of illuminated objects. While inside a dark box, they traced the outlines of object projected onto the wall opposite a pinhole. In 1839 Louis Daguerre of France developed a photographic film which could capture a permanent record of images that illuminated it. By placing this film inside a “dark pinhole box”, a picture or photograph could be obtained without the help of an artist. This box used in conjunction with photographic film became known as a **camera**” (WOLF & DEWITT, 2000: 17).

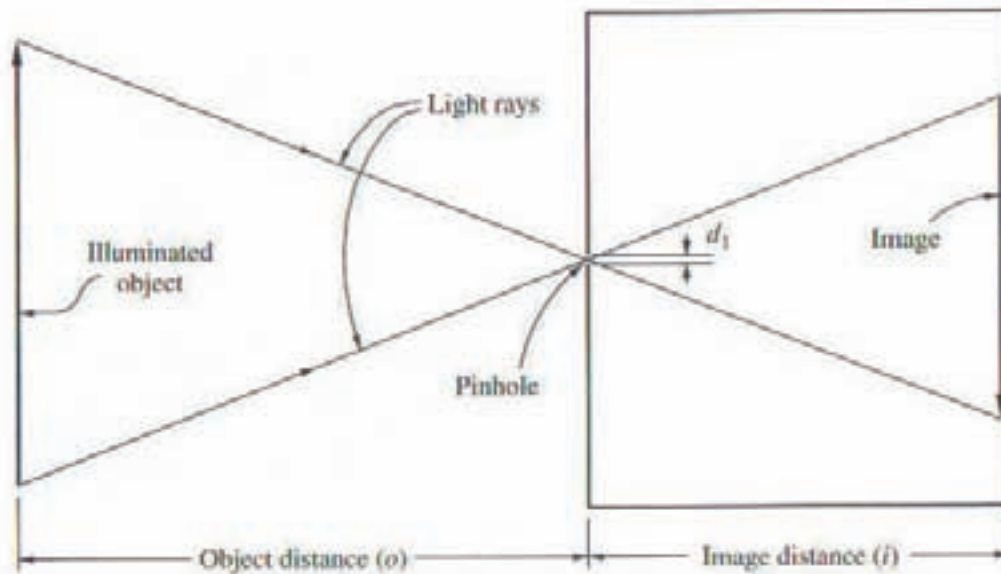


Figure 4 Principle of pinhole camera from Wolf & Dewitt, 2000.

There are two main types of cameras used in the science of Photogrammetry, aerial cameras and terrestrial camera. Terrestrial camera is a ground-based camera which takes terrestrial photographs. On the other hand, aerial cameras are “specially designed cameras to take pictures from airplanes, balloons, helicopters, or space vehicles.” (IGAC, 2009) These cameras are moved during exposure, thus the position and orientation of the photograph at the time of exposure have to be taken into account. The previous classification is known as terrestrial and aerial photogrammetry.

Aerial photogrammetry has three main types of **photographs/images**, as follows:

- Spaceborne images (taken from cameras mounted on a space vehicle)
- **Aerial images** (taken from Cameras mounted on aircrafts)
- Helicopter / balloon images (taken from Cameras mounted on Helicopter / balloon)

Aerial Cameras have been improved enormously through the years from film cameras (analog) to digital cameras, which in turn have brought digital images that are stored in computer memory allowing automatic manipulation, that in the case of photographs taken from aircrafts, are known as **digital aerial photographs/images** (It is also important to mention that digital aerial images can be obtained by scanning existing photographs). This new technology along with advances in parallel process, and increasing storage capacity among others, have lead to a new subfield of photogrammetry named **digital photogrammetry** (SCHENK, 1999: 1) . The development of digital photogrammetry, has enabled photogrammetric techniques to be integrated more easily with remote sensing and geographic information systems -GIS (IGAC,2009).

In digital photogrammetry, a digital image is “a rectangular array of pixels in which the brightness (gray level) of a scene at each discrete location has been quantified. Rather than record the reflected electromagnetic energy through silver halide crystals as in a film, digital imaging devices use solid-state detectors to sense the energy. A common type of solid-state detector in use is the **charge-coupled device** – CCD (Figure 5). At a specific pixel location, the CCD element is exposed to incident light energy, and it builds up an electric charge proportional to the intensity of the incident light. The electric charge is subsequently amplified and converted from analog to digital form. A large number of CCDs can be combined on a silicon chip in a one-dimensional or two-dimensional array” (WOLF AND DEWITT, 2000: 74). Digital frame camera (A type of digital camera) is made by a two-dimensional array of CCD elements named a *full-frame sensor* (e.g. DMC -digital modular camera from Z/I-Imaging).

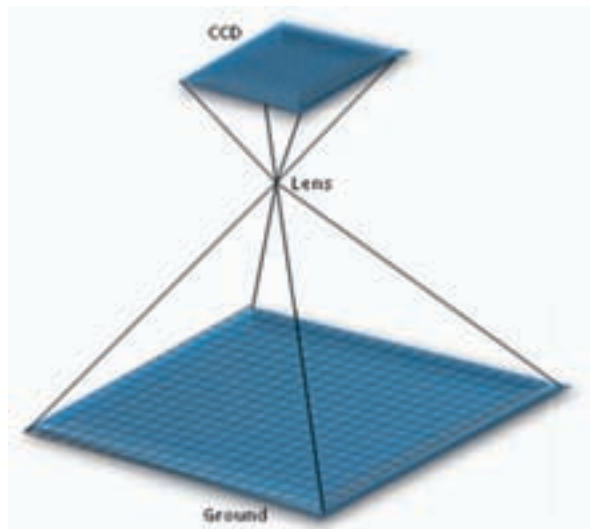


Figure 5 Array of Charge-Coupled devices –CCDs (based on WOLF & DEWITT, 2000).

It has been shown that aerial digital photogrammetry images the 3D object space through photographs/images. The 3D object space in the case of topographic mapping is a portion of the earth and natural and cultural features. Therefore, the concept of stereovision is important for determining the height component (without stereovision only X and Y, two-dimensions can be calculated). Stereovision or stereoscopic vision is the perception of depth through binocular vision (viewing with both eyes simultaneously), which enables to judge distances (WOLF & DEWITT, 2000: 147-150).

In Photogrammetry, stereovision is accomplished artificially by overlapping a pair of photographs (called stereopair) taken from different points of view. Each photograph of the stereopair is observed monoscopically, the left photo is observed with the left eye and the right photo with the right eye, so the two images of the same object reach the brain and create a three-dimensional image (IGAC,2009). For each point on the overlap area there is a continuous three-dimensional impression of the terrain in the brain, thus it is said that a three- dimensional model has been formed. The three- dimensional model is named stereoscopic model or stereomodel (WOLF & DEWITT, 2000: 152). The observation of the digital stereopair is done by means of a digital photogrammetric workstation –DPW (SCHENK, 1999: 201).

In order to obtain a digital stereoscopic model that depicts the reality (object space) as accurate as possible, it is necessary to perform pre-processing operations that correct the distortions and errors from the image acquisition process. Digital images have errors in geometry and in the measured brightness values of pixels. The last one also referred to as radiometric errors might come from instrumentation used to record the data, the wavelength dependence of solar radiation and/or from effect of atmosphere. “Radiometric correction procedures must be specific to the nature of the distortion” (RICHARDS & JIA, 2006: 27-47).

Some of the main sources of geometric distortions are: Lens distortions, atmospheric refraction, Earth curvature, variations in platform altitude, attitude (omega, phi and Kappa) and velocity (RICHARDS & JIA, 2006). Errors affect the measurement of image coordinates which have to be corrected before they are used in photogrammetric calculations, since true positions of images in the picture are required.

Image coordinates cannot be measured directly, hence an interior orientation is performed that in the case of digital cameras equipped with a CCD chip can be computed by a multiplication of the pixel addresses by the pixel size and, then, applying a shift to the principal point of the image (JACOBSEN, 2009).

Based on the image coordinates (with an image coordinate system) it can be done an exterior orientation which describes the location and orientation of an image in the object coordinate system. The exterior orientation can be found in 2 stages (DOWMAN, 2007):

- Relative orientation
- Absolute orientation

Or in 1 stage by aerial triangulation (used to treat more than 2 images at a time and reduce ground control).

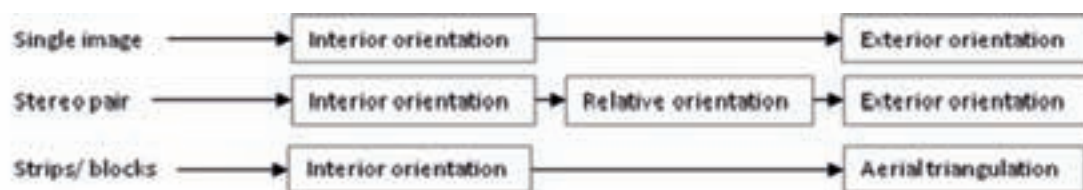


Figure 6 Absolute orientation process according to the number of images from Schenk (1999).

Relative orientation allows a stereoscopic 'model' to be found in an arbitrary co-ordinate system, for digital images image correlation techniques are used to match the stereo pair in order to achieve the relative orientation. Finally, Absolute orientation transforms the arbitrary coordinates into the ground system using ground control, thus it is possible to measure the X, Y and Z coordinates of the objects. Moreover, products such DTMs, DSMs, orthoimages, 2D and 3D reconstruction and classification of objects for mapping or thematic applications, and visualisation (maps, 3D views, animation and simulation) can be generated.

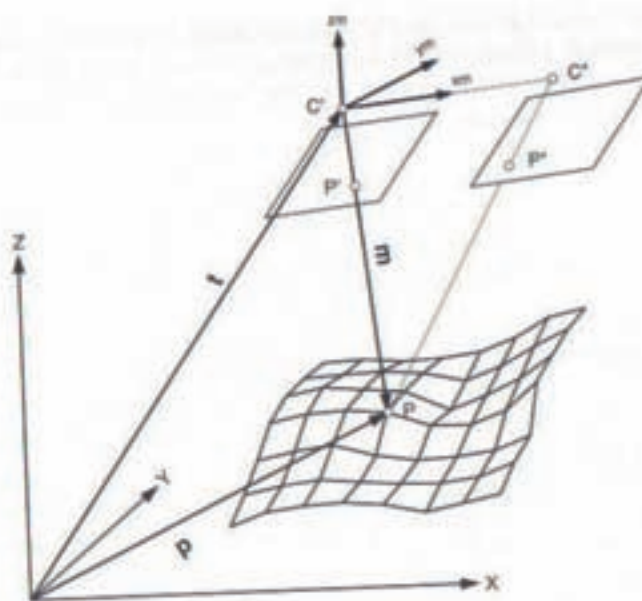


Figure 7 Absolute orientation of a stereomodel in the model coordinate system x_m, y_m, z_m , with respect to the object coordinate system X, Y, Z . From Schenk, 1999.

2.3 Registration

The process of registration aims at combining multiple datasets acquired by different sensors in order to achieve better accuracy and enhanced inference about the environment than could be attained through the use of a single sensor (HABIB, MITISHITA, & GHANMA, 2004). “In this process, one image remains without modification (the fixed image), whereas the other (the moving image) is transformed until fitting with the fixed one” (AREVALO & GONZALEZ, 2007). Image registration is frequently used in remote sensing for a wide variety of tasks such as change detection, image fusion, and image overlay.

Registration is a very important process in image processing since leads to align two or more different images that represents the same object space. There are several reasons for the misalignment between images/datasets that represents the same area, as follows:

- Images taken at different times
- Images taken from different sensors
- Images taken from different view points

A good example of registration of images taken from different sensors is the alignment of aerial images and laser scanning data, which are obtained from a passive and active sensor respectively. This process can be carrying out either by determining the sensor orientations of the aerial images and LIDAR data independently or by determining the relative orientation of the data sets (Figure 8).

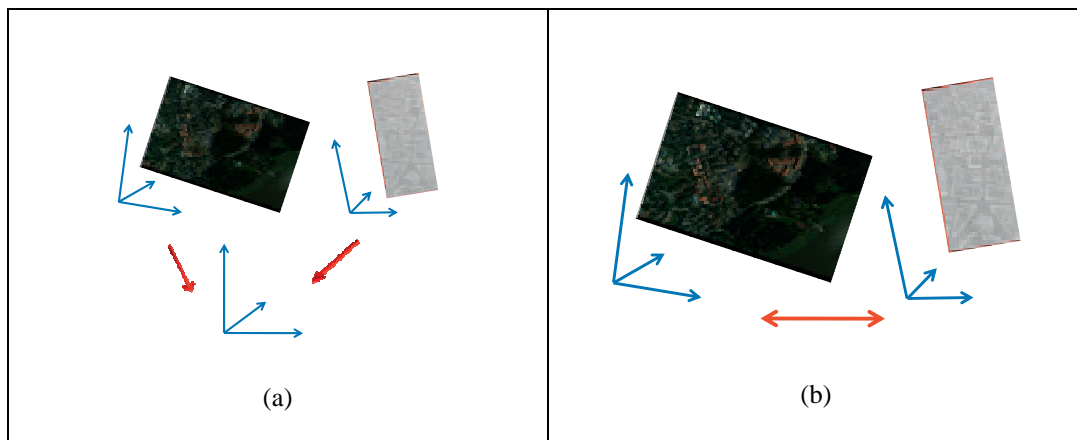


Figure 8 (a) Sensor orientations of the aerial images and LIDAR data independently. (b) Relative orientation of the datasets.

2.3.1 LiDAR and Photogrammetric data

Utilizing data from both laser altimetry (since the component is the more precise one) and photogrammetry planimetry (planimetry is more accurate) requires that the two data sets relate to the same coordinate system. Therefore, the data sets must be registered as accurately as possible

(POSTOLOV, KRUPNIK, & MCINTOSH, 1999). Thus it stands to reason to make a comparison of the characteristics of LiDAR and photogrammetric data.

“Laser altimetry provides a source of elevation information, which is both accurate and spatially dense. This information is beneficial for the production of visible surface models, especially in areas where traditional photogrammetric methods are unable to provide accurate heights” (POSTOLOV, KRUPNIK, & MCINTOSH, 1999).

As it was mentioned before, LiDAR data is the direct acquisition of three dimensional coordinates of object space points. However, there is no redundancy as any object surface is measured twice. Without redundancy, no tie points exist as in photogrammetry, and methods for checking and improving exterior orientation as well. Therefore, the quality of the derived information depends on the accuracy and the validity of the calibration parameters of the different components comprising the LiDAR system (figure 3) (HABIB, MITISHITA, & GHANMA, 2004).

Another characteristic of LiDAR is that they are mainly positional, which it is also a limitation due to its lack of thematic information (POSTOLOV, KRUPNIK, & MCINTOSH, 1999). “In contrast to LiDAR systems, photogrammetric measurements possess rich semantic information that can be easily identified in the captured imagery” (HABIB, MITISHITA, & GHANMA, 2004).

Photogrammetry measures texture, which is high at object discontinuities, i.e., edges. Point clouds that are acquired photogrammetrically are concentrated along distinct points and edges, whereas point clouds acquired by *laser scanning are more reliable inside surfaces* (SHAN & TOTH, 2009: 311).

In general terms, the major differences between photogrammetry and LiDAR are (BALTSAVIAS, 1999):

- Passive vs. Active.
- High-power collimated and monochromatic sensing (generally frame or linear sensors with perspective geometry) vs. Generally point sensors with polar geometry.
- Full area coverage vs. pointwise sampling.
- Indirect vs. Direct acquisition or encoding of 3D coordinates.
- Geometrically and radiometrically high quality images with multispectral capabilities vs. no imaging or monochromatic images of inferior quality.
- Ability for ALS to ‘see’ objects much smaller than the footprint (small openings below vegetation, power lines, etc.).

Common characteristics between photogrammetry and LiDAR are (BALTSAVIAS, 1999):

- Use of GPS. And with digital photogrammetric sensors, especially linear ones, GPS/INS.
- Methods for processing of raw data, like filtering of large errors, removal of non-DTM objects like buildings, data reduction (thin-out) and compression, and detection of breaklines, are shared between LiDAR and image matching for DSM/DTM generation.

- When laser data are regularly interpolated, they can be treated as images and various image analysis/processing techniques can be applied to them.

2.3.2 Registration methods available or under development

Traditional registration methods are based on the use of ground control points (GCPs) that are selected manually on the images, which are then used to estimate the transformation model that aligns one image to another. The fact of selecting GCPs manually leads to a laborious and time consuming process, hence automation of the registration it is desired (WONG & CLAUSI, 2007).

A classification of the current techniques that have been proposed to automate the process of image registration is:

1. **Methods based on pixel intensities:** An optimization process in which a cost function based on the radiometric similarity (The similarity between pixel intensities) of both images is maximized to determine the alignment between two images (AREVALO & GONZALEZ, 2007).
2. **Methods based on frequency-domain characteristics:** Find an optimal alignment match between two images based on characteristics in the frequency domain. A common frequency-domain technique is phase correlation, which is based on the Fourier Shift Theorem.
3. **Landmark-based methods:** that transform the moving image by a mapping function estimated from a set of representative pairs of control points (also called landmarks) identified in both images (AREVALO & GONZALEZ, 2007). This method can also be subdivided as follows:
 - **Methods based on low-level features:** Extract low-level features such as edges, ridges, and corners from the images and use the correlation between these features to determine the optimal alignment between the images (WONG & CLAUSI, 2007).
 - **High-level feature-based techniques:** Use the similarity between high-level features such as regions, buildings, and roads extracted from the images to determine the alignment between the images (WONG & ORCHARD, 2008).

Having in mind the limitations of LiDAR and aerial digital images, it is important to mention the consequent issues that make LIDAR–optical image registration a difficult process (WONG & ORCHARD, 2008):

- **Symmetric GCP detection:** Similarity-based techniques, a set of symmetric GCPs must be selected in both datasets for an image pair for the registration to function. However, it is very difficult to find the same points of interest within each image.
- **Intensity mapping:** Data acquired from these modalities (LiDAR and aerial photographs) have very different intensity mappings. This makes it very difficult to perform direct similarity comparisons between the two datasets.
- **Structural characteristics:** The structural characteristics acquired by optical imaging may not be present in the LIDAR image. This makes it difficult to perform similarity comparisons between LIDAR and optical images based solely on structural characteristics such as edges and shape.

In general terms registration is carried out in four stages (WONG & CLAUSI, 2007):

1. Control-point (CP) detection: A set of potential GCPs is accurately selected automatically from the set of images (the reference/fixed image and the moving image).
2. CP matching: Similarity analysis is performed to determine a set of matching GCPs from the GCP candidates.
3. Transformation estimation: Based on the set of matching GCPs, the geometric transformation function is estimated to provide the best alignment between the images.
4. Transformation and resampling: The moving image is transformed based on the determined function to overlap the reference/fixed image and by applying some interpolation techniques such as nearest neighbour, bilinear, bicubic, or splines.

As it is said above, a fundamental characteristic of any image registration technique is the type of spatial transformation or mapping function used to properly overlay two images, in other words, an equation that allows transforming the locations of points in one dataset to new locations of points in another dataset which is used as reference. Transformations may be global or local, a global transformation is given by a single equation which maps the entire image, whereas a local transformation map the image differently depending on the spatial location and are thus much more difficult to express succinctly. Common transformations are (GOTTESFELD, 1992):

- Rigid: Where the true shape is retained. A rigid-body transformation is composed of a combination of a rotation, a translation, and a scale change.
- Affine: are more general than rigid and can therefore tolerate more complicated distortions while still maintaining some nice mathematical properties.
- Projective and Perspective: Account for distortions due to the projection of objects at varying distances to the sensor onto the image plane.
- Global Polynomial: one of the most general global transformations (of which affine is the simplest) and can account for many types of distortions so long as the distortions do not vary too much over the image. Distortions due to moderate terrain relief can often be corrected by a polynomial transformation.
- Non-rigid: Such Polynomial functions, Piecewise-linear functions and thin-plate splines. there has been no successful technique for performing automatic nonrigid registration of optical and LIDAR images in an efficient and robust manner (WONG & ORCHARD, 2008).

There are several developments in automatic registration of LiDAR and aerial images that is worth to mention, such as:

- Fast Fourier transform (FFT), an efficient non-rigid automatic registration system approach designed to handle many of the difficulties associated with the registration of optical and light detection and ranging (LIDAR) images(WONG & ORCHARD, 2008).
- Matching LiDAR surface patches with regard to the photogrammetric digital surface model – DSM, as an alternative to other registration methodologies based on the detection of characteristic features such as planes (Roux & Pierrot-deseilligny, 2009).
- Registration of airborne laser scanning point clouds with aerial images through terrestrial image blocks (RÖNNHOLM et al., 2008a).

- Photogrammetric model orientation using centroids of building roofs that are derived from LIDAR datasets (MITISHITA, HABIB, & MACHADO, 1999).

All these methods use the LiDAR as the reference dataset, in other words the aerial images are the moving dataset that is aligned with respect to the laser scanner ground coordinate system. Since the registration of LiDAR and photogrammetric data is an emerging field there is a lot to analyze and play such performing a registration where the aerial images are the reference and LiDAR is the moving dataset.

2.3.3 Errors that affect registration

Errors in aerial images and laser scanning data affect the quality of the registration. As it was mention earlier, those errors can be internal in the case of the aerial images (Frame-based photogrammetry uses interior orientation for solving these errors) or may be in the case of LiDAR range errors, INS systematic errors, mounting errors and so on (These errors can be reduced using, e.g., overlapping laser strips and ground control features). Therefore they must be corrected before the process of registration is performed (RÖNNHOLM, P. et al., 2007).

3 Research Question

The approach of using the same registration method with different combinations of data (Empirical research) will provide a better understanding of the registration process between LIDAR and aerial data. Therefore, the next questions have been setting up:

Having registered Optech's laser data and Leica's laser data using DMC panchromatic and multispectral images as reference, How much a registration method differs in performance and accuracy since the two sets of Laser data have different density?

Having registered Optech's laser data and Leica's laser data using DMC panchromatic and multispectral images as reference, How much a registration method differs in performance and accuracy since panchromatic images and multispectral images have different resolution?

The above questions are related to the next UCGIS research agenda topics:

UCGIS(2002)

Long – term: Remotely Acquired Data and Information in GIScience.

Short – term: Geospatial data fusion.

3.1 OBJECTIVES

- Provide a better understanding of the registration process based on the detection of features of aerial images and airborne laser scanning point clouds.
- Performance a registration method for the integration of:
Optech's laser data and DMC panchromatic images.

- Leica's laser data and DMC panchromatic images.
- Optech's laser data and DMC multispectral images.
- Leica's laser data and DMC multispectral images.
- Analyze how laser scanning data's density affects on the registration method accuracy and performance.
- Analyze how the image resolution affects on the registration method accuracy and performance.

4 Data

The data were taken in Espoonlahti (approximately 60° 8'N, 24° 38'E) in southern part of Finland. The area can be characterized as low residential urban area having mainly terrace houses and detached houses.

The data listed below for this study has been provided by EuroSDR (RÖNNHOLM et al., 2008b):

4.1 LiDAR

Only one strip per sensor has been provided for this project and each one has been deflected on purpose. LiDAR data has been delivered in ASCII format and the data order is: X Y Z Intensity (X=Easting Y=Northing).

- **OPTECH ALTM 3100 STRIP:**
 - Acquired in July 2005.
 - Flying height 1000 m approximately.
 - Point density of 2-3 points/m².
 - Scanning angle 24 degrees, 20 degrees is processed ($\pm 10^\circ$).
 - PRF 100 kHz.
 - Scanning frequency 67 Hz.
 - Flying speed 75 m/s.
- **LEICA ALS50 II STRIP:**
 - Acquired in April 2007.
 - Flying height 500 m approximately.
 - Point density of 4-5 points/m².
 - Scanning angle 40 degrees ($\pm 20^\circ$).
 - PRF 148 kHz.
 - Scanning frequency 42.5 Hz.
 - Flying speed 72 m/s

4.2 Photogrammetric data

It has been provided DMC panchromatic and DMC multispectral image block of 4 images each. Aerial triangulations of both image blocks are calculated with Leica Photogrammetry Suite version 9.2 (Erdas LPS), total of 8 images were used in order to make each image block more robust, but only four images (from the middle of the block) are provided. In aerial triangulation there were no signalized points but only natural targets were used as ground control.

All image measurements were monoscopic. Forward overlap was 60% and side overlap was 20%, and the sense of the coordinate system is a conventional x, y, z system (X to right).

- **DMC PANCHROMATIC IMAGE BLOCK OF 4 IMAGES:**

Acquired in September 2005.
Pixel depth is 16 bit.
Size is 7680 x 13824.
Ground resolution is 5 cm approximately.
Projection: ETRS-TM35FIN

Interior orientation:

Focal length: 120.0000 mm (10000 pixels)
Principle point (differences from the image centre):
Px=0.000 mm
Py=0.000 mm
Pixel size: 0.012 mm
Image size: 7680 x 13824 pixels (92.16 x 165.888mm)

Exterior orientation:

Image	X (Easting)	Y (Northing)	Z	Omega(deg)	Phi(deg)	Kappa(deg)
Espo...01~0013_pan	369137.4616	6669504.5307	533.0853	-0.5966	-0.4865	-47.1581
Espo...01~0014_pan	369037.4532	6669628.9860	534.7828	-0.5513	-0.3543	-47.0364
Espo...02~0013_pan	369525.1342	6669910.7766	562.1791	0.4640	-0.4638	129.8534
Espo...02~0014_pan	369427.5298	6670029.5877	563.1658	0.6849	-0.5434	129.8055

Table 2 Exterior orientation parameters for the panchromatic block images provided by EuroSDR.

Estimated accuracy of exterior orientation parameters (meters and degrees):

image	mXs	mYs	mZs	mOMEGA	mPHI	mKAPPA
Espo_5b2_1_09_05_01~0013_pan	0.0409	0.0405	0.0138	0.0042	0.0044	0.0012
Espo_5b2_1_09_05_01~0014_pan	0.0430	0.0370	0.0168	0.0038	0.0045	0.0014
Espo_5b2_1_09_05_02~0013_pan	0.0269	0.0269	0.0089	0.0027	0.0027	0.0008
Espo_5b2_1_09_05_02~0014_pan	0.0216	0.0248	0.0085	0.0025	0.0021	0.0007

Control point RMSE (71 control points):

Ground X: 0.02169 m
Ground Y: 0.02181 m
Ground Z: 0.01083 m
Image X: 0.00302 mm (152 observations)
Image Y: 0.00291 mm (152 observations)

Check Point RMSE (7 points)

Ground X: 0.04180 m
Ground Y: 0.03396 m
Ground Z: 0.06020 m
Image X: 0.00379 mm (15 observations)
Image Y: 0.00338 mm (15 observations)

Total Image Unit - Weight RMSE: 0.00385 mm

The above parameters were used to display the panchromatic images by means of Socet Set 5.4.1 software. Once the panchromatic block of 4 images were displayed it was found Y parallax (Figure 9), thus stereovision was not possible to achieve. Y parallax occurs when the line joining corresponding images are not parallel with the direction of the flight. Most Y parallaxes usually are consequence of an improper orientation of the photos (WOLF & DEWITT, 2000: 158).

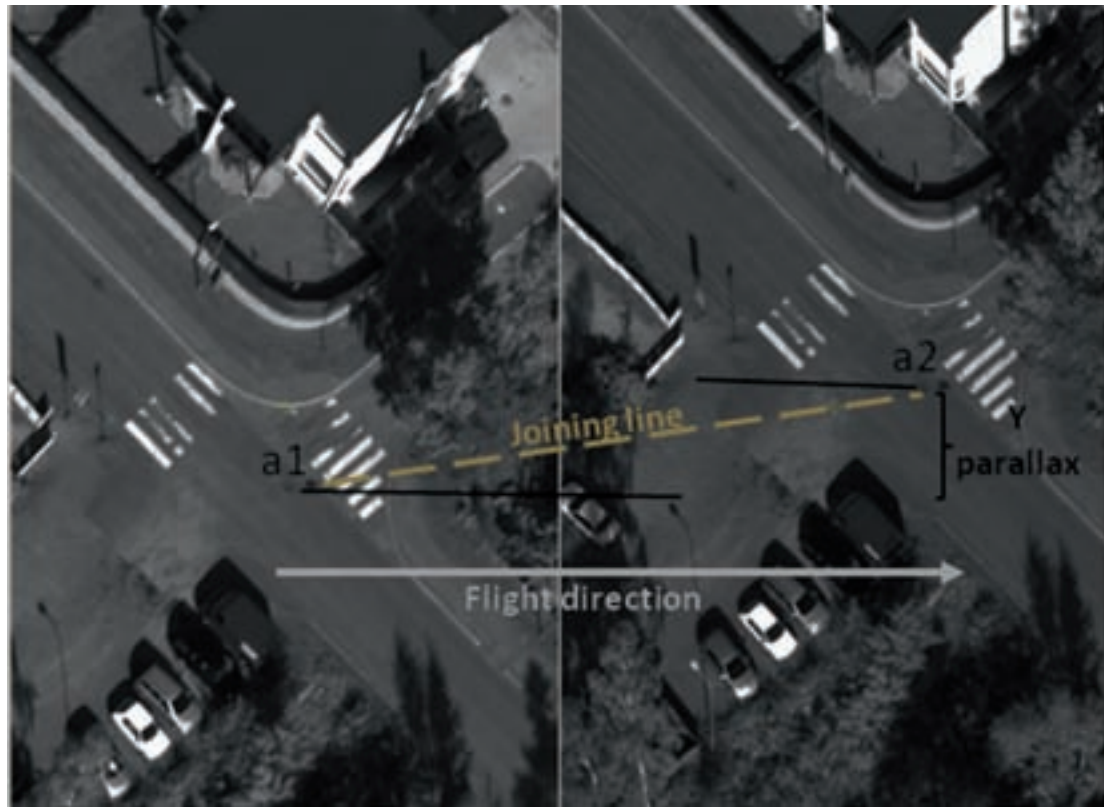


Figure 9 Y parallax.

Due to the presence of Y parallax it was necessary to carry out the absolute orientation, where the interior orientation remains the same but the aerial triangulation was performed again (Figure 6). Since ground control points (GCPs) were not provided for orientation purpose, the block of images (with the orientation provided by EuroSDR) were used in order to generate tie points automatically through the Multi-Sensor Triangulation tool in Socet Set. The generated tie points (60 points) were re-measured manually until the total RMSE was 1.013 pixels (best RMSE achieved).

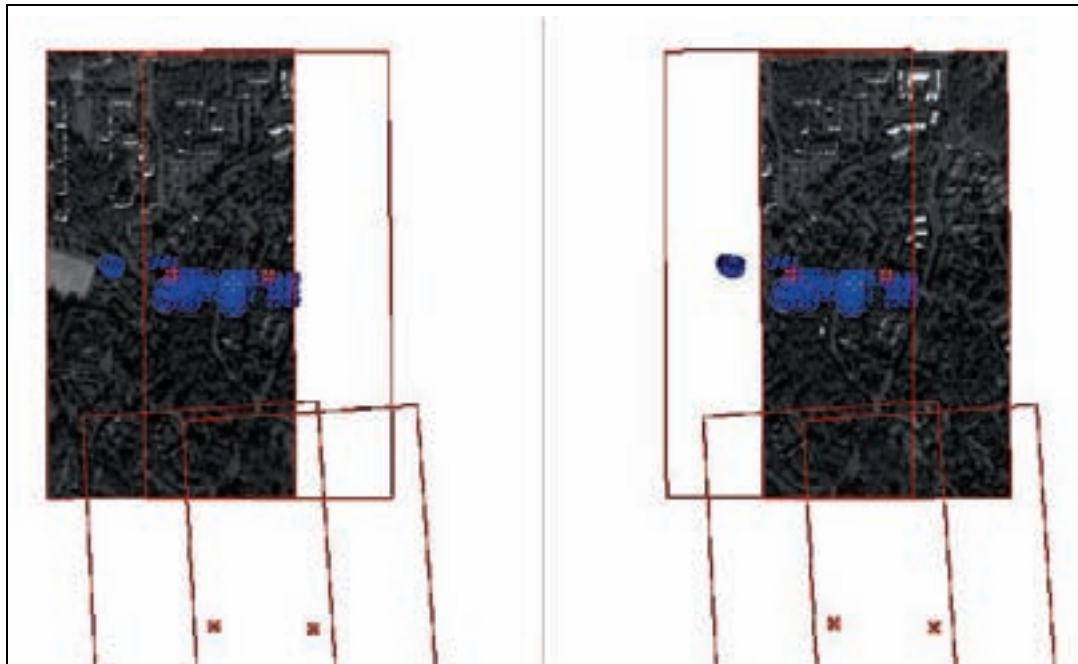


Figure 10 Distribution on the image block of Ground control points (GCPs) provided by EuroSDR.

A set of GCPs were provided from EuroSDR in order to check the accuracy of LiDAR data. These GCPs are concentrated in a specific area; hence they were not suitable for orientation as they were not properly distributed on the block of images (Figure 10). Nevertheless, these GCPs were useful to assess quality of the new aerial triangulation carried out. A statistical comparison of the 29 GCPs and their correspondence 29 points measured on the triangulated images showed the follow result:

Axis	RMSE	Standard deviation	Average Difference (Diff = Check Point File - Measured Point File)
X	1.7169	1.6206	-0.6419
Y	1.9134	1.9465	-0.0516
Z	0.7700	0.1761	0.7503

Table 3 Statistics of the new exterior orientation parameters.

New parameters of exterior orientation:

Image	Omega(deg)	Phi(deg)	Kappa(deg)
Espo_5b2_1_09_05_01~0013_pan	-0.727066	-0.35738	-45.098415
Espo_5b2_1_09_05_01~0014_pan	-0.664735	-0.186987	-44.967118
Espo_5b2_1_09_05_02~0013_pan	0.58883	-0.60035	131.90583
Espo_5b2_1_09_05_02~0014_pan	0.82810	-0.67044	131.84847

Table 4 New parameters of exterior orientation.

- **DMC MULTISPECTRAL IMAGE BLOCK OF 4 IMAGES** (only RGB channels are provided):

Acquired in September 2005.
Pixel depth is 8 bit.
Size is 2048 x 3072.
Ground resolution is 22 cm approximately.
Projection: ETRS-TM35FIN

Interior orientation:

Focal length: 25.263 mm (2105.25 pixels)
Principle point (differences from the image centre):
Px=-0.646 mm (-53.83 pixels)
Py=0.646 mm (53.83 pixels)
Pixel size: 0.012 mm
Image size: 2048x3072 pixels (24.576x36.864 mm)

EuroSDR found significant improvement when radial lens distortions were self-calibrated in aerial triangulation, thus they provided the lens distortions as follows:

The lens distortion parameters are:

$k1 = -5.4359E-005$
 $k2 = 1.1579E-007$

Exterior orientation:

Image	X (Easting)	Y (Northing)	Z	Omega (deg)	Phi(deg)	Kappa(deg)
Espo...01~0013_lrc	369137.6794	6669504.5268	530.6001	-0.5677	-0.4606	-47.1557
Espo...01~0014_lrc	369037.2651	6669628.6389	532.3045	-360.4949	-0.3727	-47.0268
Espo...02~0013_lrc	369525.1422	6669910.4982	559.6122	0.4783	-0.4725	129.8616
Espo...02~0014_lrc	369427.5371	6670029.5896	560.6816	0.6727	-0.5570	129.8225

Table 5 Exterior orientation parameters for the multispectral block images provided by EuroSDR.

Estimated accuracy of exterior orientation parameters (meters and degrees)

image	mXs	mYs	mZs	mOMEGA	mPHI	mKAPPA
Espo_5b2_1_09_05_01~0013_lrc	0.2118	0.2006	0.0903	0.0207	0.0228	0.0058
Espo_5b2_1_09_05_01~0014_lrc	0.2100	0.1943	0.1025	0.0193	0.0223	0.0070
Espo_5b2_1_09_05_02~0013_lrc	0.1340	0.1440	0.0922	0.0145	0.0136	0.0046
Espo_5b2_1_09_05_02~0014_lrc	0.0909	0.1238	0.0925	0.0127	0.0089	0.0037

Control point RMSE (77 control points)

Ground X: 0.0119 m
Ground Y: 0.0110 m
Ground Z: 0.0062 m
Image X: 0.0050 mm (187 observations)
Image Y: 0.0053 mm (187 observations)

Check Point RMSE (8 points)

Ground X: 0.1625 m
Ground Y: 0.2197 m

Ground Z: 0.3553 m
Image X: 0.0018 mm (22 observations)
Image Y: 0.0043 mm (22 observations)

Total Image Unit - Weight RMSE: 0.0058 mm

4.3 Field surveys

Ground control points from the test area collected using real time kinematic (RTK) GPS. Only points that locate within image footprints of test data were delivered (Figure 11).



Figure 11 Image of the ground control points provided by EuroSDR.

4.4 Software

- Socet Set v 5.4.1.
- Terra Solid v9.0 (TerraScan).
- LiDAR analyst tool 4.2 for ArcGIS by visual learning systems Inc.
- ArcGIS 9.2
- Matlab R2008b
- Envi 4.5

5 Methodology

The registration of LiDAR and photogrammetric data has been carried out using the aerial block of images as reference. It was used Landmark-based registration method where low-level features were determined, using as guideline the paper “CO-REGISTRATION OF PHOTOGRAMMETRIC AND LIDAR DATA: METHODOLOGY AND CASE STUDY” (HABIB, MITISHITA, & GHANMA, 2004). The steps taken in this project were:

1. To assess an initial quality of the LiDAR dataset based on the provided GCPs. This allowed having an idea of the LiDAR’s misalignment in X, Y and Z.
2. To define and extract the features from the images and LiDAR dataset. Since point clouds acquired by *laser scanning are more reliable inside surfaces* (SHAN & TOTH, 2009: 311), for the registration it was defined to extract linear features from the intersection of roof’s planes in order to obtain the end points (corners) of the lines. As experiment also, were extracted the corners of the roof in order to compare the two methods but this strategy was not used to register the data.
3. To apply a global three-dimensional transformation where the true shape is maintained based on the extracted features from the roof’s apex. Due to the registration should include at least translations and laser data may contain also rotation errors, a ten-parameter transformation was applied, so the scale, three translations, and three rotations were found.
4. To transform the LiDAR data based on the function calculated from the 3D transformation using the extracted features from the roof’s apex.
5. To validate and interpret the registration.

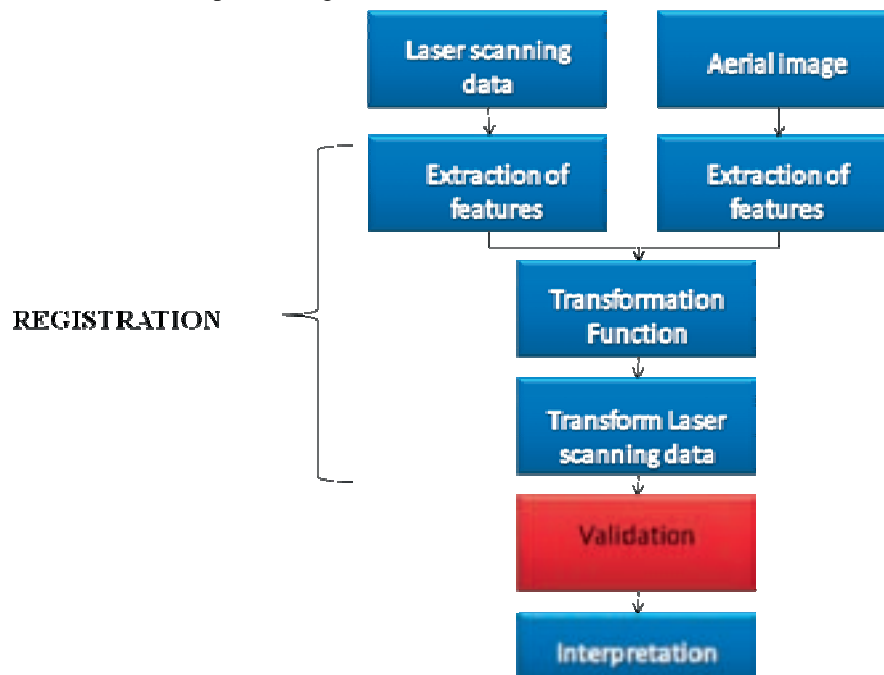


Figure 12 Methodology workflow.

The initial registration was performed based only on the panchromatic images with the new orientation, nevertheless at last minute was found how to set up the panchromatic set of images and their original orientation without Y parallax, so it was performed again the process of extracting features from the panchromatic images and multispectral as well, calculating the transformation function and finally registered the LiDAR data.

6 Results

According to the methodology presented above, the results are as follow:

6.1 Initial assessment of LiDAR data quality

6.1.1 Leica

6.1.1.1 Planimetric analysis

In order to make a visual comparison of the laser data and ground control points, it was generated a shapefile of the ground control points based on the field data provided by EuroSDR (Figure 13), acquired with Leica SR530 dual-frequency GPS-receiver and Leica AT502 GPS antenna and a RMSE of 2 cm in xy and 4 cm in z approximately. The software used to generate the .shp file was ArcGis.

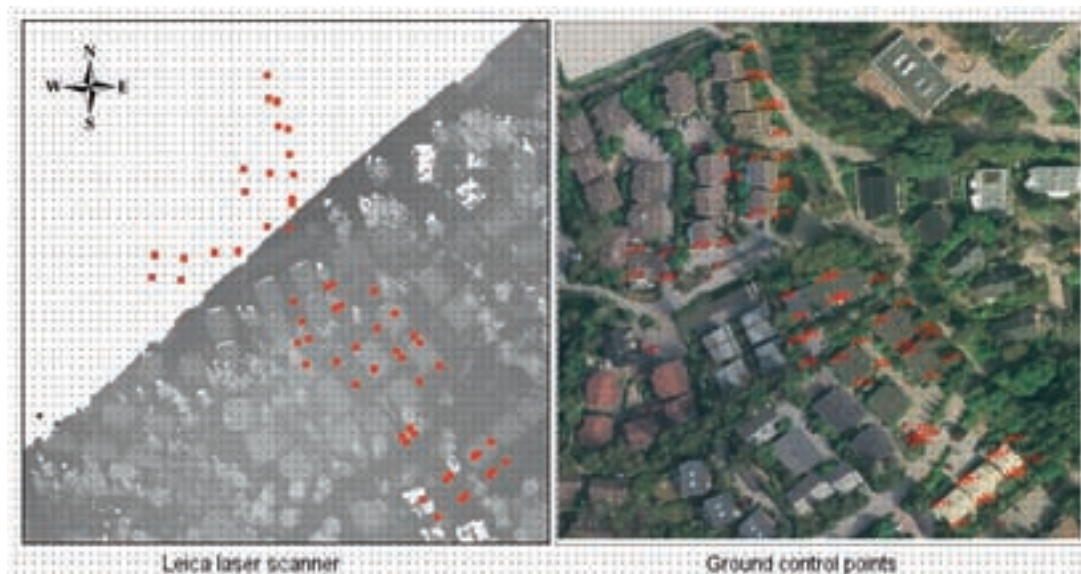


Figure 13 GCP Vs Leica Laser scanning data.

Due to ArcGis does not have the ETRS-TM35FIN coordinate system, it was necessary to download the .prj file in order to give the mentioned coordinate system to the GCP shapefile and to the project where the data was displayed.

The laser scanning data were in ASCII format which was converted to .LAS format in order to upload in ENVI and GvSIG (Open Source Software) by means of a program named **LAStools**.

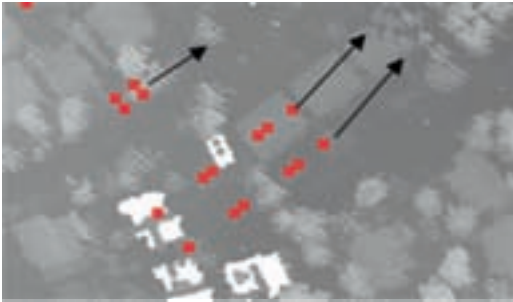

Leica laser scanning data	GCP
	

Table 6 Planimetric analysis Leica dataset.

An overall display of the laser data and the GCP of the test area shows a clear horizontal displacement of the laser data specially in the X axis. The displacement is approximately of 30 m to the north-east direction compared against the GCPs. From the above it is expected a negative translation in the X and Y axes.

6.1.1.2 Z analysis

The file .LAS created before was exported as .shp in order to visualize it in ArcMap and also to create a TIN. Once the Tin was generated by means of the 3D analyst ArcGIS extension, it was possible to make profiles of the area where the ground control points should lie (Figure 14 TIN leica data Vs GCP.). Through the profiles the value of Z (Leica laser scanning data) was calculated with the purpose of making an estimation of the RMSE of the laser data in high.



Figure 14 TIN leica data Vs GCP.

The values of **Z** in the Leica laser scanning data are **higher than** the Z values of the ground control points (GCPs), thus the registered data will need a negative translation in the Z axis. The RMSE of the Z values was calculated from the values provided by the profiles above in order to have an average of the difference in high which result is **6.1773 mts** (See Appendix A).

6.1.2 Optech

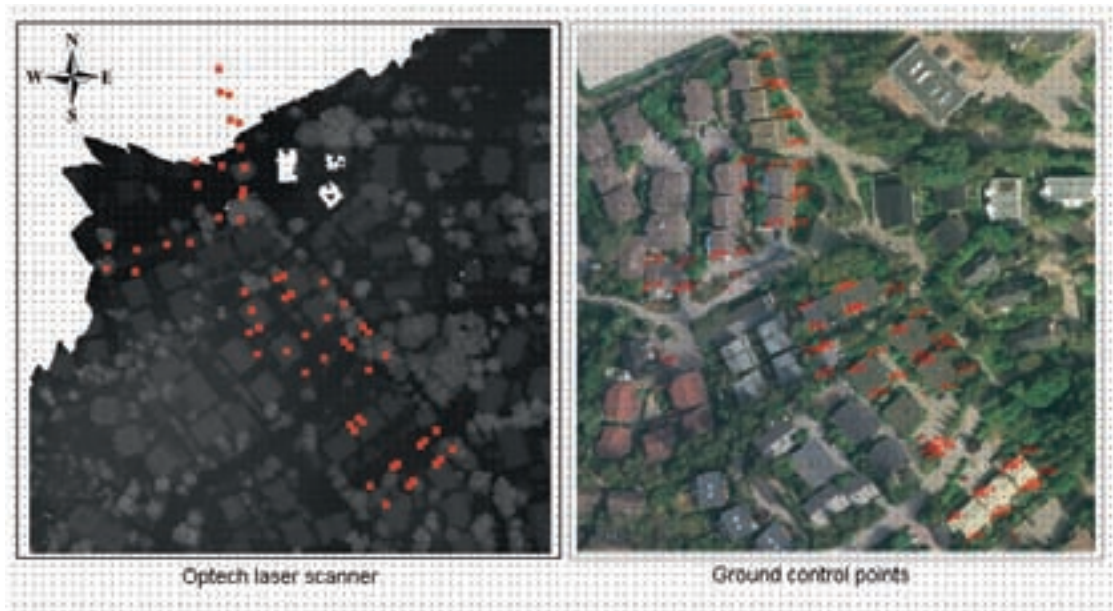


Figure 15 GCPs Vs Optech Laser scanning data.

6.1.2.1 Planimetric analysis

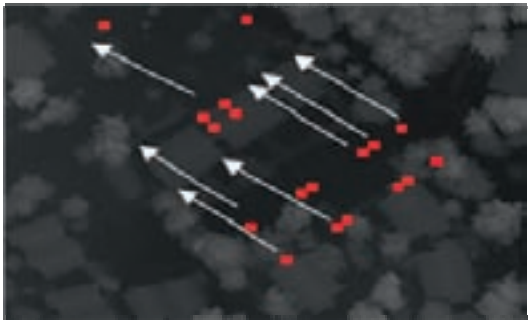

Optech laser scanning data	GCP
	

Table 7 Planimetric analysis Optech dataset.

An overall display of the laser data and the GCP of the test area shows a clear horizontal displacement of the laser data specially in the Y axis. The displacement is approximately of 30m to the north –west direction compared against the GCPs. Therefore, it is expected a negative translation in the X axis while a positive translation in the Y axis.

6.1.2.2 Z analysis

The values of **Z** in the Optech laser scanning data are **lower than** the Z values of the ground control points, so a positive translation in the Z axis is expected. The RMSE of the Z values was calculated from the values provided by the profiles above in order to have an average of the difference in high which result is **25.3501 mts** (See Appendix A).

6.2 Definition and extraction of features from the two datasets

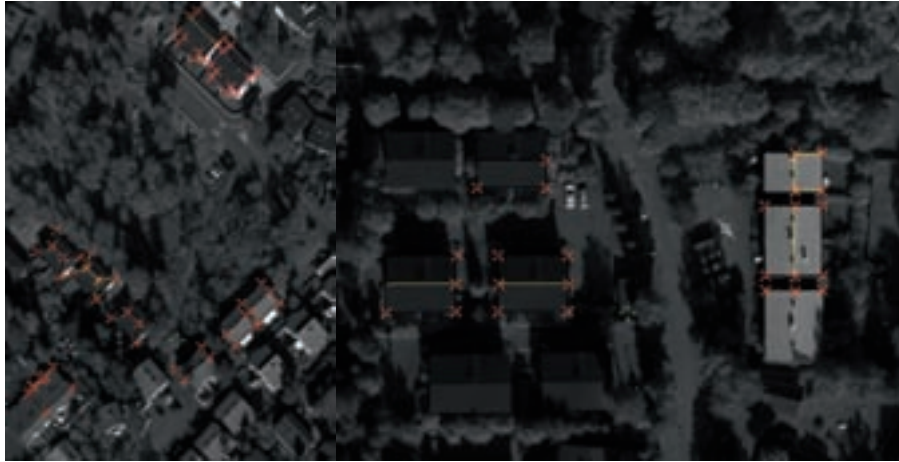
The features to carry out the registration were points. Since extraction of points in LiDAR dataset that match their corresponding image points is nearly impossible due to LiDAR's characteristics, it was necessary to extract lines first based on the intersection of roof's planes and then obtain the points of those lines; TerraScan V9.0 was used to extract the Lines from roof plane's intersections in a semi-automated way.

A second form of extraction of lines was performed by using a LiDAR tool for ArcGIS, in order to obtain the corners of the roof as it was mention before in order to make a comparison, in this case it was extracted first the boundaries of the roof then the points. This software detects automatically the buildings.

The points were selected based on the images interpretation along de overlapping area of the block focusing on buildings which roof have intersection of planes, thus the points were suitable for matching the extracted points from TerraScan.

6.2.1 Photogrammetry dataset

The extraction of the features was done manually as SocetSet software does not have an automated tool to use for this purpose (Appendix B).



(a)



(b)

Figure 16 (a) Extracted points from panchromatic images. (b) Extracted points from multispectral images.

The selected points for the panchromatic images with the new orientation and the panchromatic and multispectral images using the exterior orientation parameters provided by EuroSDR are the same; the difference is the coordinate values.

6.2.2 LiDAR dataset

6.2.2.1 Apex of Roofs

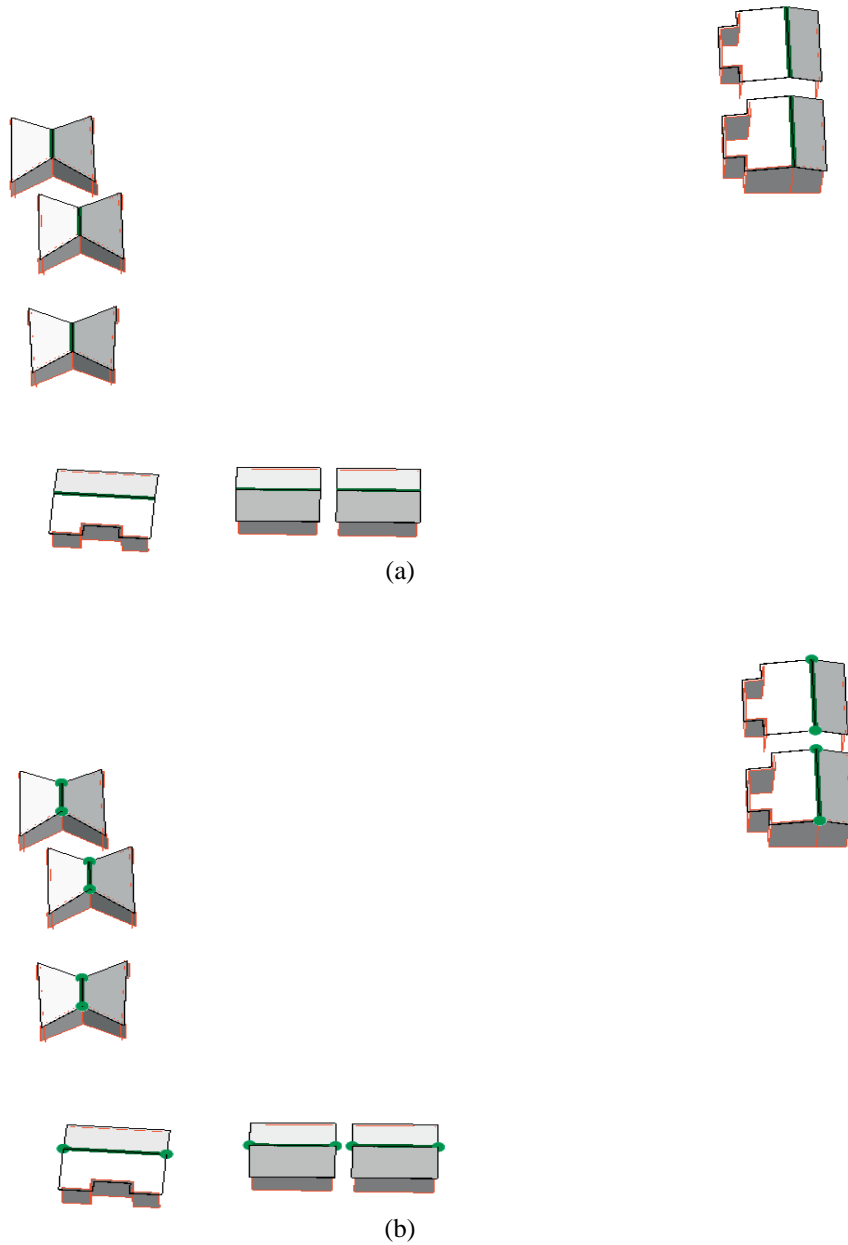


Figure 17 (a) Lines from roof plane's intersections in the Leica dataset using terraScan. (b) Points from lines.

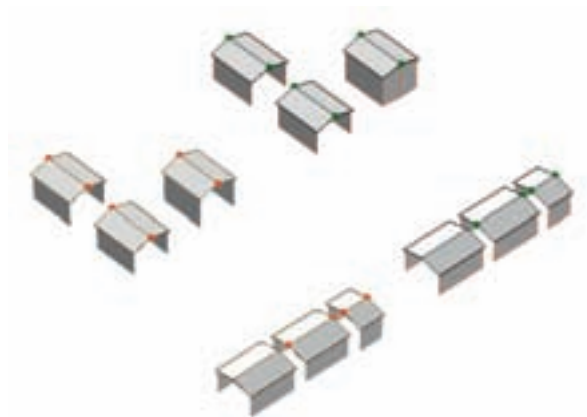


Figure 18 Orange points are the extracted points from Optech, while green points are the extracted points from Leica using TerraScan (Appendix C).

6.2.2.2 Corners of roofs

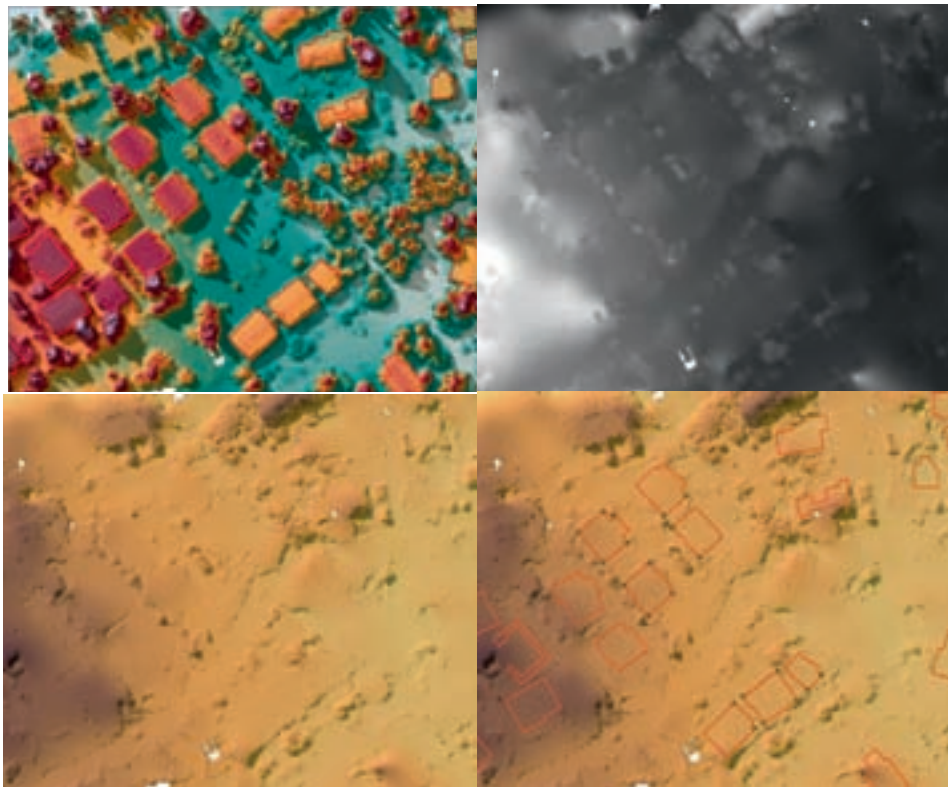


Figure 19 Extracted Leica points (roof's corners) using LiDAR tool for ArcGIS. (top) Raster hillshade of the elevation (top right) Raster using bare-Earth algorithm (bottom left) Raster hillshade of the previous one (bottom right) Points from extracted building edges based on the Raster using bare-Earth algorithm.

A total of 28 points were extracted from Terra Scan for the transformation.

6.3 Three-dimensional transformation Function

In order to calculate the parameters for a rigid transformation of the LiDAR points of clouds based on the DMC images it was performed initially a 7-parameter transformation (with only 4 points) by using least squares.

Parameter	Value
K	0.03433464
α_x	0.00727928
α_y	0.01819792
α_z	0.02085698
ΔX	-151775.971
ΔY	-221325.635
ΔZ	41854.7344

Table 8 Initial 7- parameters values, calculated from four points of Optech.

ΔX , ΔY , ΔZ are the geocentric translations from the LiDAR coordinate reference system (that is unknown) to the Images reference system (target system). α_x , α_y , α_z are the rotations about each of the three axes and the scale is $K+1$.

Since the geocentric translations (ΔX , ΔY , ΔZ) are big numbers difficult to interpret, a 10-parameters transformation was carried out, which result is:

Parameter	Value
K	0.03433303
α_x	0.00728354
α_y	0.01827601
α_z	0.02085703
ΔX	24.0496
ΔY	-18.05925
ΔZ	25.3914
X_o	369425.663
Y_o	6670013.61
Z_o	22.90155

Table 9 10-parameters values, calculated from four points of Optech.

X_o , Y_o , and Z_o are the origin of the local coordinates calculated as the average of the x, y and z values of the LiDAR's points used in the transformation.

The 10-parameter transformation is expressed as follows:

$$\begin{bmatrix} X \\ Y \\ Z \end{bmatrix}_{Images} = \mu R \begin{bmatrix} X - X_o \\ Y - Y_o \\ Z - Z_o \end{bmatrix}_{LiDAR} + \begin{bmatrix} \Delta X \\ \Delta Y \\ \Delta Z \end{bmatrix}_{LiDAR \text{ to } Images} + \begin{bmatrix} X_o \\ Y_o \\ Z_o \end{bmatrix}$$

Equation 1 10-parameter transformation expression.

6.3.1 10-parameters transformation

A script was developed in Matlab software in order to calculate the transformation function with its parameters and to transform the whole cloud of point of every LiDAR dataset as well (Appendix D).

6.3.1.1 Apex of Roofs

Initially 28 points were used to calculate the transformation function using the panchromatic images with the new orientation, then the residuals were checked which led to used finally 20 points. The same 20 points were used for the panchromatic and multispectral images with the EuroSDR orientation (Table 10).

Parameter	New orientation				EuroSDR orientation					
	Leica		Optech		Leica		Optech			
	Panchromatic		Panchromatic		Panchromatic		Panchromatic		Multispectral	
	28 points Value	20 points Value	28 points Value	20 points Value	20 points Value	20 points Value	20 points Value	20 points Value	20 points Value	20 points Value
K	0.00194078	0.00182886	0.00217027	0.00228968	-0.000695637	-0.001669653	-0.000237891	-0.001212825		
Ax(rads)	-0.00460349	-0.00522266	-0.00411432	-0.00442174	0.000109008	0.003014105	0.00092648	0.003848928		
ay(rads)	-0.0009708	-0.00244688	-0.00131525	-0.00209771	7.85E-05	0.004755203	0.000448934	0.005146315		
az(rads)	0.00066974	0.00080869	-0.00026439	-0.00033885	0.00071905	0.000673522	-0.00042298	-0.00046427		
$\Delta X(m)$	-17.9988885	-17.8971097	23.8244148	23.9025741	-18.0921919	-18.0400859	23.7074919	23.7595979		
$\Delta Y(m)$	-21.6520354	-21.5769405	-17.7670589	-17.7087255	-21.689817	-21.5316455	-17.821602	-17.6634305		
$\Delta Z(m)$	-7.80482143	-7.65223	23.7105071	23.82675	-6.21228	-6.81453	25.2667	24.66445		
Xo(m)	369359.897	369398.792	369318.074	369356.993	369398.7923	369398.7923	369356.9926	369356.9926		
Yo(m)	6669807.47	6669843.71	6669803.58	6669839.84	6669843.713	6669843.713	6669839.845	6669839.845		
Zo(m)	54.3505714	55.21583	22.8352429	23.73685	55.21583	55.21583	23.73685	23.73685		

Table 10 10-parameter transformation function parameters by using least squares. Points extracted from roof's apex.

6.3.1.2 Corners of roofs

Parameter	New orientation	
	Leica	Optech
	Panchromatic	Panchromatic
	36 points	35 points
	Value	Value
K	0.001145097	0.002025989
$\alpha_x(\text{rads})$	-0.004332053	-0.003070088
$\alpha_y(\text{rads})$	0.001628037	0.002075608
$\alpha_z(\text{rads})$	0.00359824	0.000998761
$\Delta X(\text{m})$	-17.92838956	23.66695414
$\Delta Y(\text{m})$	-21.82985861	-17.53408743
$\Delta Z(\text{m})$	-8.132333667	23.04648332
$X_o(\text{m})$	369390.822	369348.089
$Y_o(\text{m})$	6669869.863	6669868.112
$Z_o(\text{m})$	53.42347256	22.34600239

Table 11 10-parameter transformation function parameters by using least squares. Points extracted from roof's corners.

6.3.1.3 Apex and corners of roofs together

Parameter	New orientation	
	Leica	Optech
	Panchromatic	Panchromatic
	56 points	55 points
	Value	Value
K	0.001347069	0.002179287
$\alpha_x(\text{rads})$	-0.003033211	-0.001338909
$\alpha_y(\text{rads})$	0.002964032	0.00441476
$\alpha_z(\text{rads})$	2.54E-03	4.63E-04
$\Delta X(\text{m})$	-17.91721816	23.75263415
$\Delta Y(\text{m})$	-21.73953071	-17.59759218
$\Delta Z(\text{m})$	-7.960868071	23.33021666
$X_o(\text{m})$	369393.6685	369351.3267
$Y_o(\text{m})$	6669860.524	6669857.833
$Z_o(\text{m})$	54.06360021	22.85176516

Table 12 10-parameter transformation function parameters by using least squares. Points extracted from roof's apex and corners.

Residuals can be found in the appendix E.

6.4 LiDAR registered

Registration based on the transformation function using points from the apex of roofs.

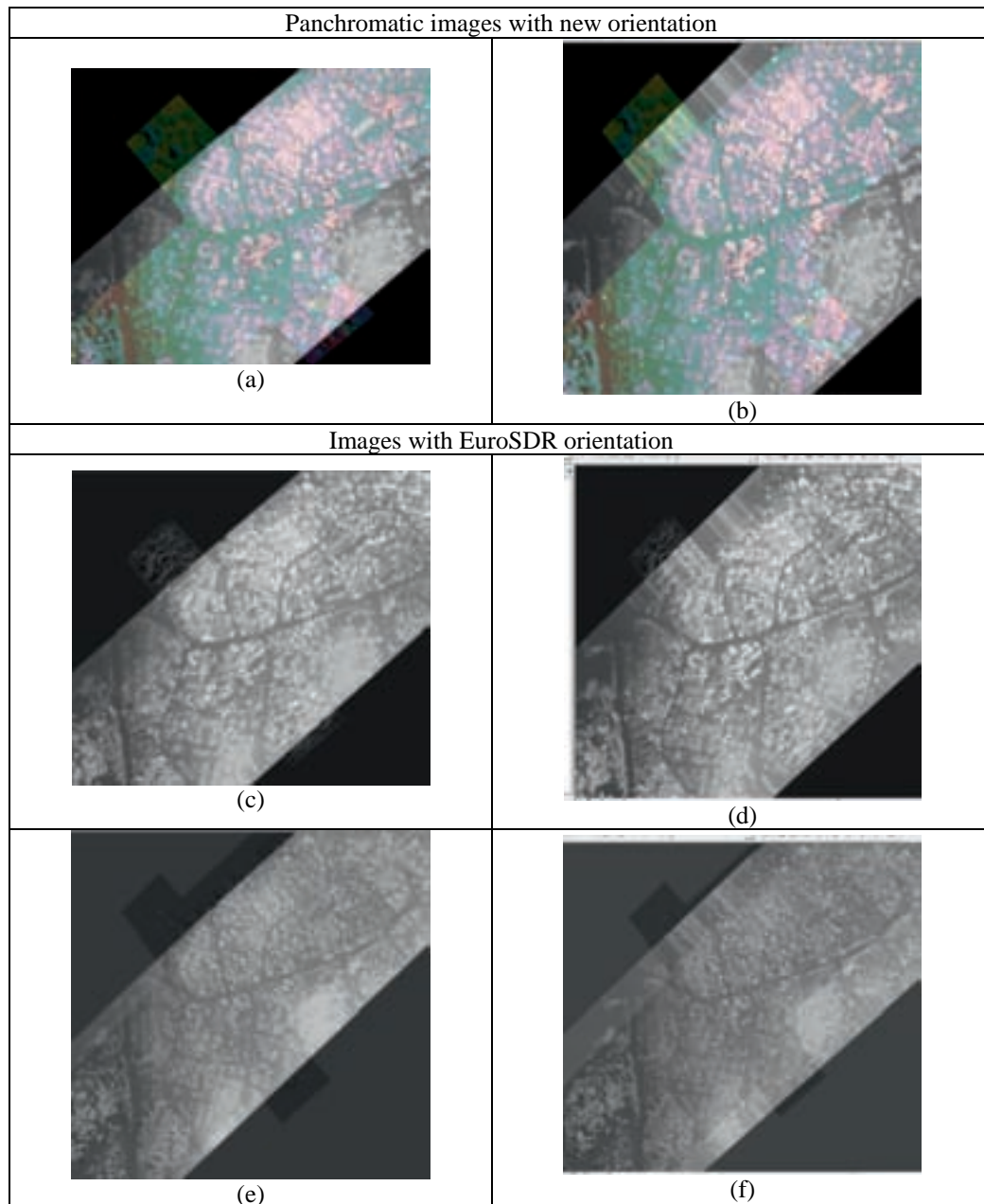


Figure 20 Overview of LiDAR data registered superimposed onto the DEM from the aerial images block. (a) Leica and Panchromatic DEM (new orientation). (b) Optech and Panchromatic DEM (new orientation). (c) Leica and Panchromatic DEM (EuroSDR orientation). (d) Optech and Panchromatic DEM (EuroSDR orientation). (e) Leica and multispectral DEM (EuroSDR orientation). (f) Optech and multispectral DEM (EuroSDR orientation).

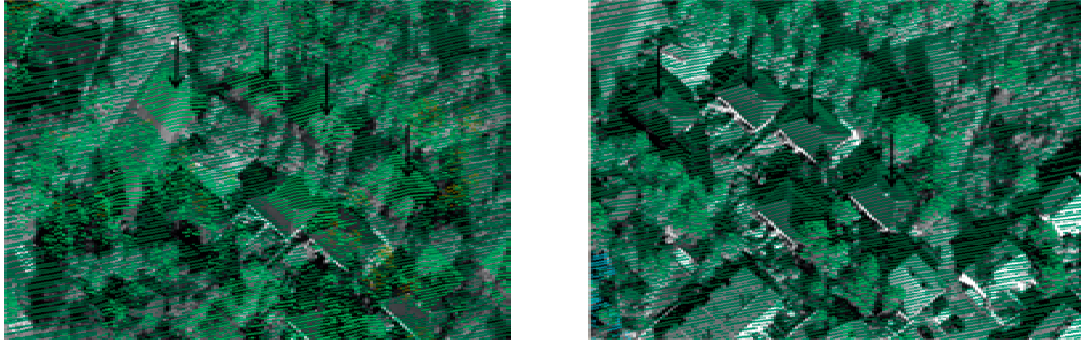


Figure 21 Leica dataset before (left) and after registration (right) based on panchromatic images (new orientation).

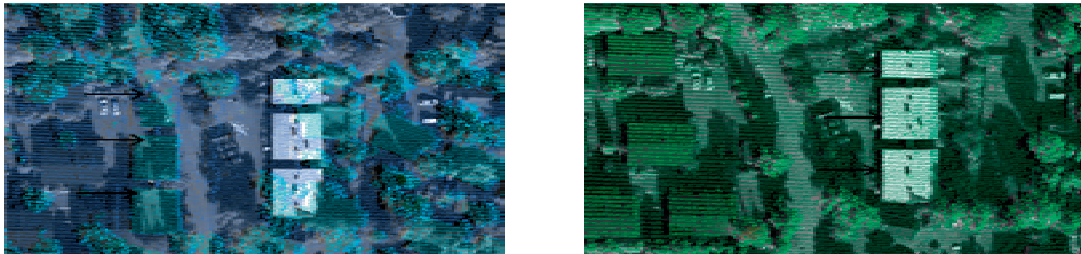


Figure 22 Optech dataset before (left) and after registration (right) based on panchromatic images (new orientation).

7 Analysis & Discussion

7.1 Extraction of features

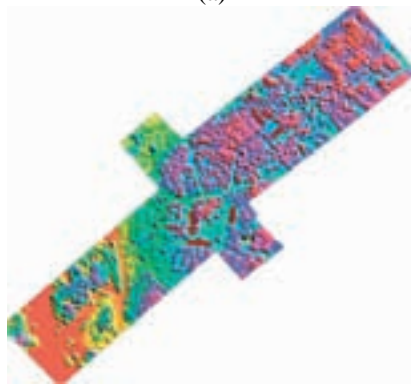
7.1.1 Block of images

7.1.1.1 Panchromatic images

In order to have a good distribution of points in the overlapping area of the images, buildings were selected from the top, centre and bottom of the mention area. However, buildings with flat roofs were rejected as only points from the edges were able to obtain (roof with no apex do not allow to get information inside the surface which is more reliable in LiDAR).



(a)



(b)

Figure 23 (a) Initial Extracted points. (b) Set of points for registration after rejecting flat roofs.

The extraction of points from the roof's apex was easier than the corners of the same roof, since the floating mark lay nicely on the top of the roof, but the corners of an inclined roof. However, the process of selecting the points from the images was quite simple, but for an inexperienced person it takes more time to get used to the tool and its modules as well as the extraction of features in an efficient way.

After the process of registration using the panchromatic images with a new orientation was carried out, it was found out that SocetSet 5.4.1 software when importing imagery with Earth - Oriented (EO) data the coordinates need to be in an Earth - Centered, Earth-Fixed (ECEF) coordinate system. Thus, the images had an excessive Y parallax. It is required to import the images into a LSR project to avoid this problem. Hence, a new project for the panchromatic images was created but only the points from the roof's apex were extracted due to time limitations, thus these points were using only to match the points extracted with TerraScan.

7.1.1.2 Multispectral Images

For the extraction of features on the multispectral images the process was much simpler since experience was acquired through the extraction of the panchromatic images.

7.1.2 LiDAR extraction

7.1.2.1 Apex of Roofs

As it was mentioned before laser scanning point clouds are more reliable inside surfaces, therefore methods that include extracting lines such as the intersection of a roof's plane are more accurate, since the line comes from the information of points inside the roof surface rather than methods based on object discontinuities such as corners or edges of buildings.

The lines extracted for this project (in order to obtain their end points), were selected in a semi-automated process using TerraScan. The process starts by classifying the LiDAR data which results in a good classification of the ground.

Since the main interest is to extract the roof's apex, the classification was focused on the ground class and the building class. However, it was necessary to make a vegetation classification since the area has an important presence of trees that in many cases were covering the roofs. Once the classification was done, the next step was to select the roof's planes. The planes are obtained by a construct planar surface tool which automatically defines the planes on a clicked roof, but these planes need to be adjusted manually since they usually do not intersect or provide the expected intersections. Automatic definition of planes was better from the Leica dataset than from the Optech dataset as well as the manual edition of them. The point density (Leica 4-5 points/m², Optech 2-3 points/m²) made a difference in the selection process and consequently the time.

The result polygons obtained were used to get the lines of the intersection and finally the end points. While the points were extracted, it was found that the Z value of end points of a line have the same values, which could have introduced a less accurate calculation of the Z values in the transformation to register the data.

7.1.2.2 Corners of roofs

Despite LiDAR data is less reliable on object discontinuities, it was performed this method by using a LiDAR tool from ArcGIS since the process is more automated for the identification of buildings. The first step was to create a raster file from the LiDAR dataset which in turn was used to generate a surface of the ground through a bare - Earth algorithm. The last result was used to extract the edges of the buildings. Having the edges of the buildings it was possible to extract the points where the edges intersect each other. The acquired Z coordinates for the four corners of a building had the same value.

Less accuracy using the corners of the roofs is expected since the extraction of features is based on a raster created from the LiDAR dataset instead of the original data which leads in a loss in precision (SHAN & TOTH, 2009: 312). The raster generated to extract the features is based on the density of points of the LiDAR, hence the better the density the better the raster resolution and so the values of the coordinates used to determine the transformation function.

The extraction of features required a considerable amount of time:

- To learn how to use software such as SocetSet, TerraScan and the ArcGIS LIDAR tool.
- To get the ability in editing and acquiring the data according to each software.

- To extract the points from the extracted linear features, since TerraScan and ArcGIS LIDAR tool output were polygons, by using ArcGIS to edit points' attributes in order to obtain the coordinates by means of spatial joins for example.

Hence, feature extraction is considered the most time consumed task of the registration process.

7.2 Transformation function

As it was shown in the results section, an initial calculation of the 3D transformation function based on 4 points were carried out where translations values had big values and thus difficult to interpret.

When the 7-parameters transformation is carry out over small areas the rotation (which is about the centre of the ellipsoid) around the coordinate system is similar to the translation, thus the translation values are so big in order to compensate the additional shift (ILIFFE & LOTT, 2008). In conclusion, 7-parameters transformation was not suitable for the registration of LiDAR data.

The alternative is to make the rotation about a location at the centre of the LiDAR points which results are easier to understand. The local coordinates of LiDAR data is the average of the X, Y and Z coordinates of the extracted LiDAR points (Table 3).

Parameter	Transformation		
	3-parameter	7-parameter	10-parameter
K		0.034334639	0.034333034
α (rads)		0.007279282	0.00728354
α y(rads)		0.018197921	0.018276006
α z(rads)		0.02085698	0.020857027
Δ X(m)	24.0496	-151775.9707	24.0496
Δ Y(m)	-18.05925	-221325.6352	-18.05925
Δ Z(m)	25.3914	41854.73438	25.3914
Xo(m)			369425.6628
Yo(m)			6670013.613
Zo(m)			22.90155

Table 13 10 – parameter transformation result values are the same that those obtained with the 3 and 7 parameter transformation. Xo, Yo and Zo are the local coordinates for LiDAR dataset.

According to the LiDAR sensors and flight specifications, the expected horizontal and vertical accuracies are:

- **OPTECH ALTM 3100 STRIP:** 0.5m horizontal accuracy and 0.15m vertical accuracy (SHAN & TOTH, 2009: 271)
- **LEICA ALS50 II STRIP:** 0.07m - 0.64m horizontal accuracy and 0.10m vertical accuracy (Leica, 2009)

7.2.1 Apex of Roofs

An initial set of 28 points were used to calculate the parameters of the transformation function for LiDAR data using the panchromatic images as reference, then the residuals were checked and it was found that some values particularly in Y were bigger than the rest of the residuals, hence the points with bigger values were revised. It was seen that the points mention before belonged to apexes made by the intersection of 4 planes where only 2 planes were used to extract the line (Figure 24), so it was decided not to use these points since they were no longer reliable.

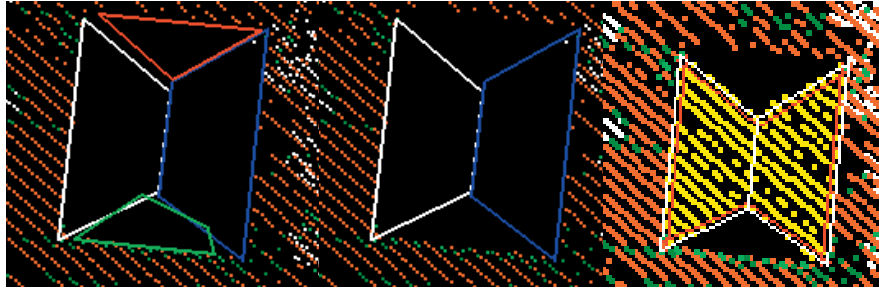


Figure 24 (Left) TerraScan Automatically generates 4 roof's planes (Centre) Only two planes were used to determine the apex (Right) Manually Edited planes.

With a final number of 20 points it was calculated again the transformation function based on the panchromatic and the multispectral images.

The RMSE of Leica dataset in X and Y using panchromatic images as reference show a good result based on the expected horizontal accuracy. On the other hand, the Z RMSE was good when using the panchromatic images with the exterior orientation provided by EuroSDR but when using the panchromatic images with the new orientation the RMSE was about 0.20m bigger. In the case of using the multispectral images as reference the Z value was higher than the expected vertical accuracy in about 0.30m.

The RMSE of Optech dataset show that only the expected vertical accuracy was not accomplished when using multispectral images as reference with a bigger value around 0.3m.

Parameter	New orientation		EuroSDR orientation			
	Leica	Optech	Leica		Optech	
	Panchromatic		Panchromatic	Multispectral	Panchromatic	Multispectral
	20 points	20 points	20 points	20 points	20 points	20 points
	Value (m)	Value(m)	Value(m)	Value(m)	Value(m)	Value(m)
RMSE X	0.08876131	0.06904741	0.090770618	0.173418046	0.07673329	0.159323239
RMSE Y	0.10765166	0.09577735	0.136482152	0.209435229	0.098360942	0.183062344
RMSE Z	0.32065186	0.35041377	0.109862636	0.429589874	0.138657026	0.442229966
stdv X	0.09106719	0.07084115	0.093128689	0.177923161	0.078726694	0.163462194
stdv Y	0.11044827	0.09826549	0.140027734	0.214876012	0.100916198	0.187818002
stdv Z	0.32898187	0.35951694	0.112716686	0.440749911	0.142259107	0.453718371

Table 14 RMSE and standard deviation values using points from the apex of buildings.

It can be seen that the RMSE of the new values (LiDAR transformed coordinates) for the extracted 20 points where points obtained from Optech dataset were more accurate in X and Y than those from Leica dataset (Table 4). Furthermore, the Z RMSE is bigger than the RMSE in X and Y. In conclusion, Optech has better Horizontal accuracy than Leica, whereas Leica has better vertical accuracy than Optech. A possible explanation can be that extraction of features from Optech data required more manual edition and attention than those from Leica since the initial planes obtained automatically looked to depict almost perfectly the roof surface (due to its better density), particularly in those areas where the roof only have two planes. Based on the above, one can think that even when the automatic selection of planes seem to be a good representation it is necessary to apply some manual edition as well.

The table above shows that the accuracy is better using panchromatic images as reference than using multispectral images, this is because the panchromatic images have better ground resolution (5 cm approximately).

Comparing the results of the points extracted from the panchromatic images with different orientations it can be seen the improvement on the accuracy of the Z value in about 20 cm using the orientation provided by EuroSDR while X and Y improvement was not that significant.

7.2.2 Corners of roofs

In this case the accuracy of the transformed points was better for Leica dataset than Optech, but none of them had the expected accuracy. Since none manual edition was done on the data, the selection of the features and its coordinates relied basically on the LiDAR's density to generate the raster file as well as the algorithm for rasterizing (SHAN & TOTH, 2009: 312).

Parameter	New orientation	
	Leica	Optech
	Panchromatic	Panchromatic
	36 points	35 points
	Value(m)	Value(m)
RMSE X	0.6848496	0.93174889
RMSE Y	0.650174977	1.157695875
RMSE Z	0.295125106	0.24884
stdv X	0.694564296	0.945351784
stdv Y	0.659397778	1.174597438
stdv Z	0.299311486	0.252472893

Table 15 RMSE and standard deviation values using points from the corners of roofs.

From the above, X and Y have more RMSE than Z and even more the Z RMSE is lower than the Z RMSE calculated from the apex of buildings (using TerraScan). One can say that this method of features extraction might determines better the Z value than the intersection of roof's plane method, but further analysis would be necessary to have a better understanding of this behave.

7.2.3 Apex and corners of roofs together

The approach of using the extracted points from the apex and the corner of roofs together shows better results than using only the corners and worse results than using the apex of roofs as it is shown below (Table 16).

Parameter	New orientation	
	Leica	Optech
	Panchromatic	Panchromatic
	56 points	55 points
	Value(m)	Value(m)
RMSE X	0.58604113	0.756088749
RMSE Y	0.562689179	0.93098111
RMSE Z	0.417431546	0.494939624
stdv X	0.591344778	0.763057456
stdv Y	0.567781492	0.939561763
stdv Z	0.421209284	0.499501376

Table 16 RMSE and standard deviation values using points from the apex and corners of roofs together.

In general, the translations on Leica and Optech data were as expected from the initial quality assessment (Table 6 and Table 7).

The process of calculating the parameters of the transformation function, the RMSE and standard deviation values and applying the transformation function to the whole LiDAR dataset was very fast and simple by creating and using a script (Appendix D).

7.3 LiDAR registered

Having in mind the previous analysis of the transformation function calculated with LiDAR points extracted in 2 different ways, it was decided to register the LiDAR data based on the points acquired from the roof's apex (intersection of roof's planes).

Once all the LiDAR data were registered using the 10 – parameter transformation function, DEMs were generated from Leica and Optech and from the images as well (as the features extracted for the registration belong to sloping roofs) in order to validate the registration outcome on a test area. It was not possible to overlay the DEM of the panchromatic block of images that have the new orientation with the LiDAR registered data since Socet Set 5.4.1 software does not give the proper projection to it because the data were not in a LSR project.

From the DEMs were generated several profiles which results show that Optech has a tendency to be higher than the panchromatic images, whereas Leica shows a tendency to be lower (Table 17), particularly comparing Optech to the multispectral images. Leica shows that fits better than Optech according to the profiles.

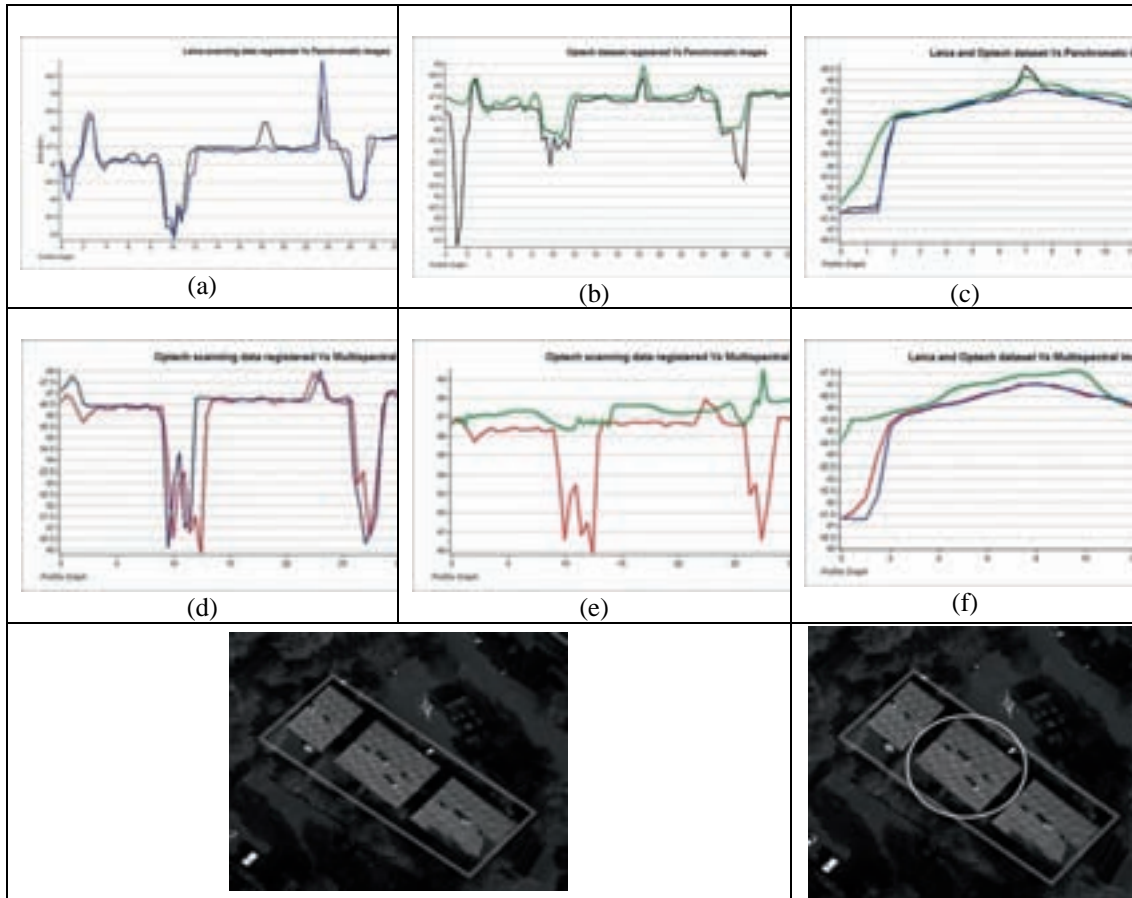


Table 17 Profiles of a test area. (a) and (b) represent the longitudinal profile of the Leica (blue) and Optech (green) comparing to the Panchromatic images. (c) Transversal profile of a house in the test area. (d) and (e) represent the longitudinal profile of the Leica (blue) and Optech (green) comparing to the Multispectral images. (f) Transversal profile of a house in the test area.

The DEMs also, allowed calculating the standard deviation between LiDAR and the images of the test area, which results are as follow:


	Panchromatic		Multispectral	
	Leica (m)	Optech(m)	Leica (m)	Optech (m)
Mean error	1.1830	1.1310	1.9571	1.9691
Mean standard deviation	1.7234	1.6438	2.2101	2.1608
				

Table 18 Mean standard deviation of a sample area calculated from DEMs.

According to the results above it is confirmed that Leica dataset have better vertical accuracy than Optech dataset using both panchromatic and multispectral images as reference. When the panchromatic images are used as reference it is achieved better vertical accuracy.

8 Conclusions & Future Work

Registered Optech laser data with a 2-3 points/m² point density shows a better horizontal accuracy than Leica laser data with a 4-5 points/m² using DMC panchromatic images as reference. However, Leica has better vertical accuracy than Optech.

it was found that density is an important characteristic when selecting and defining the planes that conform an apex, but no sufficient evidence in the quality of the registration was found since Optech (2-3 points/m²) has better horizontal accuracy than Leica (4-5 points/m²).

Leica registered dataset have a good horizontal accuracy using panchromatic images as reference. On the other hand, the vertical accuracy was good when using the panchromatic images with the exterior orientation provided by EuroSDR but when using the panchromatic images with the new orientation the RMSE was about 0.20m bigger.

In the case of using the multispectral images as reference to register Leica the Z value was higher than the expected vertical accuracy in about 0.30m.

Optech dataset show that only the expected vertical accuracy was not accomplished when using multispectral images as reference with a bigger value around 0.3m.

Registration of Optech laser data and Leica laser data show better accuracy when using panchromatic images as reference than multispectral images.

The registration performance did not exhibit a significant difference when processing the Leica and Optech dataset.

8.1 Features extraction

Feature extraction is considered the most time consumed task of the registration process as requires a considerable amount of time:

- To learn how to use software such SocetSet, TerraScan and the ArcGIS LIDAR tool.
- To get the ability in editing and acquiring the data according to each software.
- To extract the points from the extracted linear features (TerraScan and ArcGIS LIDAR tool output were polygons) by using ArcGIS to edit points' attributes in order to obtain the coordinates by means of spatial joins for example.

8.1.1 Images

Manual extraction makes the extracting features a long process and experience is required to be accurate and efficient in performing the task.

The extraction of points from the roof's apex was easier than the corners of the same roof, since the floating mark lay nicely on the top of the roof, but the corners of an inclined roof.

8.1.2 LiDAR dataset

8.1.2.1 Apex of Roofs

Automatic definition of planes was better from the Leica dataset than from the Optech dataset as well as the manual edition of them. The point density (Leica 4-5 points/m², Optech 2-3 points/m²) made a difference in the selection process and consequently the time.

It is expected that a better result of the registration would be obtained if the Z coordinate of the two end points of the apex extracted using TerraScan do not have the same value.

When extracting apex from the intersection of four planes it is important to use all of them to get a better definition of the line in the end points.

8.1.2.2 Corners of roofs

The method of corners extraction was less time consuming than the method extracting apexes, as the buildings detection was more automated and more features were able to extract.

The corner extraction method was not as accurate as the apex method since the extraction of features is based on a raster created from the LiDAR dataset instead of the original data leading a loss in precision (SHAN & TOTH, 2009: 312). The raster generated to extract the features is based on the density of points of the LiDAR, hence the better the density the better the raster resolution and so the values of the coordinates used to determine the transformation function.

Leica laser scanning registered dataset was more accurate than the Optech laser scanning registered dataset, thus when using this method the density will affect the accuracy of the registration.

The method of corners extraction exhibit lower altimetry values than those calculated from the apex extraction method (The transformation function using the extracted corners were based on the panchromatic images with the new orientation). One can say that this method of features extraction might determines better the Z value than the intersection of roof's plane method, but further analysis would be necessary to have a better understanding of this behave.

8.1.2.3 Apex and corners of roofs together

The approach of using the extracted points from the apex and the corner of roofs together shows better results than using only the corners and worse results than using the apex of roofs.

8.2 Transformation Function

When the 7-parameters transformation is carry out over small areas the rotation (which is about the centre of the ellipsoid) around the coordinate system is similar to the translation, thus the translation values are so big in order to compensate the additional shift (Illife, 2000: 98). In conclusion, 7-parameters transformation was not suitable for the registration of LiDAR data. The alternative is to make the rotation about a location at the centre of the LiDAR points which results are easier to understand by means of a 10-parameters transformation.

8.3 Automation

Automation of the registration process is not an easy task particularly when it comes to extraction of features. More than one software was necessary to use.

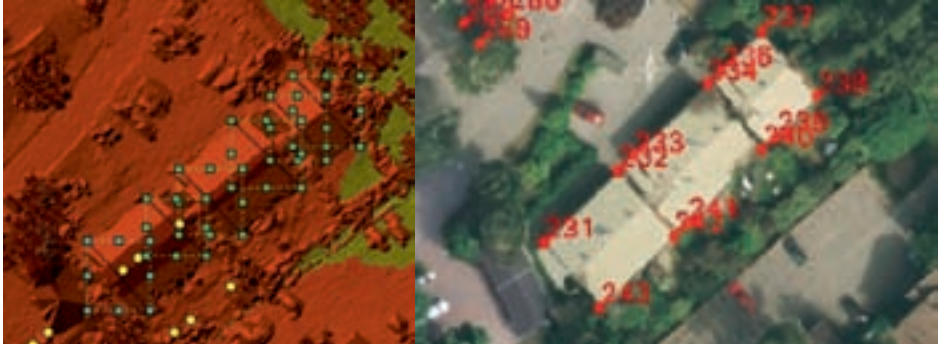
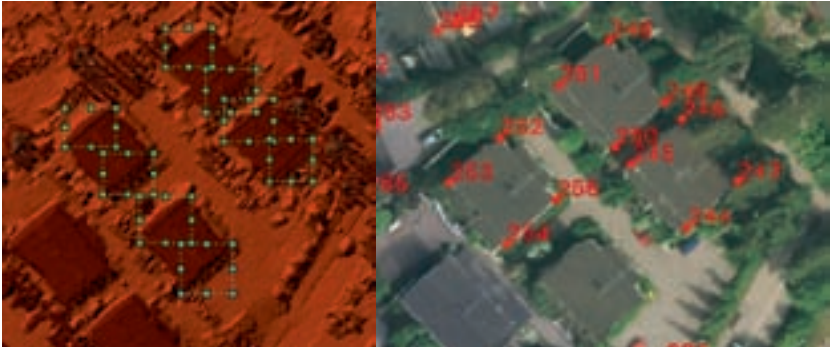
Future work will entail more automation when extracting features as well as more experiments on laser scanning point clouds with different point density in order to understand its influence on the registration.

References

- AREVALO, V., & GONZALEZ, J. (2007). An experimental evaluation of non-rigid registration techniques on Quickbird satellite imagery. *International Journal of Remote Sensing*, 29 (908567964), 513-527.
- BALTSAVIAS, E. (1999). A comparison between photogrammetry and laser scanning. *ISPRS Journal of Photogrammetry & Remote Sensing*, 54 (1), 83-94.
- DOWMAN, I. (2007). Map and Image Geometry Lecture 3 - 3D Mapping.
- GOTTESFELD, L. (1992). A Survey of Image Registration. *Computing*, (4).
- HABIB, A., MITISHITA, E., & GHANMA, M. (2004). Co-registration of photogrammetric and lidar data: methodology and case study.
- ILIFFE, J., & LOTT, R. (2008). *Datums And Map Projections: For Remote Sensing, Gis And Surveying* (2nd.). CRC Press.
- JACOBSEN, K. (2009). Photogrammetric engineering & remote sensing.
- MITISHITA, E., HABIB, & MACHADO, A. (1999). Photogrammetric model orientation using lidar dataset. *Archives*.

- POSTOLOV, Y., KRUPNIK, A., & MCINTOSH, K. (1999). Registration of airborne laser data to surfaces generated by photogrammetric means. *Image (Rochester, N.Y.)*.
- REMONDINO, F. (2005). Photogrammetry for natural and cultural heritage site documentation, mapping and visualization. *Terrain*, 1-43.
- RICHARDS, J. A., & JIA, X. (2006). *Remote sensing digital image analysis* (4 ed.).
- Roux, M., & Pierrot-deseilligny, M. (2009). Matching Topographic Surfaces: Application to lidar and photogrammetric surfaces.
- RÖNNHOLM, P., HONKAVAARA, E., LITKEY, P., HYYPPÄ, H., & HYYPPÄ, J. (2007). Integration of laser scanning and photogrammetry. *Scanning*, XXXVI, 355-362.
- RÖNNHOLM, P., HONKAVAARA, E., ERVING, A., NUIKKA, M., HAGGRÉN, H., KAASALAINEN, S., HYYPPÄ, H. & HYYPPÄ, J. (2008a). Registration of airborne laser scanning point clouds with aerial images through terrestrial image blocks.
- RÖNNHOLM, P., KAARTINEN, H., NURMINEN, K., HONKAVAARA, E., AHOKAS, E., MARKELIN, L., et al. (2008b). Registration Quality, Towards Integration of Laser Scanning and Photogrammetry. *Data Processing*, 1-11.
- SHAN, J., & TOTH, C. (2009). *Topographic Laser Ranging and Scanning: Principles and Processing*. United States of America: CRC Press.
- WONG, A., & CLAUSI, D. A. (2007). ARRSI: Automatic Registration of Remote-Sensing Images, 45 (5), 1483-1493.
- WONG, A., & ORCHARD, J. (2008). Efficient FFT-Accelerated Approach to Invariant Optical-LIDAR Registration, 46 (11), 3917-3925.

Appendix A Initial quality assessment

LEICA	
Profile	Height
<div>  </div> <div>GCP 231- 243</div>	
GCP <div> Z236 = 46.024 Z237= 45.9742 Z238 = 46.0323 Z239 = 46.0436 Z233= 46.3552 Z234 = 46.2207 Z240= 46.2400 Z241 = 46.2863 Z231=46.6117 Z232= 46.6266 Z242= 46.6187 Z243= 46.6484 </div>	Z values of the TIN according to the Profile are: <div> Z236 = 52.1994 Z237= 52.1140 Z238 = 52.2655 Z239 = 52.2133 Z233=52.4474 Z 234=52.3499 Z240=52.4519 Z241=52.6300 Z231=52.7254 Z232=52.7396 Z242=53.0647 Z243=52.9258 </div>
Profile	Height
<div>  </div> <div>GCP 244- 255</div>	


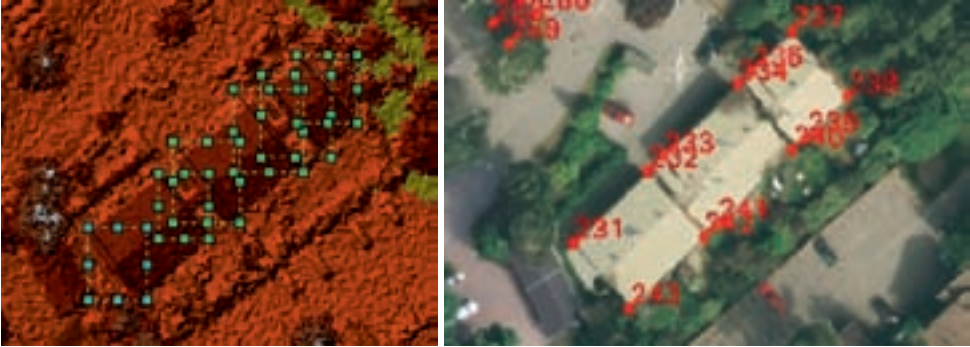
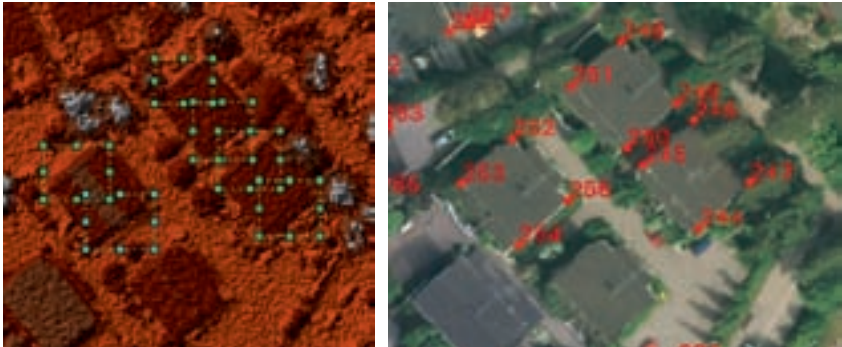
<p>GCP</p> <p>Z244 = 48.3252</p> <p>Z245= 48.3032</p> <p>Z246 = 48.2882</p> <p>Z247 = 48.2552</p> <p>Z248= 48.282</p> <p>Z249 = 48.3059</p> <p>Z250= 48.2748</p> <p>Z251 = 48.2962</p> <p>Z252=49.9965</p> <p>Z253= 49.9859</p> <p>Z254= 50.0035</p> <p>Z255= 50.0269</p>	<p>Z values of the TIN according to the Profile are:</p> <p>Z244 = 55.1715</p> <p>Z245= 54.4426</p> <p>Z246 = 54.3448</p> <p>Z247 = 54.4625</p> <p>Z248=54.4216</p> <p>Z 249=54.3755</p> <p>Z250=54.6904</p> <p>Z251=54.5221</p> <p>Z252= 56.1734</p> <p>Z253=56.3138</p> <p>Z254=56.267</p> <p>Z255=56.6919</p>
Profile	Height
 <p style="text-align: center;">GCP 256- 262</p>	
<p>GCP</p> <p>Z256=46.2124</p> <p>Z257= 46.2313</p> <p>Z259= 46.2566</p> <p>Z258=46.2291</p> <p>Z260= 46.2387</p> <p>Z261= 46.2165</p> <p>Z262= 56.2392</p>	<p>Z values of the TIN according to the Profile are:</p> <p>Z256= 52.123</p> <p>Z257=52.1559</p> <p>Z259=52.2165</p> <p>Z258= 51.9558</p> <p>Z260= 52.1928</p> <p>Z261= 52.2588</p> <p>Z262= 52.1155</p>

Figure 25 Z values of Leica Vs GCPs provided by EuroSDR.

OPTECH	
Profile	Height
 <p style="text-align: center;">GCP 231- 243</p>	
<p>GCP</p> <p>Z236 = 46.024</p> <p>Z237= 45.9742</p> <p>Z238 = 46.0323</p> <p>Z239 = 46.0436</p> <p>Z233= 46.3552</p> <p>Z234 = 46.2207</p> <p>Z240= 46.2400</p> <p>Z241 = 46.2863</p> <p>Z231=46.6117</p> <p>Z232= 46.6266</p> <p>Z242= 46.6187</p> <p>Z243= 46.6484</p>	<p>Z values of the TIN according to the Profile are:</p> <p>Z236 = 20.7654</p> <p>Z237= 20.7476</p> <p>Z238 = 20.6513</p> <p>Z239 = 20.72</p> <p>Z233=20.894</p> <p>Z 234=21.1028</p> <p>Z240=20.9823</p> <p>Z241=21.1499</p> <p>Z231=21.2322</p> <p>Z232=21.3163</p> <p>Z242=21.2473</p> <p>Z243=21.3656</p>
Profile	Height
 <p style="text-align: center;">GCP 244- 255</p>	

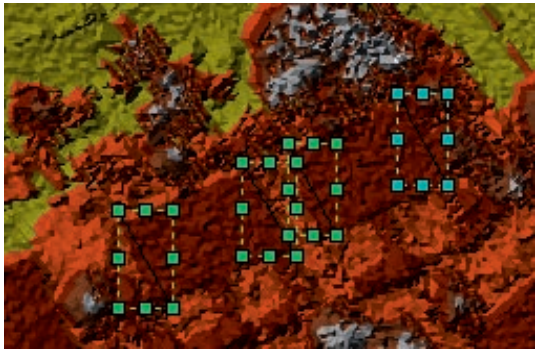

<p>GCP</p> <p>Z244 = 48.3252</p> <p>Z245= 48.3032</p> <p>Z246 = 48.2882</p> <p>Z247 = 48.2552</p> <p>Z248= 48.282</p> <p>Z249 = 48.3059</p> <p>Z250= 48.2748</p> <p>Z251 = 48.2962</p> <p>Z252=49.9965</p> <p>Z253= 49.9859</p> <p>Z254= 50.0035</p> <p>Z255= 50.0269</p>	<p>Z values of the TIN according to the Profile are:</p> <p>Z244 = 22.992</p> <p>Z245= 22.9493</p> <p>Z246 = 23.0808</p> <p>Z247 = 22.5841</p> <p>Z248=23.0774</p> <p>Z 249=23.1042</p> <p>Z250=23.1413</p> <p>Z251=23.0055</p> <p>Z252= 24.7278</p> <p>Z253=24.7444</p> <p>Z254=24.8715</p> <p>Z255=24.7263</p>
Profile	Height
	
	
<p style="text-align: center;">GCP 256- 262</p> <p>GCP</p> <p>Z256=46.2124</p> <p>Z257= 46.2313</p> <p>Z259= 46.2566</p> <p>Z258=46.2291</p> <p>Z260= 46.2387</p> <p>Z261= 46.2165</p> <p>Z262= 56.2392</p>	
<p>Z values of the TIN according to the Profile are:</p> <p>Z256= 20.7313</p> <p>Z257=20.6849</p> <p>Z259=20.8347</p> <p>Z258= 20.2836</p> <p>Z260= 20.6417</p> <p>Z261= 20.8461</p> <p>Z262= 20.6103</p>	

Figure 26 Z values of Optech Vs GCPs provided by EuroSDR.

Appendix B Socet set extracted points

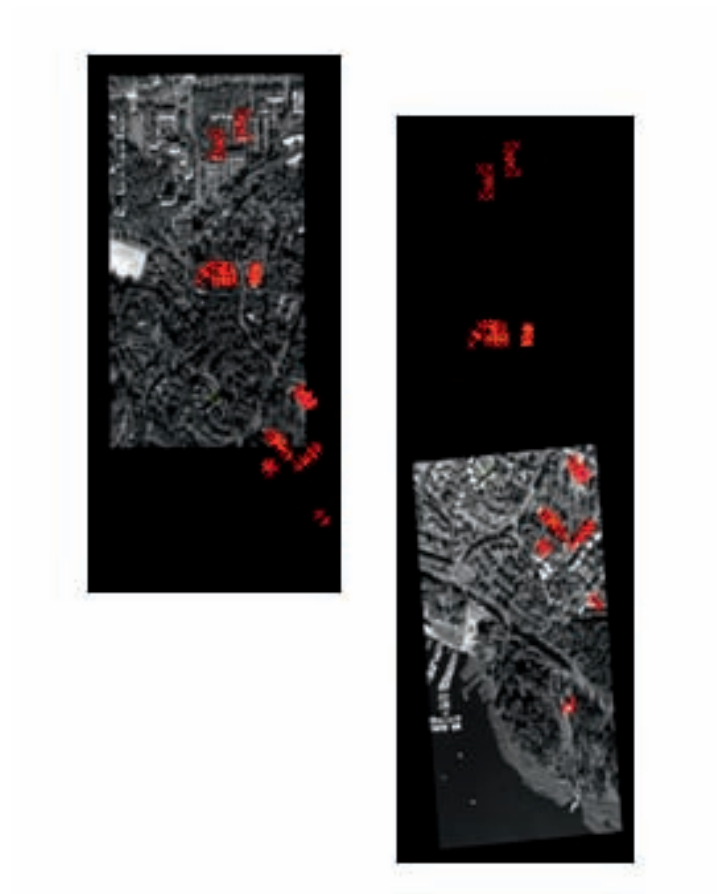


Figure 27 Distribution of the extracted points from the panchromatic images.

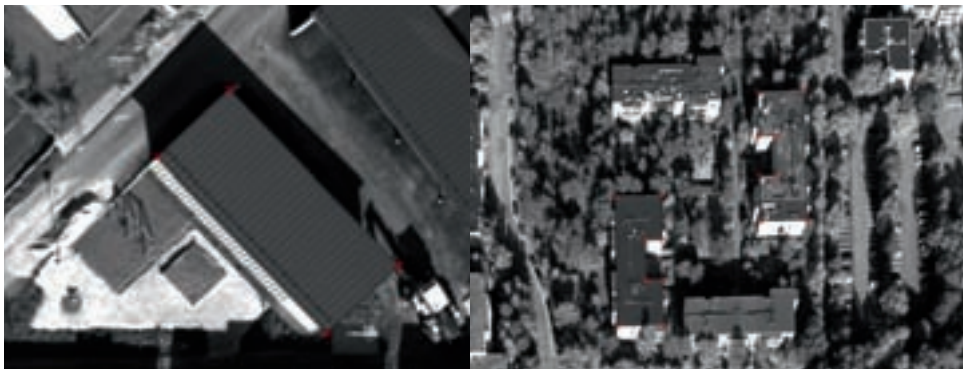


Figure 28 Points that were rejected because of their flat roof.

Appendix C Apex of roofs using TerraScan

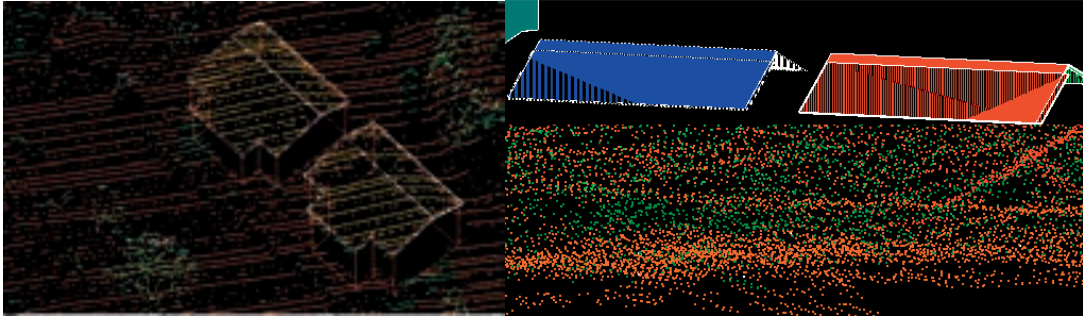


Figure 29 Example of roof plane's intersection using TerraScan.

Appendix D Matlab script

```
data(:,1) = [];

size_data = size(data);
n_points = size_data(1);
n_columns = size_data(2);
%build vector source
bSource = zeros(n_points * 3, 1);
bTarget = zeros(n_points * 3, 1);

iterator = 0;
for i=1:n_points
    for j=1:3
        iterator = iterator + 1;
        bSource(iterator,1) = data(i,j);
        bTarget(iterator,1) = data(i,j+3);
    end
end

b = bTarget - bSource;

localOrigin = mean (data);

matrixA = zeros(n_points * 3, 7);

%build matrix A
i = 1;
while i < (n_points*3)
    matrixA(i,1) = bSource(i,1) - localOrigin(1,1);
    matrixA(i,3) = localOrigin(1,3) - bSource(i+2,1);
    matrixA(i,4) = bSource(i+1,1) - localOrigin(1,2);
    matrixA(i,5) = 1;
    i = i + 3;
end

i = 2;
while i < (n_points*3)
    matrixA(i,1) = bSource(i,1) - localOrigin(1,2);
    matrixA(i,2) = bSource(i+1,1) - localOrigin(1,3);
    matrixA(i,4) = localOrigin(1,1) - bSource(i-1,1);
    matrixA(i,6) = 1;
    i = i + 3;
end

i = 3;
while i <= (n_points*3)
    matrixA(i,1) = bSource(i,1) - localOrigin(1,3);
    matrixA(i,2) = localOrigin(1,2) - bSource(i-1,1);
    matrixA(i,3) = bSource(i-2,1) - localOrigin(1,1);
    matrixA(i,7) = 1;
```



```

        i = i + 3;
    end

    matrixAT = matrixA';

    ATA = matrixAT*matrixA;
    ATAInv = minv(ATA);

    ATb = matrixAT*b;

    X = ATAInv * ATb;

    %build transformed values matrix
    R=zeros(3, 3);
    R(1,1)=1;
    R(1,2)=X(4,1);
    R(1,3)=0-X(3,1);

    R(2,1)=0-X(4,1);
    R(2,2)=1;
    R(2,3)=X(2,1);

    R(3,1)=X(3,1);
    R(3,2)=0-X(2,1);
    R(3,3)=1;

    Scale=1+X(1,1);

    New_data=zeros(n_points * 3, 1);

    i=1;

    while i <= (n_points*3)

        RbSource=R*(bSource(i:i+2,1)-localOrigin(1,1:3)');
        SRbSource=Scale* RbSource;
        New_data(i:i+2,1)=SRbSource+localOrigin(1,1:3)'+X(5:7,1);
        i=i+3;
    end

    newX = zeros(n_points, 1);
    newY = zeros(n_points, 1);
    newZ = zeros(n_points, 1);
    i=1;
    j=1;
    while i <= (n_points*3)
        newX(j) = New_data(i,1);
        newY(j) = New_data(i+1,1);
        newZ(j) = New_data(i+2,1);
        j=j+1;
        i=i+3;
    end
end

```

```

%build Residuals
v = bTarget - New_data;

vX = zeros(n_points, 1);
vY = zeros(n_points, 1);
vZ = zeros(n_points, 1);
i=1; j=1;
while i <= (n_points*3)
    vX(j) = v(i,1);
    vY(j) = v(i+1,1);
    vZ(j) = v(i+2,1);
    j=j+1;
    i=i+3;
end
%calculate standard deviation and RMSE values
stdvX=std(vX);
stdvY=std(vY);
stdvZ=std(vZ);

rmseX = rmse(newX,data(:,4));
rmseY = rmse(newY,data(:,5));
rmseZ = rmse(newZ,data(:,6));

calcddata=zeros(n_points, 4);
calcddata(:,2) = newX;
calcddata(:,3) = newY;
calcddata(:,4) = newZ;
%transformation of whole LiDAR dataset
size_lidar = size(points);
n_pointslidar = size_lidar(1);
n_columnslidar = size_lidar(2);

pointsTra = zeros(n_pointslidar, 3);

i=1;

while i <= (n_pointslidar)

    RbSourceLidar=R*(points(i,1:3)'+localOrigin(1,1:3)');
    SRbSourceLidar=Scale* RbSourceLidar;
    pointsTra(i,1:3)=SRbSourceLidar+localOrigin(1,1:3)'+X(5:7,1);
    pointsTra(i,4) = points (i,4);
    i=i+1;
end

```

Appendix E Values of Extracted Points

Point_Leica_ID	Xs	Ys	Zs	Xt	Yt	Zt
1	369463.292	6670022.61	55.9441	369445.742	6670001.23	48.967
2	369471.923	6670012.14	55.9441	369454.282	6669990.83	48.967
3	369433.475	6670021.11	57.6463	369415.868	6669999.65	50.523
4	369442.165	6670010.61	57.6463	369424.485	6669989.27	50.594
5	369447.342	6670004.27	57.1524	369429.767	6669982.84	50.11
6	369456.004	6669993.81	57.1524	369438.351	6669972.43	49.946
7	369503.805	6669975.56	53.4835	369486.08	6669954.16	46.637
8	369498.062	6669970.82	53.4835	369480.459	6669949.52	46.637
9	369495.956	6669969.07	53.7967	369478.248	6669947.67	47.014
10	369485.219	6669960.27	53.7967	369467.7	6669938.98	46.849
11	369381.561	6669755.65	55.9184	369363.439	6669733.98	47.389
12	369379.738	6669740.3	55.9184	369361.703	6669718.73	47.275
13	369379.24	6669736.27	55.9757	369361.159	6669714.63	47.372
14	369377.427	6669720.95	55.9757	369359.488	6669699.38	47.189
15	369316.315	6669660.74	54.1296	369298.045	6669638.93	45.874
16	369304.824	6669662.38	54.1296	369286.734	6669640.45	46.026
17	369302.57	6669662.69	54.1254	369284.162	6669640.8	46.019
18	369291.101	6669664.29	54.1254	369272.886	6669642.39	46.032
19	369279.755	6669663.93	53.9862	369261.436	6669642.02	45.926
20	369266.071	6669666.77	53.9862	369247.869	6669644.83	45.926
21	369272.104	6669696.35	52.6928	369253.842	6669674.36	44.541
22	369272.744	6669702.19	52.6928	369254.496	6669680.92	44.539
23	369276.049	6669721.18	51.7919	369257.786	6669698.87	43.454
24	369276.656	6669727	51.7919	369258.519	6669705.5	43.454
25	369274.148	6669738.37	51.4837	369255.854	6669716.01	43.337
26	369274.798	6669744.4	51.4837	369256.527	6669722.62	43.337
27	369234.903	6669701.49	52.7813	369216.55	6669679.74	44.613
28	369219.876	6669703.85	52.7813	369201.677	6669682.1	44.734

Table 19 Xs, Ys and Zs are the coordinates of the source dataset which in this case is LiDAR whereas Xt, Yt and Zt are the coordinates of the corresponding points in the target coordinate system which in this case is the images block's ground coordinate system with the new orientation (ETRS89 / ETRS-TM35FIN) .Blue shaded cells are the points that were removed after cheking the residuals.

X	Y	Z
0.101963094	-0.07269465	-0.06714767
0.001840877	0.02985048	-0.01045175
0.10266907	-0.16146144	-0.2387132
0.019876835	-0.01071475	-0.11081319
0.119053238	-0.08588733	-0.06570736
0.031993194	-0.01269777	-0.17302022
-0.116745762	0.02287258	0.32466587
0.018719041	0.12463801	0.3409419
-0.08090514	0.0248472	0.41013746
0.135222409	0.13942056	0.27528159
-0.1317121	0.10490378	-0.46756116
-0.031577527	0.2324111	-0.51253445
-0.073649513	0.17037616	-0.45480961
0.08203439	0.26162698	-0.56894742
-0.087482331	0.09253092	0.1840146
0.113506108	-0.02718951	0.31730456
-0.200588585	0.00317638	0.31088903
0.0135089	-0.01434599	0.30535134
-0.068097851	-0.0386111	0.32942659
0.072938279	-0.08621903	0.30300838
-0.016919892	-0.19083367	0.08335377
-0.007502928	0.52496812	0.05505536
-0.040397716	-0.55640935	-0.21168215
0.079213609	0.24009595	-0.23792851
-0.080061185	-0.6504918	-0.10102844
-0.061563454	-0.07716154	-0.12819244
-0.038359502	0.01184563	0.00678967
0.143024444	0.00115412	0.10231745

Table 20 Leica residuals of 28 points extracted using TerraScan. Blue shaded cells are the points that were removed after checking the residuals.

X	Y	Z
-0.06711046	0.15684597	-0.13022599
0.05539662	-0.0572753	-0.07725976
0.01458146	-0.03297877	-0.25742328
0.0549708	-0.14929599	-0.13291261
-0.03467161	0.20521475	-0.09790703
0.04647302	-0.09692439	-0.2091043
-0.04122677	-0.01176938	0.40208495
-0.05728453	-0.07575365	0.41354584
0.12096808	0.08526198	0.47366639
0.05017422	-0.12930873	0.32976357
-0.12314708	0.00472384	-0.49378631
-0.04269897	0.07245788	-0.54715809
-0.1207383	0.07283478	-0.47997493
-0.0124632	0.02953464	-0.60276011
0.12570003	-0.03184121	0.19525755
0.05009917	-0.12612277	0.32580899
0.0358526	-0.09391486	0.29572375
-0.03631824	-0.11453493	0.2873341
0.05125085	-0.13700135	0.32793711
-0.0275019	-0.10934623	0.29873908
-0.00961847	-0.11026937	0.06413314
-0.08016558	0.14736374	0.03714616
0.06209508	0.43768497	-0.19464685
0.12447121	1.14306656	-0.21812175
-0.22927316	-0.95410916	-0.08856251
-0.12996522	0.22171879	-0.11016632
-0.00043132	-0.07219564	0.0491338
0.22058167	-0.27406617	0.13973541

Table 21 Residuals Optech with 28 points extracted using TerraScan. Blue shaded cells are the points that were removed after checking the residuals.

Optech			Leica			Panchromatic images			Multispectral images		
Xs	Ys	Zs	Xs	Ys	Zs	Xt	Yt	Zt	Xt	Yt	Zt
369421.814	6670018.35	24.634	369463.292	6670022.61	55.9441	369445.364	6670000.59	49.625	369445.339	6670000.57	48.139
369430.211	6670008.19	24.634	369471.923	6670012.14	55.9441	369453.907	6669990.35	49.520	369453.776	6669990.69	47.823
369391.921	6670016.98	26.2799	369433.475	6670021.11	57.6463	369415.486	6669999.15	51.484	369415.436	6669999.06	50.498
369400.476	6670006.73	26.2799	369442.165	6670010.61	57.6463	369424.160	6669988.75	51.461	369424.123	6669988.74	50.498
369405.835	6669999.97	25.7969	369447.342	6670004.27	57.1524	369429.354	6669982.26	50.889	369429.504	6669982.28	50.972
369414.317	6669989.87	25.7969	369456.004	6669993.81	57.1524	369437.897	6669972.02	50.879	369438.059	6669972.13	50.972
369462.03	6669971.54	22.0234	369503.805	6669975.56	53.4835	369485.653	6669953.64	47.478	369485.528	6669953.72	47.029
369456.436	6669966.97	22.0234	369498.062	6669970.82	53.4835	369480.105	6669949.08	47.376	369480.131	6669949.07	46.88
369454.051	6669964.97	22.3447	369495.956	6669969.07	53.7967	369477.806	6669947.19	47.612	369477.592	6669947.18	46.984
369443.595	6669956.51	22.3447	369485.219	6669960.27	53.7967	369467.270	6669938.60	47.622	369467.476	6669938.44	47.075
369339.675	6669751.86	24.4106	369381.561	6669755.65	55.9184	369363.592	6669734.18	49.403	369363.467	6669734.36	49.147
369337.858	6669736.57	24.4106	369379.738	6669740.3	55.9184	369361.531	6669719.04	49.700	369361.498	6669719.52	49.147
369337.392	6669732.48	24.4566	369379.24	6669736.27	55.9757	369361.096	6669714.73	49.758	369360.884	6669714.7	49.576
369335.613	6669717.3	24.4566	369377.427	6669720.95	55.9757	369359.276	6669699.59	49.767	369359.139	6669699.98	49.576
369274.152	6669657.06	22.5152	369316.315	6669660.74	54.1296	369298.042	6669639.18	47.953	369298.225	6669639.47	47.491
369262.942	6669658.67	22.5152	369304.824	6669662.38	54.1296	369286.753	6669640.75	47.988	369287.025	6669641.09	47.491
369260.389	6669658.99	22.5336	369302.57	6669662.69	54.1254	369284.259	6669641.16	47.849	369284.571	6669641.41	47.133
369249.21	6669660.6	22.5336	369291.101	6669664.29	54.1254	369272.933	6669642.70	47.985	369273.099	6669642.93	47.139
369237.697	6669660.25	22.3736	369279.755	6669663.93	53.9862	369261.468	6669642.34	47.888	369261.716	6669642.81	47.228
369224.239	6669663.03	22.3736	369266.071	6669666.77	53.9862	369248.052	6669645.17	47.834	369248.456	6669645.48	47.228

Table 22 Values of points extracted from the images using the EuroSDR exterior orientation related with the extracted points with TerraScan.

Extracted points using ArcGIS LiDAR tool											
Panchromatic						Multispectral					
Residuals leica 36 puntos			Residuals optech 35 points			Residuals Leica 29 points			Residuals optech 30 points		
X	Y	Z	X	Y	Z	X	Y	Z	X	Y	Z
-0.335	0.335	-0.196	-0.152	1.149	-0.021	-0.457	0.243	-0.226	-0.196	1.187	-0.022
0.289	0.550	-0.197	1.075	0.952	-0.028	0.531	-0.869	-0.346	-0.529	-1.085	-0.033
-0.122	-0.897	-0.138	-0.501	-1.404	0.017	1.116	-0.695	0.068	0.468	-1.652	0.314
0.650	-0.769	-0.330	0.874	-1.688	-0.181	-0.663	-0.050	-0.061	-0.284	1.281	-0.316
0.792	0.982	-0.047	-0.379	1.280	0.049	0.170	-0.249	0.704	0.734	0.999	-0.508
1.235	-0.593	0.081	1.012	0.970	0.178	0.125	-0.147	0.706	0.497	-0.181	-0.520
-1.190	-0.326	0.037	-0.778	-0.268	0.119	-1.933	1.643	-0.466	-0.395	0.761	-0.530
-0.733	-1.848	0.018	0.628	-0.525	0.101	0.535	0.748	-0.521	-1.392	-1.203	0.729
0.100	0.481	-0.118	-0.387	0.864	0.045	-0.413	-0.684	-0.445	0.793	1.573	-0.210
-0.532	0.067	-0.057	-1.206	-0.991	0.084	-0.439	-0.364	0.081	0.665	0.940	0.498
0.304	-0.123	0.697	0.277	-1.202	0.422	0.827	0.194	-0.041	0.145	-1.046	0.486
0.254	-0.018	0.688	0.501	1.889	-0.519	-0.249	-0.642	-0.318	-0.208	-0.838	-0.596
-0.132	0.083	0.502	1.023	1.659	-0.491	-0.378	0.108	-0.534	0.878	0.356	-1.537
-1.856	1.751	-0.521	0.299	-0.658	-0.516	0.540	-0.757	0.130	0.785	-1.149	-0.663
0.608	0.858	-0.583	-0.090	-1.239	-0.008	1.206	-0.038	0.067	-0.944	0.080	-0.421
-0.337	-0.568	-0.513	1.265	-0.086	-0.124	0.160	0.357	-0.003	0.610	-1.651	0.066
-0.437	-0.380	0.108	0.976	-1.535	-0.083	-0.239	-0.117	0.090	1.282	-0.607	1.726
0.825	0.175	-0.016	-1.200	-0.009	-0.274	0.048	-0.225	-0.075	-1.146	0.989	1.613
-0.250	-0.651	-0.306	0.778	-1.956	0.073	0.475	-0.455	-0.104	-1.557	0.127	0.112
-0.377	0.093	-0.511	1.326	-0.605	0.014	-0.491	-0.129	-0.146	0.003	-1.448	0.271
0.555	-0.770	0.163	-1.162	1.065	-0.028	-0.902	0.269	-0.137	0.911	-0.370	0.652
1.215	-0.053	0.097	-1.678	-0.230	0.059	-1.147	-0.007	0.055	-0.371	1.151	0.698
0.172	0.337	0.038	0.008	-1.521	-0.146	0.293	-0.104	0.028	-1.661	0.137	0.320
-0.222	-0.136	0.133	1.101	-0.345	-0.166	-0.035	0.047	0.232	-1.212	-0.903	0.150
0.057	-0.228	-0.061	-0.573	1.338	-0.178	0.309	-0.201	0.345	-0.520	-1.229	-0.183
0.480	-0.460	-0.092	-1.732	0.256	-0.179	0.144	1.405	0.293	1.071	0.501	-0.420
-0.484	-0.140	-0.123	-1.580	-0.703	0.306	-0.740	0.605	0.057	0.367	0.880	0.113
-0.890	0.260	-0.113	-0.713	-1.220	0.397	1.096	-0.082	0.252	0.912	-0.564	-0.173
-1.162	0.009	0.021	1.037	0.665	0.350	0.511	0.196	0.316	0.624	0.970	-0.128
0.276	-0.090	-0.006	0.132	1.262	0.142				-0.330	1.994	-1.487
-0.039	0.062	0.213	0.986	-0.368	0.247						
0.303	-0.182	0.317	0.523	1.341	0.337						
0.132	1.423	0.260	-1.587	0.460	0.442						
-0.751	0.618	0.034	0.049	-1.072	-0.343						
1.092	-0.062	0.225	-0.152	2.477	-0.097						
0.509	0.211	0.297									

Table 23 Residuals from points extracted with ArcGIS LiDAR tool using the new orientation.

Appendix F Registered LiDAR



Figure 30 Overview Optech registered based on panchromatic images.



Figure 31 Overview Leica registered based on panchromatic images.

Report of the Institute for Photogrammetry, University of Stuttgart

EuroSDR "Registration Quality – Towards Integration of Laser Scanning and Photogrammetry"

Jan Böhm, Institute for Photogrammetry, jan.boehm@ifp.uni-stuttgart.de



Method A

In this approach the registration is based on the registration of point clouds using the iterative closest point algorithm (ICP) [1]. While the point cloud for the LiDAR data is naturally given, the point cloud from images has to be produced as a first step. We used the orientation of the images as provided; no further processing was done. We used MatchT for the generation of a dense grid of points. To avoid outliers and points in noisy areas (vegetation, etc.) only reliable points were used. Filtering was done by MatchT (standard Grid_OK points).

For the computation of ICP we used Polyworks. For initialization 3 corresponding points have to be (coarsely) picked in both point clouds. After this initialization, iterative registration is computed automatically. As a result the transformation matrix is reported along with internal accuracy parameters. An example of the accuracy information is given in Figure 11. Figure 2 shows the deviation of LiDAR DSM versus the DSM from aerial images. Hotspots have deviations of up to 25 cm.

The method is somewhat similar to the strategy suggested in [2] for video streams. We have previously used ICP to align terrestrial LiDAR data to aerial LiDAR data [3] (where a similar discrepancy in scale exists) and were able to achieve accuracies at the decimetre level.

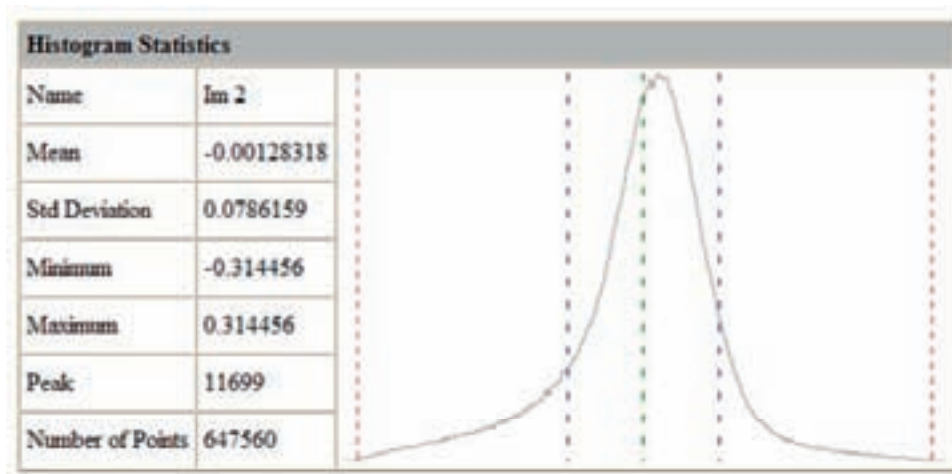


Figure 1: Example for internal accuracy information of the ICP processing. The numbers indicate a very good alignment of the two point clouds.

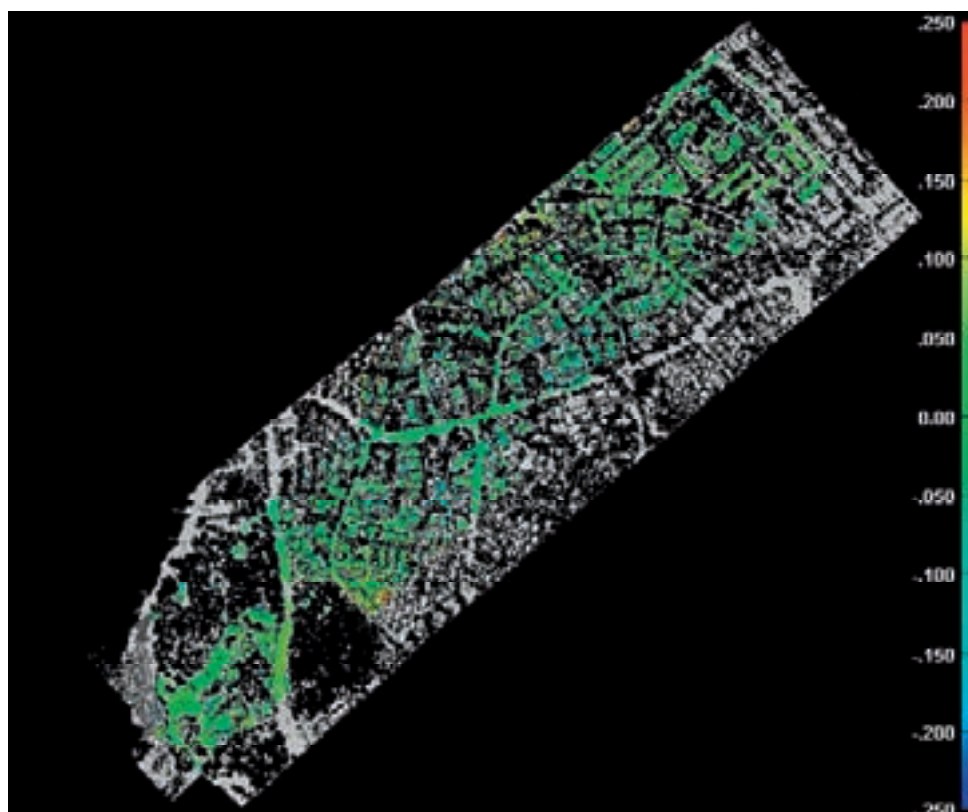


Figure 2: Error map showing the difference of image-based point cloud to LiDAR point cloud after registration. Deviation is scaled from -0.25 meters to +0.25 meters. Some ‘hot spots’ of deviation can be identified. They indicate problems in the input data.

Results

Panchromatic images

We report the transformation as a homogeneous 4x4 transformation matrix. The direction of transformation is from the LiDAR reference system to aerial triangulation (AT) reference system. If a LiDAR point with coordinates X, Y, Z is given the transformation is applied as follows:

$$P = A \begin{bmatrix} X \\ Y \\ Z \\ 1 \end{bmatrix}$$

Numerical values for the matrix are given separately for each case. While numerical values are stated with full decimals as computed, it is obvious that their accuracy is limited.

Case: Leica

0,999999272	0,000343667949	0,00115671056	-2309,93892
-0,000342911826	0,999999727	-0,000653818214	106,898577
-0,00115693494	0,000653421088	0,999999117	-3936,83903
0	0	0	1

Case: Optec

0,999999853	0,0000568428681	0,000538854824	-355,353879
-0,0000569591766	0,999999975	0,00021583098	3,50632043
-0,000538842542	-0,000215861641	0,999999832	1664,28665
0	0	0	1

RGB/NIR images

RGB/NIR images were not processed.

Level of Automation

The level of automation in DSM generation from oriented aerial imagery is well known. ICP is an automated method; however initial alignment parameters have to be given. In this example the original alignment was not good enough for the automated approach to converge, so coarse manual pre-alignment had to be performed. In practical cases we assume, that the georeferencing of both datasets is good enough to serve as initial alignment for ICP. In that case processing can be fully automated.

Discussion

The computational cost for computing a dense DSM is quite high, if the DSM is only used for registration. In this example DSM computation took 0 hour 17 min. 34 sec. Together with project set-up and data formatting, we were just under 1 hour.

ICP is very fast and takes clearly under 1 minute for the tested example. It is however problematic to choose the correct parameters for data import. In order to avoid matches in unreliable areas (forest, vegetation, etc.), we choose to omit triangles with an angle above 75 degrees from the vertical axis and triangles with an edge longer than 2 meters. These parameters are highly project/sensor dependent.

Conclusions

The approach provides a smooth data flow using mature commercial applications at high computational costs. A clear advantage of the approach is the fact that it uses information from all available images and provides a high degree of redundancy. One disadvantage is the computational cost of the DSM generation.

References

1. Besl, P.J. and N.D. McKay, A Method for Registration of 3-D Shapes. IEEE Transactions on Pattern Analysis and Machine Intelligence, 1992. 14(2): p. 239-256.
2. Zhao, W., D. Nister, and S. Hsu, Alignment of Continuous Video onto 3D Point Clouds. IEEE Trans. Pattern Anal. Mach. Intell., 2005. 27(8): p. 1305--1318.
3. Schuhmacher, S. and J. Boehm. Georeferencing of terrestrial laser scanner data for applications in architectural modeling. in 3D-ARCH 2005: Virtual Reconstruction and Visualization of Complex Architectures. 2005.

Method B

In this approach registration is based on the spatial resection of one aerial image using control points from the LiDAR data. In order to identify corresponding points the intensity information from LiDAR data is used. The intensity information is resampled to a regular grid to obtain an image-like representation. Within this image seven points were manually identified. Since the intensity is perfectly co-registered with X, Y and Z these points can immediately be used as control points for spatial resection. We used ArcGIS to import the LiDAR data and resample the intensity information of the point cloud to a 1 m and 0.5 m raster. Figure shows an overview of the raster intensity image for the Optech data and the position of the control points. We have previously used a similar approach for the registration of terrestrial LiDAR and terrestrial imagery [1] and were able to achieve accuracies in the order of magnitude of the point spacing.

The seven control points were then used to compute the spatial resection of one DMC image. We chose the scene “Espo_5b2_1_09_05_02~0013_pan” for the resection. Figure shows an example for two corresponding points. Due to the discrepancy in resolution identification of points was difficult. We chose points on planar surfaces with high contrast. Street crossings were good candidates. For simplicity we used PhotoModeler for point measurement in the image and to compute the resection. The ideal camera parameters as given were used; no additional parameters were estimated. The result of the resection (orientation and translation) can then be compared with the provided exterior orientation (result of the AT). The discrepancy in-between the two exterior orientations provides the transformation of the two reference systems. If X is a point in some arbitrary world coordinate system the following equations describe the transformation to the reference system of the AT and the reference system after resection (RS) which refers to the LiDAR reference system and the transformation in-between.

$$\begin{aligned}X_{AT} &= R_{AT}X + T_{AT} \\X_{RS} &= R_{RS}X + T_{RS} \\X_{AT} &= R_{AT}R'_{RS}X_{RS} - R_{AT}R'_{RS}T_{RS} + T_{AT}\end{aligned}$$



Figure 3: Resampled LiDAR intensity data and measured points.

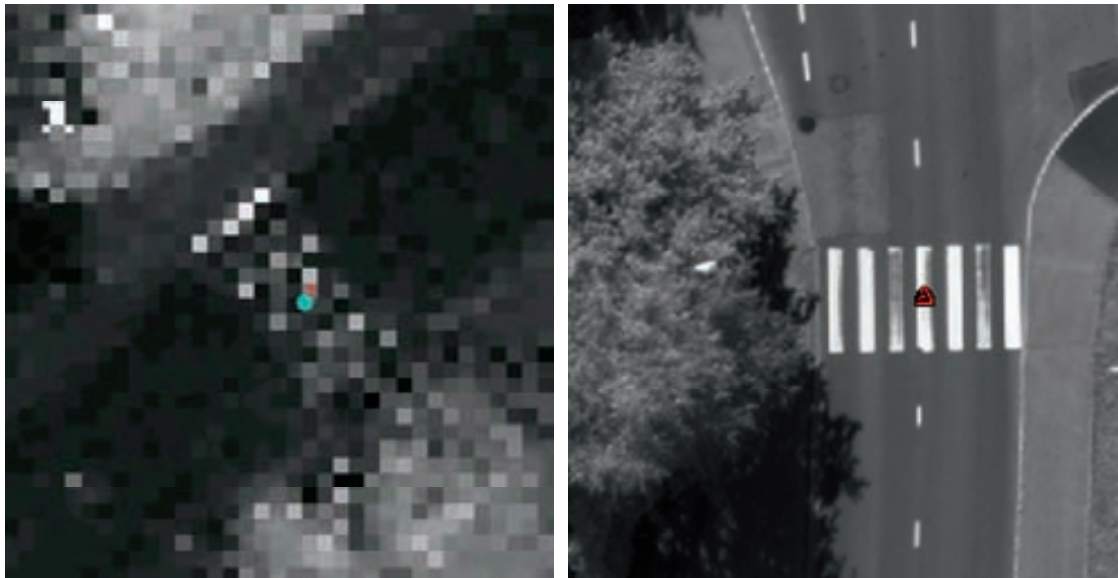


Figure 4: Corresponding point in LiDAR intensity image (left) and DMC pan image (right).

Results

Panchromatic images

We report transformation as a homogeneous 4x4 transformation matrix. The direction of transformation is from LiDAR reference system to aerial triangulation (AT) reference system. If a LiDAR point with coordinates X, Y, Z is given the transformation is applied as followed:

$$P = A \begin{bmatrix} X \\ Y \\ Z \\ 1 \end{bmatrix}$$

Numerical values for the matrix are given separately for each case. While numerical values are stated with full decimals as computed, it is obvious that their accuracy is limited.

Case: Leica

0,999997324908846	0,001032786869777	0,002069668194034	-6907,497237053001
-0,001028279390113	0,999997100002791	-0,002177757448383	377,0275847353041
-0,002071911351301	0,002175623425535	0,999995486912847	-13752,308657210364
0	0	0	1

Case: Optech

0,999999591318362	0,000207780517161	0,000879880881115	-1362,6883233173285
-0,000207198315889	0,99999759596801	-0,000661721389713	60,24832623824477
-0,000880018162402	0,000661538809443	0,999999393967035	-4061,7613589333273
0	0	0	1

RGB/NIR images

RGB/NIR images were not processed.

Level of Automation

Our current processing pipeline is of an experimental nature. We currently do not succeed in finding correspondences automatically. Grid interpolation and photogrammetric spatial resection are computed using standard commercial software and the level of automation is sufficiently high.

Discussion

The interpolation of LiDAR intensities to a regular raster was more problematic than expected. While the point density is specified with 2-3 points/m² and 4-5 points/m² respectively, we were only able to reliably extract a 1 m raster for both cases. We extracted a 0.5 m raster in addition for both cases, which was used as an overlay to “visually sharpen” the image. An example is given in Figure. We can clearly see a problem in raster interpolation with the Leica dataset. Visually it appears to be more blurred.

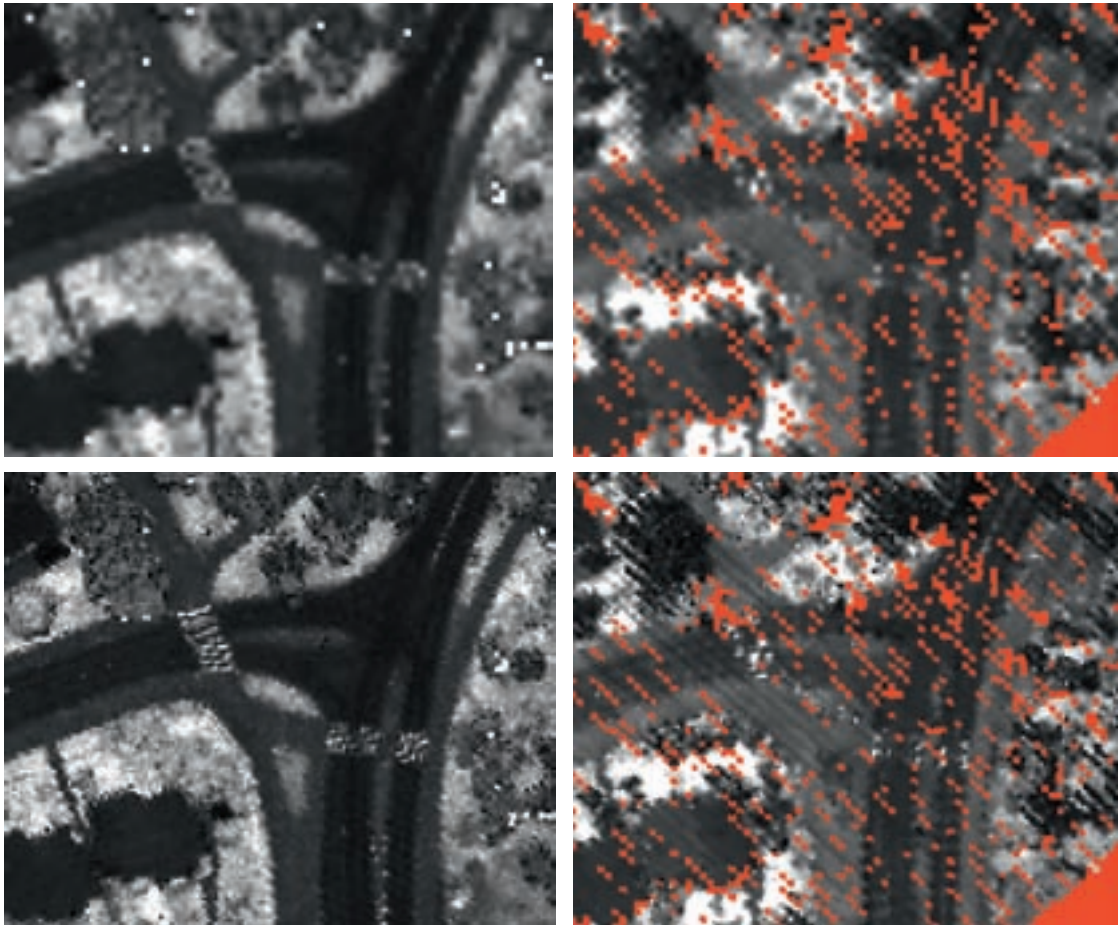


Figure 5: Examples for interpolated LiDAR intensity images. The top row shows a raster at 1 m. The bottom row shows the 1m raster with an overlay of a 0.5 m raster. The left column displays the Optech dataset, the right column the Leica dataset. Red indicates raster cells that could not be interpolated.

Measuring corresponding points was therefore problematic. We currently do not succeed in finding correspondences automatically. This should be a subject of further investigations. Given the recent progress in image feature extraction and matching, it is highly likely that successful strategies can be developed to fully automate the procedure. At the moment uncertainty of manual point identification is

still very high. Below we give a table of residuals after resection indicating the problems of precise point measurement, again especially for the Leica dataset.

Point ID	Optech control RMS Residual (pixel)	Leica control RMS Residual (pixel)
1	5,8	10,9
2	3,8	4,5
3	5,1	8,3
4	3,0	33,8
5	4,8	20,2
6	2,6	6,8
7	2,0	37,9

As far as run time is concerned, both raster interpolation and resection are very quick. Pure processing time is below 10 minutes total. However, as indicated above the processing pipeline is still experimental and parameters have to be tweaked manually.

Conclusions

The method has the clear advantage that only a single image needs to be processed. Potentially the method can be fully automated. An obvious disadvantage is the fact that, depending on the opening angle of lens and the distribution of control points, the spatial resection can be unreliable. Automation and the influence of different interpolation strategies should be further investigated.

References

1. Böhm, J. and S. Becker. Automatic Marker-Free Registration of Terrestrial Laser Scans using Reflectance Features. in Proceedings of 8th Conference on Optical 3D Measurement Techniques. 2007. Zurich, Switzerland.

Report of the Vienna University of Technology EuroSDR "Registration Quality – Towards Integration of Laser Scanning and Photogrammetry"

Camillo Ressl

Institute of Photogrammetry and Remote Sensing,
Vienna University of Technology
car@ipf.tuwien.ac.at

December 3rd, 2009

Method

First from the set of given aerial images with their given orientation a point cloud was derived by means of image matching using the software Match-T (version 5.2.0). For this only the panchromatic images were used. We did not use the RGB or infrared images.

The remainder of the method corresponds to our publications [Ressl et al., 2008] and [Ressl et al., 2009].

For each point cloud (from image matching, Leica ALS points, Optech ALS points) a grid surface model (DSM) was interpolated using the moving planes interpolation. For this a grid width of 1m was used, and at each grid location the interpolating plane was determined from the 9 closest points (within a circle of radius 2.1m). Additionally for each interpolation two other grids are stored. A sigma-grid and an eccentricity-grid. The sigma-grid stores the standard deviation from the moving planes interpolation (i.e. a small value for smooth surfaces and a large value for rough surfaces (like vegetation)). The eccentricity-grid stores the 2D-distance between the location of interpolation and the centre of gravity (CoG) of the points used for the determination of the plane (i.e. a small value if the CoG is closer and thus the points are scattered around the location of interpolation, and large value if the CoG is farther away (in case the points are only located on one side of the location of interpolation, thus indicating extrapolation)).

Then least squares matching (LSM) is applied to pairs of DSMs. The following pairs are considered: Photo-DSM/Leica-DSM and Photo-DSM/Optech-DSM. In each pair the DSM derived from the images is kept fixed, and the laser DSM is transformed. Additionally, in a third pair the two laser DSMs are used (for which the Optech DSM was fixed). LSM works by minimizing the height differences between the two grids. For this it is necessary that both DSMs model the same "feature" of the Earth's surface. This is only possible in smooth surface parts (e.g. streets, roofs, etc.) but not at rough surface parts (e.g. all types of vegetation). Therefore a roughness mask is used to mask out all "rough" grid cells. This roughness mask is derived for each DSM from the sigma grid and eccentricity grid mentioned above. For each DSM a cell is considered smooth, if its sigma-value $< 0.1\text{m}$ and its eccentricity-value $< 0.8\text{m}$; [Ressl et al., 2008]. During our LSM computation only the smooth cells are considered. This way the whole computation is already very robust from the beginning. Nevertheless, a few cells remain in the data with wrong heights, which need to be eliminated during the LSM adjustment. For this a simple threshold was used.

Originally, this LSM approach was intended for quality control of ALS strips [Ressl et al., 2008], where both DSMs are already well orientated (with residual shifts <1m). For this EuroSDR project, however, the orientation of the given laser data was (obviously deliberately) changed to be rather different with respect to each other and with respect to the aerial images (with detected shifts of about 20m). If the orientation of the two DSMs is that different, then the initial orientation does not allow a convergence of the LSM computation. Therefore, the initial orientation has to be improved. For this, a simple correlation approach between the two DSMs was used: one DSM was shifted cell by cell within (+- 100m) in steps of 10m. At each shifted location the height differences were computed. Around the shifted position of the minimum height differences a sub-pixel refinement was then computed (by fitting a parabola through the height differences of the 8 neighbouring shifts). This correlation approach yielded the following initial shifts for the three considered pairs:

Photo-DSM = Leica-DSM + (-18.9 / -20.6 / -5.7)
 Photo -DSM = Optech -DSM + (23.6 / -17.8 / 25.0)
 Optech-DSM = Leica-DSM + (-41.0 / -2.4 / -29.8)

The LSM computation used these shifts for the initial transformation.

Type of transformation used for LSM

Usually the transformation determined by LSM is only a shift from the moving grid to the fixed grid. If LSM is applied to central perspective images the geometric transformation is often extended to have affine parameters to correct for the central perspective distortions caused by different viewing angles. Additional transformation parameters for the grey values (contrast, brightness) are considered. The latter are not of concern for the matching of DSMs as considered in this work. However, the geometric transformation must be considered. As outlined in [Ressl et al., 2009], the correction of errors in ALS data caused by residual errors of the mounting calibration require an affine transformation. Because ALS data is also used in this EuroSDR project also a 3D affine transformation (12 parameters) is used for LSM. Additionally, in order to compare the effect of the 3D affine transformation with simpler transformations, a rigid body transformation (6 parameters) and a simple 3D shift (3 parameters) were used.

All three transformations are realized in the same way: $X_{new} = T \cdot (X_{old} - R) + R$

With T being a 4x4 transformation matrix, R is a constant reduction point, Xold and Xnew are the 3D points before and after the transformation in homogenous coordinates. R has 0 as fourth homogenous coordinate.

The layout of the transformation matrix T is therefore:

3D affine (12 par.):

x	y	z	shifts
1+a	b	c	d
e	1+f	g	h
i	j	1+k	l
0	0	0	1

3D rigid (6 par.):

x	y	z	shifts
1	b	c	d
-b	1	g	h
-c	-g	1	l
0	0	0	1

3D shift (3 par.):

x	y	z	shifts
1	0	0	d
0	1	0	h
0	0	1	l
0	0	0	1

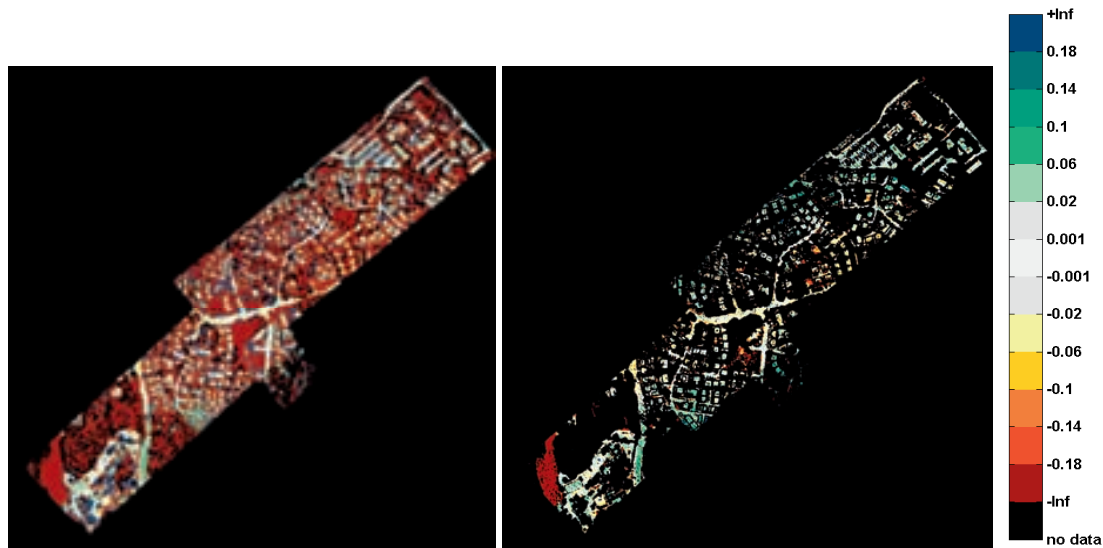
With a – l being the up to 12 unknown transformation parameters. Note, that the rigid body transformation realised in this way is approximate because it uses only differential rotation angles.

Results

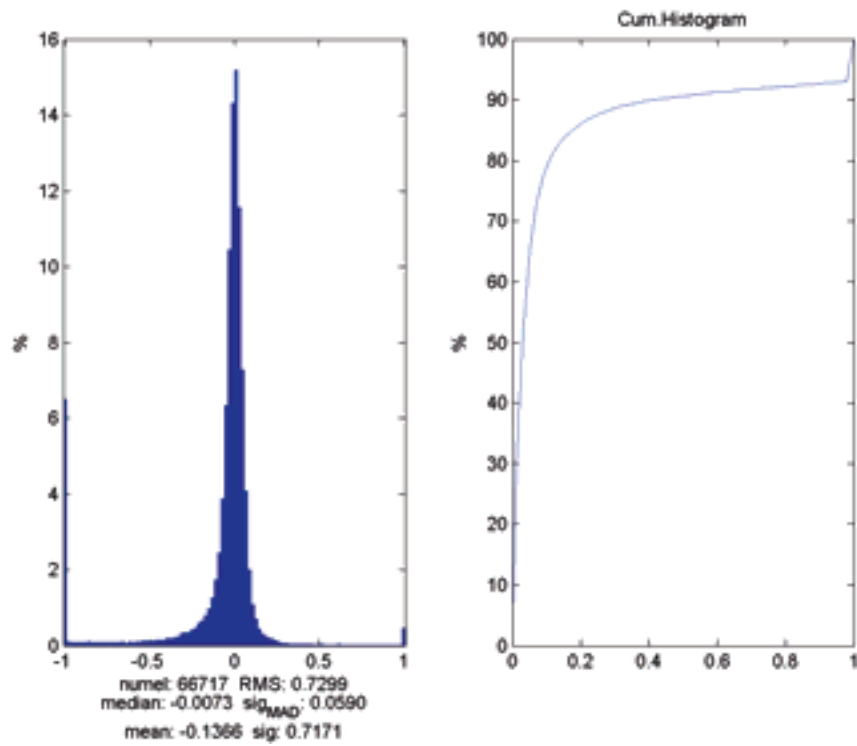
Panchromatic images

After computing the transformation between each pair, a difference between the two DSMs (the fixed DSM and the transformed DSM) can be computed (following the idea of strip differences in [Ressl et al., 2008] and [Ressl et al., 2009]). The colour-coding of this strip difference represents a continuous visualisation of the registration quality of the two DSMs. If also the roughness masks mentioned above are used to mask out rough cells (mainly vegetation and building outlines), the remaining cells with dark red and blue colours indicate larger residual errors of the registration. Additionally, a histogram of these masked strip differences can be computed, which gives a quantitative measure of the registration quality.

The following figure shows an example of an original colour coded strip difference and the respective masked difference, together with the used colour table (given in metres):



For the masked differences a histogram can be computed, which for this example looks like the following:



From this histogram various statistics can be derived. The quantity used in the following is σ_{MAD} which is the standard deviation derived from the median of absolute differences (the so-called MAD) as $\sigma_{\text{MAD}} = 1.4826 \cdot \text{MAD}$.

Pair: Photo-DSM vs. Leica-DSM

Reduction point for transformation: 369379 6669813 46

Transformation type: 3D affine

0.998363626	0.001557057	0.008682271	-18.161980663
0.001420606	0.998681334	-0.007429841	-21.529556014
-0.000276053	0.000190176	1.000773320	-6.058756283
0	0	0	1



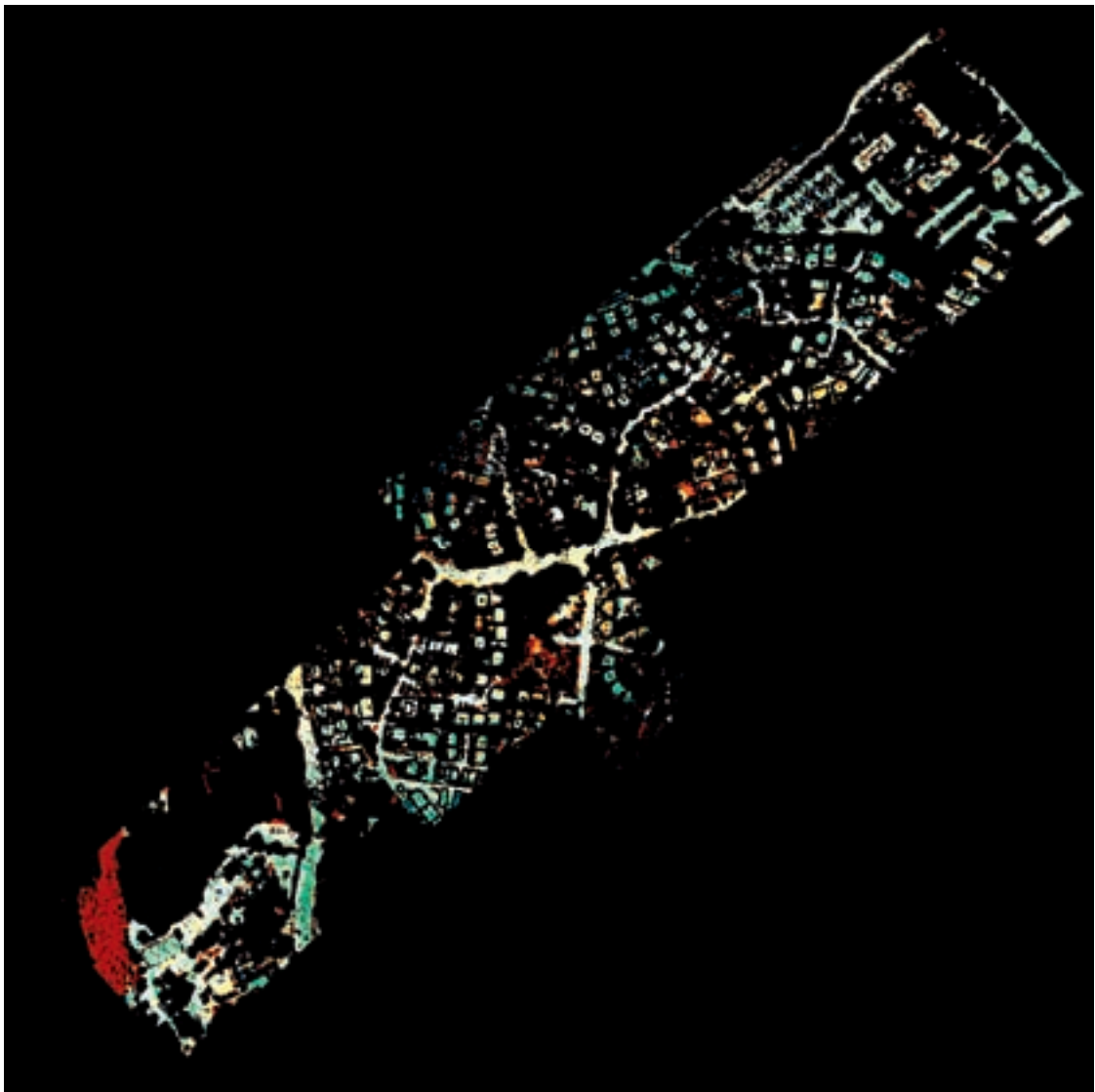
The σ_{MAD} of these masked differences is 5.9cm, derived from 66717 masked differences.

Pair: Photo-DSM vs. Leica-DSM

Reduction point for transformation: 369379 6669813 46

Transformation type: 3D rigid body

1.000000000	0.000138318	0.000249667	-18.042616757
-0.000138318	1.000000000	-0.000182346	-21.632987349
-0.000249667	0.000182346	1.000000000	-6.058895233
0	0	0	1



The σ_{MAD} of these masked differences is 6.4cm, derived from 68472 masked differences.

Pair: Photo-DSM vs. Leica-DSM

Reduction point for transformation: 369379 6669813 46

Transformation type: 3D shift

1.000000000	0.000000000	0.000000000	-18.039034296
0.000000000	1.000000000	0.000000000	-21.630752267
0.000000000	0.000000000	1.000000000	-6.049698448
0	0	0	1



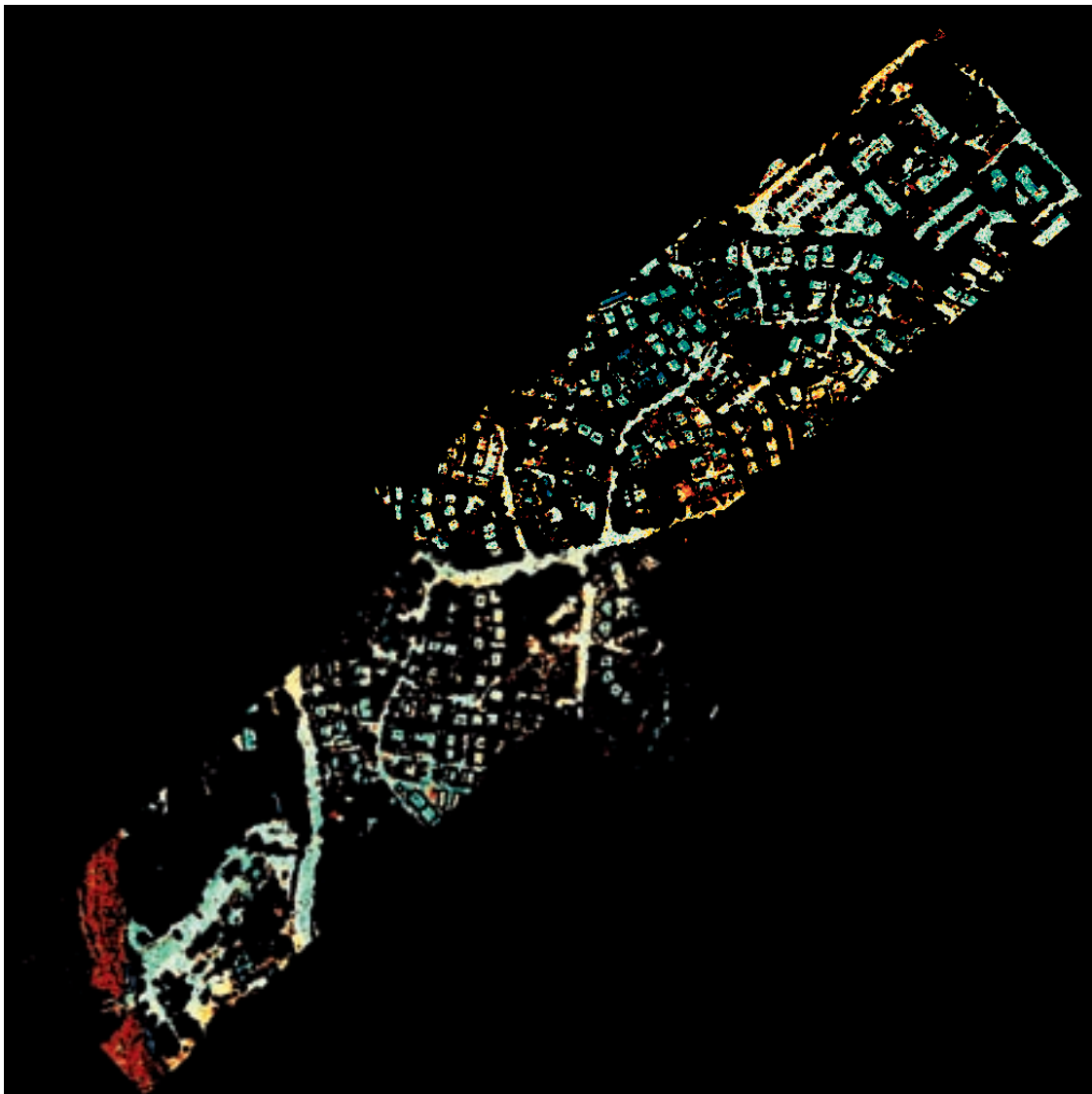
The σ_{MAD} of these masked differences is 7.4cm, derived from 68470 masked differences.

Pair: Photo-DSM vs. Optech-DSM

Reduction point for transformation: 369318 6669788 13

Transformation type: 3D affine

1.000029232	-0.000299979	0.006152293	23.598023210
-0.000154822	1.000111725	0.007204183	-17.735511187
-0.000285257	-0.000317157	1.001207212	25.488743254
0	0	0	1



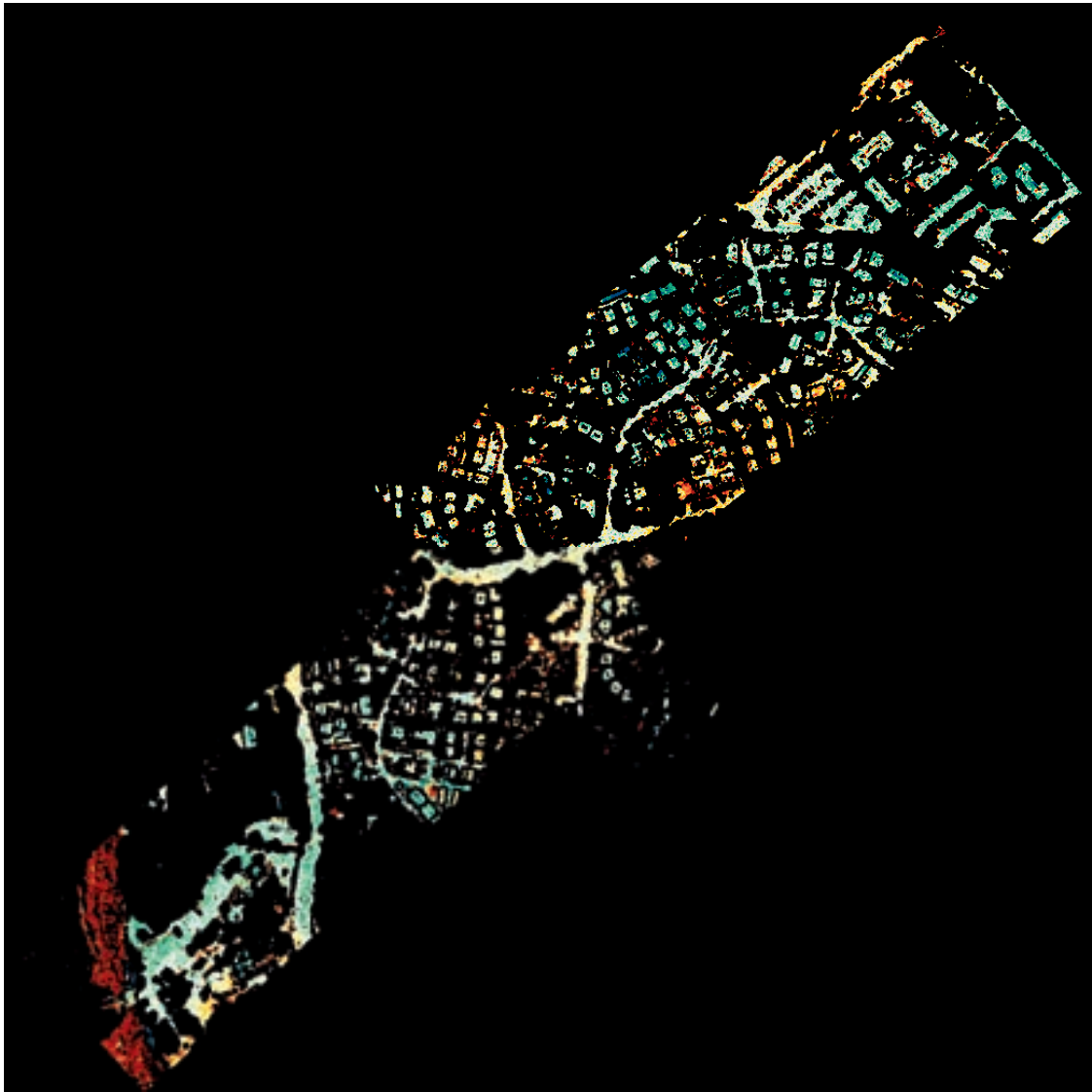
The σ_{MAD} of these masked differences is 6.5cm, derived from 65779 masked differences.

Pair: Photo-DSM vs. Optech-DSM

Reduction point for transformation: 369318 6669788 13

Transformation type: 3D rigid body

1.000000000	-0.000077273	0.000262093	23.675534986
0.000077273	1.000000000	0.000302274	-17.760988898
-0.000262093	-0.000302274	1.000000000	25.487630480
0	0	0	1



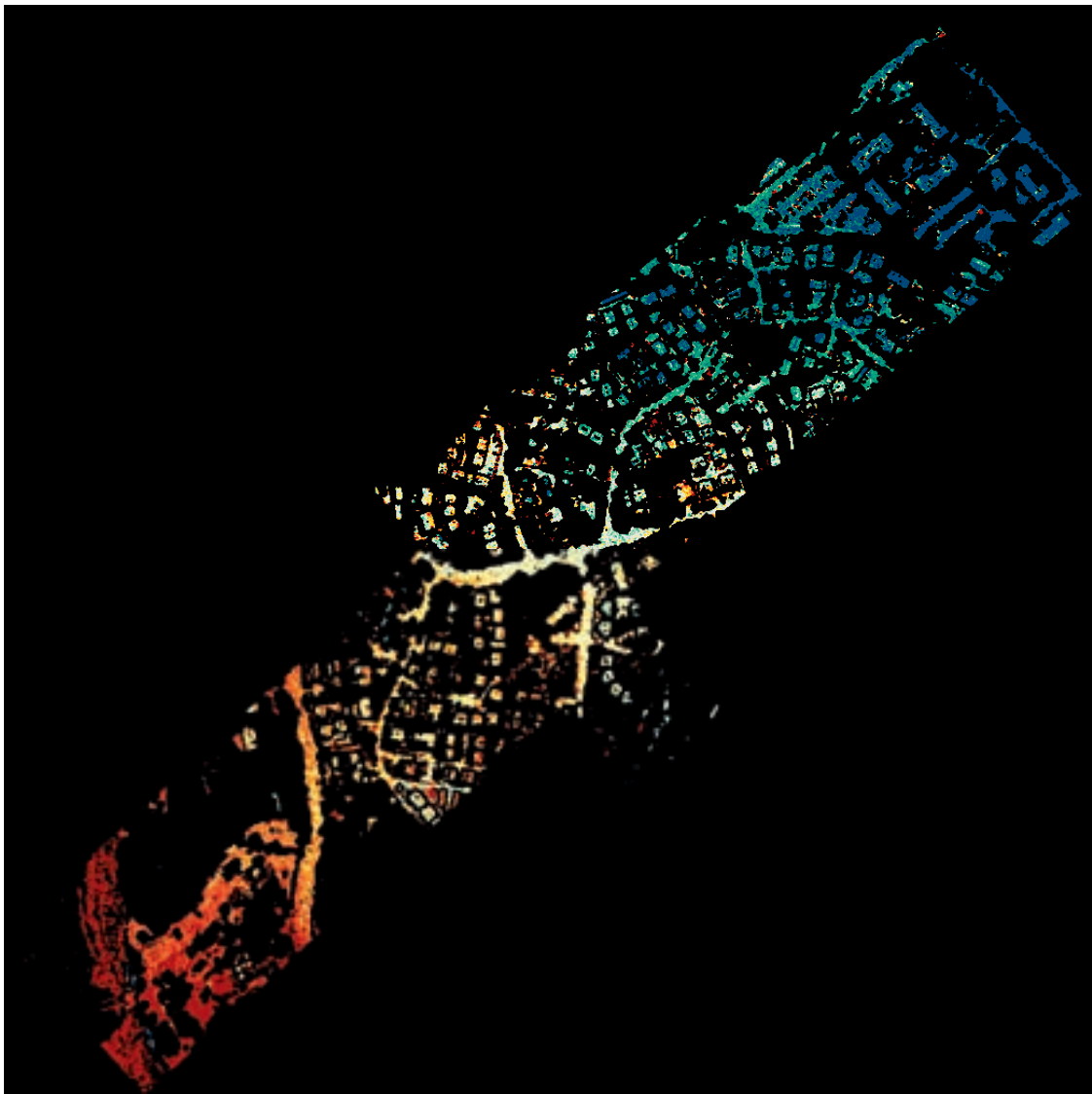
The σ_{MAD} of these masked differences is 6.6cm, derived from 65516 masked differences.

Pair: Photo-DSM vs. Optech-DSM

Reduction point for transformation: 369318 6669788 13

Transformation type: 3D shift

1.000000000	0.000000000	0.000000000	-18.039034296
0.000000000	1.000000000	0.000000000	-21.630752267
0.000000000	0.000000000	1.000000000	-6.049698448
0	0	0	1



The σ_{MAD} of these masked differences is 19.1cm, derived from 67089 masked differences.

Pair: Optech-DSM vs. Leica-DSM

Reduction point for transformation: 369379 6669813 46

Transformation type: 3D affine

0.998537541	0.001810713	0.000989442	-41.756392812
0.001733753	0.998075657	-0.004994463	-3.747815238
-0.000167958	0.000698489	0.999329923	-31.545522766
0	0	0	1



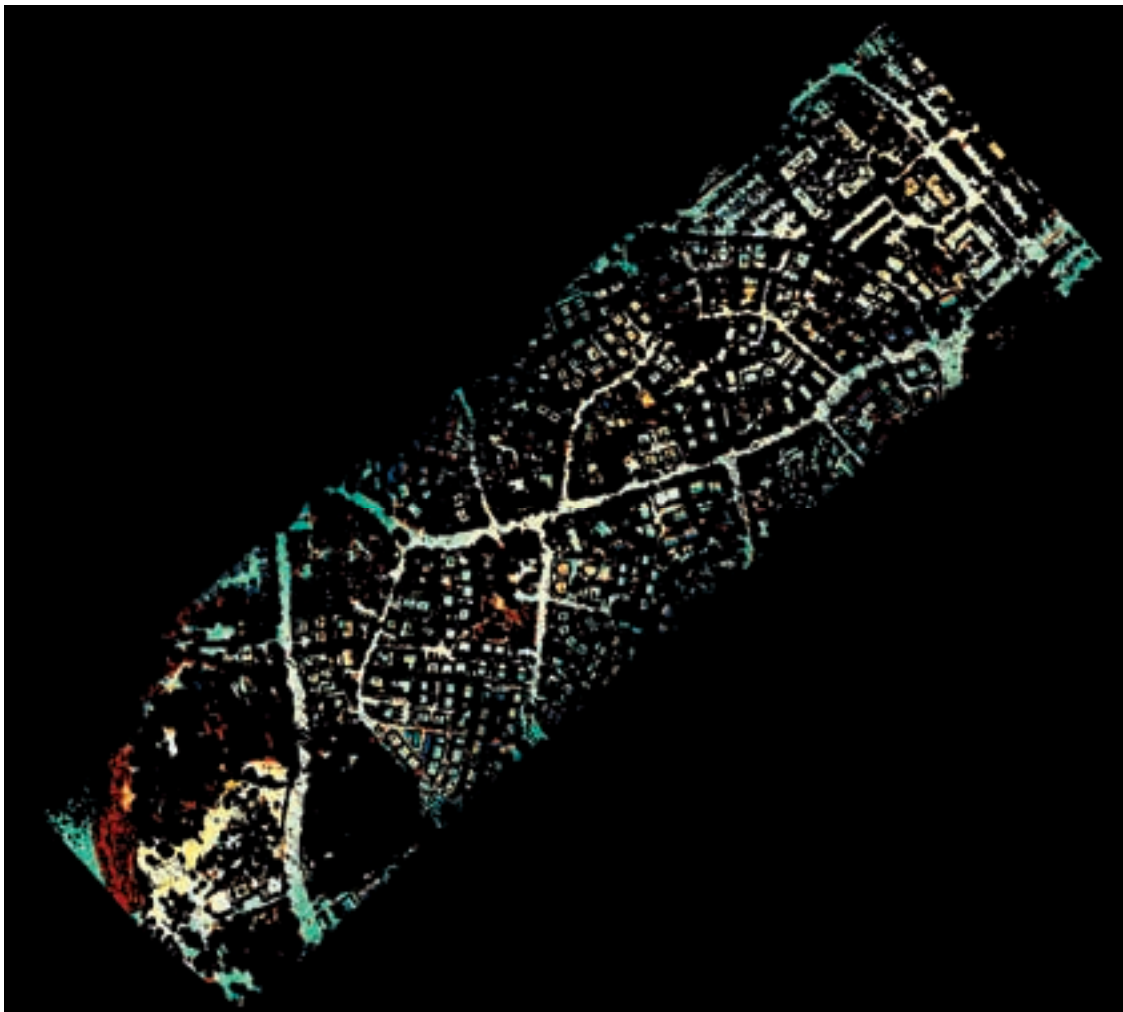
The σ_{MAD} of these masked differences is 5.6cm, derived from 110632 masked differences.

Pair: Optech-DSM vs. Leica-DSM

Reduction point for transformation: 369379 6669813 46

Transformation type: 3D rigid body

1.000000000	0.000504763	0.000141571	-41.834721697
-0.000504763	1.000000000	-0.000652836	-3.795450198
-0.000141571	0.000652836	1.000000000	-31.545027620
0	0	0	1



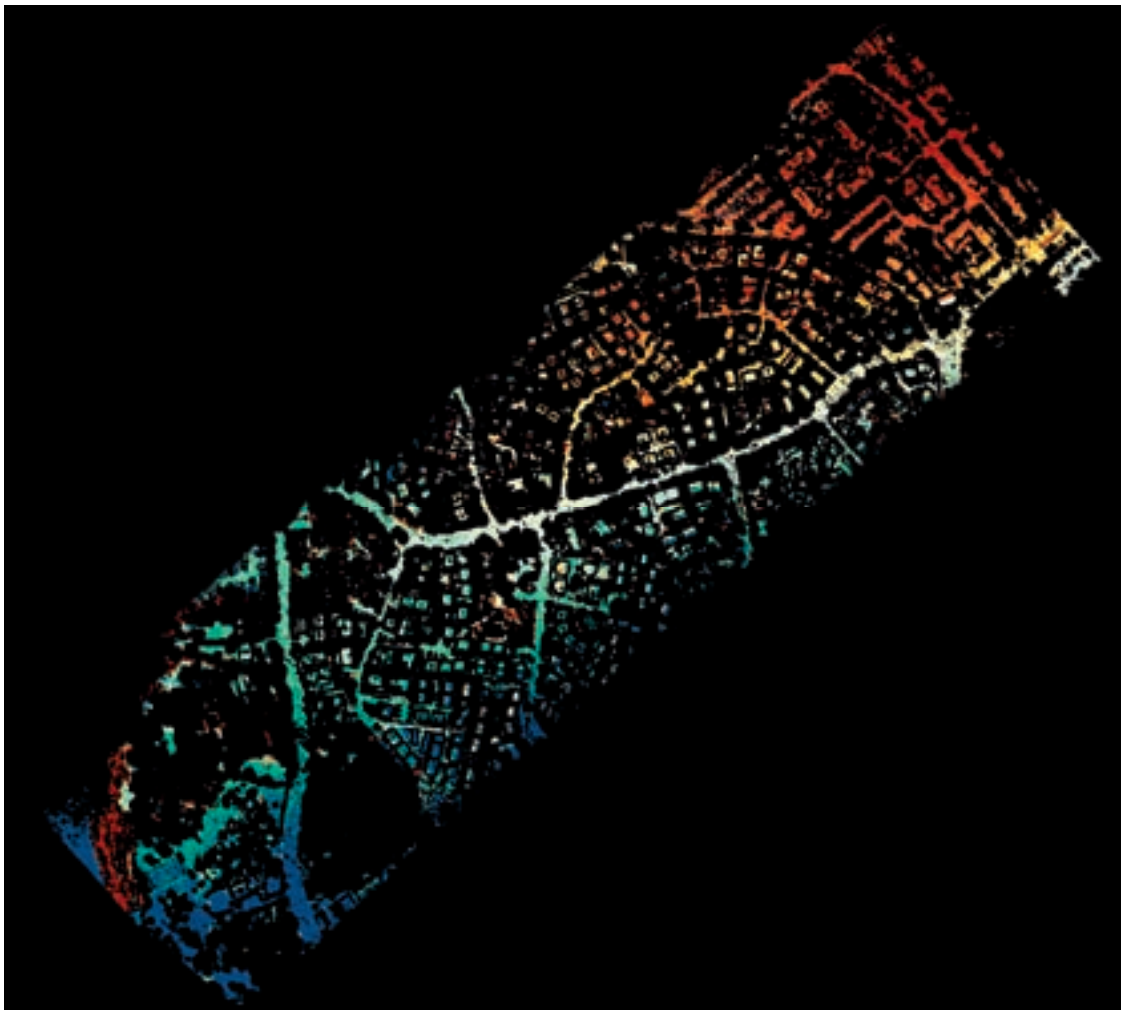
The σ_{MAD} of these masked differences is 6.1cm, derived from 111764 masked differences.

Pair: Optech-DSM vs. Leica-DSM

Reduction point for transformation: 369379 6669813 46

Transformation type: 3D shift

1.000000000	0.000000000	0.000000000	-41.746667975
0.000000000	1.000000000	0.000000000	-3.780158248
0.000000000	0.000000000	1.000000000	-31.534515735
0	0	0	1



The σ_{MAD} of these masked differences is 17.6cm, derived from 1011998 masked differences.

RGB/NIR images

TU Vienna did not use RGB or NIR images.

Level of Automation and Run time

Except for the project setups (Match-T software and own LSM implementation) and choice of certain parameters (Match-T parameters, grid width, mask parameters, threshold for robust adjustment) the whole registration process runs fully automatically. There is no manual intervention (e.g. measurement or selection of corresponding features) involved.

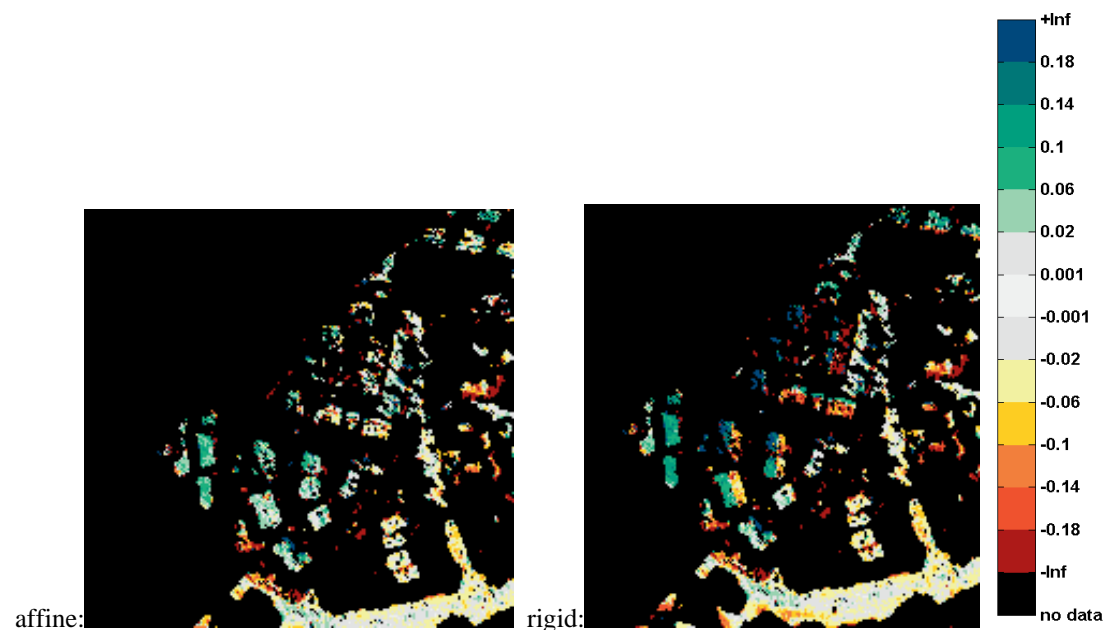
Run time:

- 1) image matching in Match-T software: 16 minutes for the entire image block
- 2) DSM interpolation by moving planes: ca. 30 seconds for each point cloud
- 3) LSM for each pair of DSMs: ca. 1 minute for each pair once the initial shift is found
(time for finding the initial shift by correlation: ca. 1.5 minutes for each pair)

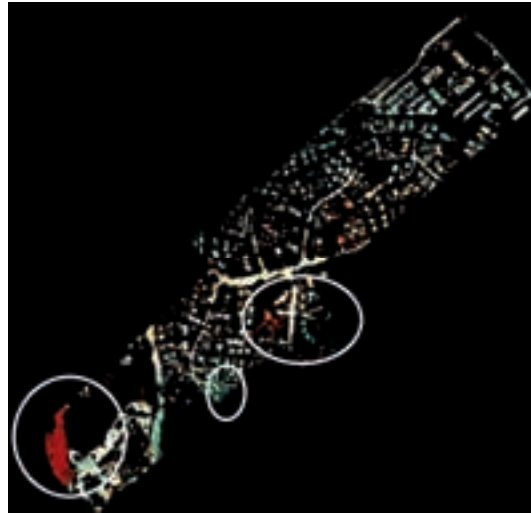
Discussion and Conclusions

As expected the affine transformation always performs best, although the rigid body transformation is close behind. Therefore the laser point clouds uploaded on the ftp-server are the ones after the affine transformation. A simple 3D shift is dangerous, as can be seen from the Optech data.

A closer look at the colour-coded strip differences of the affine and rigid body transformation shows local problems of the rigid body transformation. See figure below (section from Photo-DSM vs. Leica-DSM), where large height errors exceeding $\pm 18\text{cm}$ can be seen at the roofs of the buildings:



In general in all color coded strip differences local regions with large residual height differences can be spotted:



Here either certain rough surface parts were able to survive the roughness mask thresholds, or the terrain changed between the time of data acquisition of the three different sensors (very likely for the west-southern part), or uncorrected errors from the (laser) sensor data (e.g. laser angular error, etc.), whose correction requires the GPS/INS trajectory as some of these errors cannot be compensated by a transformation which only relies on the points.

In the past we used this LSM method with the affine transformation quite successfully for several ALS flights. There a σ_{MAD} of the strip differences usually below 3cm could be achieved. For the (ALS) data here it is only slightly below 6cm. This is probably due to some remaining large errors in the mounting calibration or other laser parameters, which cannot be modeled very well with the affine transformation. For this it would be interesting to perform a rigorous ALS strip adjustment [Kager 2004] for this EuroSDR ALS data and to see what σ_{MAD} of the strip differences can be reached afterwards. This rigorous ALS strip adjustment, however, requires the GPS-INS-trajectory of the two ALS strips.

References

- H. Kager: "Discrepancies Between Overlapping Laser Scanning Strips- Simultaneous Fitting of Aerial Laser Scanner Strips"; Poster: International Society for Photogrammetry and Remote Sensing XXth Congress, Istanbul; 07-12-2004 - 07-23-2004; in: "Proceedings", O. Altan (ed.); Vol XXXV, Part B/1 (2004); 555 - 560.
- C. Ressler, H. Kager, G. Mandlbauer: "Quality Checking Of ALS Projects Using Statistics Of Strip Differences"; International Society for Photogrammetry and Remote Sensing XXIst Congress, Beijing, China; 07-03-2008 - 07-11-2008; in: "Proceedings", Vol. XXXVII. Part B3b (2008), ISSN: 1682-1750; 253 - 260.
- C. Ressler, G. Mandlbauer, N. Pfeifer: "Investigating Adjustment Of Airborne Laser Scanning Strips Without Usage Of GNSS/IMU Trajectory Data"; Laserscanning 2009, Paris; 09-01-2009 - 09-02-2009; in: "ISPRS Workshop Laserscanning '09", IAPRS, Vol. XXXVIII, Part 3/W8 (2009), ISSN: 1682-1750; 195 - 200.

EuroSDR-Project

Atlas of INSPIRE Implementation Methods

Final Report

Project team

Ingrid Vanden Berghe (National Geographic Institute, Belgium)

Joep Crompvoets (K.U.Leuven- Public Management Institute, Belgium)

Walter de Vries (ITC, The Netherlands)

Jantien Stoter (Delft University of Technology & Kadaster, Apeldoorn, The Netherlands)

February, 2011

Abstract

This report is the final report of the EuroSDR project “Atlas of INSPIRE Implementation Methods”. In two two-day workshops and one pre-workshop of the INSPIRE Conference in Krakow, June, 2010 we investigated strategies to implement INSPIRE in several members states. We focused specifically on the relations between the implemented strategy and how successful the INSPIRE implementation is perceived in a specific country. A questionnaire was carried out as well. This report describes the project, presents the conclusions and contains the main deliverables of the project which are:

- Two workshop reports
- Research agenda for the implementation of INSPIRE
- A network of SDI-practitioners and scientists across Europe that are strongly involved in the development of INSPIRE SDI-strategies
- Scientific paper publications Scientific paper publications: published IJSDIR article [1] and article in progress for CEUS (Journal for Computers, Environment and Urban Systems)
- INSPIRE-Conference pre-conference workshop, abstract and presentation
- Key documents collection regarding INSPIRE-implementation
- Prototype INSPIRE atlas (see: <http://www.spatialist.be>)

We are grateful to all participants of the workshops as well as to all who carefully completed the questionnaire. The exchange of knowledge and experiences has been a very valuable result to all of us.

February, 2011

Ingrid Vanden Berghe, Joep Crompvoets, Walter de Vries and Jantien Stoter

1 Introduction

Implementing well-performing Spatial Data Infrastructures (SDIs) is not a straightforward, linear process. This is because a complex of interdependent aspects determine the success of SDIs such as legal, economic, technological, organisational, and public administrative aspects. In order to have successful SDI's and to meet the INSPIRE directive in particular, it is relevant for EU member states to know the key elements that lead to successful SDI implementation. In addition, identifying key areas for further research gives the scientific community the possibility to carry out research supporting the INSPIRE implementation requirements. The EuroSDR-project 'INSPIRE atlas of implementation methods' addresses these issues by studying the current (on-going) experiences of the INSPIRE implementations, and by providing a structured overview of INSPIRE implementation methods across the member states with references to their key documents. Moreover, the project aims to define a research agenda for INSPIRE related topics. The project is different other similar projects such as ESDIN, eSDInet+ and INSPIRE State of Play, since it is a research project aiming at understanding the factors of successful SDI's rather than implementing solutions or monitoring INSPIRE.

The input of EU member states has been very valuable for our project as it helps the states to learn from each other and to define common areas for further research. To accomplish the objectives of this project and to involve the member states in this project, two workshops were organised: one in April 2009 and the second one in January 2010. In addition a follow up workshop was organised as a pre-conference workshop of the INSPIRE Conference in Krakow, June 2010. To structure the experiences of the EU member states with implementing INSPIRE, a questionnaire was used as well. This helped to get a first overview of the current implementation methods and experiences as well as a preliminary list of areas for further research. In discussions during the workshop, the participants elaborated on their INSPIRE experiences in the context of every theme (i.e. technical, organisational, legal, economical): what are good examples and what are bad examples of implementation? What further research is required to support the INSPIRE implementation as well as future requirements with respect to the INSPIRE directive.

This report presents the main results of the project. Chapter 2 reports on the questionnaire. The two workshops that were organized are described in Chapter 3 and 4. Chapter 5 describes the workshop that was organized as a pre-event of the INSPIRE conference in Krakow, June 2010 and Chapter 6 ends with conclusions.

2 Questionnaire

2.1 Introduction

We considered input from the participants in advance of the workshops in the form of a questionnaire essential input for the discussions. Therefore we compiled a questionnaire to learn more about the specific INSPIRE implementation strategies in the different states and how it is evaluated by the specific member state. The answers were structured according the following themes: Organisational, Economic, Legal, and Technological. Note that the questions were not structured on these topics to give the respondents the freedom to answer in any direction. In the answers and the follow-up discussions, the participants were able to express their INSPIRE experiences in the context of these themes, and to learn from each other in a structured way. In addition, the input formed a basis for an overview of the current implementation methods and experiences.

This chapter presents the questionnaire and summarizes the outcomes.

2.2 Questions

The questionnaire contained the following 14 questions:

- Which organisations of your country are the most active in complying to INSPIRE?
- Which professional sector in your country has been the most influential in the preparation to implement INSPIRE?
- Which initiatives/changes to cope with INSPIRE have been completed?
- Which initiatives to cope/comply with INSPIRE are still on hold?
- Which articles of the INSPIRE directive cause the biggest headaches, and why?
- Which laws and/or regulations are adapted as a direct result of INSPIRE?
- Which organisations have adapted their internal structures and activities in order to cope with INSPIRE?
- Which changes in operational management have been enforced or observed as a direct result of INSPIRE?
- Which changes in maintenance management have been enforced or observed as a direct result of INSPIRE?
- Which policy is applied to the investment management of INSPIRE?
- Where do you think are still ineffective structures and/or operations when dealing with spatial data?
- Which uncertainties are you still coping with?
- What is the main success of the introduction of INSPIRE so far?
- What key strategies do you recommend for the implementation of INSPIRE?

2.3 Analysis of the questionnaire responses

The questionnaire was completed by the following countries: Belgium, Bulgaria, Croatia, Cyprus, France, Germany, the Netherlands, Poland, Slovakia, Sweden, Switzerland and the United Kingdom.

The responses can be summarized as follows:

- Organizational results:
 - Internal structures have not been changed much, but new partnerships and projects are more regularly developed and set up. Ultimately, this has resulted in a different ratio of task allocations (regular vs. project work)
 - None of the respondents has undertaken any measures or changes in maintenance of data.
- Economic results:
 - There is very little knowledge in terms of investments. There are no clear policies or guidelines; neither do any respondents have a clear idea where to invest. This seems even more remarkable given the responses that many new activities need to be undertaken. Part of the reason may be that organizations have to comply with many new EU and national regulations and directives.
 - The issue of inefficiencies is seldom described in economic (production; customer; market; cost price) terms, but contributed to poor coordination, lack of standards, pending legal requirements.
 - None of the respondents mention any economic success factors or success stories.
- Legal results:
 - Articles on data sharing and responsibilities for each data theme seem to confuse a number of respondents.
 - Pending legal reform/compliance causes many legal uncertainties.
 - To provide insight into which organizations have to comply with / act upon INSPIRE, the NL made a tool.
- Technological results:
 - Data specifications are still unclear, and create uncertainty how to specify internally in organizations.

2.4 *Conclusions of the questionnaire*

From the results above it can be concluded that an incremental approach is useful when awaiting certain decisions on details, and when anticipating a negotiated SDI environment. Another remarkable result is that most of the participants expressed the awareness of spatial issues to the introduction of INSPIRE. As a final result it can be mentioned that the INSPIRE State-of-Play documents (from other countries) are considered to be useful in the development of strategic plans.

These questionnaire results formed the basis for the INSPIRE Conference 2010 presentation (Appendix I) and an article published in the International Journal of Spatial Data Infrastructures Research.

3 Report of 1st project workshop, 29 & 30 April 2009



3.1 Introduction

The first workshop was held on 29/30 April 2009 in Brussels, as part of the National Geoweeek in Vlaanderen. This chapter presents the outcomes of the first workshop, i.e. a brief description of the workshop (Section 3.2), the research questions identified by the participants (Section 3.3), the main workshop observations (Section 3.4) and finally some noteworthy quotes that characterise the workshop (Section 3.5).

The participants of the workshop were:

Name	Organisation	Country
Joep Cromptvoets	KU Leuven	Belgium
Ine De Cubber	KH Sint-Lieven	Belgium
Ezra Dessers	KU Leuven	Belgium
Leen De Temmerman	Agency for Geo-Information Flanders	Belgium
Walter De Vries	ITC International Training Centre	The Netherlands
Tessa Geudens	Vrije Universiteit Brussel	Belgium
Christine Giger	Swisstopo	Switzerland
Erwin Goor	Flemish institute for technological research	Belgium
Katarina Leitmannova	Geodesy Cartography and Cadastre Authority	Slovakia
Per-Ola Lindberg	Lantmäteriet	Sweden
Roger Longhorn	Dynamics Research Associates Ltd	Belgium
Stefan Moyzes	Geodesy Cartography and Cadastre Authority	Slovakia

Andres Östman	University of Gävle	Sweden
Ivan Philipov	Agency for Sustainable Development and Eurointegration	Bulgaria
Patrick Rudloff	EADS Astrium	Germany
Jantien Stoter	ITC International Training Centre	The Netherlands
Glenn Vancauwenberghe	KU Leuven	Belgium
Ingrid Vanden Berghe	National Geographic Institute	Belgium
Danny Vandenbroucke	KU Leuven	Belgium
Luc Van Linden	1Spatial Belgium NV	Belgium
Jos Van Orshoven	KU Leuven	Belgium
Sandra Van Wijngaarden	Geonovum	The Netherlands
Désirée Veschetti Holmgren	Lantmäteriet	Sweden
Andres Von Dömming	Federal Agency for Cartography and Geodesy	Germany
Kristoft Vydts	Esri Belux nv	Belgium
Peter Woodsford	Snowflake Software Ltd	United Kingdom
and Sanja Zekusic	State Geodetic Administration	Croatia

Participants of the first workshop were: Joep Cromptvoets (KU Leuven, Belgium), Ine De Cubber (KH Sint-Lieven, Belgium), Ezra Dessers (KU Leuven, Belgium), Leen De Temmerman (Agency for Geo-Information Flanders, Belgium), Walter De Vries (ITC International Training Centre, The Netherlands), Tessa Geudens (Vrije Universiteit Brussel, Belgium), Christine Giger (Swisstopo, Switzerland), Erwin Goor (Flemish institute for technological research, Belgium), Katarina Leitmannova (Geodesy, Cartography and Cadastre Authority, Slovakia), Per-Ola Lindberg (Lantmäteriet, Sweden), Roger Longhorn (Dynamics Research Associates Ltd, Belgium), Stefan Moyzes (Geodesy, Cartography and Cadastre Authority, Slovakia), Andres Östman (University of Gävle, Sweden), Ivan Philipov (Agency for Sustainable Development and Eurointegration, Bulgaria), Patrick Rudloff (EADS Astrium, Germany), Jantien Stoter (ITC International Training Centre, The Netherlands), Glenn Vancauwenberghe (KU Leuven, Belgium), Ingrid Vanden Berghe (National Geographic Institute, Belgium), Danny Vandenbroucke (KU Leuven, Belgium), Luc Van Linden (1Spatial Belgium NV, Belgium), Jos Van Orshoven (KU Leuven, Belgium), Sandra Van Wijngaarden (Geonovum, The Netherlands), Désirée Veschetti Holmgren (Lantmäteriet, Sweden), Andres Von Dömming (Federal Agency for Cartography and Geodesy, Germany), Kristoft Vydts (Esri Belux nv, Belgium), Peter Woodsford (Snowflake Software Ltd, United Kingdom), and Sanja Zekusic (State Geodetic Administration, Croatia)

3.2 *Brief description of the Workshop 29- 30 April 2009*

29 April 2009

After a welcome and Introduction to the Programme by Ingrid Vanden Berghe (Head IGN, Belgium), several speakers presented their national strategy examples from an organisational perspective dealing with issues such as coordination, task division and capacity building (Ivan Philipov (Bulgaria), Désirée Veschetti Holmgren (Sweden), Christine Giger (Switzerland), and Sandra Wijngaarden (The Netherlands)). The morning session was closed by questions and remarks referring to the content of the presentations (see main observations and noteworthy quotes further in this chapter). In the afternoon, there was the opportunity to participate in the Staten-Generaal “Flanders Geoland”, a

formal meeting with key decision makers in Flanders (Belgium). The aim of this event was to contribute to the development of a strategy for the Flemish SDI. The main difficulty in participating in this afternoon event was the Dutch language of communication.

30 April 2010

The second day started with presentations about strategy examples from a more technological perspective dealing with issues such as web services, standards and e-government facilities (Andreas von Dömming (Germany), Sanja Zekušić (Croatia), Katarina Leitmannova (Slovakia), Ingrid Vanden Berghe (Belgium)). After the lunch break, Peter Woodsford (United Kingdom) and Roger Longhorn (Belgium) presented strategy examples from a more economic perspective dealing with issues such as funding and pricing. The workshop ended with agreeing on follow-up activities by the organisers and participants. Discussing the strategies from a more legal perspective, the mentioned strategies and SDI-research agenda in more detail was proposed for the second workshop.

3.3 Research questions identified by the participants

The participants of the workshop identified the following issues as topics for further research:

- How to coordinate INSPIRE implementation in one country?
- Has something similar been coordinated before? Can we, for example, learn from e-governance and PSI interoperability that has been started since 2000?
- Is the basic question for implementing INSPIRE successfully, how to manage information?
- How to coordinate a network required for INSPIRE (technical part is similar for every country; coordination is different)?
- How to involve stakeholders in the INSPIRE implementation process (in many countries the stakeholders are limited to the governmental organizations)?
- Who are the users of INSPIRE and how to involve them?

3.4 Main observations during the workshop

The following observations summarise the results of the workshop:

- Coordination of SDI appears to be problematic and the type of coordination needed was) unprecedented (for the public sector). Never before has coordination of the technology been so invasive in the operational activities of each SDI stakeholder. Key characteristics of new SDI-coordination strategies that might be included in the Atlas are: “do not compete with each other, but complete with each other” (Belgium); “seduce and align” (The Netherlands); “leave discretionary space for organizational flexibility” (Switzerland), “what is resolved, creates confusion at the same time” (UK).
- People are eager to learn from other countries, and share with other countries and professionals, yet do not know how this can be done best (regular meetings? professional coaching? Web-based guidelines?).
- Compliance with INSPIRE remains context and contingency specific because of existing national, organizational, economic and legal structures and cultural histories. Yet, a few general similarities exist:
 - All countries have to comply, one way or another, and will all be punished if they don’t comply, also one way or another;

- Coordination of INSPIRE related activities seems to work best if applying softer steering instruments – incremental approaches; seduction rather than coercion; complete with rather than compete with; seek complement rather than compliance; keep flexibility rather than tight organizational and decision structures;
- SDIs are a negotiated result. It is therefore necessary to build up skills and capacity in negotiating;
- There is a need to balance INSPIRE requirements with other EU or national requirements (E-government related, PSI related, etc.).
- There is still a clear difference in how to position and embed INSPIRE in existing regulations, activities and organizational structures between new (e.g. Bulgaria, Slovakia) and accession members (e.g. Croatia) of the EU versus older members of the EU (Germany, Netherlands, Belgium, UK, Sweden). Hence, no uniform guideline or best practice can be generated.
- The Swiss model of seeking INSPIRE compliance seems to be working, even though (or maybe because?) Switzerland is not an EU member.
- There are no clear guidelines or economic models to follow for the respective agencies. Rather than focusing on absolute cost and benefit assessments (ex post / ex ante), which are rather static and represent only one moment in time, perhaps one could use the changes of costs and changes of benefits that working with INSPIRE brings about. In other words what are the extra costs that compliance with INSPIRE brings about, and what are the extra benefits and opportunities that compliance brings about.

3.5 *Noteworthy quotes*

The following remarkable quotes characterise the results of the first workshop:

- “Quite a lot has been resolved; yet, quite a lot of confusion has been generated as well”.
- “We learned how to cooperate in the process of developing our national SDI”.
- “Do not compete with each, but complete each other”,
- “Seduce and align”
- “Leave discretionary space for organizational flexibility”

4 Report of 2nd project workshop 14/15 January 2010

4.1 Introduction



The second workshop was organised on 14/15 January 2010 in Brussels. The workshop contained three main elements: discussion of successes and disappointments around INSPIRE implementation by every participant (Section 4.2); discussions of propositions prepared by the organisers (Section 4.3) and a discussion of the research agenda for successful SDI implementation (Section 4.4). Apart from these working sessions, Hans Dufourmont from JRC gave a key note speech.

The participants of the workshop were:

Name	Organisation	Country
Ingrid vanden Berghe	NGI Nationaal geografisch instituut	Belgium
Joep Cromptoets	KU Leuven	Belgium
Danny van den Broeke	SADL KU Leuven	Belgium
Dimitrios Biliouris	SADL KU Leuven	Belgium
Pierrette Fraisse	FOD Financien	Belgium
Roger Longhorn	I-DRA Info-Dynamics Research associates	Belgium
Luc van Linden	1spatial	Belgium
Hans Dufourmont	EU Brussel Joint Research Centre	Ispra (VA)

Marie-Louise Zambon	Chef de projet INSPIRE@IGN	France
Daniela Hogrebe	Federal Agency for Cartography and Geodesy	Germany
Dieter Fritsch	University Stuttgart	Germany
Jantien Stoter	TU Delft & Kadaster	The Netherlands
Walter de Vries	Fac. ITC / UT	The Netherlands
Ewa Surma	HEAD OFFICE OF GEODESY AND CARTOGRAPHY	Poland
Desiree Verschetti Holmgren	Lantmäteriet	Sweden
Christina Wasström	INSPIRE Co-ordinator	Sweden
Christine Giger	Federal office of topography Swisstopo	Switzerland
Clare Hadley	Ordnance Survey	UK

4.2 *Successes and disappointments*

In the first working session, the participants were asked to present aspects of their SDI implementation which they are proud of and aspects that made them disappointed. These successes and disappointments” are summarised in this section for every country.

Switzerland

Successes:

First with a law on SDI, although not an EU country. Much convincement involved. Successfully voted for the law in 2007 and the law came into force into 2008.

Disappointment:

Did not succeed in an operational structure of cooperation. Problem is to find a legal body that serves public and private institutions. Especially involving private sector is hard. Already three years busy to accomplish this. Problem: who is responsible for national portal, only public? To serve the whole infrastructure also involves private sector to economically benefit by building services on top of it (e.g. enriching data). There may be a difference between strictly national SDI and wider SDI serving public and private sector.

Questions are: How to get together with public and private partners? How to divide responsibilities? Legal and organizational aspects cause problems in implementing INSPIRE.

Croatia

Successes:

Law that came into force before INSPIRE Directive. The Directive helped to raise awareness of SDI, i.e. the obligation to meet INSPIRE raised political support

Disappointment:

Complexity of INSPIRE Directive and the bureaucratic procedure to get it to happen. Not sure if all users’ needs can be met in time. NSDI is progressing very slowly. Therefore we may consider a private SDI, which can be a thread for implementation.

UK

Successes:

Horizontal collaboration and the establishment of a location council. Technical: top down implementation strategy. Department of Environment and Rural Affairs (DEFRA) leads. Conceptual model established.

Disappointment:

No strong political lead. Fragmented. No connection of successful initiatives to Location Council.

Unstable situation because of election this year.

We read nothing in the directive of access to citizens, instead it focuses on access between governmental organizations, i.e. public authorities. But what is a public authority?

France

Successes:

Technically we established a national portal developed by IGN and Geological Agency conforms with INSPIRE. We also developed tests with other countries (view service). But: the portal is not official yet.

Disappointment:

No law. Very complicated to transpose the INSPIRE law. We have now finally decided to have a law but on edict. But still no clear decision on how to improve France SDI. The edict is very close to INSPIRE Law, but does not contain any transpose. Question from the public: "But do you need a law?". Answer: Yes: to enforce every authority with geo data (France has 36000 municipalities and many local authorities)

Netherlands

Successes:

Established Law on key registers and a strategy document for SDI. We have a framework for geo standards.

Disappointment:

It is complicated to bring the good ideas as supported by Law and policies into reality. This is therefore a long process.

Belgium

Successes:

Agreement to set up national portal. Law goes further than INSPIRE implementation requires. Specific for the Flemish: we apply a networked approach. Every public authority has to define itself as a node in the network. Hierarchy and responsibilities are clear.

Disappointment:

Takes too long. Motivation decreases. No support at political level.

Sweden

Successes:

Budget of 50 million Swedish kronor available for developing portal and coordination. Also for authorities that need to make services and metadata.

Disappointment:

No law yet, although a draft has been ready for one year. Not easy to identify who are the authorities responsible for which data set.

Germany

Successes:

Established coordination structure and network. Processes are very clear. Network represents public and private sectors.

Disappointment:

Not an appropriate way to involve municipalities. Saxony was an example of strong involvement of municipalities. Federal law in force since 2007.

Poland

Successes:

Geo portal established by Office for Cartography and Geodesy.

Disappointment:

Not a lot of collaboration. Might change with new law on SDI that hopefully comes into force in April 2010.

Ireland

Waiting for benefit/costs analysis before law comes into force

Successes:

INSPIRE was a good driving factor to put attention on importance of geo-information. However the financial crisis has decreased this attention again.

Disappointment:

Not easy to implement INSPIRE because personnel responsible for INSPIRE implementation has to do it as part of their regular job

Europe

Successes:

Inspire is the only European initiative that has strong involvement of stakeholders and experts of the member states to establish legal framework.

Disappointment:

The sharing concept is hard to bring in reality. Although successful in European institutions, no sustainable program for sharing data.

From this summary of INSPIRE success and disappointments, the existence of a high diversity in INSPIRE implementation is evident. The main success can be considered to be the establishment of the INSPIRE transposition law in many countries, meanwhile the main weakness can be considered to be the low political support.

4.3 Propositions

The perception of the degree of influence from INSPIRE on National Mapping Agencies (NMA) was evaluated in a session where participants had to indicate how they perceived the influence of certain developments through opposing propositions. The propositions were not necessarily opposite / exclusive (see table below). The proposition sheet acted as a tool for discussion. Prior to the discussion the group was required to indicate (by a cross or an arrow) for each row how much they would agree with either of the two propositions. In addition, they had to provide an explanation or provide examples why they came to this conclusion. Four groups were formed, representing 4 more or less similar communities.

	Proposition 1		Proposition 2
1	Organizational		
	Implementing INSPIRE rules has changed our organizational processes and structures in a much more drastic way than having to implement other rules from national agencies.	↔	In practice it does not make any difference to our organization whether rules come in from INSPIRE or whether we have to implement rules from other policies. Both lead to similar types of organizational changes.
2	Legal		
	Overall, cooperation and exchange of data according to INSPIRE rules is just a matter of (practical) organisation through individual (layers of) legal contracts	↔	Overall, cooperation and exchange of data according to INSPIRE rules is a long, difficult and uncertain process of institutional negotiations, and complex legal structures
3	Technological		
	The increasing possibilities of webGIS have made cooperation and collaboration in the dissemination of geodata or geoservices increasingly easier.	↔	The increasing possibilities of webGIS have made cooperation and collaboration in the dissemination of geodata or geoservices increasingly more complex.
4	Economic		
	I am sure that INSPIRE has made me work more efficiently, and I have evidence and indicators to prove that.	↔	It is unknown to me whether INSPIRE has made me work more efficiently, and even if it did, I would not know from what type of indicator how much.

From this working session the following observations can be made (note that there was no significant difference between the groups):

- Having to comply to INSPIRE rules changed some of the internal rules of national organizational rules in a more drastic way than any other similar rules from national and supranational agencies. Most did however not see any change in other organizations than the national coordinating organizations themselves. It depends furthermore if the NMA is really the leading agency which has to coordinate INSPIRE.
- Overall, the cooperation and exchange of data according to INSPIRE rules is felt to be a long, difficult and uncertain process of institutional negotiations and complex legal structures. It was definitely not felt to be a matter of just practical organization through individual layers of (sub)contracts. There is some difference, however, between the countries. In Spain and the Netherlands, for example, most of the implementation is guided by sets of individual contracts which each need to be negotiated. Still the negotiations are felt complex and difficult. In Germany and Belgium on the other hand, most of the implementation is guided by hierarchical regulations. In these cases the process is (almost) complex by definition.
- Most felt that the increasing possibilities of web technology made the technical data sharing increasingly easier, but made the overall policy of dissemination of geodata and geoservices more complex. Furthermore, the general feeling was that webGIS enabled cooperation and collaboration. Yet problems in cooperation and collaboration were not immediately solved by

new technology only. Being in a network does not guarantee better cooperation. The technique of dissemination of data, on the other hand, has become easier with webGIS. The dissemination of geodata can however not be seen in isolation from the dissemination of other data. That's why cooperation still needs to be improved.

- Most of the respondents and participants could not indicate whether compliance with INSPIRE has made any effect on efficiency of their work. It would be too early to comment on this aspect. Nor could anyone indicate in which area and how much efficiency had changed since introduction of INSPIRE.

4.4 Research agenda

The last working session was dedicated to setting up a research agenda. This session was divided into two parts. At first the participants were asked where they would invest € 50 mill if available. Secondly they were asked to formulate research questions that need attention within the context of SDIs (as follow up of the research questions identified in the first workshop).



The participants compiled the following list of projects for investing € 50mill in INSPIRE implementation (per project):

1. Evaluation methods
2. Multilingualism
3. Ontology and automated schema translation
4. Further development of geo-portal
5. Interoperability of datasets
6. Best organizational structure for INSPIRE
7. Legal structures (make software package which makes regulations more insightful)
8. Implement information networks of geo-info
9. Standardized meta-data
10. (how to) capacity building for INSPIRE implementation
11. Social service oriented governance
12. Technical transformation data quality
13. Technology adoption
14. How to invest in ICT
15. Towards processing cloud computing, cloud processing
16. On –the-fly3D portal
17. Social mechanism to enhance cooperation
18. Effective architectures
19. Use of Google
20. New technologies to make easier use of geo-information
21. Software agent theory
22. Data sharing regulations
23. Restrictive data set models in data collection
24. How to engage in relevant collaboration
25. Business models with IT with end user approach
26. Producing multi-resolution supply needs to meet user needs
27. Automatic change detection and generalization
28. Legal base for creative commons

The research questions as formulated by the participants are summarised in the following list:

1. How to achieve INSPIRE from a supplier point of view (currently INSIPRE is formulated from a user point of view)?
2. How to link INSIPRE to other infrastructures?
3. How to build capacity for SDI?
4. How to close the (mis)match between user and producer?
5. How to prioritise research problems?
6. How to evaluate information infrastructures?
7. How to redefine SDI, without a single mapping agency?
8. How to involve national politicians?
9. What is the benefit of INSPIRE to social change?
10. What is the co-interest of INSPIRE in society?
11. What is the tension between crowd sourcing, reference sourcing?
12. Which datasets are most useful in terms of INSPIRE?
13. How to bring mainstream IT-development into geo-business? How to fill the formalism in a MDA (Model Driven Architecture) approach)?
14. What are the social problems / multiple realities, and how to overcome these?
15. What are the indicators for data sharing?
16. What are costs and benefits?

17. How to design effective infrastructures?

From these lists it appears that the main research topics for the research agenda deal with geoportals, metadata, standardisation, implementation evaluations, coordination structures, and legal issues.

4.5 *Concluding remarks*

A few final conclusions can be drawn from the second workshop.

The research agenda as formulated by the participants identifies the knowledge gap that is experienced by the participants, but mostly it addresses a gap between design and reality. The issue for science is therefore to go beyond collecting current knowledge, and create new knowledge.

Also science may have a role in generating a paradigm shift to better align with other domains.

Finally it is interesting to see that many 'how to do', 'what' and 'how much' questions were formulated (typical for engineers), few 'where' questions (typical for geographers) and not many 'when' and 'who' questions (typical for social sciences, politicians). It requires further attention to find out the reason, i.e. is it because of the background of the participants or are these really the research questions that bring us closer to successful SDI/INSPIRE implementation?

5 Pre-conference INSPIRE workshop, 22 June 2010

The proposal “EuroSDR-project Atlas of INSPIRE Implementation methods” was selected as a pre-conference workshop of the INSPIRE Conference 2010 (Krakow, Poland). This section reports on the 90 minutes workshop.

Around 25 participants joined this workshop (see list below). They were mainly SDI/INSPIRE-practitioners (e.g. managers and policy makers) who would like to know more about experiences regarding SDI/INSPIRE-implementations, and scientists who are interested in the development, utility and requirements of SDIs. The participants came from Belgium, Germany, Hungary, The Netherlands, Norway, Poland, Portugal, and Spain:

Name	Organization	Country
Mindaugas Pazemys	GIS-Centras	Lithuania
Frank Eyraud	CID,JRC,EC	EU
Engels Patrick	SPW,Environment, BE	Belgium
Peter Schwarzberg	CARIS,NL	Nederland
Rui Reis	IGP Portugal	Portugal
Gobe Hobona	Nottingham University	UK
Pàl Lèvai	FÖMI-Institute of Geodesy	Hungary
Aleksandra Kuczerawy	KU Leuven	Belgium
Zelyho Becic	State Geodetic Administration, Croatia	Croatia
Gregorio Urquia Osorio	Tragsatec	Spain
Michael Lutz	JRC	EU
Wouter Schaubroeck		Belgium
Alex van de Ven	VROM	Netherlands
Mabek Snitkowski		
Rafał Petrykowski	Mapmatic	EU

The aim of this workshop was to introduce the EuroSDR project to the wider SDI-community, to inform them about the latest results and seek feedback on these results, and determine key topics for the INSPIRE implementation research agenda.

The topics of the workshop were:

1. Introduction to the EuroSDR-project Atlas of INSPIRE implementation methods
2. Key results of the workshops and questionnaire analyses
3. INSPIRE implementation research agenda

The first two topics were presented and discussed. The topic regarding the INSPIRE implementation research agenda was done in an interactive way. As in the second workshop participants were asked to write down research topics that they would like to fund if they had € 50 mln for funding research on INSPIRE-implementation in their country.

The following list of issues came out of this discussion:

- Structuring standard framework for spatial data modelling
- Support national and thematic nodes

- Institutional coordination
- Coordination management
- Cooperation development of SDIs
- Capacity building
- Needs – evaluation of user needs
- How to make it user friendly
- User orientation
- Awareness raising / education / training
- Increase cooperation from local to national level
- Workflows becoming INSPIRE compliant
- Legal-technical cooperation
- Legal aspects of future usage of spatial data (public, professional, responsibility, liability)
- Development of data exchange node (like Norge Digital)
- Security of the data
- Security
- Efficiency
- Return on investment
- Impact on organizations
- Structural funding SDI
- Improving transparency for governmental data
- What service market needs
- Data sharing
- Sharing
- Data harmonization
- Standards

- Interoperability
- Themes
- INSPIRE killer application
- Geoportal possibilities
- Technology
- 3D Cadastral info system
- Large scale mapping
- Best practice strategies
- INSPIRE architecture

The results were very similar to the ones of the assignment performed in the January 2010 workshop, which were presented at the end of this workshop.

In addition to the pre-conference workshop, Walter de Vries presented the main results of the EuroSDR-project at the INSPIRE conference and its related workshop (see Appendix I). This presentation was also selected for writing a paper in the International Journal of Spatial Data Infrastructures Research [1]. Finally, this all resulted in two statements made at the closing session of the INSPIRE-conference.

- It is necessary to study experiences related to INSPIRE implementation
- Organisational issues matter and need to be studied in detail

6 Conclusion

The inventory of experiences, success and headache perceptions of European national mapping implementers of INSPIRE shows a large variety in national endeavours. This variety makes a standard recipe for INSPIRE implementation, let alone SDI implementation, impossible. However, the inventory provides the respective mapping agencies with a palette of current possibilities and alternatives, which enables the construction of an Atlas of INSPIRE implementation strategies. This Atlas is not prescriptive, but descriptive.

An advantage of the descriptive nature of how the actors perceive the INSPIRE implementation is that it enabled a first step towards conceptualizing how SDIs actually develop in practice. Whereas often the current paradigm is that SDIs can be planned and steered towards fixed goals, and in a sequential planned manner, the interpretation of the results shows that a conceptualization of the cultivation approach reflects the INSPIRE implementation experiences better than a conceptualization of the design approach. This conclusion implies that SDI research needs to be better embedded in information infrastructure research in social sciences. Experiences and perceptions of success and failure strongly relate to socio-organizational conditions, and to contextual and historical contingencies. An additional implication for the implementation of INSPIRE is cultivation of INSPIRE objectives is likely to be more effective than a blueprint design strategy. While such a cultivation strategy might still require evident national leadership with clear objectives, mandate and frame of reference, at the same time, it would also require a more gradual approach towards more innovative inter-organizational working relations, and a scaling up approach which is more strongly linked to societal windows of opportunity.

The final deliverables of this EuroSDR-project are:

- Two workshop reports
- A research agenda for the implementation of INSPIRE
- A network of SDI-practitioners and scientists across Europe that are strongly involved in the development of INSPIRE SDI-strategies
- Scientific paper publications: published IJSDIR article [1] and article in progress for CEUS (Journal for Computers, Environment and Urban Systems)
- INSPIRE-Conference pre-conference workshop, abstract and presentation
- Key documents collection regarding INSPIRE-implementation
- Prototype INSPIRE atlas (see, www.spatialist.be)

Acknowledgments

We would like to thank all participants of the workshops for their fruitful contributions. We are also grateful to everyone who completed the questionnaire.

Reference

- [1] W. T. de Vries, J. Crompvoets, J. Stoter and I. Vanden Berghe, Atlas of INSPIRE – evaluating SDI development through an inventory of INSPIRE experiences of European national mapping agencies, in Journal: International Journal of Spatial Data Infrastructures Research (IJS DIR), Volume: 6, Issue: special issue - selected articles from INSPIRE 2010, <http://ijsdir.jrc.ec.europa.eu/index.php/ijsdir/article/download/208/277>

Appendix I Presentation at INSPIRE conference, Krakow, June 2010

De Vries, W., Cromptoets, J., Stoter, J., and Vanden Berghe, I., 2010. Atlas of INSPIRE implementation – an inventory of experiences, successes and headaches of national mapping agencies. INSPIRE Conference 2010, Krakow, Poland.

ATLAS OF INSPIRE IMPLEMENTATION –

An Inventory of Experiences, Successes And Headaches of European National Mapping Agencies

Walter T. de Vries
(Joep Crompvoets, Jantien Stoter, Ingrid Vanden Berghe)

23 June 2010



UNIVERSITY OF TWENTE.

ITC

FACULTY OF GEO-INFORMATION SCIENCE AND EARTH OBSERVATION



Studying INSPIRE implementation as development process of information infrastructure

- (Hanseth & Monteiro, 1998): information infrastructures are enabling, shared, open, relying on socio-technical networks, connected to other infrastructures
- (Bowker et. al, 2007): information infrastructure are *pervasive enabling resources*, containing of the technologies, organizations, and individuals (designers, developers, users, mediators, managers and administrators) which enable knowledge work



ITC



Information Infrastructure vs. Information Systems

Info system:

- Stand alone, developed from scratch, life cycle,

Info Infrastructure:

- shared, evolving & open, heterogeneous, **installed base**, which is also standardized in one way or another
- Positive network externalities (vs. other techno)
- **No life cycle**, only maintenance and transformation



Characteristics of IIs

1. Network value (Metcalfe's law: value of a network grows exponentially with users' number. Potential value of services increases for providers and customers)
2. Path dependency and Installed base (lock-ins and irreversibility)
3. Control and complexity / standardization and flexibility
4. Standards and Gateways
5. Where is innovation, in the center of IIs or on the fringes of IIs?



I.I. example

Understanding IIs (Bowker, 2007; Hanseth & Monteiro, 1998)

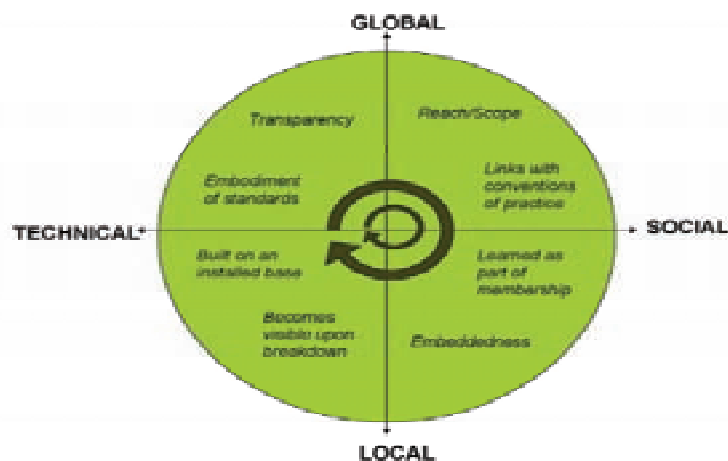
-> Cultivation approach for information infrastructure constellation , relying on:

- Installed base and lock-in effects
- Standardization processes – as processes of institutionalization
- Bootstrapping & Scaling up approaches

<http://heim.ifi.uio.no/~oleha/Publications/bok.html>



Information infrastructure (Bowker et al, 2007) scaling up approaches



Cyberinfrastructure as distributions along technical/social & global/local axes



Cultivation versus design approach

- | | |
|---|--|
| <ul style="list-style-type: none"> ▪ Installed base, path dependency and lock-in effects ▪ Standardization as processes of institutionalization ▪ (Coincidental) bootstrapping and scaling up ▪ Co-evolution of socio-techn. developments | <ul style="list-style-type: none"> ▪ Clear base, path independency, and neutrality of techn. ▪ Standards as technological solutions ▪ Planned, sequential development process ▪ Technology and context separated |
|---|--|



II questions and INSPIRE survey questions

- | | |
|--|--|
| <ul style="list-style-type: none"> ▪ Do GISs scale up to an SDI? ▪ Consequences of an installed base and what are lock-in effects? ▪ Choices on standards; which standards adopted? ▪ How and why are certain design choices and activities cultivated across different organizations? ▪ How do complex systems adapt to changing environments? ▪ How are processes institutionalized? | <ul style="list-style-type: none"> ▪ Most active organizations? ▪ Which initiatives completed / on hold? ▪ Which INSPIRE articles headaches and why? ▪ Which laws and/or regulations are adapted as direct result of INSPIRE? ▪ Which changes in organizational & investment management? ▪ Which ineffective structures and uncertainties? |
|--|--|



Survey statistics



■ Respondents:

April 2009	December 2009
Belgium	Croatia (2x)
Bulgaria	Cyprus
Germany	France
Netherlands	Germany (GDI-DE)
Slovakia	Poland
Sweden	Sweden
	Switzerland
	UK
6	8(9)
Total of 12 countries	



Country	Most active organizations in complying to INSPIRE	Sectors
Belgium	AGIV, NGI, Kadastral administration, Wallon Geomatics department, Brussels Env. Institute	GI sector
Bulgaria	State agency for ICT, Agency for sustainable development and eurointegration	Informatics, IT
Croatia	State Geodetic administration; Ministries; private sector; geodetic institute; Univ. of Zagreb	Geodesy & (geo) ICT
Cyprus	Department of lands, surveys Environment service	Not yet involved
France	IGN; Geological survey; local authorities	
Germany	Administration of Environment; Surveys	Public sector
Netherlands	Kadaster, KNMI, PBL, provinces	VROM, Geonovum, IdSW
Poland	HQ Geodesy & Cartography	Geodesy, cartogr., cadastre
Slovakia	Min. of Environment; Env. Agency; Geodesy, Cartography and Cadastre Authority	GIS community in env. Agency
Sweden	Landmateriet – geodata advisory board; SMHI; SGU	Public sector
Switzerland	Federal Offices of Topography, of the Environment and Statistics	Geomatics
UK	Dep. of Environment, Food & Rural Affairs (Defra), Highways Agency (HA), Land Registry (LR), Ordnance Survey (OS), Northern Ireland government, and Welsh Assembly government and many others are actively preparing	GI; recently much wider info. User community



Country	Which initiatives are Completed?	On hold – awaiting progress?
Belgium	GDI working group established; Transposition in national legislation ; Metadata already compatible	All other initiatives
Bulgaria	Spatial data access law approved by government	Metadata
Croatia	Legally mandated NSDI body; Public awareness campaign Transposition of legal framework	Full legal framework has to be worked out
Cyprus	New law has been drafted – submitted to government legal service	
France		Transposition still to be issue; there will be several decrees
Germany	Federal SDI steering committee established; National working groups	
Netherlands	Full adoption in legislation; cooperation agreement between public parties	
Poland	All activities / initiatives are ongoing and in different stage of completion	
Slovakia		Establishing GI as Basic E-gov register
Sweden	National coordination structure established; Version 1.0 of geodata portal completed	Identification of data providers awaiting adaption of env. Law; Financing and price models
Switzerland	none (only national law)	no dedicated initiatives but several specific investigations in institutions with European connections
UK	Location Strategy and Location Programme ; Location Council and supporting structure	Nothing really on hold, but some things have not been looked at in much detail yet. In some cases waiting for Regulations

Country	Headache articles / issues	Reasons for headaches
Belgium	Data sharing ,interoperability, network services	
Bulgaria	Article 10, article 11 Article 18	Requires too big investments Requires additional resources (human & finances) to implement
Croatia	Data distribution not yet possible - Metadata	Will require significant investment to complete
Cyprus	Article 9	Implementation time and due date – difficult to meet.
France	Coordination & role of different decentral public authorities; Article 17 – requires data sharing among public authorities without any restrictions at the point of use	Unclear: what authority for which type of spatial data ; Seems difficult as we look at the numbers of actors involved.
Germany	Providing thematic datasets Arrangements of data sharing	To which & by which administrative level? Too many parties involved
Netherlands	Data specifications	
Poland	Articles 7, 11 and 12	Seem the first articles to tackle after transposition
Slovakia	The wide extent of themes and associated authorities of themes	Problem of coordination
Sweden	Article 17 Security and secrecy	Implications of this article are unclear
Switzerland	none	since it is not legally binding for Switzerland
UK	Within Network Services, the transformation services and 'invoke spatial data services'	are still very unclear.



Headaches – observations


- Very diverse; different per country; per administrative level
- Common headaches:
 - Sharing and interoperability
 - Coordination & authority
- Administrative hierarchies cause uncertainties in :
 - Organizational (coordination) responsibilities
 - Distribution of thematic responsibilities




Country	Which laws and/or regulations are adapted as direct result of INSPIRE?
Belgium	GDI-decree(t)
Bulgaria	New special law
Croatia	Law on state survey and real estate cadastre – gazette 16 / 2007
Cyprus	A new law has been drafted
France	Local coordinating structures will be organised by local authorities, the link between the national level and the local levels will be established (probably on a consensus basis)
Germany	At Federal level: Geodata access law – GEOZG; At state level comparable laws in preparation
Netherlands	Anchoring in Dutch legislation
Poland	Spatial data infrastructure law – currently in Parliament
Slovakia	Amendment of law on geodesy and cartography
Sweden	A law and an ordinance, replacing present law (2005:181) on environmental information
Switzerland	none
UK	Directive itself will be transposed into a Statutory Instrument for all parts of the UK except Scotland




Country	Which organizations have adapted internal structures / activities to cope with INSPIRE?
Belgium	All organizations that own INSPIRE datasets
Bulgaria	Some divisions in the Ministry of Environment
Croatia	State geodetic administration has changed organizational schema, and introduced NSDI sector.
Cyprus	No changes so far
France	No changes to report yet
Germany	Coordination office SDI Germany has been improved , e.g. additional personal resources and budget
Netherlands	Very little to none
Poland	Establishment of coordination structure; Creation of spatial information departments within public agencies
Slovakia	Awareness of INSPIRE is low, hence very little adaptation
Sweden	Landmateriet in coordinating NGI; establishment of geodata advisory board
Switzerland	none, but some processes and data models (e.g. at the Federal Office for the Environment) may change in future
UK	Defra (re-organised existing programme for INSPIRE); SRO



Observations



- Type and sequence of changes (if any) are very contingent (= dependent on local development paths and priorities)
- Currently changes tend to focus on structures and/or responsibilities rather than on changing the behavior / attitude
- Direct (intra-)organizational (back office) effects are not immediately felt / visible, yet are required (in terms of different resources and different distribution of resource allocation)
- The back office changes are not always visible to external stakeholders (hence may not be appreciated sufficiently)



Country	Which changes in operational management have you enforced to cope with INSPIRE?
Belgium	Creation of partnership agreement between regions and federal authorities; creation of working groups
Bulgaria	Preliminary studies on partial or full re-organization of public authority databases
Croatia	Depends on re-organization of SGA as first step; Many working groups are defined to implement in different sectors.
Cyprus	Changes have not yet been implemented
France	No changes to report yet
Germany	The SDI coordination office has been assigned national point of contact
Netherlands	Emergence of projects within organizations to shape the implementation of INSPIRE
Poland	HOGC established a council for INSPIRE implementation
Slovakia	Once new NSDI law is in force, the intention is to change operational and maintenance management
Sweden	Strategy comprises rules and guidelines for operative management, and focus on 7 areas: financing, organization, internal processes, external cooperation, communication, INSPIRE and e-government
Switzerland	None, too early
UK	As part of governance for the Location Programme there is a Location Information Interoperability Board – gathering together experts to determine common policy, standards and guidance. There is increasingly a more horizontal way of working.



Observations operational management




(despite coercive character INSPIRE, and despite having to encapsulate a uniform INSPIRE within a heterogeneous environment)

only some innovation in ways of working and associated management – e.g.


- Horizontal working methods
- Different types of project based work;
- chain management;
- cross-boundary approaches;
- (inter-national) joined-up approaches
- cross-organizational management structures
- Shared-responsibility



Country	Which changes in maintenance management have you enforced / observed as a result of INSPIRE?
Belgium	-
Bulgaria	No changes in data maintenance. It will await legal changes.
Croatia	Geoportal and cooperation concepts are fostered
Cyprus	Changes have not yet been implemented
France	-
Germany	Geodatencatalog-DE, a central catalogue service
Netherlands	-
Poland	Modernization of data models, harmonization of DBs, use of ISO norms, exchange standards based on XML, GML and implementing rules
Slovakia	-
Sweden	Awareness of information overlap between different organizations has increased, and underlying causes to this have been better understood
Switzerland	None
UK	too soon to answer this question



Country	Which policy is applied in investment management as an effect of INSPIRE?
Belgium	-
Bulgaria	Standard policy of public investment management apply
Croatia	INSPIRE is based on state budget funds supported with co-financing models, developed by some authorities involving local government and public enterprises
Cyprus	N/A
France	No decisions to report yet; each public authority is responsible for its own investment policy
Germany	No overall budget or investment management of INSPIRE
Netherlands	Limited investment through VROM ministry. INSPIRE considered important, yet not crucial for VROM
Poland	Policy consistent with national policy related to activities in SDI
Slovakia	No investment yet; yet, lots is anticipated – we intend to obtain finances from EU structural funds
Sweden	Geodataprojektet will analyse cost and benefits for society as a whole and for different stakeholders; Government invests 50Mkr (≈4.65 M€)/year for the coming 3 years; 30 Mkr is earmarked for coordination activities
Switzerland	none directly, investments concerning the NSDI are currently mainly provided by the Federal Office of Topography (swisstopo) and the cantons; internal measures in federal administrations are provided by the respective organisations
UK	The costs of complying with INSPIRE must come from BAU expenditure of each individual organisation.



Country	Where are still ineffective structures and/or operations when dealing with spatial data?
Belgium	-
Bulgaria	Still 'foggy' requirements for spatial data operations in the public administration before national law and set of regulations to be in force
Croatia	We are still building new structures, but already facing data sharing policy as major problem
Cyprus	A central management board is lacking with authoritative powers to all INSPIRE stakeholders
France	Coordination and cooperation should be improved; reference data sets for cadastral parcels
Germany	Finding thematic responsibilities; raising other stakeholders' awareness; integration of business processes ; E-government could be more effectively integrated in decision support systems
Netherlands	-
Poland	Cooperation between public authorities, and access to spatial data sets
Slovakia	So far only few organizations in environmental sector are affected. No national standard beyond this.
Sweden	Interoperability; standardization methods ; test environments of data and service conformity, including certification mechanisms
Switzerland	Everywhere. Despite many efficient and effective local structures nation-wide provision of data and services has to take into account the overall federal structure. This structure causes e.g. different data sharing policies in cantons and municipalities, which have to be provided on the national level in a way that is consistent and usable.
UK	Everywhere. Data still very silo-bound which leads to a lot of duplication and disconnections. The UK Government has now recognised this in wider field and announced plans to make public data public. At local government level there is little coordination on INSPIRE or real appreciation of what they have to do at this stage.

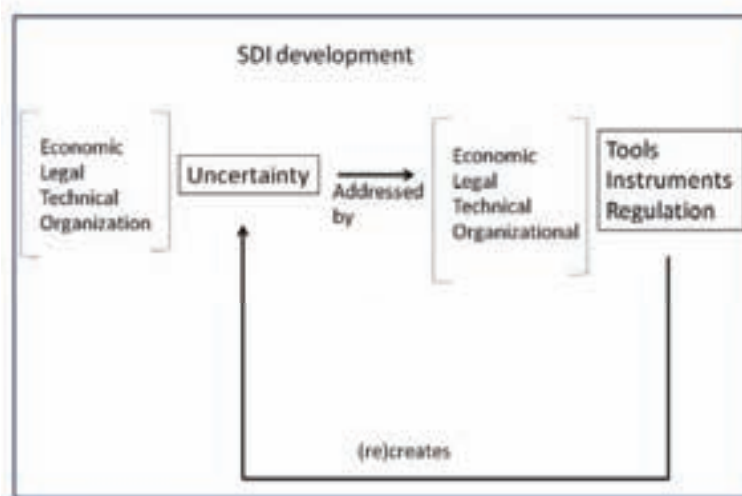


Country	Which uncertainties are you still coping with?			
	Economic	Legal	Organizational	Technical
Belgium				Demarcation of reference datasets
Bulgaria		synchronization local texts with EU texts with many iterations.		
Croatia	Financial resources			quality of data
Cyprus		new law	Central authority	
France		Regulations cannot be too specific politically, as this will raise interoperability issues;		New products through INSPIRE are not compliant/adapted to GIS users
Germany		Heterogeneity of stakeholders backgrounds, leading to different interpretations of INSPIRE, implementing rules and guidelines; legal binding of technical specifications	thematic responsibility;	unexpected questions emerging during implementation

Country	Which uncertainties are you still coping with?			
	Economic	Legal	Organizational	Technical
Netherlands	Who pays? Currently, various organizations declaring funds to coordinating Ministry	Consequences of coercion of key data usage.		
Poland	Economic aspects;		Coordination with other programs, e.g. GMES; large amounts of implementing rules of different EU activities ; coping with people's mentality, and convincing them about INSPIRE benefits	
Slovakia			Coordination structures. Difference between national SDI and INSPIRE	
Sweden			Identification of key datasets, and related responsible organizations; need for awareness and co-understanding amongst stakeholders	
Switzerland		budgets other than federal are not yet available;	Availability of human resources; organizational and working cultures	
UK			Still a challenge to get organisations to work collaboratively. Organisations may seek to provide minimal compliance	No implementing rules yet. Much to be resolved on network services.



Uncertainty (re-)generation



Country	What is the main success that introducing INSPIRE has achieved so far?
Belgium	Rise of awareness of importance of GI; creation of new initiatives for collaboration in Belgium
Bulgaria	Better structured information about how public administration is dealing with spatial and other types of data
Croatia	Necessity to harmonize and reduce multiple data collections has grown visibility. This has created good platform for action. NSDI concept has been legally adopted and accepted by stakeholders.
Cyprus	Adoption of common standards and rules. Storing and maintaining each category of spatial information once.
France	It is a good framework to incite GI stakeholders to strive for interoperability (even though not all interoperability is achieved)
Germany	Awareness of spatial issues has been improved; the legal requirements push existing SDI activities
Netherlands	Awareness has been created; now there is clarity about which data source holder is responsible for what feature
Poland	Better understanding of INSPIRE idea. Geoportal is already available.
Slovakia	INSPIRE forces us to innovate data provision and invent new web services
Sweden	It has infosized the need for standardization and information management; realization of national geodata portal with business models for data sharing; it has resulted in efficient coordination structure, incorporating all organizations.
Switzerland	In the last 6-8 years many projects to implement SDI for Switzerland. New law was a joint effort of many (public and private) institutions in Switzerland; is regarded as a major milestone.
UK	Because there is <u>legislation</u> to make it happen, it has forced the need for a governance framework for cross government working and more collaborative working



Observations

- INSPIRE not as end goal, but as vehicle to promote public sector back office integration and cooperation
- The effect of the formalizing processes through INSPIRE has raised awareness about spatial issues, and is pushing innovation in older (inert) institutions



Country	What key strategy do you recommend for the implementation of INSPIRE?
Belgium	
Bulgaria	Ensure significant new budgets for implementation. Seek co-funding with other projects (e.g. GMES)
Croatia	Legally mandated leadership to implement INSPIRE. Use weaknesses (i.e. not having national GI) as opportunities ; develop centralized data model structure; spend a few years in checking national data
Cyprus	Implementation through management board and director's team. Creation of working teams with experts from all organizations
France	Expand INSPIRE horizontally, e.g. link and be consistent to GMES for example
Germany	Establish a coordination structure involving broad participation – all levels of administration, research, business; accompany implementing phase by pilots and projects; cooperation between member states
Netherlands	Choose for a grow model; first do what is required and feasible, then expand.
Poland	Establish framework program for NSDI , including measures of coordination and organization.
Slovakia	No particular key strategy.
Sweden	Persistent communication and information about background and goals is essential. Showing good examples; a step-by-step implementation is recommended
Switzerland	Our main approach is to keep things simple (organisational and technical aspects).
UK	

Observations

- Evident leadership while using more flatter inter-organizational working relations
- Cultivation approach (not single /static design or coercive)
- A grow , step-by-step, model is common (scaling up approach) with global to local implementation plans
- Actual INSPIRE implementation reflects more II cultivation approach than II design approach -> hence relevance social sciences theory



LIST OF OEEPE/EuroSDR OFFICIAL PUBLICATIONS

State – August 2011

- 1 *Trombetti, C.*: „Activité de la Commission A de l'OEEPE de 1960 à 1964“ – *Cunietti, M.*: „Activité de la Commission B de l'OEEPE pendant la période septembre 1960 – janvier 1964“ – *Förstner, R.*: „Rapport sur les travaux et les résultats de la Commission C de l'OEEPE (1960–1964)“ – *Neumaier, K.*: „Rapport de la Commission E pour Lisbonne“ – *Weele, A. J. v. d.*: „Report of Commission F.“ – Frankfurt a. M. 1964, 50 pages with 7 tables and 9 annexes.
- 2 *Neumaier, K.*: „Essais d'interprétation de »Bedford« et de »Waterbury«. Rapport commun établi par les Centres de la Commission E de l'OEEPE ayant participé aux tests“ – „The Interpretation Tests of »Bedford« and »Waterbury«. Common Report Established by all Participating Centres of Commission E of OEEPE“ – „Essais de restitution »Bloc Suisse«. Rapport commun établi par les Centres de la Commission E de l'OEEPE ayant participé aux tests“ – „Test »Schweizer Block«. Joint Report of all Centres of Commission E of OEEPE.“ – Frankfurt a. M. 1966, 60 pages with 44 annexes.
- 3 *Cunietti, M.*: „Emploi des blocs de bandes pour la cartographie à grande échelle – Résultats des recherches expérimentales organisées par la Commission B de l'O.E.E.P.E. au cours de la période 1959–1966“ – „Use of Strips Connected to Blocks for Large Scale Mapping – Results of Experimental Research Organized by Commission B of the O.E.E.P.E. from 1959 through 1966.“ – Frankfurt a. M. 1968, 157 pages with 50 figures and 24 tables.
- 4 *Förstner, R.*: „Sur la précision de mesures photogrammétriques de coordonnées en terrain montagneux. Rapport sur les résultats de l'essai de Reichenbach de la Commission C de l'OEEPE“ – „The Accuracy of Photogrammetric Co-ordinate Measurements in Mountainous Terrain. Report on the Results of the Reichenbach Test Commission C of the OEEPE.“ – Frankfurt a. M. 1968, Part I: 145 pages with 9 figures; Part II: 23 pages with 65 tables.
- 5 *Trombetti, C.*: „Les recherches expérimentales exécutées sur de longues bandes par la Commission A de l'OEEPE.“ – Frankfurt a. M. 1972, 41 pages with 1 figure, 2 tables, 96 annexes and 19 plates.
- 6 *Neumaier, K.*: „Essai d'interprétation. Rapports des Centres de la Commission E de l'OEEPE.“ – Frankfurt a. M. 1972, 38 pages with 12 tables and 5 annexes.
- 7 *Wiser, P.*: „Etude expérimentale de l'aérotiangulation semi-analytique. Rapport sur l'essai »Gramastetten«.“ – Frankfurt a. M. 1972, 36 pages with 6 figures and 8 tables.
- 8 „Proceedings of the OEEPE Symposium on Experimental Research on Accuracy of Aerial Triangulation (Results of Oberschwaben Tests)“ *Ackermann, F.*: „On Statistical Investigation into the Accuracy of Aerial Triangulation. The Test Project Oberschwaben“ – „Recherches statistiques sur la précision de l'aérotiangulation. Le champ d'essai Oberschwaben“ – *Belzner, H.*: „The Planning. Establishing and Flying of the Test Field Oberschwaben“ – *Stark, E.*: „Testblock Oberschwaben, Programme I. Results of Strip Adjustments“ – *Ackermann, F.*: „Testblock Oberschwaben, Program I. Results of Block-Adjustment by Independent Models“ – *Ebner, H.*: „Comparison of Different Methods of Block Adjustment“ – *Wiser, P.*: „Propositions pour le traitement des erreurs non-accidentelles“ – *Camps, F.*: „Résultats obtenus dans le cadre du project Oberschwaben 2A“ – *Cunietti, M.*; *Vanossi, A.*: „Etude statistique expérimentale des erreurs d'enchaînement des photogrammes“ – *Kupfer, G.*: „Image Geometry as Obtained from Rheidt Test Area Photography“ – *Förstner, R.*: „The Signal-Field of Baustetten. A Short Report“ – *Visser, J.*; *Leberl, F.*; *Kure, J.*: „OEEPE Oberschwaben Réseau Investigations“ – *Bauer, H.*: „Compensation of Systematic Errors by Analytical Block Adjustment with Common Image Deformation Parameters.“ – Frankfurt a. M. 1973, 350 pages with 119 figures, 68 tables and 1 annex.
- 9 *Beck, W.*: „The Production of Topographic Maps at 1 : 10,000 by Photogrammetric Methods. – With statistical evaluations, reproductions, style sheet and sample fragments by

Landesvermessungsamt Baden-Württemberg Stuttgart.“ – Frankfurt a. M. 1976, 89 pages with 10 figures, 20 tables and 20 annexes.

- 10 „Résultats complémentaires de l’essai d’«Oberriet» of the Commission C de l’OEEPE – Further Results of the Photogrammetric Tests of «Oberriet» of the Commission C of the OEEPE“
Hárry, H.: „Mesure de points de terrain non signalisés dans le champ d’essai d’«Oberriet» – Measurements of Non-Signalized Points in the Test Field «Oberriet» (Abstract)“ – *Stickler, A.*; *Waldhäusl, P.*: „Restitution graphique des points et des lignes non signalisés et leur comparaison avec des résultats de mesures sur le terrain dans le champ d’essai d’«Oberriet» – Graphical Plotting of Non-Signalized Points and Lines, and Comparison with Terrestrial Surveys in the Test Field «Oberriet»“ – *Förstner, R.*: „Résultats complémentaires des transformations de coordonnées de l’essai d’«Oberriet» de la Commission C de l’OEEPE – Further Results from Co-ordinate Transformations of the Test «Oberriet» of Commission C of the OEEPE“ – *Schürer, K.*: „Comparaison des distances d’«Oberriet» – Comparison of Distances of «Oberriet» (Abstract).“ – Frankfurt a. M. 1975, 158 pages with 22 figures and 26 tables.
- 11 „25 années de l’OEEPE“
Verlaine, R.: „25 années d’activité de l’OEEPE“ – „25 Years of OEEPE (Summary)“ – *Baarda, W.*: „Mathematical Models.“ – Frankfurt a. M. 1979, 104 pages with 22 figures.
- 12 *Spiess, E.*: „Revision of 1 : 25,000 Topographic Maps by Photogrammetric Methods.“ – Frankfurt a. M. 1985, 228 pages with 102 figures and 30 tables.
- 13 *Timmerman, J.*; *Roos, P. A.*; *Schürer, K.*; *Förstner, R.*: On the Accuracy of Photogrammetric Measurements of Buildings – Report on the Results of the Test “Dordrecht”, Carried out by Commission C of the OEEPE. – Frankfurt a. M. 1982, 144 pages with 14 figures and 36 tables.
- 14 *Thompson C. N.*: Test of Digitising Methods. – Frankfurt a. M. 1984, 120 pages with 38 figures and 18 tables.
- 15 *Jaakkola, M.*; *Brindöpke, W.*; *Kölbl, O.*; *Noukka, P.*: Optimal Emulsions for Large-Scale Mapping – Test of “Steinwedel” – Commission C of the OEEPE 1981–84. – Frankfurt a. M. 1985, 102 pages with 53 figures.
- 16 *Waldhäusl, P.*: Results of the Vienna Test of OEEPE Commission C. – *Kölbl, O.*: Photogrammetric Versus Terrestrial Town Survey. – Frankfurt a. M. 1986, 57 pages with 16 figures, 10 tables and 7 annexes.
- 17 *Commission E of the OEEPE*: Influences of Reproduction Techniques on the Identification of Topographic Details on Orthophotomaps. – Frankfurt a. M. 1986, 138 pages with 51 figures, 25 tables and 6 appendices.
- 18 *Förstner, W.*: Final Report on the Joint Test on Gross Error Detection of OEEPE and ISP WG III/1. – Frankfurt a. M. 1986, 97 pages with 27 tables and 20 figures.
- 19 *Dowman, I. J.*; *Ducher, G.*: Spacelab Metric Camera Experiment – Test of Image Accuracy. – Frankfurt a. M. 1987, 112 pages with 13 figures, 25 tables and 7 appendices.
- 20 *Eichhorn, G.*: Summary of Replies to Questionnaire on Land Information Systems – Commission V – Land Information Systems. – Frankfurt a. M. 1988, 129 pages with 49 tables and 1 annex.
- 21 *Kölbl, O.*: Proceedings of the Workshop on Cadastral Renovation – Ecole polytechnique fédérale, Lausanne, 9–11 September, 1987. – Frankfurt a. M. 1988, 337 pages with figures, tables and appendices.
- 22 *Rollin, J.*; *Dowman, I. J.*: Map Compilation and Revision in Developing Areas – Test of Large Format Camera Imagery. – Frankfurt a. M. 1988, 35 pages with 3 figures, 9 tables and 3 appendices.
- 23 *Drummond, J.* (ed.): Automatic Digitizing – A Report Submitted by a Working Group of Commission D (Photogrammetry and Cartography). – Frankfurt a. M. 1990, 224 pages with 85 figures, 6 tables and 6 appendices.
- 24 *Ahokas, E.*; *Jaakkola, J.*; *Sotkas, P.*: Interpretability of SPOT data for General Mapping. – Frankfurt a. M. 1990, 120 pages with 11 figures, 7 tables and 10 appendices.

- 25 *Ducher, G.*: Test on Orthophoto and Stereo-Orthophoto Accuracy. – Frankfurt a. M. 1991, 227 pages with 16 figures and 44 tables.
- 26 *Dowman, I. J.* (ed.): Test of Triangulation of SPOT Data – Frankfurt a. M. 1991, 206 pages with 67 figures, 52 tables and 3 appendices.
- 27 *Newby, P. R. T.; Thompson, C. N.* (ed.): Proceedings of the ISPRS and OEEPE Joint Workshop on Updating Digital Data by Photogrammetric Methods. – Frankfurt a. M. 1992, 278 pages with 79 figures, 10 tables and 2 appendices.
- 28 *Koen, L. A.; Kölbl, O.* (ed.): Proceedings of the OEEPE-Workshop on Data Quality in Land Information Systems, Apeldoorn, Netherlands, 4–6 September 1991. – Frankfurt a. M. 1992, 243 pages with 62 figures, 14 tables and 2 appendices.
- 29 *Burman, H.; Torlegård, K.*: Empirical Results of GPS – Supported Block Triangulation. – Frankfurt a. M. 1994, 86 pages with 5 figures, 3 tables and 8 appendices.
- 30 *Gray, S.* (ed.): Updating of Complex Topographic Databases. – Frankfurt a. M. 1995, 133 pages with 2 figures and 12 appendices.
- 31 *Jaakkola, J.; Sarjakoski, T.*: Experimental Test on Digital Aerial Triangulation. – Frankfurt a. M. 1996, 155 pages with 24 figures, 7 tables and 2 appendices.
- 32 *Dowman, I. J.*: The OEEPE GEOSAR Test of Geocoding ERS-1 SAR Data. – Frankfurt a. M. 1996, 126 pages with 5 figures, 2 tables and 2 appendices.
- 33 *Kölbl, O.*: Proceedings of the OEEPE-Workshop on Application of Digital Photogrammetric Workstations. – Frankfurt a. M. 1996, 453 pages with numerous figures and tables.
- 34 *Blau, E.; Boochs, F.; Schulz, B.-S.*: Digital Landscape Model for Europe (DLME). – Frankfurt a. M. 1997, 72 pages with 21 figures, 9 tables, 4 diagrams and 15 appendices.
- 35 *Fuchs, C.; Gülch, E.; Förstner, W.*: OEEPE Survey on 3D-City Models.
Heipke, C.; Eder, K.: Performance of Tie-Point Extraction in Automatic Aerial Triangulation. – Frankfurt a. M. 1998, 185 pages with 42 figures, 27 tables and 15 appendices.
- 36 *Kirby, R. P.*: Revision Measurement of Large Scale Topographic Data.
Höhle, J.: Automatic Orientation of Aerial Images on Database Information.
Dequal, S.; Koen, L. A.; Rinaudo, F.: Comparison of National Guidelines for Technical and Cadastral Mapping in Europe (“Ferrara Test”) – Frankfurt a. M. 1999, 273 pages with 26 figures, 42 tables, 7 special contributions and 9 appendices.
- 37 *Koelbl, O.* (ed.): Proceedings of the OEEPE – Workshop on Automation in Digital Photogrammetric Production. – Frankfurt a. M. 1999, 475 pages with numerous figures and tables.
- 38 *Gower, R.*: Workshop on National Mapping Agencies and the Internet. *Flotron, A.; Koelbl, O.*: Precision Terrain Model for Civil Engineering. – Frankfurt a. M. 2000, 140 pages with numerous figures, tables and a CD.
- 39 *Ruas, A.*: Automatic Generalisation Project: Learning Process from Interactive Generalisation. – Frankfurt a. M. 2001, 98 pages with 43 figures, 46 tables and 1 appendix.
- 40 *Torlegård, K.; Jonas, N.*: OEEPE workshop on Airborne Laserscanning and Interferometric SAR for Detailed Digital Elevation Models. – Frankfurt a. M. 2001, CD: 299 pages with 132 figures, 26 tables, 5 presentations and 2 videos.
- 41 *Radwan, M.; Onchaga, R.; Morales, J.*: A Structural Approach to the Management and Optimization of Geoinformation Processes. – Frankfurt a. M. 2001, 174 pages with 74 figures, 63 tables and 1 CD.
- 42 *Heipke, C.; Sester, M.; Willrich, F.* (eds.): Joint OEEPE/ISPRS Workshop – From 2D to 3D – Establishment and maintenance of national core geospatial databases. *Woodsford, P.* (ed.): OEEPE Commission 5 Workshop: Use of XML/GML. – Frankfurt a. M. 2002, CD.
- 43 *Heipke, C.; Jacobsen, K.; Wegmann, H.*: Integrated Sensor Orientation – Test Report and Workshop Proceedings. – Frankfurt a. M. 2002, 302 pages with 215 figures, 139 tables and 2 appendices.
- 44 *Holland, D.; Guilford, B.; Murray, K.*: Topographic Mapping from High Resolution Space Sensors. – Frankfurt a. M. 2002, 155 pages with numerous figures, tables and 7 appendices.

- 45 Murray, K. (ed.): OEEPE Workshop on Next Generation Spatial Database – 2005. Altan, M. O.; Tastan, H. (eds.): OEEPE/ISPRS Joint Workshop on Spatial Data Quality Management. 2003, CD.
- 46 Heipke, C.; Kuittinen, R.; Nagel, G. (eds.): From OEEPE to EuroSDR: 50 years of European Spatial Data Research and beyond – Seminar of Honour. 2003, 103 pages and CD.
- 47 Woodsford, P.; Kraak, M.; Murray, K.; Chapman, D. (eds.): Visualisation and Rendering – Proceedings EuroSDR Commission 5 Workshop. 2003, CD.
- 48 Woodsford, P. (ed.): Ontologies & Schema Translation – 2004. Bray, C. (ed.): Positional Accuracy Improvement – 2004. Woodsford, P. (ed.): E-delivery – 2005. Workshops. 2005, CD.
- 49 Bray, C.; Rönsdorf, C. (eds.): Achieving Geometric Interoperability of Spatial Data, Workshop – 2005. Kolbe, T. H.; Gröger, G. (eds.): International Workshop on Next Generation 3D City Models – 2005. Woodsford, P. (ed.): Workshop on Feature/Object Data Models. 2006, CD.
- 50 Kaartinen, H.; Hyypä J.: Evaluation of Building Extraction. Steinmocher, K.; Kressler, F.: Change Detection. Bellmann, A.; Hellwich, O.: Sensor and Data Fusion Contest: Information for Mapping from Airborne SAR and Optical Imagery (Phase I). Mayer, H.; Baltsavias, E.; Bacher, U.: Automated Extraction, Refinement, and Update of Road Databases from Imagery and Other Data. 2006, 280 pages.
- 51 Höhle, J.; Potuckova J.: The EuroSDR Test “Checking and Improving of Digital Terrain Models”. Skaloud, J.: Reliability of Direct Georeferencing, Phase 1: An Overview of the Current Approaches and Possibilities. Legat, K.; Skaloud, J.; Schmidt, R.: Reliability of Direct Georeferencing, Phase 2: A Case Study on Practical Problems and Solutions. 2006, 184 pages.
- 52 Murray, K. (ed.): Proceedings of the International Workshop on Land and Marine Information Integration. 2007, CD.
- 53 Kaartinen, H.; Hyypä, J.: Tree Extraction. 2008, 56 pages.
- 54 Patrucco, R.; Murray, K. (eds.): Production Partnership Management Workshop – 2007. Ismael Colomina, I.; Hernández, E. (eds.): International Calibration and Orientation Workshop, EuroCOW 2008. Heipke, C.; Sester, M. (eds.): Geosensor Networks Workshop. Kolbe, T. H. (ed.): Final Report on the EuroSDR CityGML Project. 2008, CD.
- 55 Cramer, M.: Digital Camera Calibration. 2009, 257 pages.
- 56 Champion, N.: Detection of Unregistered Buildings for Updating 2D Databases. Everaerts, J.: NEWPLATFORMS – Unconventional Platforms (Unmanned Aircraft Systems) for Remote Sensing. 2009, 98 pages.
- 57 Streilein, A.; Kellenberger, T. (eds.): Crowd Sourcing for Updating National Databases. Colomina, I.; Jan Skaloud, J.; Cramer, M. (eds.): International Calibration and Orientation Workshop EuroCOW 2010. Nebiker, S.; Bleisch, S.; Gülch, E.: Final Report on EuroSDR Project Virtual Globes. 2010, CD.
- 58 Stoter, J.: State-of-the-Art of Automated Generalisation in Commercial Software. Grenzdörffer, G.: Medium Format Cameras. 2010, 266 pages and CD.

The publications can be ordered using the electronic order form of the EuroSDR website
www.eurosdrr.net